

APPENDIX B

IDENTIFICATION OF FACTORS CONTROLLING THE DEVELOPMENT OF SUBSIDENCE IMPACTS FORECASTING METHODOLOGY TO THE I-70 ALIGNMENT OVER LONGWALL MINING OF THE TUNNEL RIDGE MINE, WASHINGTON COUNTY, PA

Task 2: Undermining Activities Report
Submitted 3 February 2020; Finalized on 4 January 2021

The University of Pittsburgh Master Agreement
Contract No. 4400018535

Project Team

Anthony Iannacchione, Associate Professor, Principal Investigator*

Luis Vallejo, Professor, Co-Principal Investigator

Julie Vandenbossche, Professor

Mingzhou Li, Graduate Research Student

Emily Adelsohn, Graduate Research Student

Robert Winn, Graduate Research Student

** - Email ati2@pitt.edu, Phone: 412-624-8289*

Task 2 Report Outline

| | | |
|-----|--|------|
| I | Introduction..... | B4 |
| | a) Project Scope | |
| | a) Objective | |
| | b) Overview | |
| II | Longwall Mining Under I-70..... | B8 |
| | a) What is Longwall Mining? | |
| | b) The Mining of Panel 15 | |
| | c) Prevention Controls and Recovery Measures | |
| | d) University Field Activity | |
| III | Discussion of Data Collected..... | B19 |
| | a) Highway Alignment Surveys Data | |
| | b) Embankment and Cut Slope Surveys | |
| | c) Observational Data | |
| | d) Inclinator Data | |
| | e) Tiltmeter Data | |
| | f) Piezometer Data | |
| | g) LiDAR Accuracy Assessment | |
| IV | Characterization of Subsidence Basin..... | B82 |
| | a) Subsidence Movement Explained Through Survey Data and Observations | |
| | b) Calibration of SDPS Models Using Survey Data | |
| | c) Comparison of Subsidence Observations with Empirical Models | |
| V | Embankment Behavior..... | B110 |
| | a) Stress-Strain Response of the Soil Samples from Embankment #1 | |
| | b) Embankment Observations during Subsidence | |
| | c) Consolidation and Lateral Spreading | |
| | d) Analysis of Piezometers Data | |
| | e) FEM Analysis of Embankment #1 Subjected to Limited (2D) Simulated Subsidence | |
| | f) Discussion of Challenges in Utilizing the SDPS Subsidence Numerical Regression within the Embankment #1 FEM | |
| VI | Future Work..... | B181 |
| | a) Orientation Influence | |
| | b) Overburden Influence | |

- c) Embankment Stability
- d) I-70 Highway Alignment Damage Susceptibility Maps

ReferencesB190

Appendix I - Detailed SPK Survey Stake Data.....B193

Appendix II - Complete Record of Observed Features on Pavement.....B221

Appendix III - Inclometers Data.....B233

SECTION I – INTRODUCTION

Subsection Ia – Project Scope

1.0 Background

Longwall coal mining was introduced to Pennsylvania in the late 1960's. Since that time, almost 800 hundred longwall panels have extracted huge reserves of coal. Of this total, twenty-five panels have undermined parts of two interstate highways, I-70 and I-79. These twenty-five panels were located in four mines: Gateway, Eight-Four, Cumberland, and Emerald.

Over the last five decades, there has been a great deal of effort to understand how longwall subsidence basin formation impacts surface features, such as buildings, water supplies, streams and wetlands. Less is known as to how subsidence can impact interstates, and even less is known about the impact to embankments and cuts that carry these highway alignments. In some areas, careful monitoring of conditions and asphalt re-surfacing repaired the subsidence damage with only minimal impact to highway traffic. In other cases, bridges carrying I-79, as well as certain overpass structures, had to be replaced (Iannacchione, et al., 2011). Traffic delays were most noticeable during milling and paving activities. The University is not aware of any subsidence impacts causing an accident or injuring the traveling public.

2.0 Contract

The University of Pittsburgh (herein referred to as 'the University' submitted a proposal to PennDOT in May 2018. This proposal has the University studying data collected by PennDOT and its contractors during periods where interstate I-70 was impacted by longwall subsidence. It also requires the University to assess the risk to other areas along Pennsylvania interstate alignments that might be impacted by longwall subsidence in the future.

The University received a notice to proceed with this effort on 3 October 2018. The contract was to end, no later than, 4 January 2021 at a cost of \$516,348.30. The project is administered by Shelley Scott and Roy Painter is the technical advisor. The project Kickoff meeting occurred on 23 October 2018 with work activities started in late November after the necessary University approvals were in-place. Communication and reporting on contract activities occurred through regularly scheduled monthly meetings and through required reporting activities. This report is an example of a required reporting task.

The five major reporting tasks are listed below:

- Task 1: Pre-Undermining Activities - A report containing a summary of the pre-undermining activities, along with a PowerPoint presentation of research findings by 5 August 2019, **COMPLETED 14 July 2019**
- Task 2: Undermining Activities - A report containing a summary of the undermining activities, along with a PowerPoint presentation of research findings by 3 April 2020, **THE DRAFT OF THIS REPORT AND THE CORRESPONDING PRESENTATION WERE DELIVERED TO PennDOT ON 17 DECEMBER 2019 AT PennDOT'S UNIONTOWN OFFICE.**
- Task 3: Post-Undermining Activities - A report of the Subsidence Forecasting, along with a PowerPoint presentation of research findings by 3 October 2020
- Task 4: Draft Final Report by 17 November 2020
- Task 5: Final Report by 19 December 2020

The Final Report will summarize the most important information contained in Tasks Reports 1, 2 and 3. This report, referred to as the Task 2 Report, focuses on undermining activities associated with the extraction of Tunnel Ridge's Panel 15.

Subsection Ib – Objective

Alliance Coal's Tunnel Ridge Mine plans to undermine I-70 with the longwall mining method in both Pennsylvania and West Virginia over the next two decades. One of their panels, Panel 15, undermined I-70 early in 2019 and more are planned in the future.

- 1) Investigate the influence of longwall mining on highway alignments and associated slopes and embankments.
- 2) Evaluate how the highway deforms during undermining with a focus on determining its transient characteristics.
- 3) Utilize models to better understand subsidence impacts to the highway alignment, and where possible,
- 4) Determine how other future highway alignments could be impacted.

Subsection Ic – Overview

This project has two distinct study areas. The first has to do with detailed monitoring of the I-70 highway alignment during the undermining by longwall Panel 15 of the Tunnel Ridge Mine. The results of this monitoring effort are presented within this report. It should be noted that monitoring stopped a few months after Panel 15 passed under the study area. No attempt was made to monitor I-70 study area conditions when the adjacent Panel 16 was extracted in the fall of 2019.

Panel 15 lies less than one mile southwest of the West Alexander I-70 interchange. The initial study area is hereby designated as the 3,300-ft of I-70 that spans the subsidence basin developed by the extraction of Panel 15 (Figure Ic.1). Panel 15 underlies approximately 2,130-ft of I-70. The gate entries underlie another 340-ft of highway with another 325-ft buffer zone over the unmined coal. The western end lies some 700-ft within the State of West Virginia and the remaining 2,600-ft within the Commonwealth of Pennsylvania.

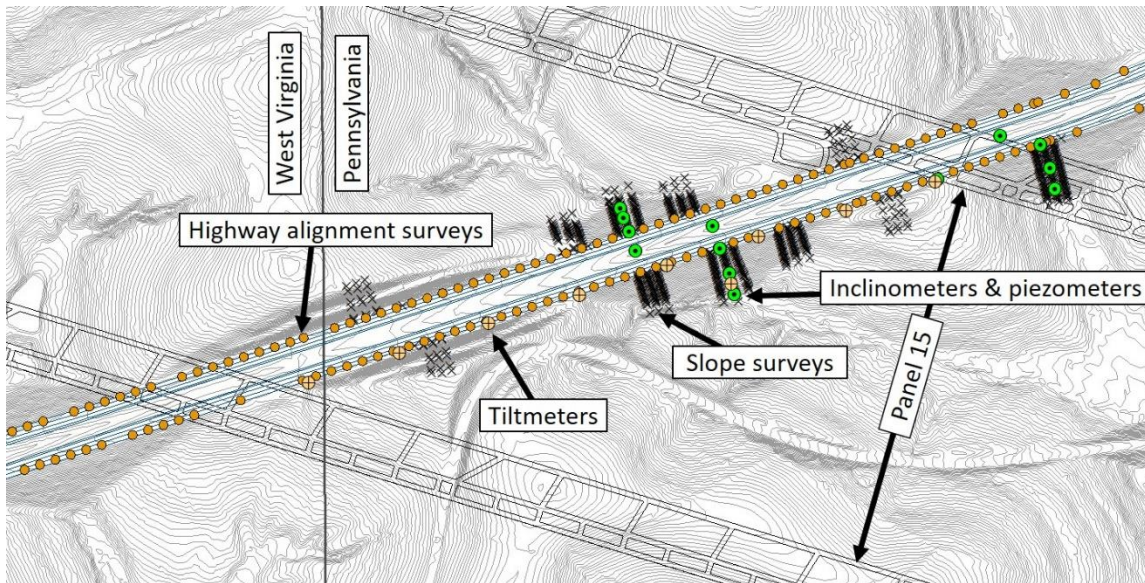


Figure Ic.1 - The initial study area and the location of monitoring instrumentation

The extended study area encompasses the Tunnel Ridge reserves of Pittsburgh Coalbed in western Pennsylvania (Figure Ic.2). A portion of these reserves has the potential to be mined in the next two decades by the longwall mining method. The University plans to take the knowledge gained during the undermining of Panel 15, where a considerable array of monitoring equipment was assembled, to evaluate potential longwall mining subsidence impacts within the extended study area.

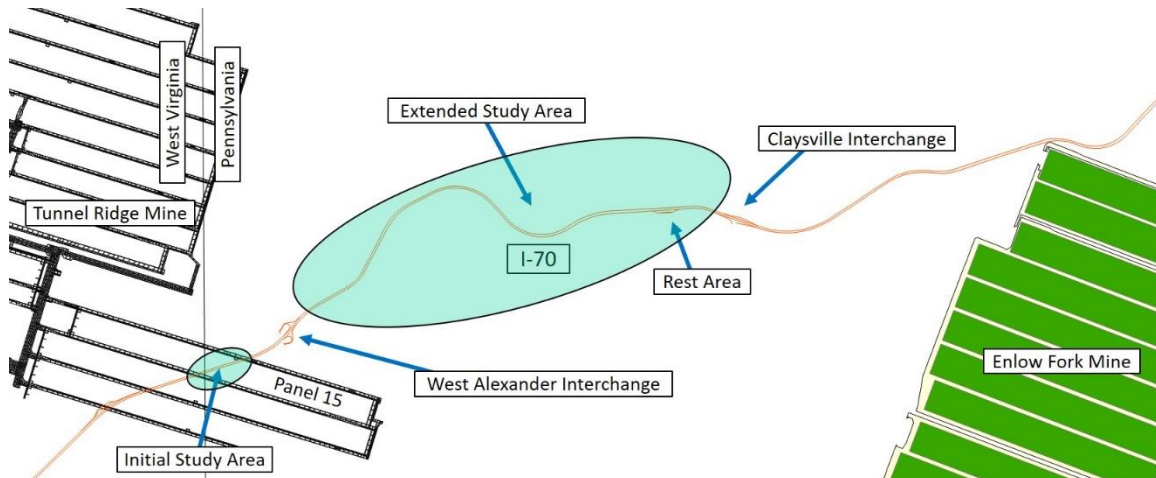


Figure Ic.2 – Extent of I-70 overlain by unmined portion of the Tunnel Ridge Mine reserves in Washington County, Pennsylvania. Also shown are the initial and extended study areas

The following report summarizes observations and measurements made during the undermining of I-70 by Panel 15. The formation of the subsidence basin was characterized and compared with other empirical and analytical models. The complex behavior of the highway was established by comparing observations with alignment surveys and LiDAR imagery. Impacts to embankments and slopes within the I-70 alignment were measured and compared to monitoring instrumentation. These data have been used to validate models constructed by the University. All of these efforts are providing a foundation for future project reporting, i.e. the Task 3 Report.

SECTION II – LONGWALL MINING UNDER I-70

Section IIa – What is Longwall Mining?

In a recently published assessment of underground bituminous coal mining from 2013 to 2018, forty-nine (49) operations undermined over 28,000 acres in Pennsylvania (Bain, et al., 2019). Seven of these mines used the longwall mining method (the Emerald Mine was idled in 2016) and account for 61.2-pct of the total acreage mined. The Tunnel Ridge Mine is one of these seven. In a longwall mine, the room-and-pillar method is used for developing mains, gate roads, and bleeder entries. Longwall panels are outlined by these developments. During this same period, panels range in width from 1,000 to 1,600-ft. Panel 15 at the Tunnel Ridge Mine is approximately 14,450-ft long and 1,230-ft wide.

The longwall face extends between parallel gate road developments and is equivalent to the width of the panel (Figure IIa.1). An electro-hydraulic cutting machine known as a shearer, extracts a slice of coal approximately 30 to 40-in thick along the 1,230-ft longwall face in one pass. The longwall face work area is protected by massive hydraulic support known as shields. With each pass of the shield, the entire mechanism moves forward, allowing the overlying strata to cave into the recently created void. The longwall mining method extracts nearly 100-pct of the coal within the panel.

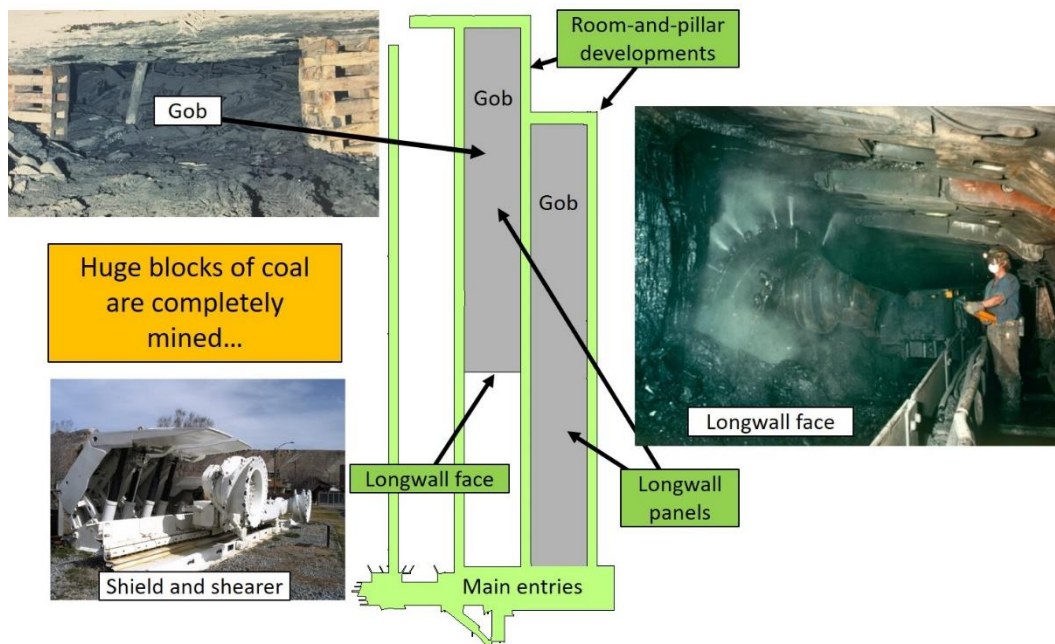


Figure IIa.3 – Example of longwall mining where the shearer and shields operate along a longwall production face that extracts the coal and allows the overlying strata to cave into the extraction zone, creating 'gob'.

A typical Pittsburgh Coalbed longwall face normally advances from 100 to 130-ft per day. That means the shearer can make over a dozen passes between the gate roads per shift. The University was able to visit the Tunnel Ridge mine in May of 2018 and observed a highly mechanized, engineered system. The longwall mines operating within Pennsylvania are some of the most productive coal mining operations in the world.

Over 600 longwall panels have been mined in the Pittsburgh Coalbed in Greene and Washington Counties, Pennsylvania in the last 50 years (Adelsohn, et. al, 2019). Twenty-five of those panels undermined interstate highways. An investigation of past undermining of PA interstate highways was completed and reported on in Section 2 of the Task 1 Report (Iannacchione, et. al, 2019). Panel 15 at the Tunnel Ridge Mine was the 26th panel to undermine an interstate and was studied to a greater degree than any of the previous undermining of Pennsylvania interstate highways. Subsidence related impacts to the highway alignments are diverse and dependent primarily on overburden, panel dimension, strata conditions, and highway orientation. As will be presented here within, some of the observed and measured conditions fell within predicted ranges, while others produced results that seem to be unique and somehow tied to local site-conditions. These similarities and differences with past experiences will be highlighted and discussed throughout this report.

Subsection IIb – The Mining of Panel 15

To better understand the observations and measurements discussed within this report, one must know how Panel 15 was mined. Surface features can be linked to the shape and location of the developing subsidence basin. Because the highway is oriented at a 55-deg angle with the direction of longwall advance (Figure IIb.1), the longwall face was directly under some part of I-70 for approximately 1,800-ft of advance. The subsidence basin drapes over the adjacent gate roads, extending the zone of potential influence 265-ft into the solid coal. These two factors combine to form a length of 3,300-ft of highway for detailed monitoring (Figure IIb.1). Panel 15 began coal extraction on 28 October 2018 (144+60) and cut the longwall chain and began recovering equipment on 1 May 2019 (0+0).

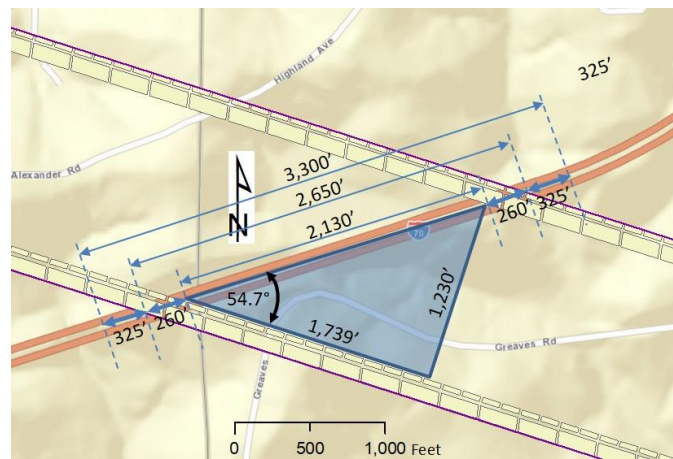


Figure IIb.1 - Location and dimensions of the initial study area

It is helpful to examine the mining of Panel 15 in context of the history of longwall mining in the area. Panel 15 is currently part of an active underground coal mining permit approved by the PA DEP (Figure IIb.2). The next four to five Tunnel Ridge longwall panels are covered under this permit and will be mined south of Panel 15 in both Pennsylvania and West Virginia. The Tunnel Ridge Mine is believed to have significant reserves of coal to the north and northeast of Panel 15 and will likely mine additional longwall panels in this area over the next two decades. To the south is the abandoned Valley Camp 3 Mine and to the east is the active and expansive Enlow Fork Longwall Mine and the abandoned Lincoln 1 Mine.

The final or permanent subsidence basin was almost completely developed under I-70 in a span of less than two months. Detailed monitoring occurred over a 50 days period from 14 January to 5 March 2019. During this period, thirty-six (36) production days advanced the longwall face approximately 4,063-ft, averaging 113-ft/production day (Table IIb.1).

Table IIb.1 – Longwall face advancement rate during the detailed monitoring period.

| | Date | Day | Distance between face positions, ft | Production days | Distance per production day, ft |
|----|-------------|-----------|-------------------------------------|-----------------|---------------------------------|
| 1 | 14 Jan 2019 | Monday | | | |
| 2 | 21 Jan 2019 | Monday | 506 | 5 | 101 |
| 3 | 25 Jan 2019 | Friday | 495 | 4 | 124 |
| 4 | 29 Jan 2019 | Tuesday | 223 | 2 | 112 |
| 5 | 31 Jan 2019 | Thursday | 266 | 2 | 133 |
| 6 | 1 Feb 2019 | Friday | 120 | 1 | 120 |
| 7 | 4 Feb 2019 | Monday | 103 | 1 | 103 |
| 8 | 5 Feb 2019 | Tuesday | 121 | 1 | 121 |
| 9 | 6 Feb 2019 | Wednesday | 124 | 1 | 124 |
| 10 | 7 Feb 2019 | Thursday | 127 | 1 | 127 |
| 11 | 8 Feb 2019 | Friday | 81 | 1 | 81 |
| 12 | 11 Feb 2019 | Monday | 108 | 1 | 108 |
| 13 | 12 Feb 2019 | Tuesday | 106 | 1 | 106 |
| 14 | 13 Feb 2019 | Wednesday | 116 | 1 | 116 |
| 15 | 14 Feb 2019 | Thursday | 121 | 1 | 121 |
| 16 | 18 Feb 2019 | Monday | 202 | 2 | 101 |
| 17 | 19 Feb 2019 | Tuesday | 74 | 1 | 74 |
| 18 | 20 Feb 2019 | Wednesday | 113 | 1 | 113 |
| 19 | 25 Feb 2019 | Monday | 357 | 3 | 119 |
| 20 | 5 Mar 2019 | Tuesday | 700 | 6 | 117 |
| | Total | | 4,063 | 36 | 113 |

Subsection IIc – Prevention Controls and Recovery Measures

1.0 Prevention Controls

One of PennDOT's primary reasons for monitoring conditions along the I-70 highway alignment during the mining of Panel 15 was to continually assess the safety of the traveling public. The emphasis on safety prevention controls can be seen in a photograph taken of the study area just prior to the passage of the longwall face (Figure IIc.1). Traffic was limited to one-lane in each direction with a speed limit of 45-mph. The traveling lane was restricted, allowing work related activities by PennDOT, their contractors, and the University to be performed from the shoulder. During the detailed monitoring period, the site was under continuous surveillance by PennDOT.



Figure IIc.1 – View of the I-70 study area over Panel 15 just prior to undermining.

One of the most interesting engineered prevention controls is the application of asphalt relief sections. Each section is 60-ft in length and occupies both the travel and passing lanes. The existing asphalt overlay and underlying concrete slab were removed and filled with a special asphalt mix. Four asphalt relief sections were installed and located in areas where horizontal deformation is expected to peak (Figure IIc.2). The effectiveness of this engineered prevention control works is a central focus of the project and will be discussed more in this task report.

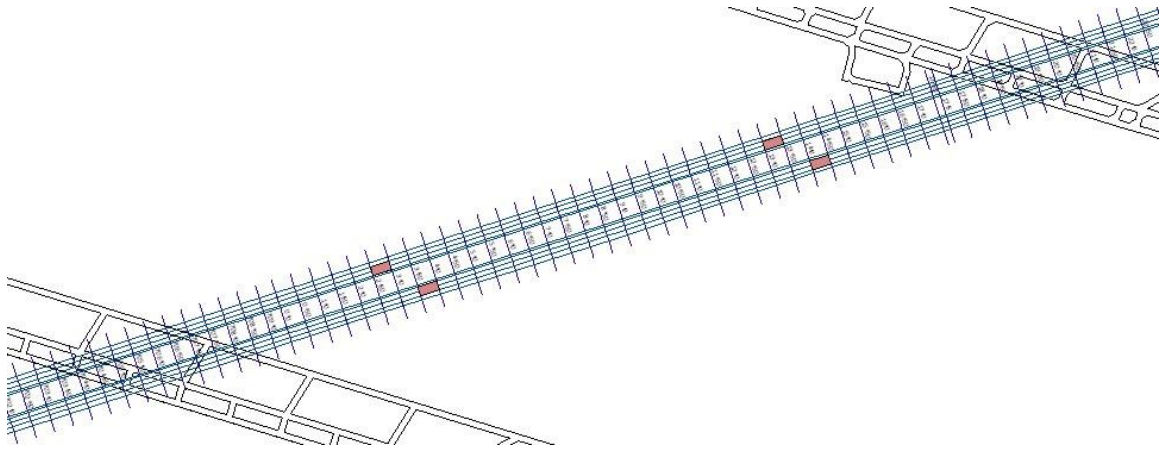


Figure IIc.2 – I-70 highway alignment showing the location of the four asphalt relief sections and the highway alignment survey marks.

2.0 Recovery Measures

A wide array of recovery measures were utilized within the study area to quickly and effectively recover from subsidence related impacts to the highway alignment. Light stands were located approximately every 400-ft to assist with night-time observations. Milling and paving equipment needed to grind compression bumps and/or patch the roadway were located close-by. Lastly, a real-time camera system was installed to allow for remote access by PennDOT staff. The camera had over a dozen settings allowing for complete viewing of the study area.

Several examples of subsidence impact recovery measures were observed. For example, on 2 February a compression bump formed on the east-bound highway alignment, cutting across both lanes of traffic, the shoulder, and both berms (Figure IIc.3). A detailed description of subsidence impacts is presented in Section 3. When this kind of impact occurred to the highway, PennDOT personnel:

- 1) monitored conditions,
- 2) alerted vehicles to slow-down with flagging, signs, and flares,
- 3) mobilized surface grinders, often stored close-by, and
- 4) applied asphalt patches.

These actions helped to protect the travelling public, minimized delays, and kept the highway open to traffic.

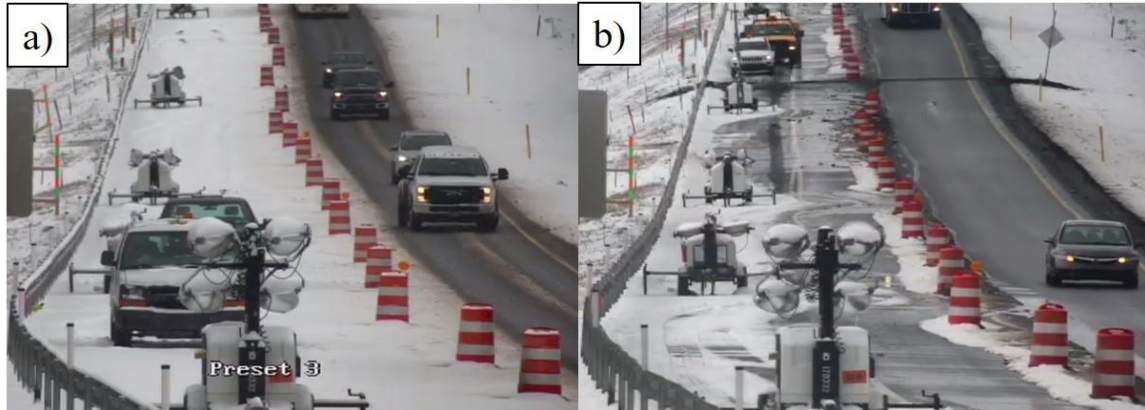


Figure IIc.3 – a) photograph taken at 12:50 on 1 February 2019; b) photograph taken at 12:09 on 2 February 2019 showing a compression bump forming across the entire East Bound highway alignment.

Another example is shown in Figure IIc.4 where a compression bump formed in the westbound lanes and an effective recovery measure was successfully implemented with minimal traffic interruptions. Subsidence impacts of this scale were continuously monitored by PennDOT and its contractors. During University visits to the study area, subsidence impacts (both large and small) were observed, measured, photographed, and located using highway alignment survey markings. The results of activities helped to build a rich inventory of information which is chronicled throughout this report.



Figure IIc.4 – a) 15 February 2019 at 14:23 the longwall face is under this section of highway, b) 17 February at 15:49 compression bump begins to form, c) 1 March at 13:16 the asphalt patch applied to a previously milled surface, and d) 2 March at 10:50 repair work completed.

The University aided in monitoring activities by producing field observation activity reports and scroll maps especially when subsidence impacts were the greatest. The field observation activity reports were in the form of memorandums to Roy Painter, Uniontown District Office, PennDOT and were typically provided to answer a question or indicate concern. Five of these reports were completed and are available on request.

- 8 November 2018, Memorandum to Roy Painter, PennDOT Uniontown Office, “19 December 2017 Visit to the I-70 Panel 15 Undermining Site”, 3 p.
- 28 January 2019, Memorandum to Roy Painter, PennDOT Uniontown Office, “Examination of the South Facing Slopes, Embankments 1 and 2”, 6 p.
- 12 February 2019, Memorandum to Roy Painter, PennDOT Uniontown Office, “Examination of the I-70 Alignment above Panel 15”, 7 p.
- 16 February 2019, Memorandum to Roy Painter, PennDOT Uniontown Office, “Examination Slopes Associated with Embankment 1 and 2, I-70 Alignment above Panel 15”, 4 p.
- 28 February 2019, Memorandum to Roy Painter, PennDOT Uniontown Office, “Development of the Permanent Subsidence Basin over Longwall Panel 15”, 4 p.

Scroll maps were generated from the University’s ArcGIS database and contained detailed information about site conditions within study area, an example of which can be seen in Figure IIc.5. In the transportation community, these maps can take on the shape of scroll since highway alignments are best displayed in a continuous median that unrolls to different sections of the study area. The University provided PennDOT with both printed and digital scroll maps of the study area and met with PennDOT staff to discuss maps at the Uniontown District Office and Taylorstown Maintenance Office. It is the opinion of the University that the generated scroll maps were commonly used by maintenance workers and supervisors to record and analyze current activity, especially during the most active period of 2 February to 19 February 2019.



Highway Extent with Geotechnical Properties

Figure IIc.5 – The third scroll map section of eight showing highway alignment survey lines and other important information about site conditions.

Subsection IId – University Field Activities

The first visit to the I-70 study area occurred on 19 December 2017, prior to the initiation of the contract. A second pre-contract visit occurred when the project team visited the Tunnel Ridge Mine and examined the longwall face environment. The University met with PennDOT staff at the study area to discuss local conditions and plans for monitoring on 13 November 2018 and 18 January 2019. Eleven field visits were conducted during the undermining, during which the entire 3,300-ft within the I-70 study area were walked along both the eastbound and westbound lanes. Details of the impacts were measured and recorded on field copies of the scroll maps. Updates from these visits were supplied through field observation and monthly project meetings reports. A record of the visits and other important dates can be seen in Table IId.1.

Table IId.1 – Important dates associated with the undermining of I-70 by Panel 15.

| Dates | Comment | Slope evaluation |
|------------------|--|------------------|
| 19 December 2017 | First site visit to examine conditions of the highway and adjacent slopes | Yes |
| 17 May 2018 | Visit of Tunnel Ridge Mine | |
| 28 October 2018 | Extraction of Panel 15 begins | |
| 13 November 2018 | Met with PennDOT to examine study area conditions | |
| 11 December 2018 | Examined conditions within the study area | Yes |
| 8 January 2019 | Examined conditions within the study area | Yes |
| 3 January 2019 | Provided examples of subsidence impacts to maintenance workers, Uniontown Office | |
| 15 January 2019 | Examined conditions within the study area | Yes |
| 18 January 2019 | Met with PennDOT to examine study area conditions | |
| 22 January 2019 | Examined conditions within the study area | Yes |
| 29 January 2019 | Examined conditions within the study area | Yes |
| 5 February 2019 | Examined conditions within the study area | Yes |
| 12 February 2019 | Examined conditions within the study area | Yes |
| 13 February 2019 | Examined conditions within the study area | Yes |
| 19 February 2019 | Examined conditions within the study area | Yes |
| 25 February 2019 | Examined conditions within the study area | Yes |
| 5 March 2019 | Examined conditions within the study area | |
| 1 May 2019 | Extraction of Panel 15 ends | |
| 6 May 2019 | Repaving and guiderails installation within the study area | |

SECTION III – DISCUSSION OF DATA COLLECTED

Subsection IIIa – Highway Alignment Surveys Data Analysis

The University has analyzed the data from the highway alignment surveys provided by PennDOT. The centerline alignment was staked for approximately 3,500-ft with 2,600-ft in Pennsylvania and 900-ft extending into West Virginia. The alignment was offset 62-ft right and left to create the two baselines with 147 points along the alignment to be monitored. The locations of these points can be seen in Figure IIIa.1. This set of points was surveyed regularly during the undermining, for a total of 11 contracted monitoring surveys. The surveys resulted in a horizontal accuracy of 0.02-ft and a vertical accuracy of 0.05 to 0.10-ft.

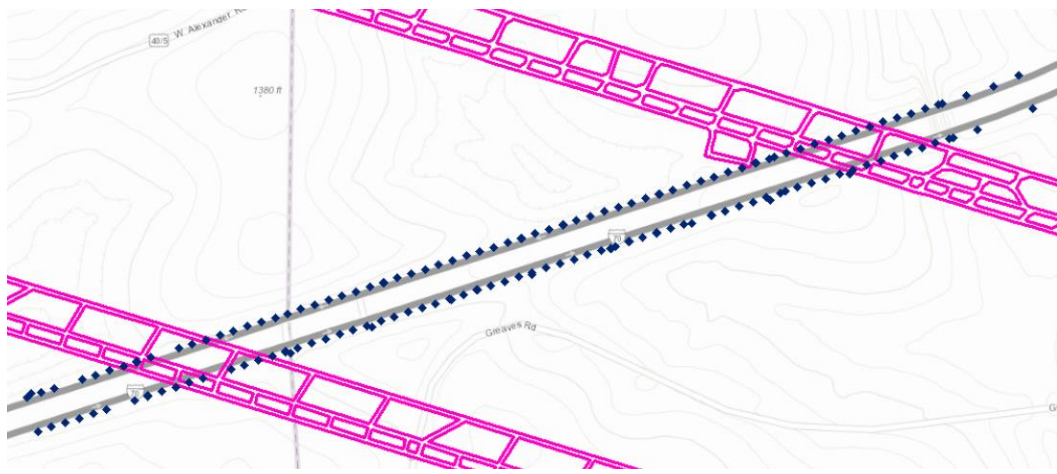


Figure IIIa.1 – Points monitored by highway alignment surveys

1.0 Vertical Movement

The points observed on the highway alignment extended the full width of the longwall panel. This means that the amount of maximum vertical subsidence observed varied along the roadway. The most vertical movement observed was just over 5-ft of subsidence. This maximum subsidence was observed on the road along the southern slope of Embankment #1. It is also noteworthy that this data shows as much as 0.25-ft of heave over the gate road entries of Panel 15. The impact of the final subsidence basin can be seen in Figure IIIa.2.

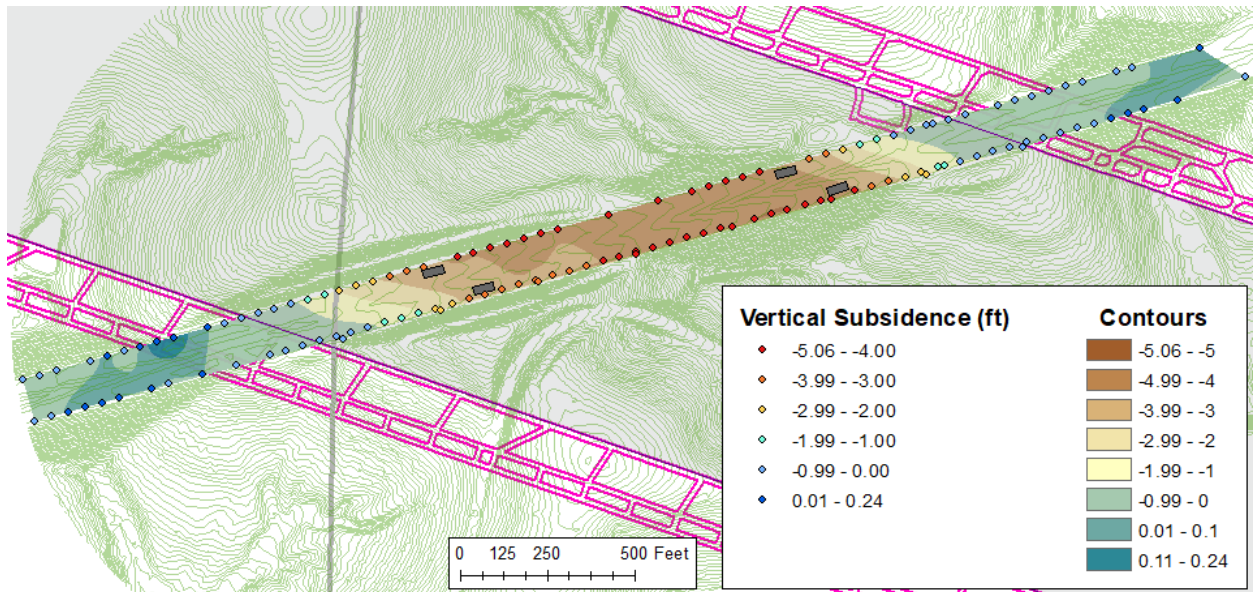
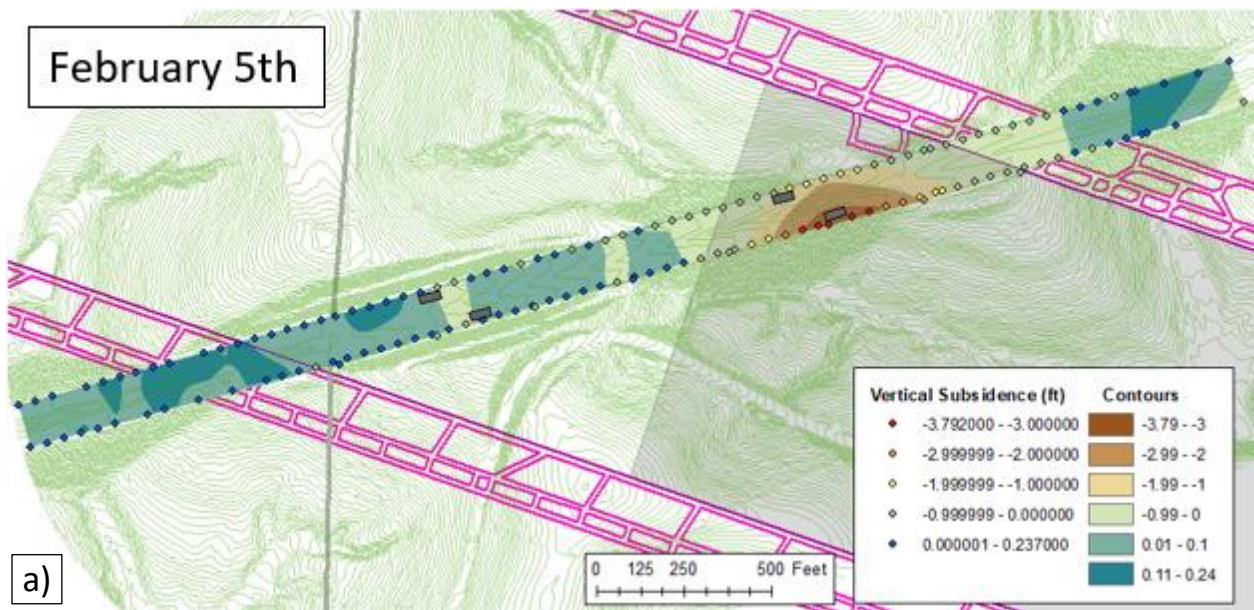


Figure IIIa.2 – Vertical drop of highway surface due to subsidence after longwall mining

Subsidence caused by longwall mining is not instantaneous. As the longwall face advanced, the subsidence basin deformed the ground behind it. The progression of subsidence increases as the longwall face progresses, as can be seen in Figure IIIa.3.



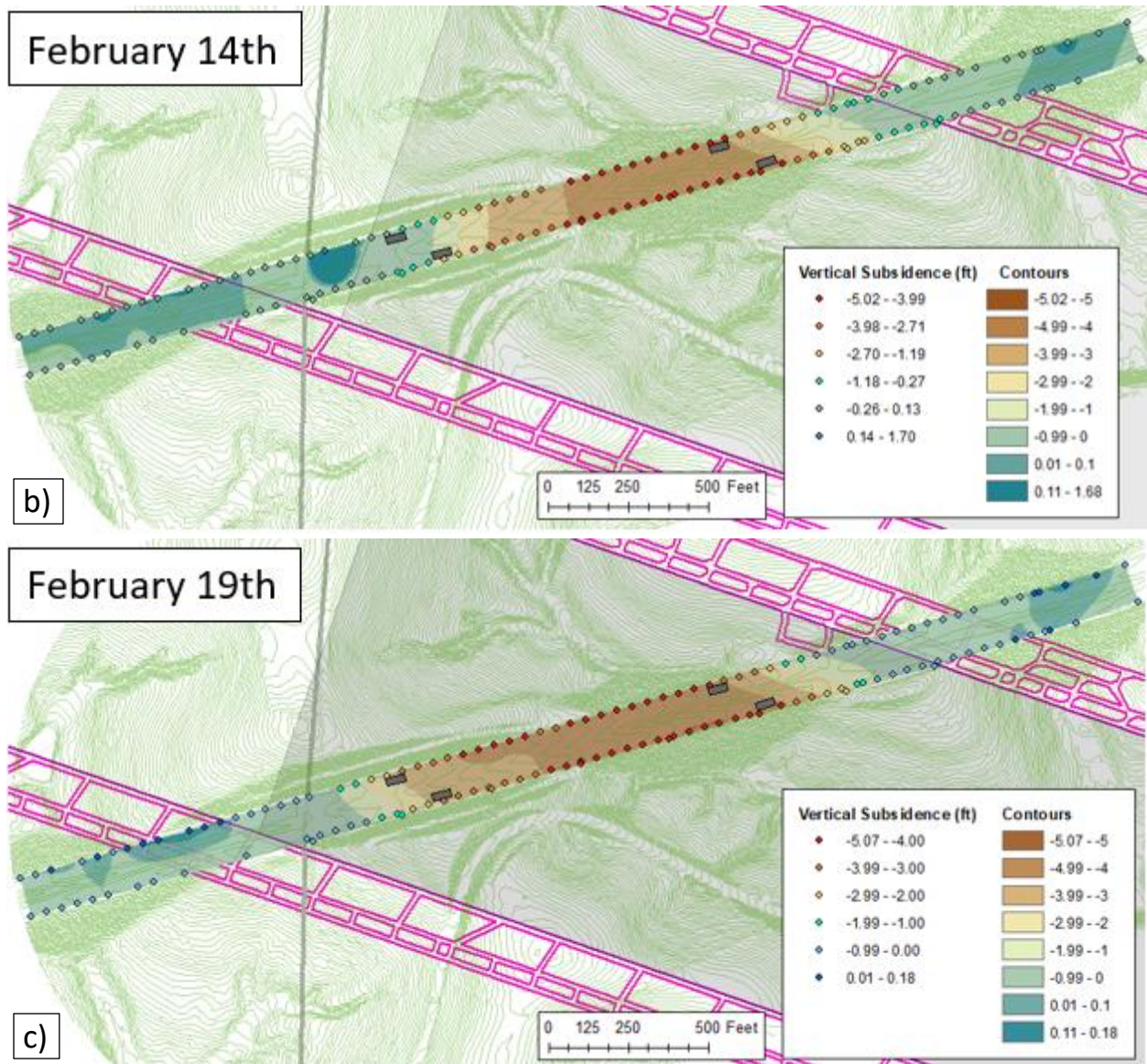


Figure IIIa.3 – Vertical subsidence as longwall face progresses

On 5 February, the longwall face was in the middle of the study area, below Embankment #1, as can be seen in Figure IIIa.3a. The data from the survey taken on this day shows the maximum vertical displacement occurring over the eastbound asphalt relief section, located about 315-ft behind the longwall face. At this point, the maximum displacement observed was just under 4-ft, meaning that it has not reached the maximum subsidence. Very little movement was observed beyond the longwall face.

Weather delays caused surveys to be suspended until 14 February, when the longwall face was just beyond the western asphalt relief section, as can be seen in Figure IIIa.3b. At this point in time a maximum subsidence of between 4-ft and 5-ft was observed above the entirety of the central embankment. As the central embankment is slightly east of the center of the panel, the

subsidence basin at this point in time is concentrated towards the eastern half of the panel. It can also be seen that the change in surface drop between the gate road and the maximum subsidence occurs in a shorter distance on the eastern side of the highway than the western, meaning the slope is steeper on the eastern half of the road.

The next survey was taken on 19 February, when the longwall face was at the end of the highway section, as can be seen in Figure IIIa.3c. The eastern side of the subsidence basin looks the same as it did during the previous observational period. However, the longwall face progression caused the area of 4 to 5-ft of subsidence to extend further beyond the central embankment. The maximum subsidence observed on this day was about 5.07-ft of vertical displacement and occurred in the center of Embankment #1 on the eastbound lanes. On the western side of the highway, the slope is closer to that on the eastern side, making the subsidence basin symmetrical throughout the panel.

2.0 Horizontal Movement

In the horizontal plane, survey points throughout the highway moved in both the north-south and east-west directions. Like in the vertical plane, the extent of horizontal movement of these points varied depending on their location in the longwall panel. The points on the eastern side of the highway experienced more horizontal movement than those on the western side. As can be seen in Figure IIIa.4 below, points were observed to move as much as 1.4-ft in the horizontal plane.

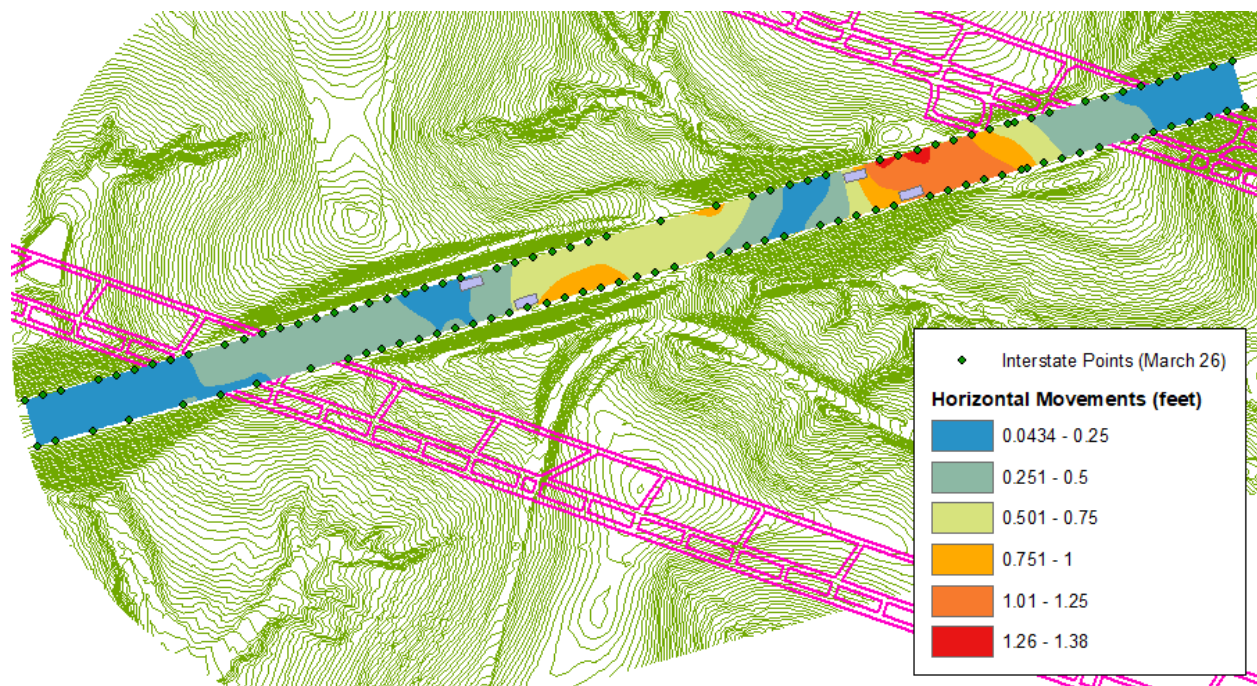


Figure IIIa.4 – Horizontal movement of highway surface due to subsidence after longwall mining

Figure IIIa.4 above does not account for the direction of the movement observed on the highway alignment. As the ground surrounding the highway is not flat, the presence of slopes can impact the impact of horizontal movement observed. As such, it is worth looking at the data directionally. Figure IIIa.5 shows the magnitude and direction of horizontal movement as the longwall face moved through the highway study area.

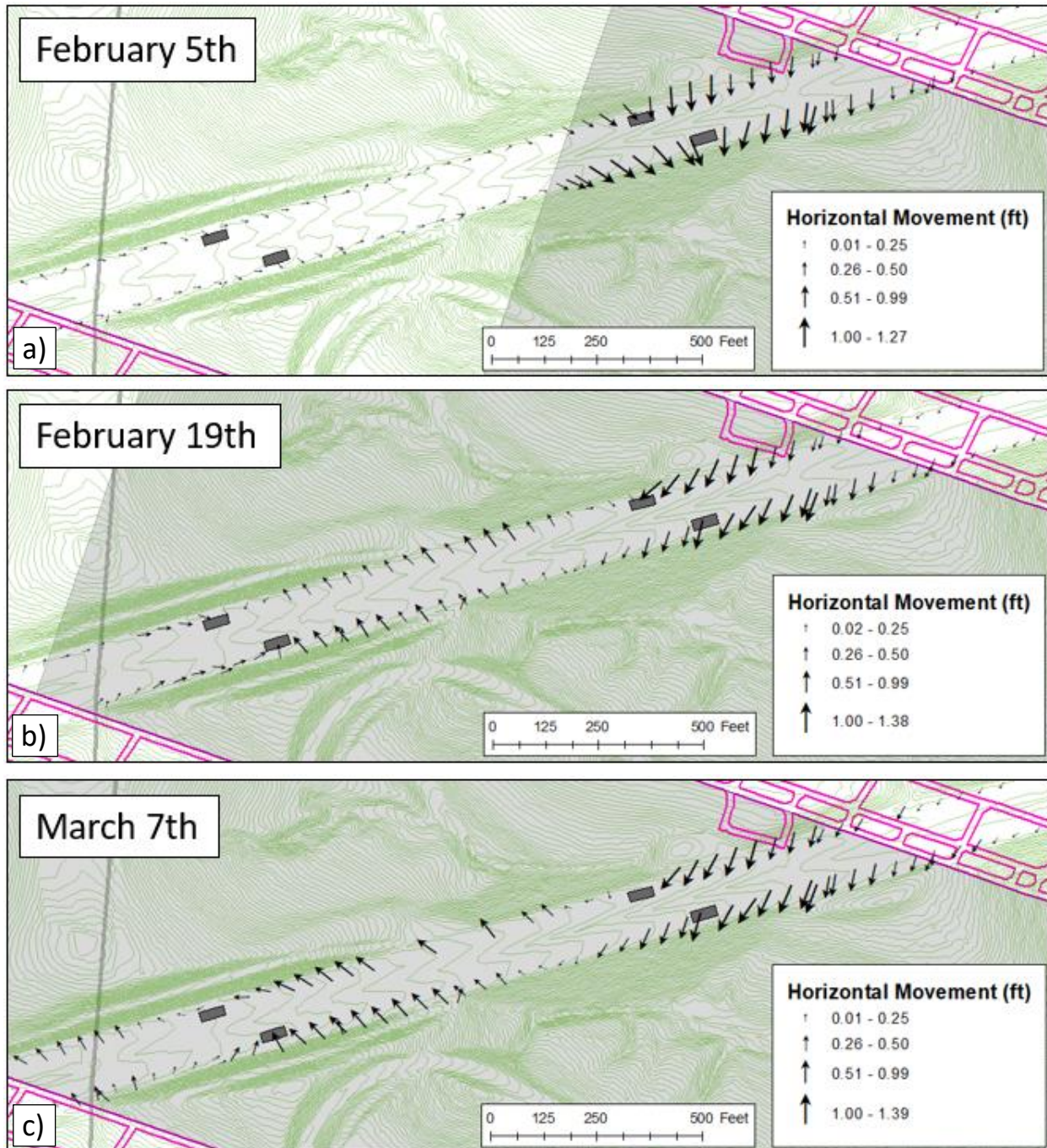


Figure IIIa.5 – Magnitude and direction of horizontal movement as longwall face progresses

On 5 February, the longwall face was in the middle of the study area, below Embankment #1, as can be seen in Figure IIIa.5a. The data from the survey taken on this day shows horizontal movements of up to 1.3-ft concentrating around the eastern asphalt relief sections just behind the longwall face and that the highway moved down the southern slope of the embankment. It also shows that there was little to no horizontal movement beyond the longwall face.

The next survey was taken on 19 February, when the longwall face was at the end of the highway section, as can be seen in Figure IIIa.5b. The movement observed at this moment in time show that there is significantly more movement on the eastern side of the highway than on the western side. Large movements up to 1.4-ft were observed pointing towards the center of the longwall basin leading up to the eastern asphalt relief sections. The asphalt relief sections dissipated the stress, which resulted in almost no movement being observed over the center embankment. On the western side of the embankment, the magnitude of horizontal movements was lower, primarily ranging between 0.5 and 1.0-ft, and movement tended to move towards the longwall face.

Another survey was performed on 7 March, when the longwall face was approximately 1,200-ft beyond the highway. The movement observed on the eastern side of the highway matches that which was observed on 19 February, with large movement pointing towards the center of the longwall basin. Once again, these movements dissipate at the first asphalt relief sections. However, with the longwall face so far away, much more movement is observed on the western side of the highway. In the section of highway adjacent to the cut slope leading up to the second set of asphalt relief sections, movements of 0.5 to 1.0-ft were observed pointing towards the longwall face. Once again, the asphalt relief sections dissipate the stress causing the western most side of the highway to experience little horizontal movement. This movement can be seen in Figure IIIa.5c.

Through a review of the surveys in the horizontal plane of the highway alignments, the horizontal movement of the highway can be characterized. The eastern side of the highway moved primarily in the south-west direction, while the western side of the highway moved primarily in the north-west direction. The movement of the west side of the highway is atypical. Normally, points on a surface will move more towards the center of the subsidence basin, which means that under normal circumstances the western side of the highway would move in the north-east direction. The observed movement appears more like the highway is twisting than it is sliding towards the center of the subsidence basin. The University hypothesizes that the difference in the direction of movement on the road is due to the structural construction of the interstate. Because the highway base is composed of concrete slabs 20-ft long that are tied together with dowels, the movement of one slab causes the movement of adjacent slabs.

Subsection IIIb – Embankment and Cut Slope Surveys

The University team analyzed the survey stake data provided by SPK Engineering. Of the 590 survey points, a sample of 160 survey points scattered throughout the study area have been considered to characterize the movement of the slopes throughout the panel. Movement was monitored both in the horizontal and vertical planes. These surveys are accurate to 0.03 to 0.04-ft. An overview of the study area can be seen below in Figure IIIb.1 and displays the survey stake group locations and longwall face positions on select days.

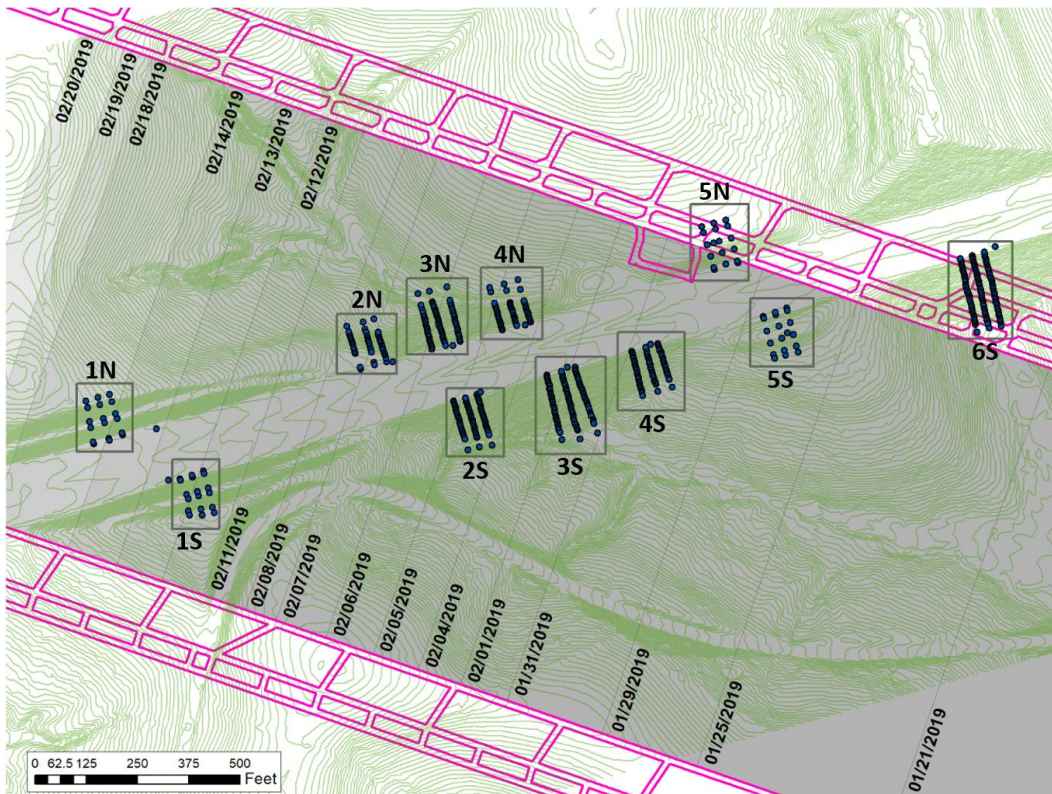


Figure IIIb.1 – Total extent of study area with face positions

1.0 Embankment #2 South

The second embankment is located on the eastern edge of the study area. The south side of the embankment is located above the gate road entries of panel 15. A total of 26 points were selected on Embankment #2 to be analyzed. These points can be seen below in Figure IIIb.2.

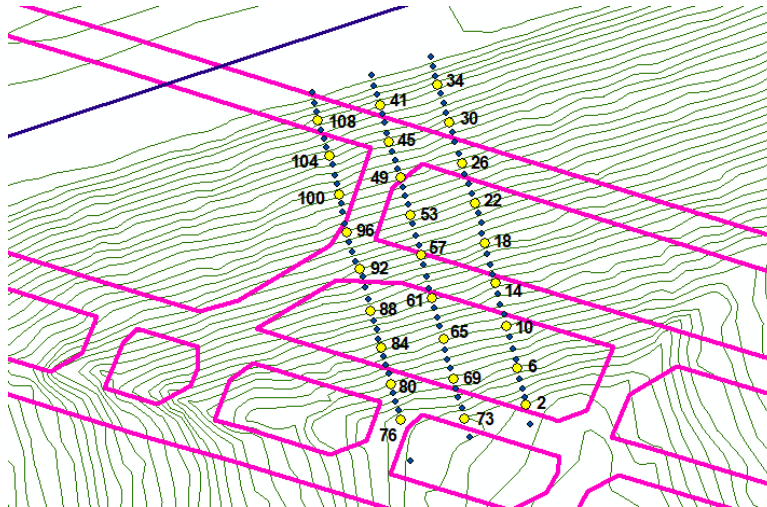


Figure IIIb.2 – Selected SPK survey points located on Embankment #2 survey group 6S

1.1 Vertical Movement

As Embankment #2 is located over the gate road entries, it experienced minimal amounts of vertical movement. The vertical movement in this area ranged from -0.06 to 0.22-ft. The majority of vertical movement in this area was heave rather than subsidence. Figure IIIb.3 below shows the vertical movement from a selection of points. The vertical movement from the remainder of points that have been analyzed can be seen in Appendix I. When this data was compared with the longwall face positions, it can be determined that the spike in vertical movement occurred when the longwall face was about 1000-ft passed the points on Embankment #2.

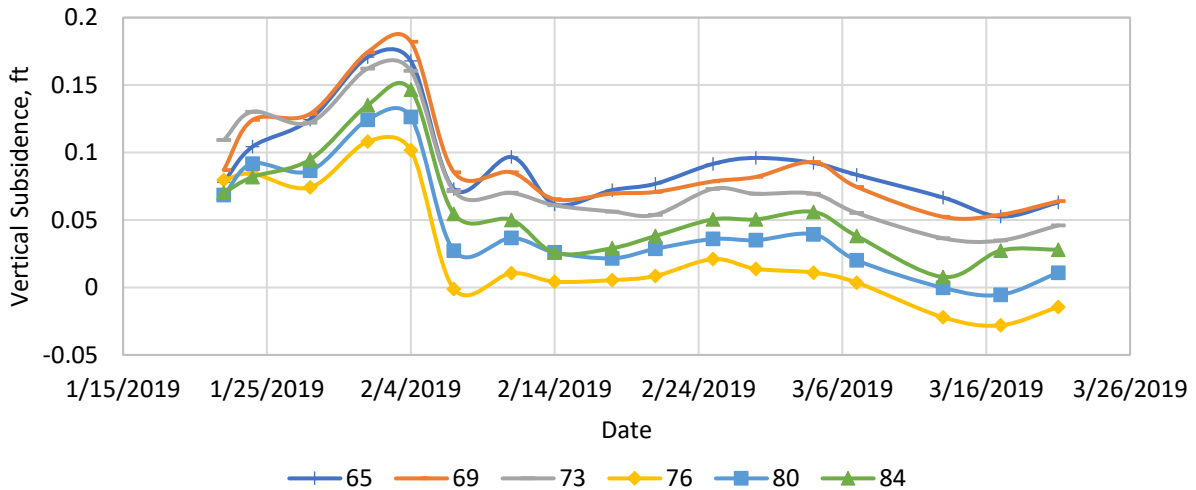


Figure IIIb.3 – Vertical subsidence of select points on Embankment #2 (Figure IIIb.2) within survey group 6S

1.2 Horizontal Movement

In the horizontal plane, survey points on Embankment #2 moved in both the north-south and east-west directions. In the east-west direction, the movement in this area ranged from -0.33 to 0.19-ft; in the north-south direction, the movement in this area ranged from -0.53 to 0.02-ft. Most of these points moved in the south and west directions, meaning that the points along these embankments moved toward the center of the basin. However, the movement of these points fluctuated in both the north-south and east-west directions. Figures IIIb.4 and IIIb.5 below show the horizontal movement from a selection of points on Embankment #2. The horizontal movement from the remainder of points that have been analyzed can be seen in Appendix I.

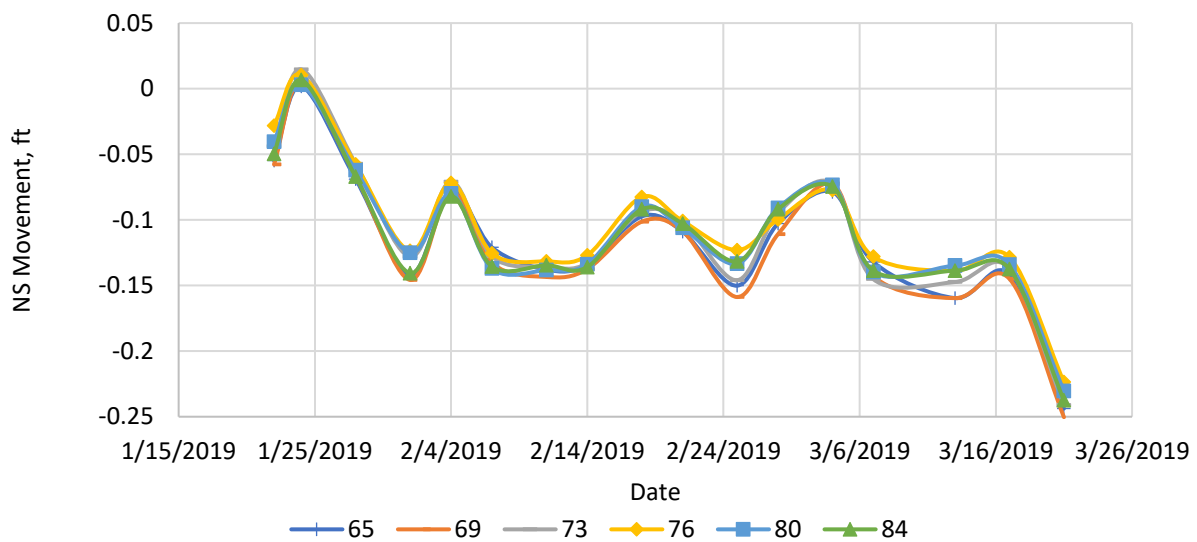


Figure IIIb.4 – Horizontal movement in the north-south direction of select points on Embankment #2 survey group 6S

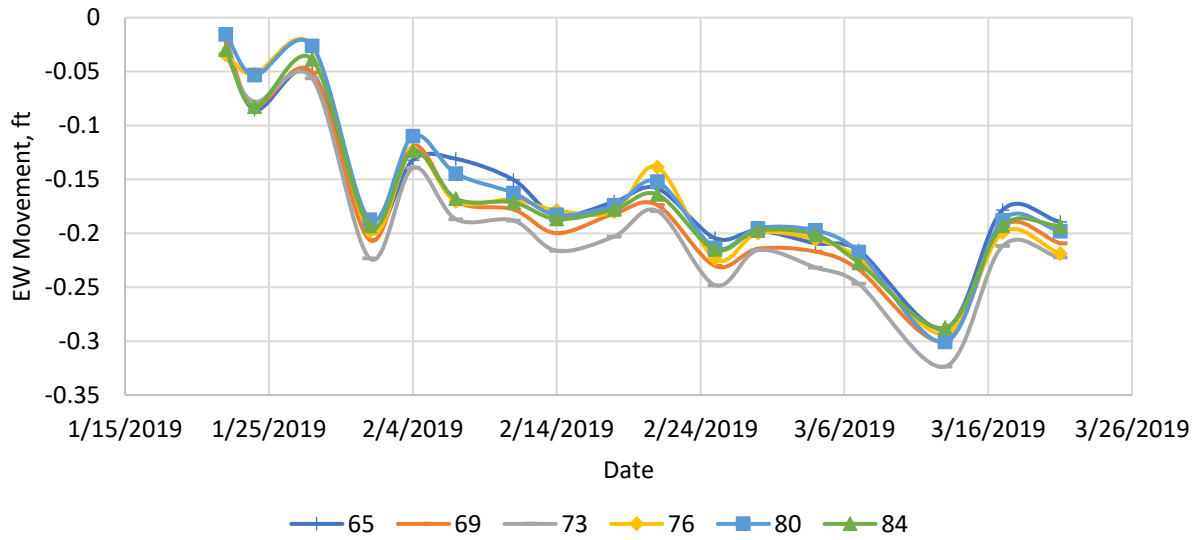


Figure IIIb.5 – Horizontal movement in the east-west direction of select points on Embankment #2 survey group 6S

2.0 Eastern Cut Slope

2.1 North (5N)

The 5N group of survey stakes is located on the eastern side of the study area and north of the interstate. These survey stakes are located primarily over the gate road entries. A total of six points were selected on this cut slope to be analyzed. These points can be seen below in Figure IIIb.6.

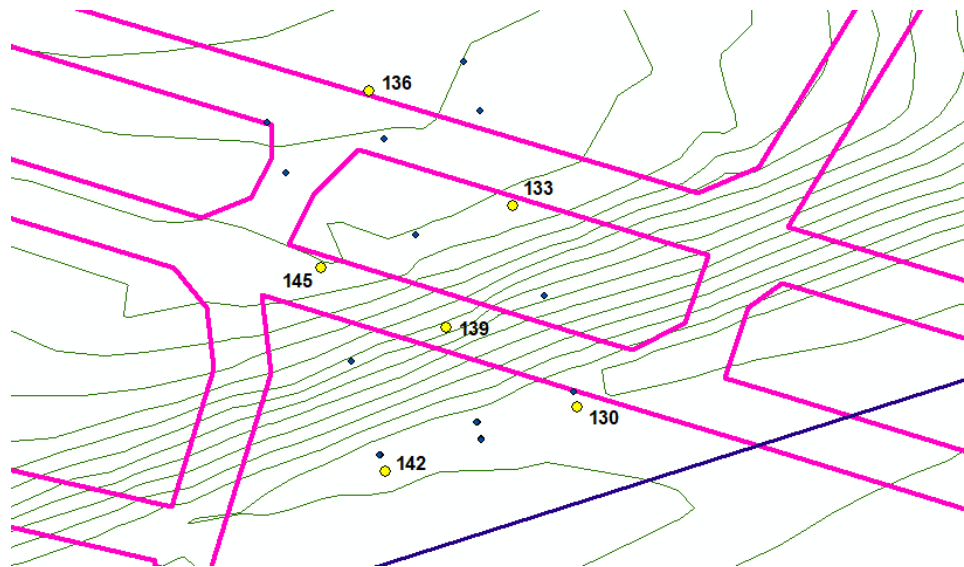


Figure IIIb.6 – Selected SPK survey points located on north eastern cut slope survey group 5N

2.1.1 Vertical Movement

As the north eastern cut slope is located between the gate road entries and the inflection line, it experienced varied amounts of vertical movement. The vertical movement in this area ranged from -0.98 to 0.05-ft. Most of the vertical movement in this area was subsidence, but many points experienced heave before subsiding. Figure IIIb.7 below shows the vertical movement from a selection of points. This data was compared with the face positions and it was determined that the initial surface heave occurred when the face was approaching the points and maximum subsidence is reached when the face was approximately 500-ft passed the point. As seen in this figure, the vertical subsidence on this slope fluctuates just as it does on Embankment #2. This trend of fluctuation indicates that subsidence is irregular over the gate road entries.

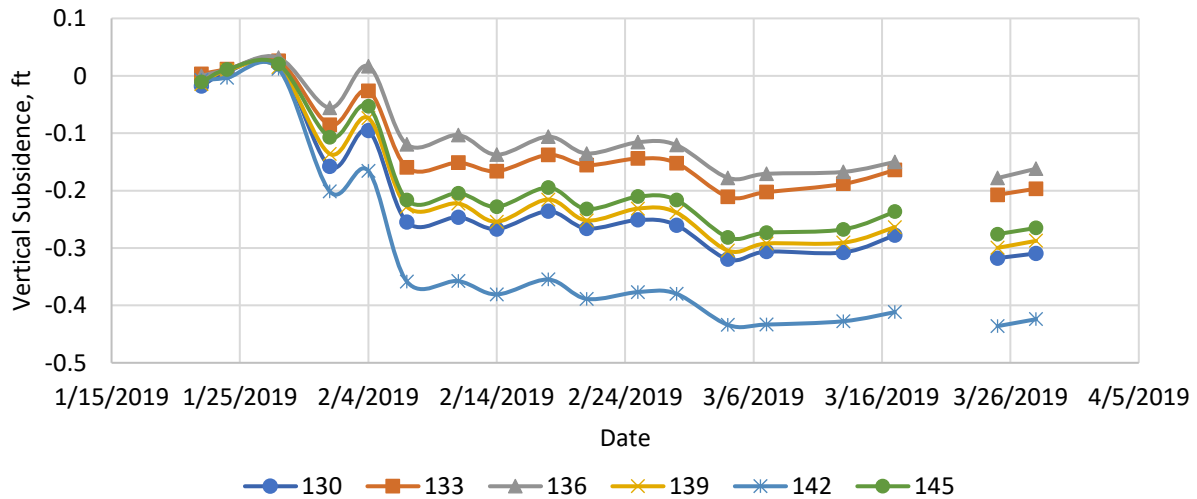


Figure IIIb.7 – Vertical subsidence of select points on north eastern cut slope survey group 5N

2.1.2 Horizontal Movement

In the horizontal plane, survey points on the eastern cut slope north moved in both the north-south and east-west directions. Most of these points moved primarily in the south and west directions, meaning that these points move toward the center of the basin. In the north-south direction, the movement in this area ranged from -0.54 to 0.04-ft. As can be seen in Figure IIIb.8, the points moved gradually south, then north, before settling in their new southern locations. In the east-west direction, the movement in this area ranged -0.21 to 0.13-ft. As can be seen in Figure IIIb.9, the points fluctuated from east to west movement in small increments.

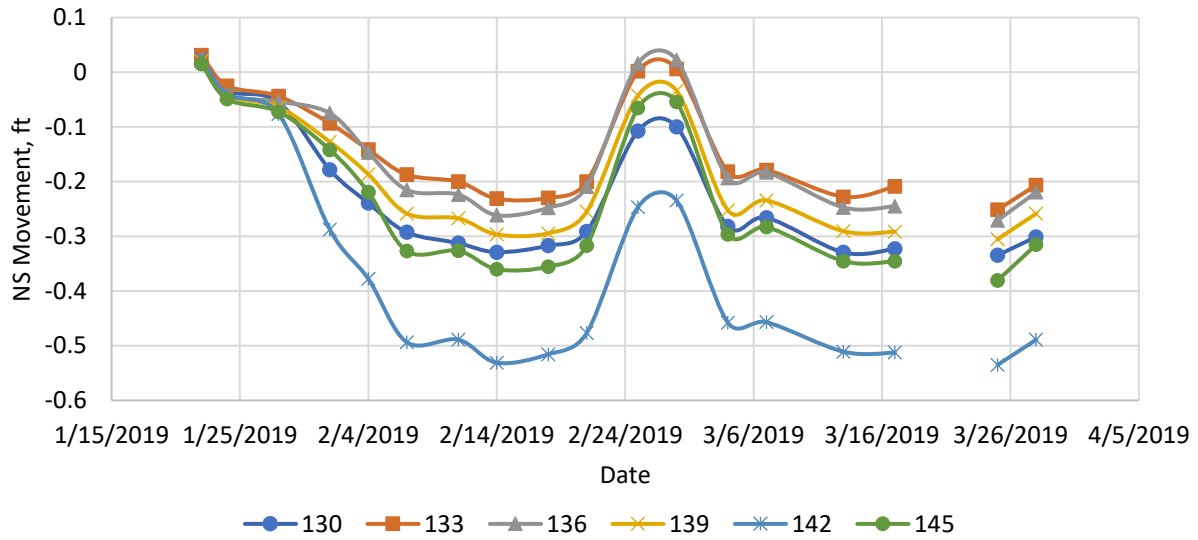


Figure IIIb.8 – Horizontal movement in the north-south direction of select points on north eastern cut slope survey group 5N

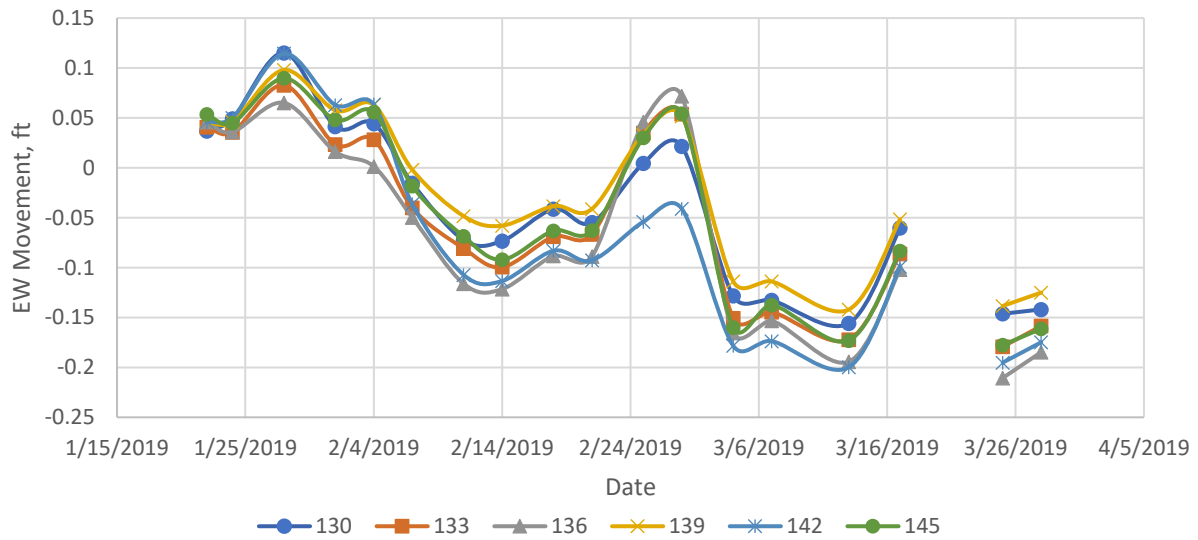


Figure IIIb.9 – Horizontal movement in the east-west direction of select points on north eastern cut slope survey group 5N

2.2 South (5S)

The 5S group of survey stakes is located on the eastern side of the study area and south of the interstate. These survey stakes are located primarily between the gate road entries and the inflection line of the subsidence basin. A total of six points were selected on this cut slope to be analyzed. These points can be seen below in Figure IIIb.10.

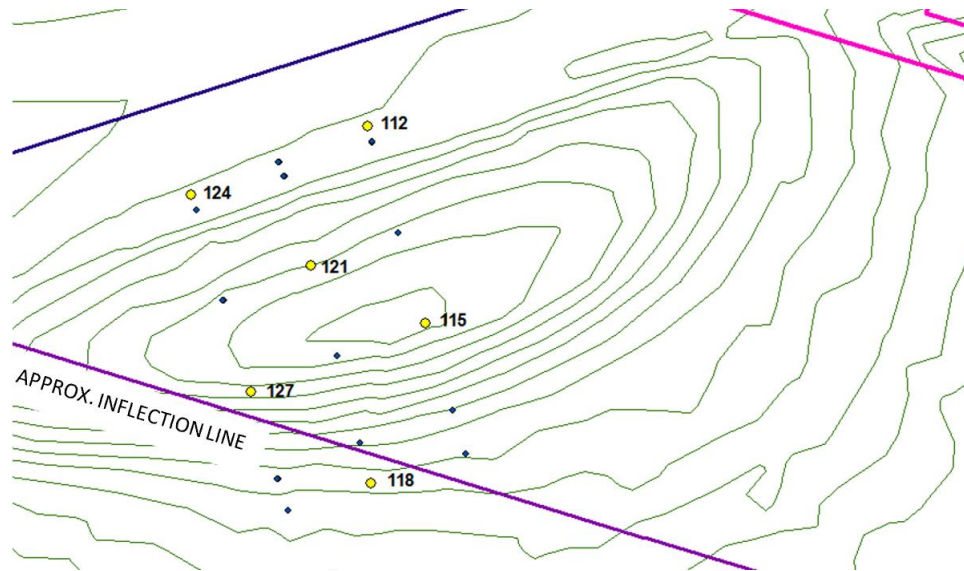


Figure IIIb.10 – Selected SPK survey points located on south eastern cut slope survey group 5S

2.2.1 Vertical Movement

As the south eastern cut slope is located between the gate road entries and the inflection line, it experienced varied amounts of vertical movement. The vertical movement in this area ranged from -2.79 to 0.005-ft. Most of the vertical movement in this area was subsidence, but many points experienced heave before subsiding. Figure IIIb.11 below shows the vertical movement from a selection of points. This data was compared with the face positions and it was determined that a small amount of initial surface heave occurred when the face was approaching the points and maximum subsidence is reached on 7 February when the face was approximately 900-ft passed the point.

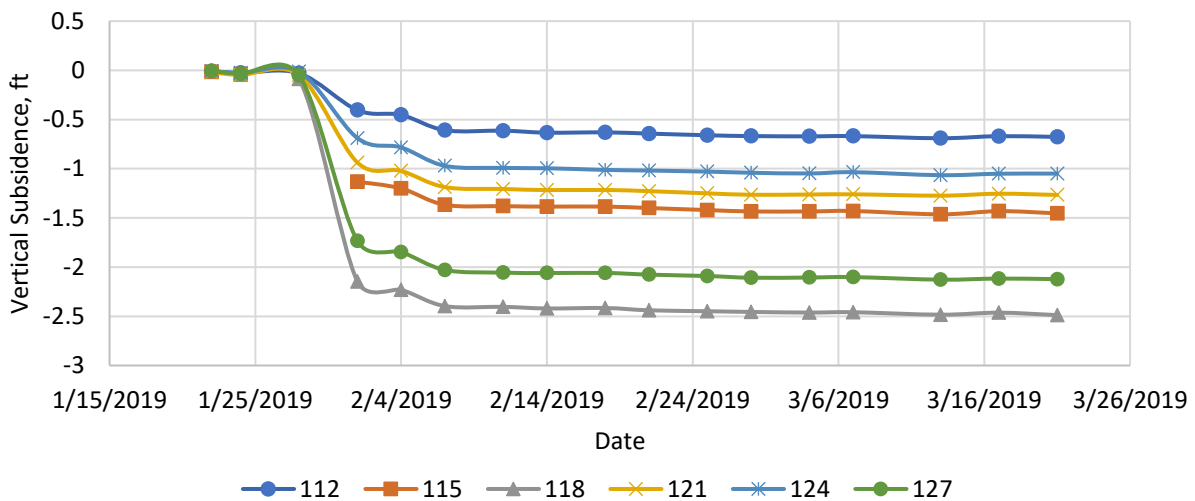


Figure IIIb.11 – Vertical subsidence of select points on south eastern cut slope survey group 5S

2.2.2 Horizontal Movement

In the horizontal plane, survey points on the eastern cut slope south moved in both the north-south and east-west directions. Most of these points moved primarily in the south and west directions, meaning that these points move toward the center of the basin. In the north-south direction, the movement in this area ranged from -1.605 to 0.005-ft. As can be seen in Figure IIIb.12, the points moved south rapidly when the longwall face is about 450-ft passed the points and then remain in that location. In the east-west direction, the movement in this area ranged -0.62 to 0.12-ft. As can be seen in Figure IIIb.13, the points moved east first as the longwall face passes and then settled west in the direction of the longwall face progression.

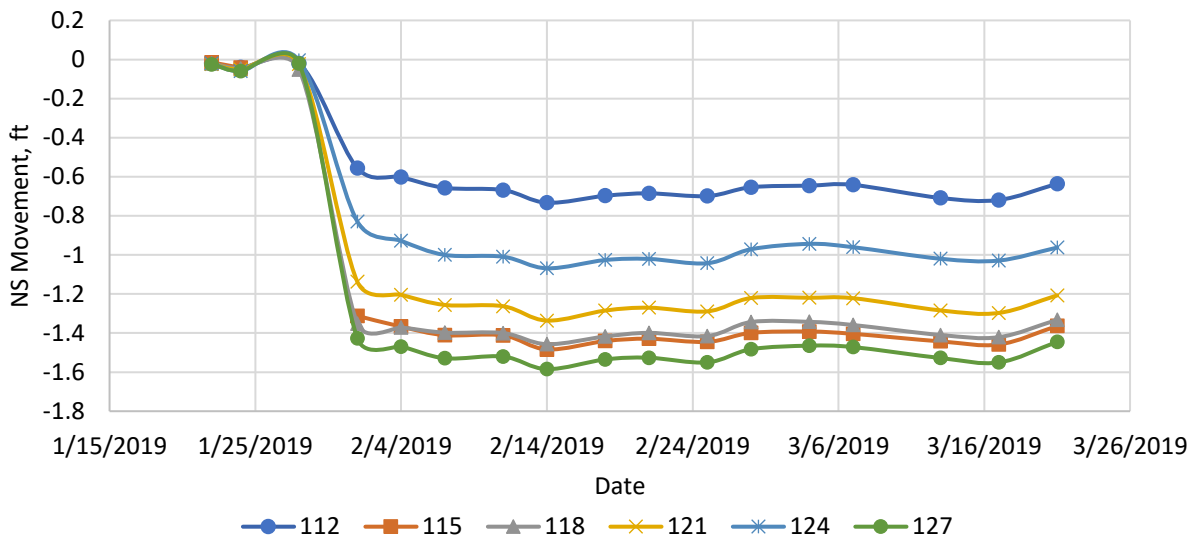


Figure IIIb.12 – Horizontal movement in the north-south direction of select points on south eastern cut slope survey group 5S

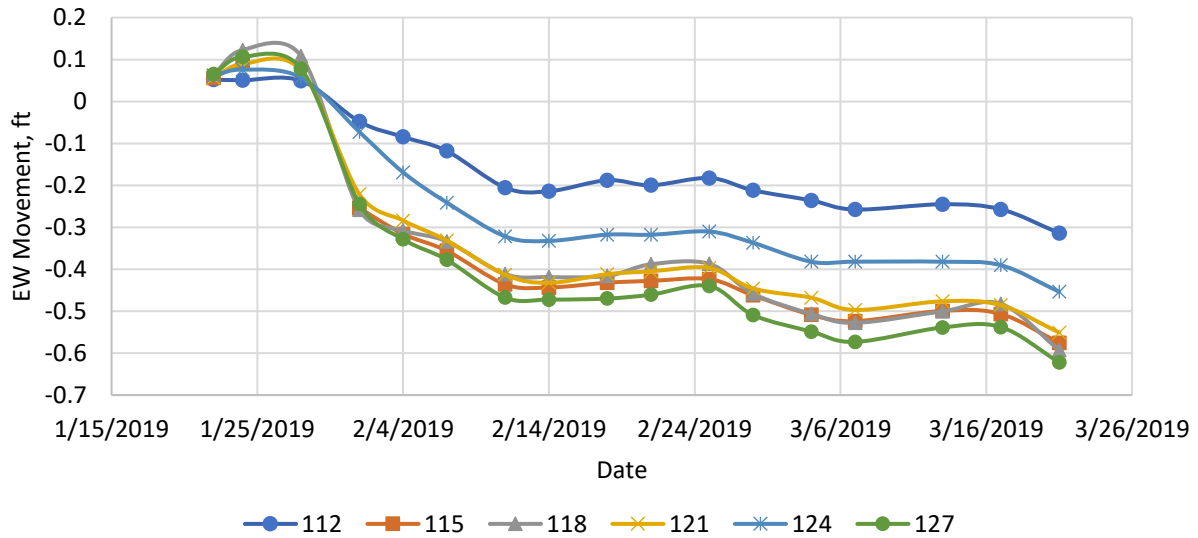


Figure IIIb.13 – Horizontal movement in the east-west direction of select points on south eastern cut slope survey group 5S

3.0 Embankment #1 North

The survey stakes located on the northern side of Embankment #1 were divided into three groups: 2N, 3N, and 4N. Though separate groups, they behaved similarly, so the groups were considered as a single entity. These survey stakes are located in the center of the longwall panel, primarily in the area of maximum subsidence, as seen in Figure IIIb.14. A total of 49 points were selected on this side of the embankment to be analyzed, as can be seen in Figure IIIb.14.

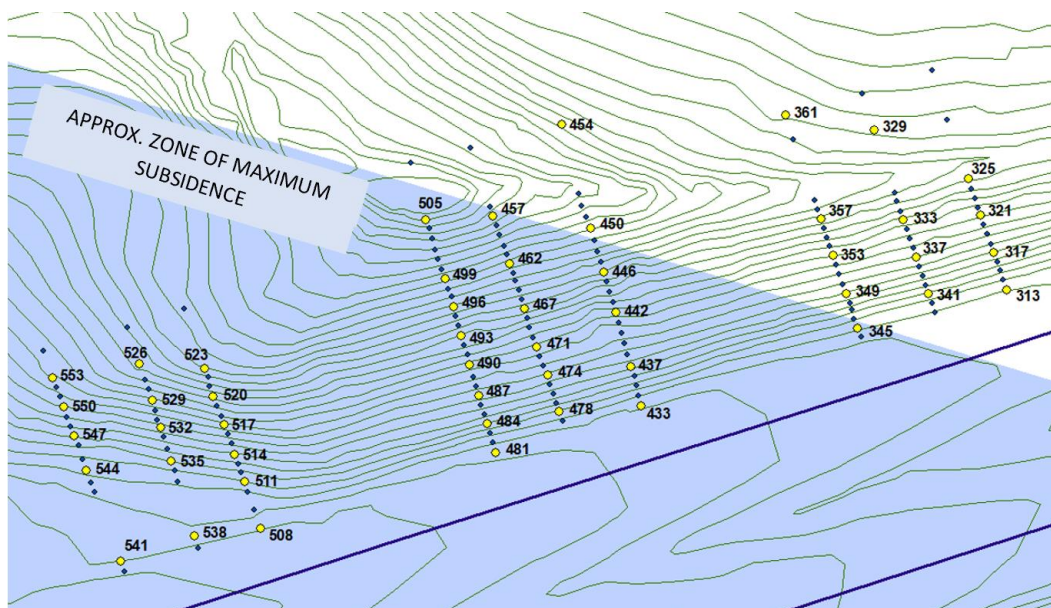


Figure IIIb.14 – Selected SPK survey points located on Embankment #1 north (2N, 3N, and 4N)

3.1 Vertical Movement

Though the northern side of Embankment #1 is located in the center of the panel, it is not entirely in the zone of maximum subsidence, meaning it experienced small variations in amount of vertical movement between points. The vertical movement in this area ranged from -4.91 to 0.44-ft. Most of the vertical movement in this area was subsidence, but many points experienced heave before subsiding. Figure IIIb.15 below shows the vertical movement from a selection of points. This data was compared with the face positions and it was determined that a small amount of initial surface heave occurred when the face was approaching the points and maximum subsidence is reached on 14 February when the face was approximately 700-ft passed the point. The vertical movement from the remainder of points that have been analyzed can be seen in Appendix I. It is worth noting that stakes at the top of the embankment experienced more subsidence than points at the bottom of the embankment. This differential movement is likely due to factors other than subsidence, such as consolidation or spreading of the embankment.

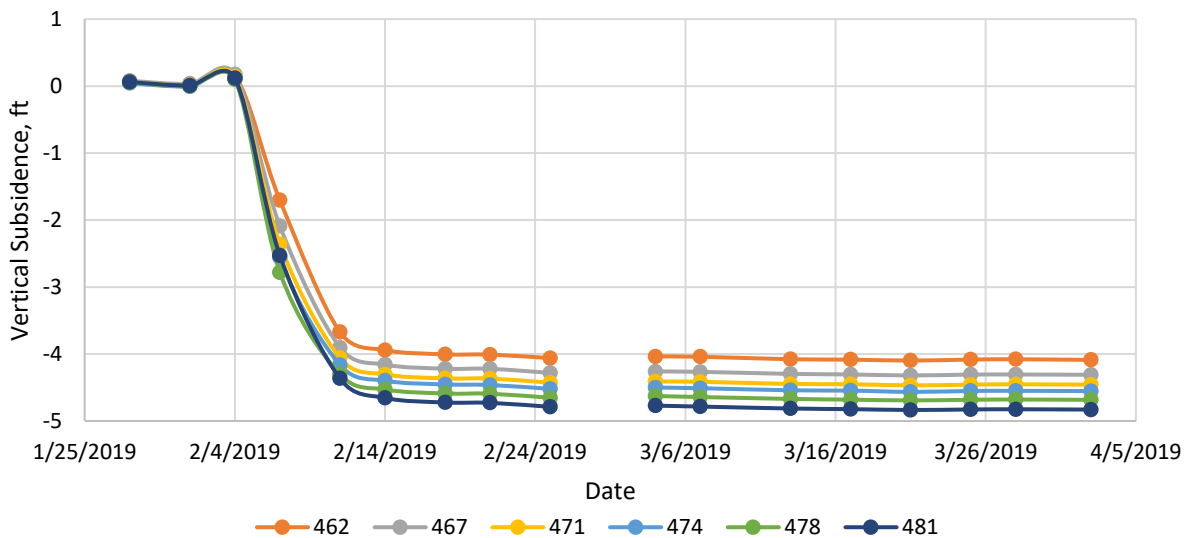


Figure IIIb.15 – Vertical subsidence of select points on north Embankment #1 survey group 3N

3.2 Horizontal Movement

In the horizontal plane, survey points on the northern side of Embankment #1 moved in both the north-south and east-west directions. Movement in the horizontal plane differed between groups, likely due to the points' proximity to the zone of maximum subsidence. In the north-south direction, the movement on this side of the embankment ranged from -0.75 to 2.56-ft. In group 4N, the points tended to move south at smaller magnitudes, beginning as the longwall face approached, as can be seen in Figure IIIb.16. In groups 2N and 3N, the points tended to move north at much large magnitudes, reaching maximum movement when the longwall face was about 900-ft from the points, as can be seen in Figure IIIb.17.

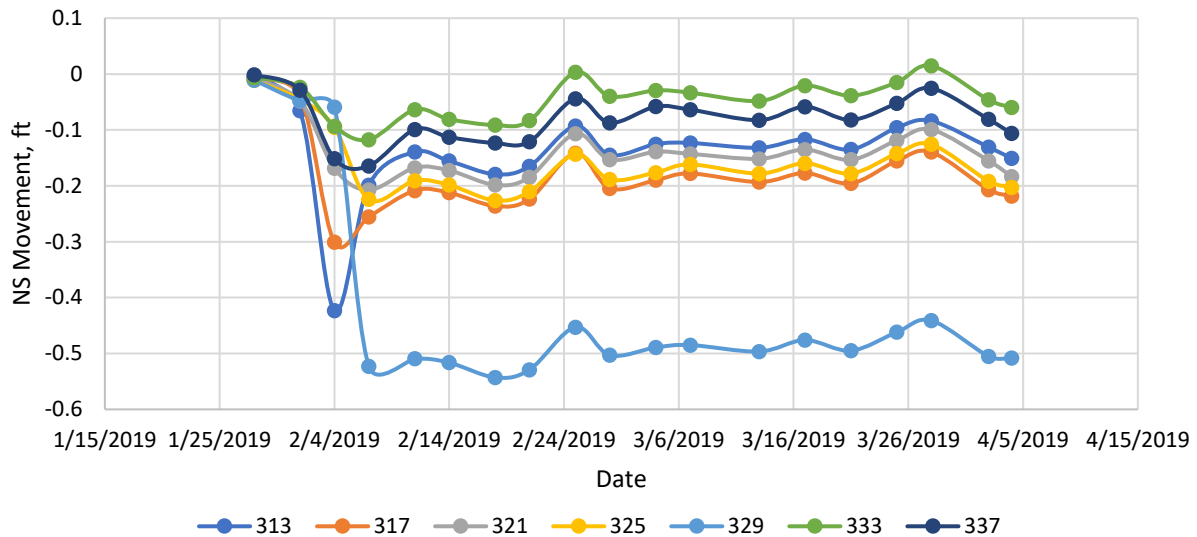


Figure IIIb.16 – Horizontal movement in the north-south direction of select points on north Embankment #1 survey group 4N

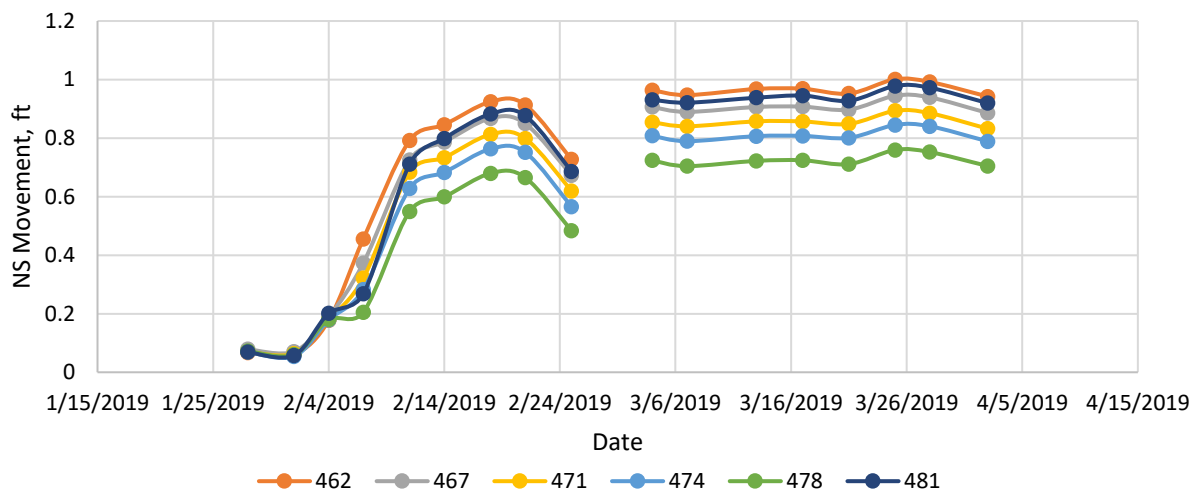


Figure IIIb.17 – Horizontal movement in the north-south direction of select points on north Embankment #1 survey groups 2N and 3N

In the east-west direction, the movement on this side of the embankment ranged from -0.71 to 1.52-ft. The movement for all of the points on this side of the embankment follows similar trends, in which there was a spike in movement east as the wall approached and passed the point. In groups 3N and 4N, after the spike in movement east, the points then move west passed their initial locations, as shown in Figure IIIb.18. This movement means that the points are first moving into the gob (area of panel that have already been mined) and then move in the direction of the longwall face to settle. Contrarily, in group 2N, the movement after the initial spikes

moved west in small increments and remained east of their initial locations, as seen in Figure IIIb.19 below. The data for the remainder of the points analyzed can be found in Appendix I.

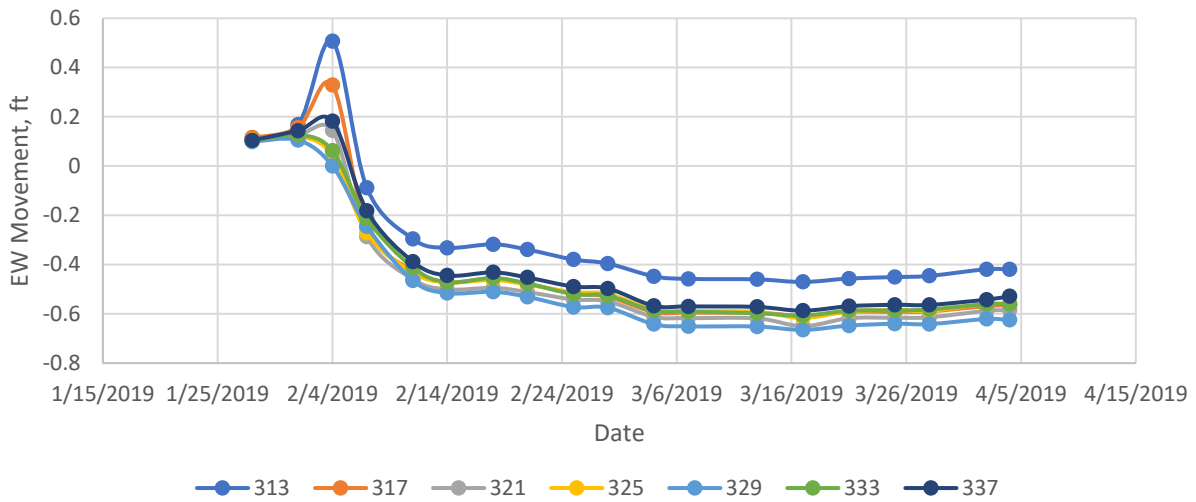


Figure IIIb.18 – Horizontal movement in the east-west direction of select points on north Embankment #1 survey groups 3N and 4N

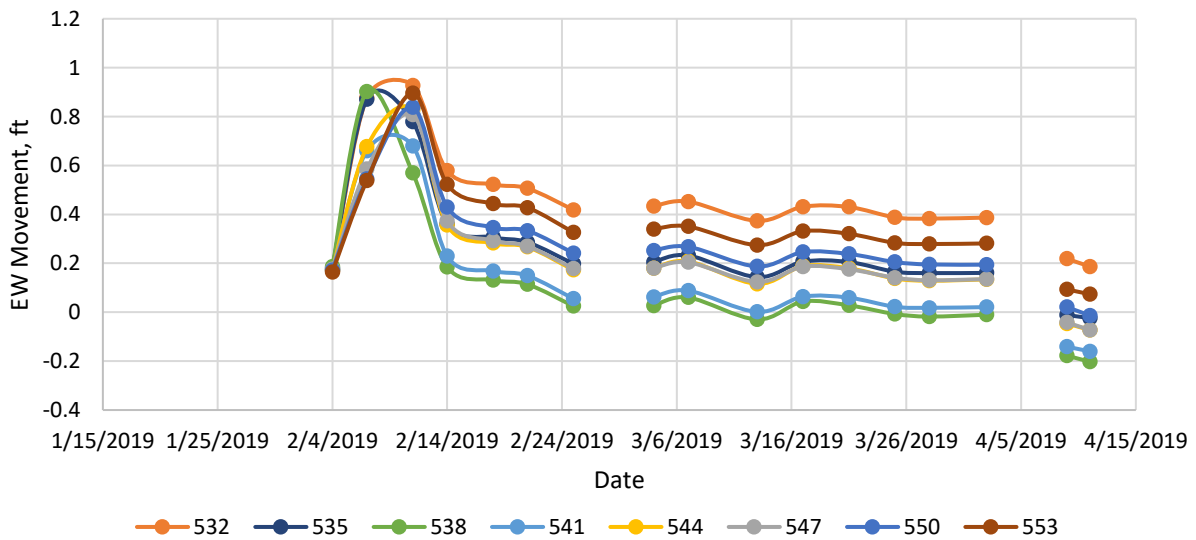


Figure IIIb.19 – Horizontal movement in the east-west direction of select points on north Embankment #1 survey group 2N

4.0 Embankment #1 South

The survey stakes located on the southern side of Embankment #1 were divided into three groups: 2S, 3S, and 4S. Though they are separate groups, they behaved similarly, so were considered as a single entity. These survey stakes are located in the center of the longwall panel,

primarily in the area of maximum subsidence, as seen in Figure IIIb.20. A total of 60 points were selected on this side of the embankment to be analyzed, as can be seen in Figure IIIb.20.

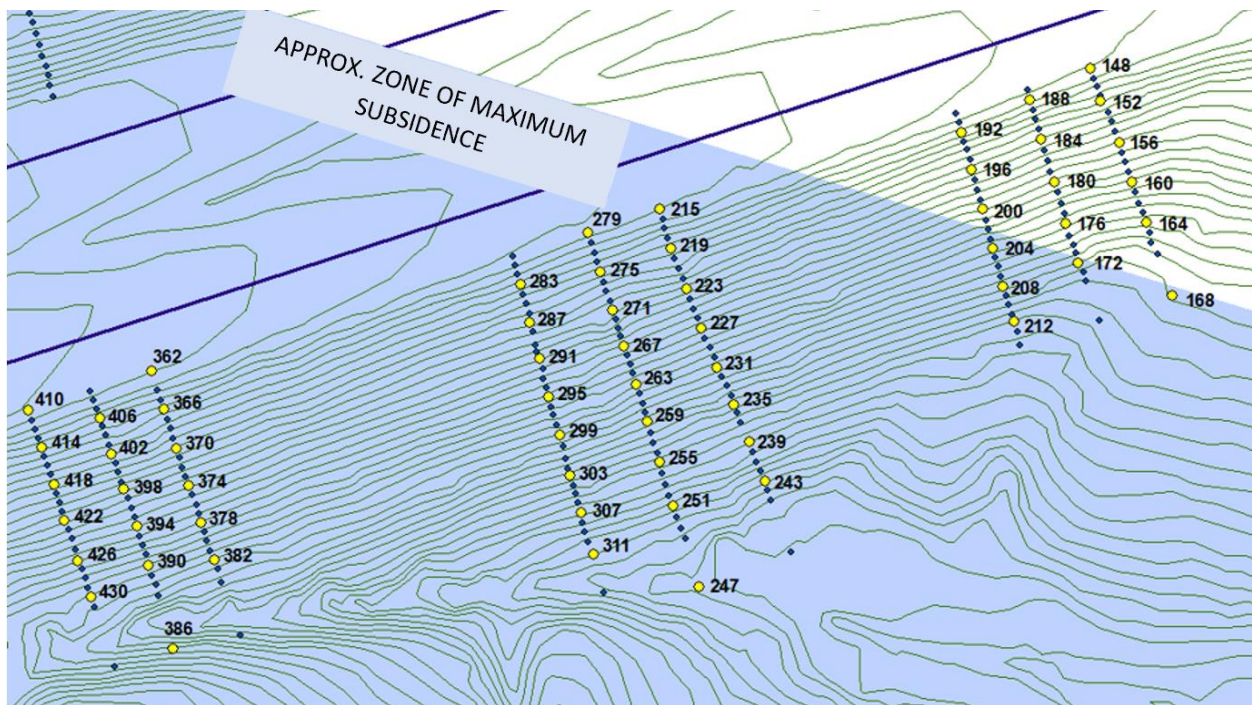


Figure IIIb.20 – Selected SPK survey points located on south Embankment #1 survey groups 2S, 3S, and 4S

4.1 Vertical Movement

As the southern side of Embankment #1 is in the center of the panel but not entirely in the zone of maximum subsidence, it experienced small variations in amount of vertical movement between points. The vertical movement in this area ranged from -5.13 to 0.074-ft. Most of the vertical movement in this area was subsidence, but many points experienced small amounts of heave before subsiding. Figure IIIb.21 below shows the vertical movement from a selection of points. This data was compared with the face positions and it was determined that a small amount of initial surface heave occurred when the face was approaching the points and maximum subsidence is reached on 11 February when the face was approximately 700-ft passed the point. The vertical movement from the remainder of points that have been analyzed can be seen in Appendix I. It is worth noting that stakes at the top of the embankment experienced more subsidence than points at the bottom of the embankment. This differential movement is likely due to factors other than subsidence, such as consolidation or spreading of the embankment.

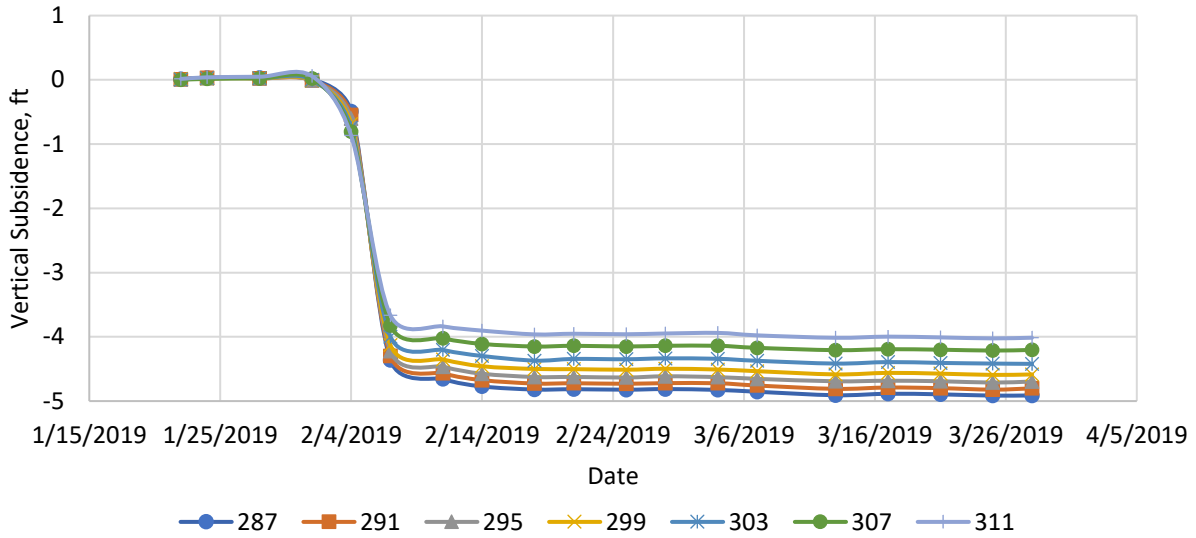


Figure IIIb.21 – Vertical subsidence of select points on south Embankment #1 survey group 3S

4.2 Horizontal Movement

In the horizontal plane, survey points on the northern side of Embankment #1 moved in both the north-south and east-west directions. Movement in the horizontal plane differs between groups, likely due to the points’ proximity to the zone of maximum subsidence. In the north-south direction, the movement on this side of the embankment ranged from -1.13 to 0.59-ft. In groups 3S and 4S, the points tended to move north first as the wall passed beneath the points and then south at larger magnitudes, as can be seen in Figure IIIb.22. In group 2S, the points tended to move at smaller magnitudes, moving south first and then north, as can be seen in Figure IIIb.23.

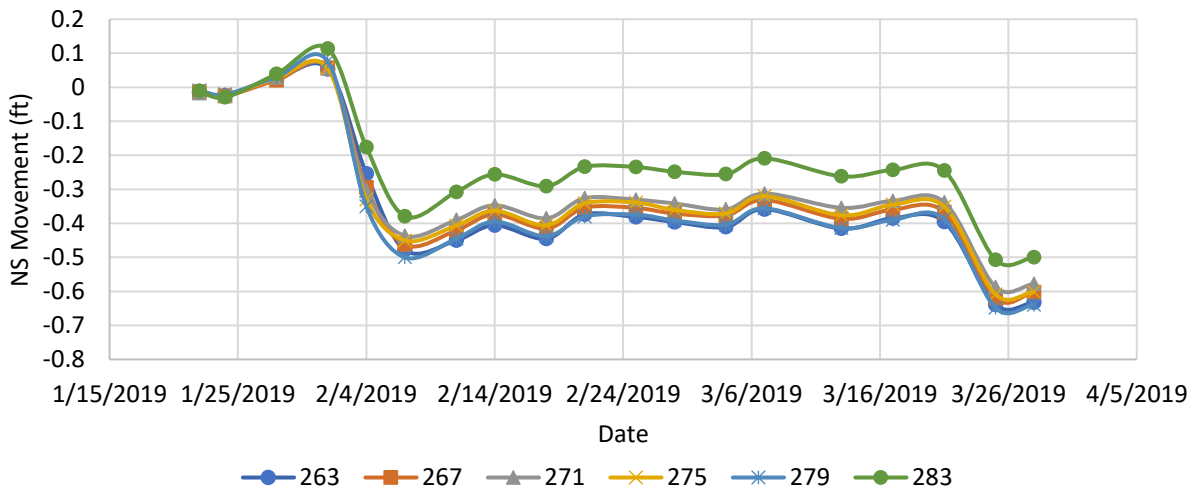


Figure IIIb.22 – Horizontal movement in the north-south direction of select points on south Embankment #1 survey groups 3S and 4S

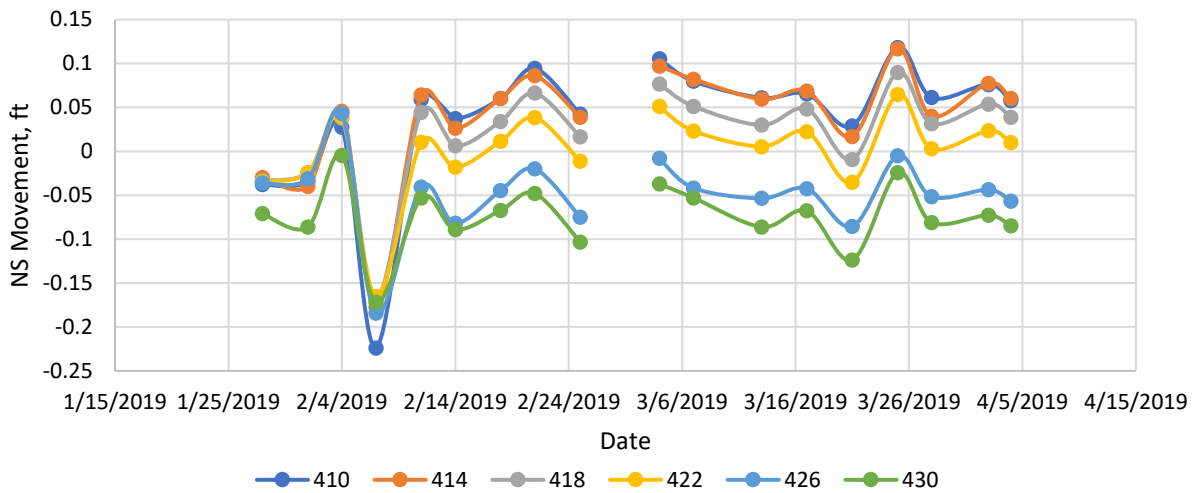


Figure IIIb.23 – Horizontal movement in the north-south direction of select points on south Embankment #1 survey group 2S

In the east-west direction, the movement on this side of the embankment ranged from -0.79 to 0.83-ft. The movement for the points on this side of the embankment followed similar trends, in which there was a spike in movement east as the wall passes the point. In group 4S, after the spike in movement east, the points then moved west, passed their initial locations, as shown in Figure IIIb.24. This movement means that the points are first moved into the gob (area of panel that have already been mined) and then moved in the direction of the longwall face to settle. Contrarily, in groups 2S and 3S, the movement after the initial spikes moved west in small increments and remained slightly east of their initial locations, as seen in Figure IIIb.25 below. The data for the remainder of the points analyzed can be found in Appendix I.

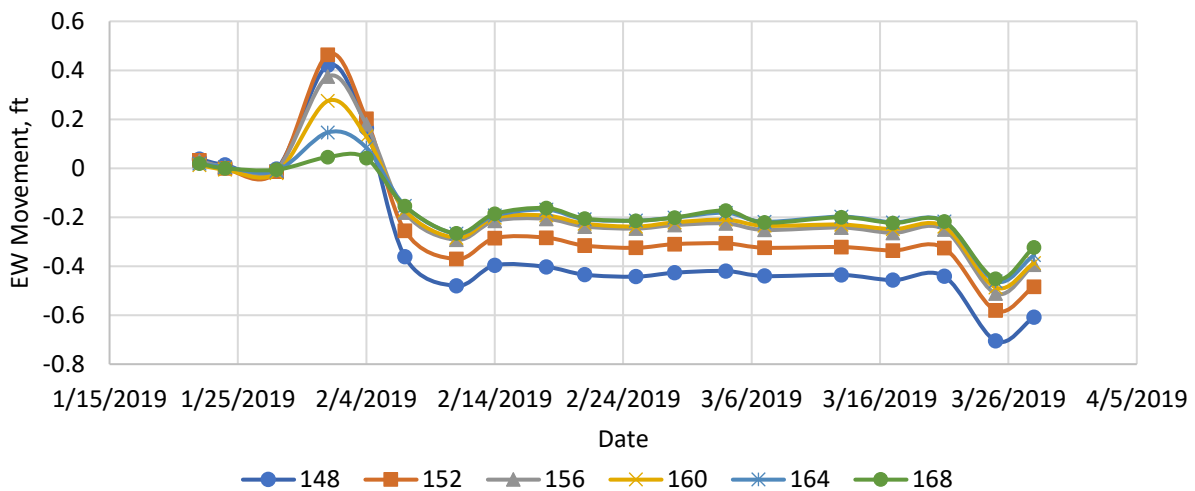


Figure IIIb.24 – Horizontal movement in the east-west direction of select points on south Embankment #1 survey group 4S

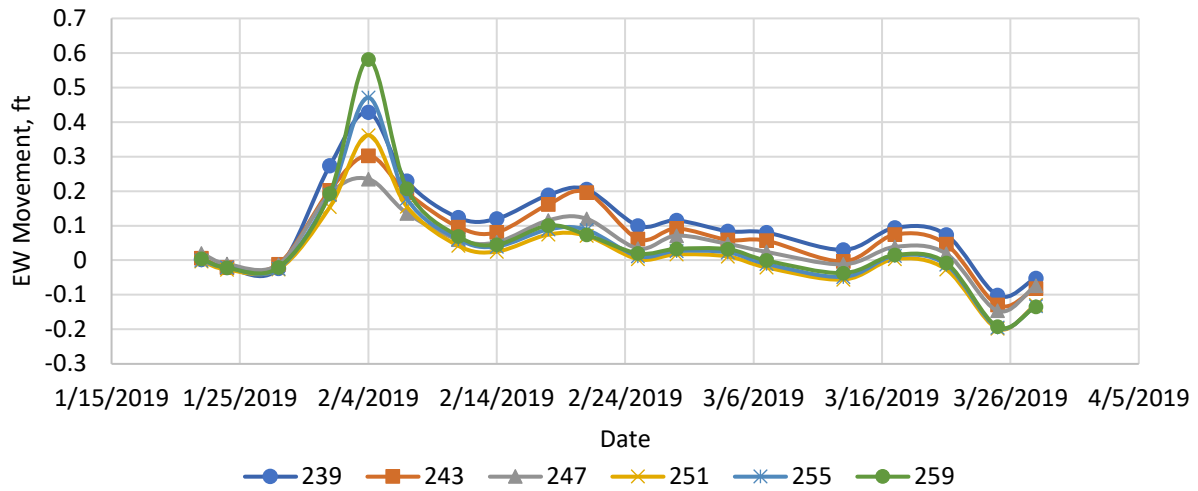


Figure IIIb.25 – Horizontal movement in the east-west direction of select points on south Embankment #1 survey groups 2S and 3S

5.0 Western Cut Slope

5.1 North (1N)

The 1N group of survey stakes is located on the western side of the study area and north of the interstate. These survey stakes in the center of the subsidence basin. A total of six points were selected on this cut slope to be analyzed. These points can be seen below in Figure IIIb.26.

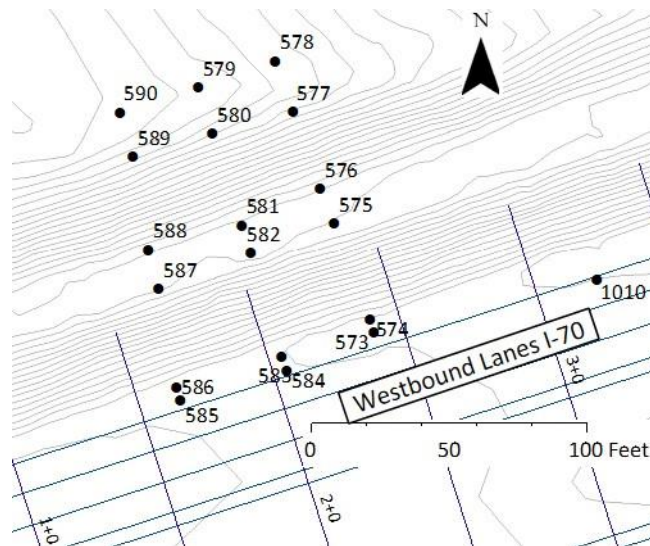


Figure IIIb.26 – Selected SPK survey points located on north western cut slope survey group 1N

5.1.1 Vertical Movement

The northern eastern cut slope is located near the center of the basin but is not entirely in the zone of maximum subsidence, so it experienced varied amounts of vertical movement. The vertical movement in this area ranged from -4.43 to 0.17-ft. Most of the vertical movement in this area was subsidence, but many points experienced small amounts of heave before subsiding. Figure IIIb.27 below shows the vertical movement from a selection of points. This data was compared with the face positions and it was determined that a small amount of initial surface heave occurred when the face was approaching the points and maximum subsidence is reached on 25 February when the face was approximately 700-ft passed the point.

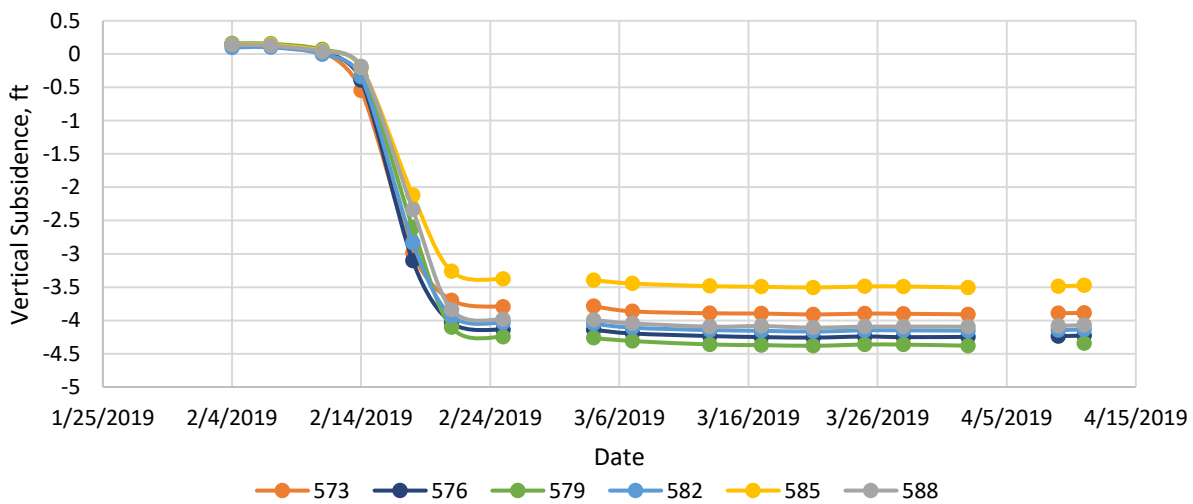


Figure IIIb.27 – Vertical subsidence of select points on north western cut slope survey group 1N

5.1.2 Horizontal Movement

In the horizontal plane, survey points on the eastern cut slope north moved in both the north-south and east-west directions. Most of these points moved primarily in the south and east directions, meaning that these points move toward the center of the basin. In the north-south direction, the movement in this area ranged from -0.27 to 0.35-ft. As can be seen in Figure IIIb.28, the points do not all follow a trend but many of them move south and then north, at small magnitudes. In the east-west direction, the movement in this area ranged -0.50 to 1.42-ft. As can be seen in Figure IIIb.29, the points spiked east first when the longwall face is about 175-ft from the slope and then moved west in smaller increments, ending east of their original location.

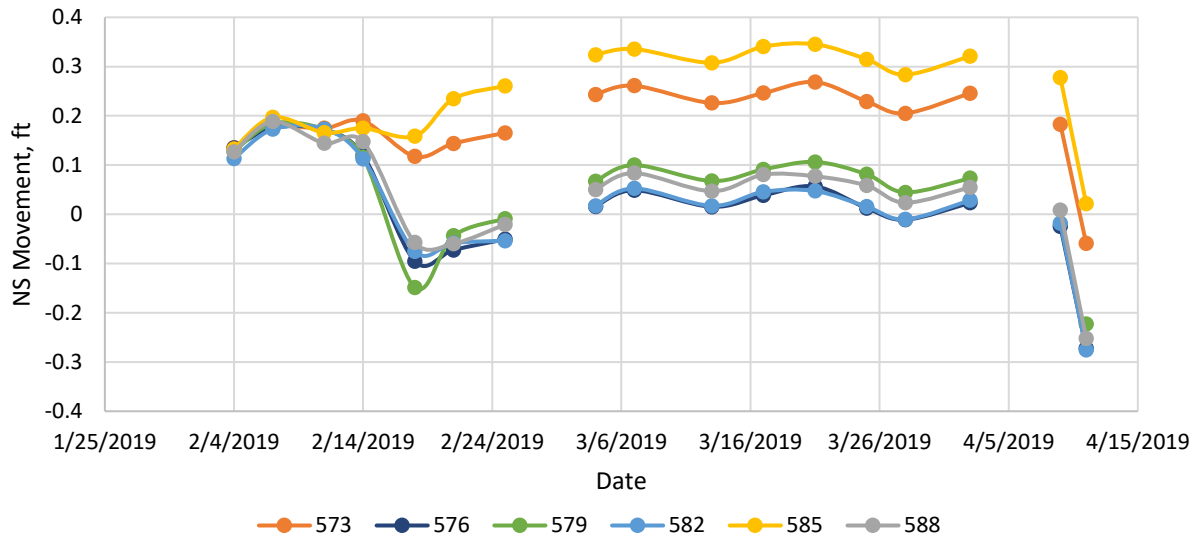


Figure IIIb.28 – Horizontal movement in the north-south direction of select points on north western cut slope survey group 1N

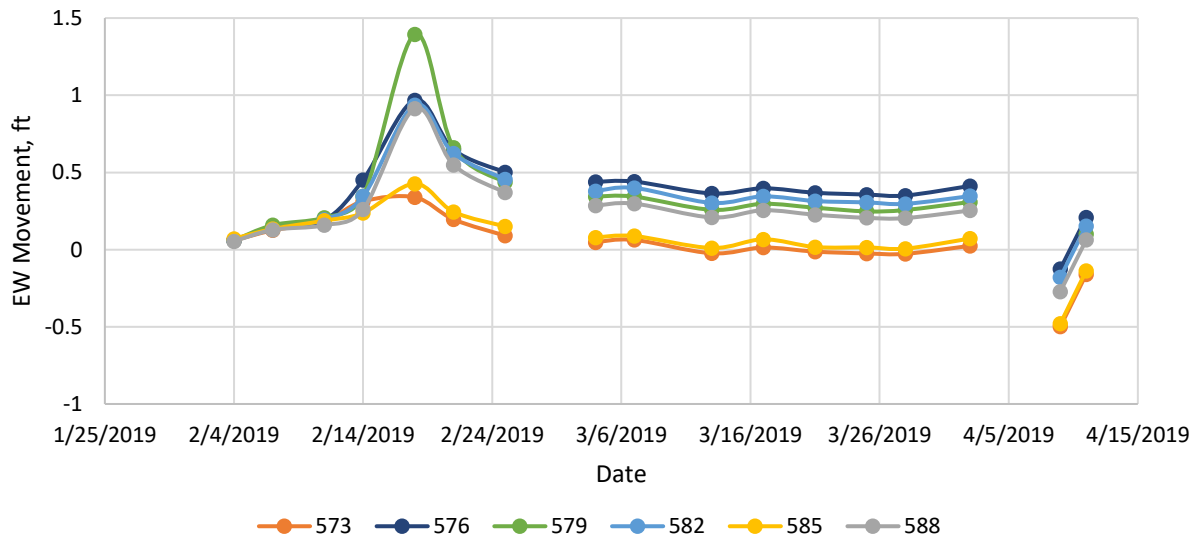


Figure IIIb.29 – Horizontal movement in the east-west direction of select points on north western cut slope survey group 1N

5.2 South (1S)

The 1S group of survey stakes is located on the western side of the study area and south of the interstate. These survey stakes are located between the inflection line and bottom of the subsidence basin. A total of six points were selected on this cut slope to be analyzed. These points can be seen below in Figure IIIb.30.

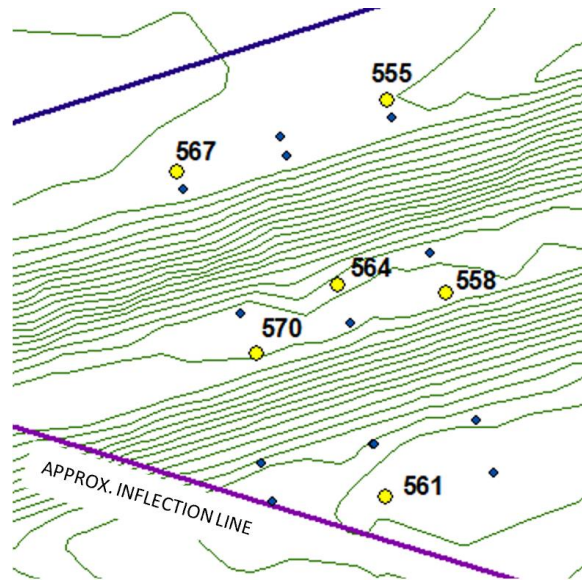


Figure IIIb.30 – Selected SPK survey points located on south western cut slope survey group 1S

5.2.1 Vertical Movement

The western cut slope south is located near the center of the basin, but it is not entirely in the zone of maximum subsidence, so it experienced varied amounts of vertical movement. The vertical movement in this area ranged from -3.64 to 0.15-ft. Most of the vertical movement in this area was subsidence, but many points experienced heave before subsiding. Figure IIIb.31 below shows the vertical movement from a selection of points. This data was compared with the face positions and it was determined that a small amount of initial surface heave occurred when the face was approaching the points and maximum subsidence is reached on February 21st when the face was approximately 750-ft passed the point.

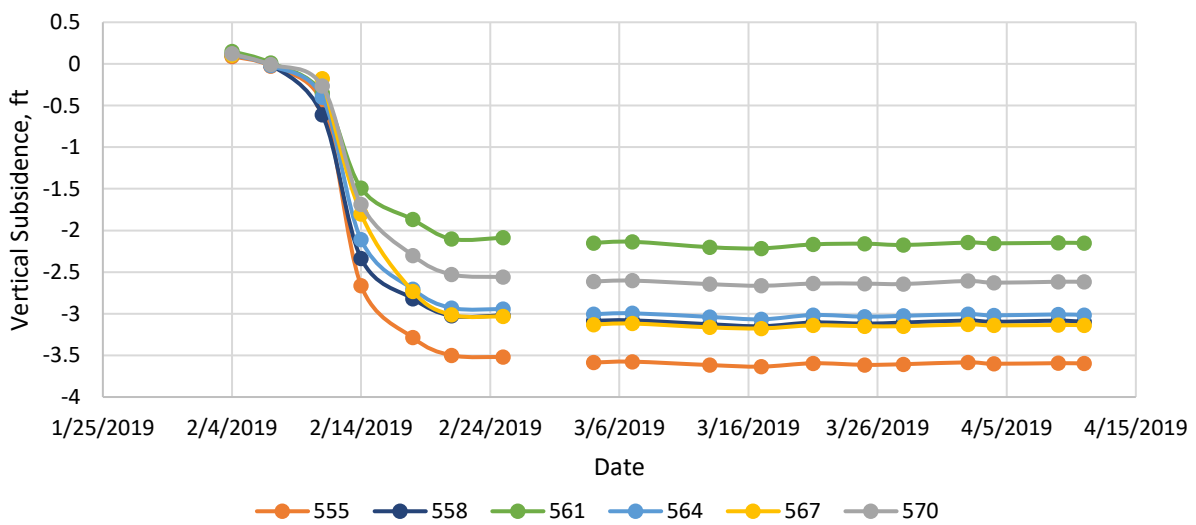


Figure IIIb.31 – Vertical subsidence of select points on south western cut slope survey group 1S

5.2.2 Horizontal Movement

In the horizontal plane, survey points on the western cut slope south moved in both the north-south and east-west directions. Most of these points moved primarily in the north and east directions, meaning that these points move toward the center of the basin. In the north-south direction, the movement in this area ranged from 0.06 to 2.17-ft. As can be seen in Figure IIIb.32, the points move north rapidly when the face is about 250-ft passed the points and then they remain in that location. In the east-west direction, the movement in this area ranged -0.35 to 0.81-ft. As can be seen in Figure IIIb.33, points spiked east first when the face is about 250-ft passed the points and then the points moved west in small increments before they ended east of their original positions.

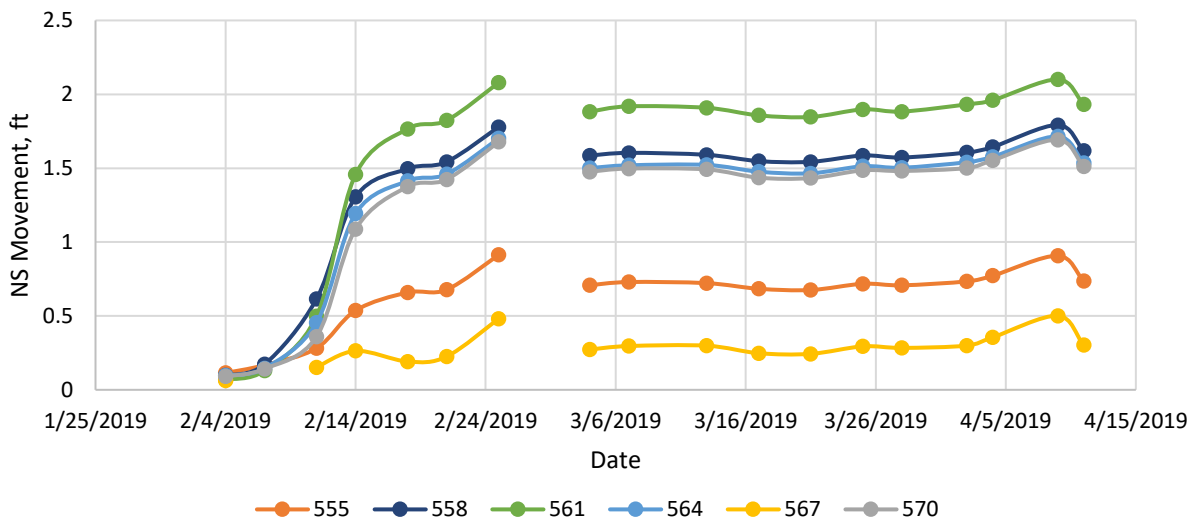


Figure IIIb.32 – Horizontal movement in the north-south direction of select points on north western cut slope survey group 1S

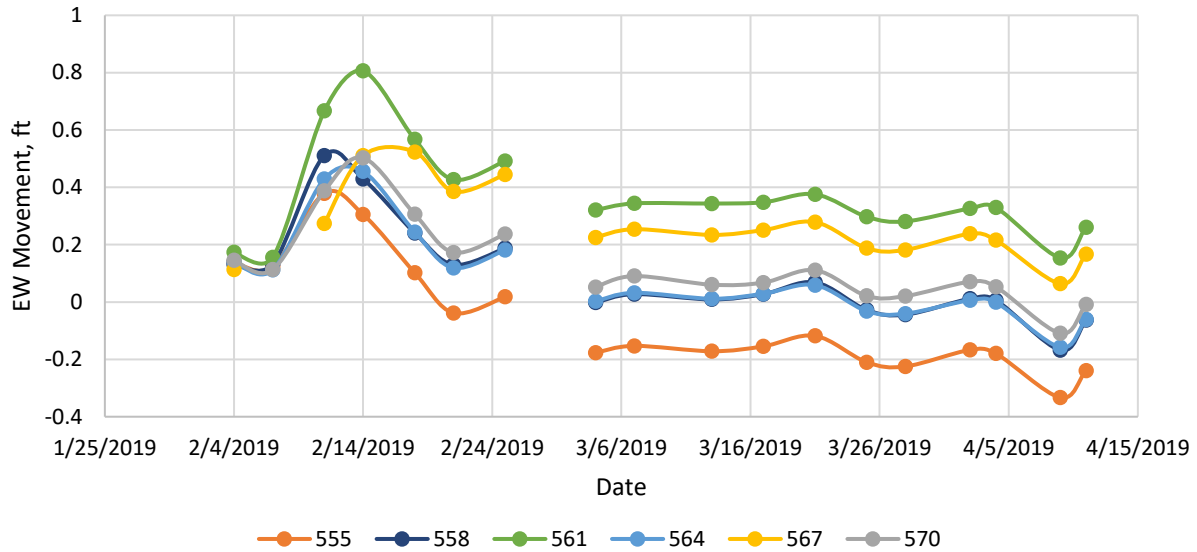


Figure IIIb.33 – Horizontal movement in the east-west direction of select points on south western cut slope survey group 1S

6.0 Summary of the Analysis of the Embankment and Cut Slope Surveys

Through the review of the slope stake data, the Pitt team was able to draw some conclusions on the behavior of the cut slopes and embankments throughout the undermining process. Based on this analysis, it appears that most points reach their maximum subsidence when the longwall face is between 700 and 900-ft passed the points. This means at a face advance rate of 115-ft per day, the points will experience their maximum subsidence values about six to eight days after the longwall face passes. On the other hand, horizontal movement tended to peak within two days of the longwall face approaching and passing a point.

Through this analysis, some conclusions regarding the behavior of Embankment #1 were also reached. After reviewing the data, the University determined that most of the horizontal movement on the south side of the slope moved in the south-west direction, which means that the points were moving down the slope. On the other side of the road, the horizontal movement on the north side of the slope moved in the north-east direction, which means that the points were also moving down the slope. This means that the different sides of the embankment were moving away from each other, providing evidence to support the theory that the embankment is spreading.

Subsection IIIc – Observational Data

Throughout the undermining of I-70 by Panel 15, the University visited the site weekly to observe the state of the pavement surface and the adjacent slopes associated with road cuts and embankments. The site conditions were provided to PennDOT through scroll maps and memorandum reports, which were used to continually assess roadway conditions. The failures of the pavement observed during these site visits were recorded in the field and then digitized in ArcGIS. These field site observations were recorded on scroll maps and supplied to the PennDOT for continual assessment of the roadway conditions. There were eight types of failures observed during these site visits. It is worth noting that the pavement surface in Pennsylvania was repaved shortly before the mining occurred, so it was devoid of any failures prior to the effects of subsidence.

The following is a list of distress features observed within the I-70 highway alignment. Some of the distress features are discussed in the “Distress Identification Manual for the Long-Term Pavement Performance Program” (Miller and Bellinger, 2014).

- Transverse cracks – cracks that predominately perpendicular to the pavement centerline
- Longitudinal cracks – cracks that are predominately parallel to the pavement centerline
- Corner breaks - A portion of the slab is separated by a crack, which intersects the adjacent transverse and longitudinal joints, describing approximately a 45-deg angle with the direction of traffic. The length of the sides is from 0.3-m to half the width of the slab on each side of the corner.
- Blowups - localized upward movement of the pavement surface at transverse joints or cracks, often accompanied by shattering of the concrete in the area; also known as blowups
- Faulting of transverse joints and cracks – difference in elevation across a joint or crack
- Lane-to-shoulder dropoffs – difference in elevation between the edge of slab and outside shoulder; typically occurs when the outside shoulder settles.
- Lane-to-shoulder separation - widening of the joint between the edge of the slab and the shoulder

Some distress features are unique to this kind of large deformation event.

- Longitudinal shear cracks – cracks caused by shear forces that run predominately parallel to the pavement centerline resulting from differential movement between pavement slabs
- Joints with separations – the opening of expansion joints cut into the pavement due to tensile forces
- Guiderail deformations – shear or compression failure of guiderail due to differential movement of the highway surface
- Compression bumps – this feature occurs when thick asphalt compresses into a bump

Because the pavement was overlain with 4-in of asphalt prior to undermining, many distress features associated with aging pavements were not observed.

The longwall face was mined five days a week and progressed at an average rate of 115-ft/day, meaning that in a week it progresses about 575-ft. The longwall face first interacted with the highway when the face passed beneath the gate road entries below the interstate on 25 January 2019.

1.0 29 January 2019

The observed damage highway surface was seen on 29 January 2019 when the panel first crossed beneath the highway. During this visit, four expansion joints at the edge of the study area began to open from the subsidence forces. These expansion joints were located over the edge of the gate roads approximately 250-ft behind the longwall face. The location of the observed features can be seen in Figure IIIc.1.

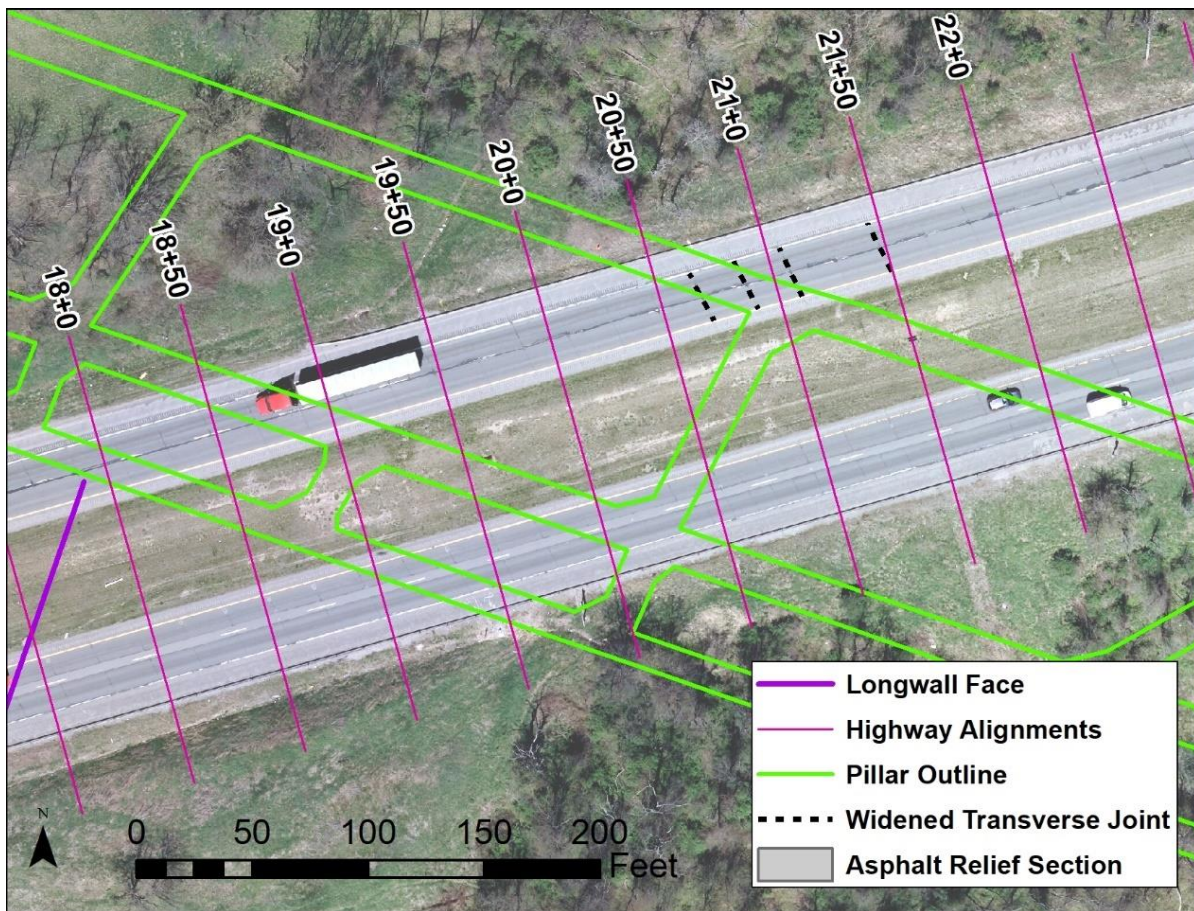


Figure IIIc.1 – Pavement features observed on 29 January

2.0 5 February 2019

The University returned to the site on 5 February 2019 to observe the condition of the pavement surface. By 5 February, the longwall panel had progressed about 835-ft since it first impacted the highway, which caused impacts on approximately 1,450-ft of the interstate. Damage was observed as far as 725-ft behind the longwall face and 450-ft in front of the longwall face. The damage observed during this site visit included expansion joint separations, transverse cracking, shear cracking, longitudinal cracking, blowups, compression bumps, and separations between the pavement and adjacent soil. The location of the features closest to the longwall face can be seen in Figure IIIc.2 and the remainder of the features can be seen in Appendix II.

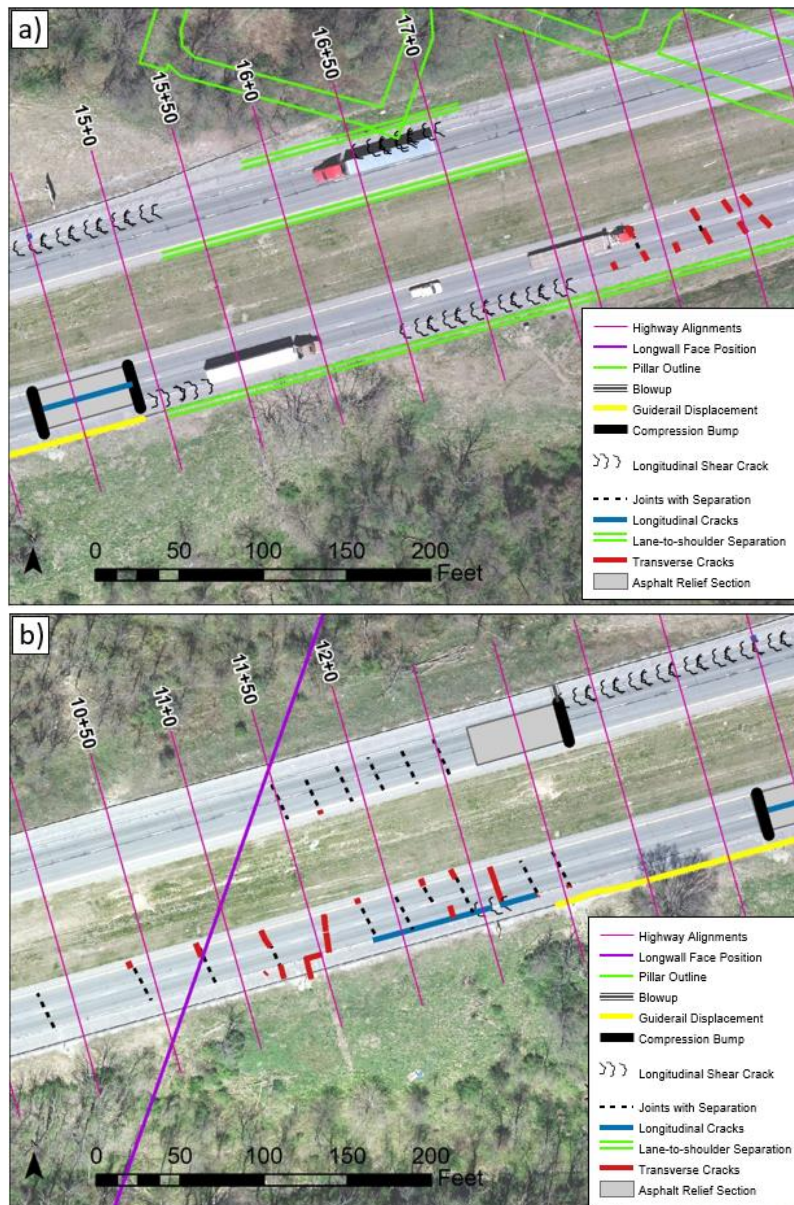


Figure IIIc.2 – Pavement features observed on 5 February

Some of the most notable features observed during this site visit were the three compression bumps and a large transverse crack. The compression bump and adjacent blowup on the westbound lane formed on 5 February, approximately 150-ft behind the longwall face. The two compression bumps on the eastbound lane formed on 4 February, between 175-ft and 225-ft behind the longwall face. Two of the three compression bumps formed in the asphalt relief sections. The large transverse crack formed about 60-ft behind the longwall face and opened to a width of more than 2.5-in wide. Images of these failures can be seen in Figure IIIc.3 below.



Figure IIIc.3 – Field images of observed features from left to right; eastbound blowup 1-ft tall, westbound blowups, eastbound large transverse crack 2.5-in wide

3.0 14 February 2019

Due to inclement weather, the University was unable to return to the site until 14 February 2019, which was seven active mining days after the prior visit. In this time period, the longwall face progressed about 800-ft. During this site visit, damage was observed on approximately 1,900-ft of the interstate. The types of damages observed throughout the highway included transverse cracking, longitudinal cracking, longitudinal shear cracking, blowup, compression bumps, open expansion joints, displaced guiderails, and separations between the pavement edge and the adjacent soil. The locations of the failures observed on 14 February closest to the longwall face can be seen in Figure IIIc.4 and the remainder of the features can be seen in Appendix II.

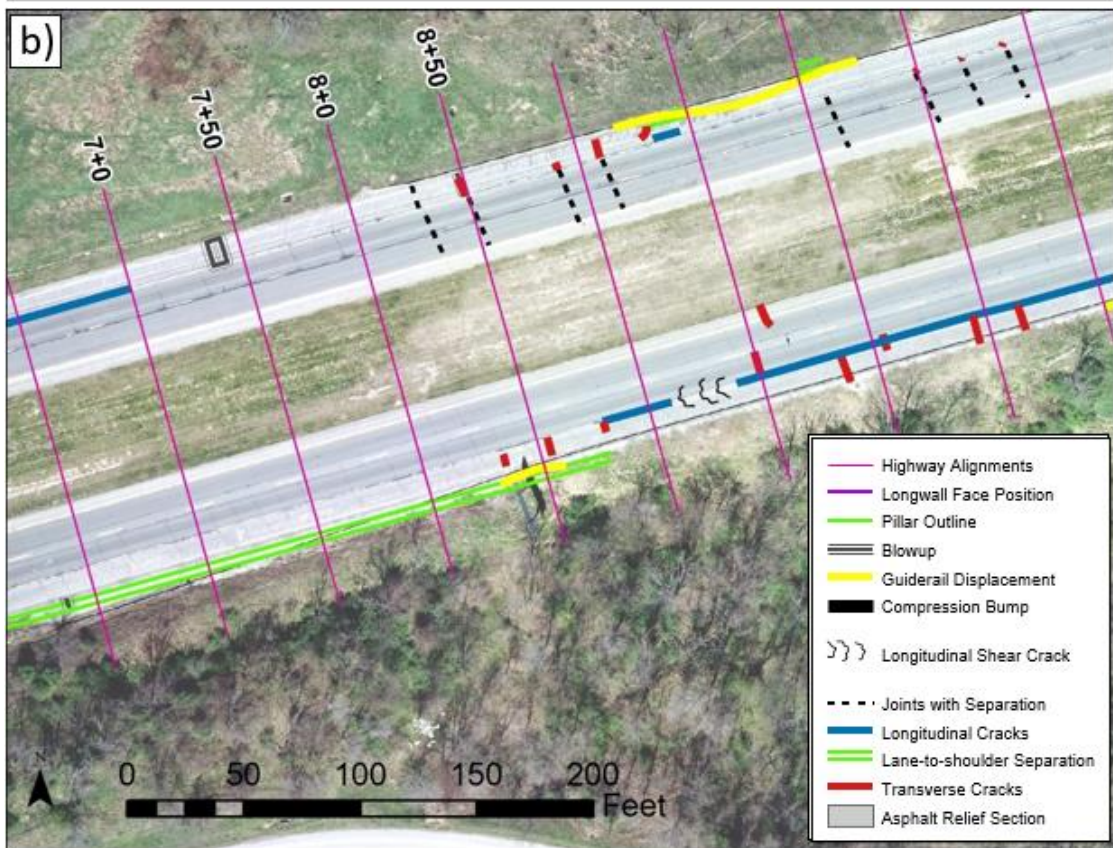
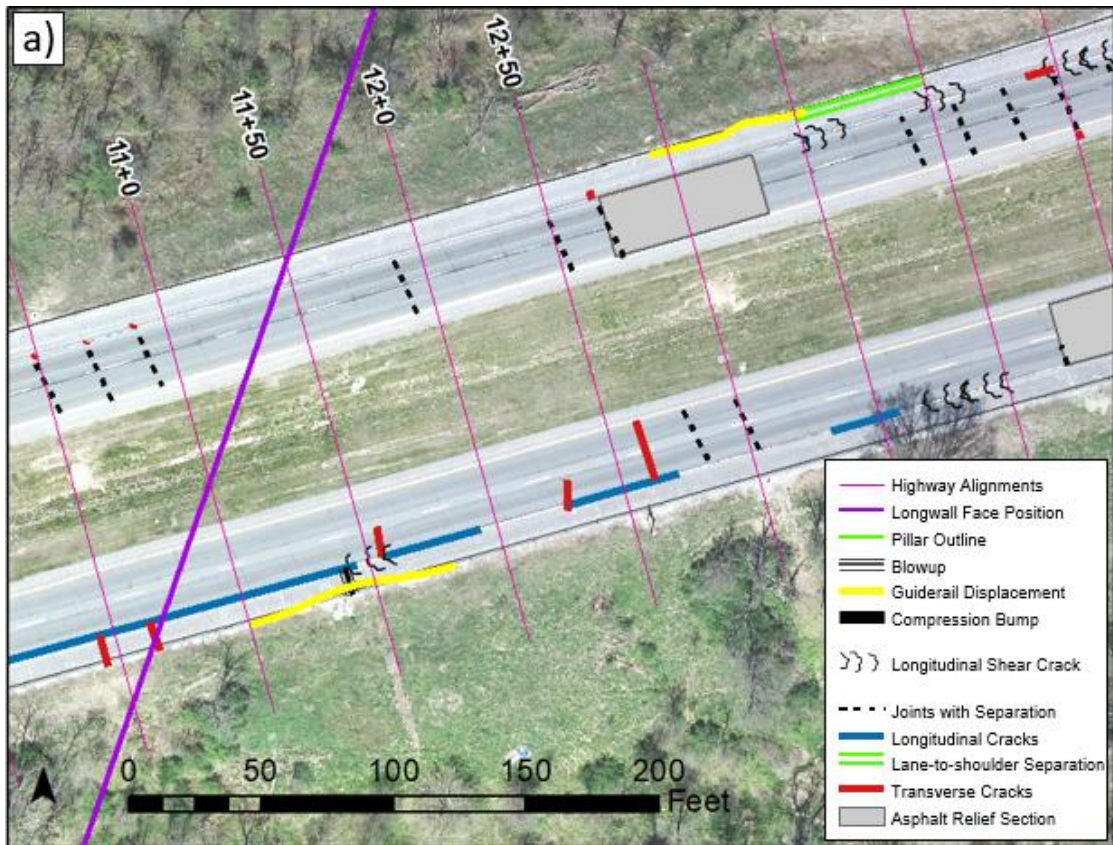




Figure IIIc.4 – Pavement features observed on 14 February

Two new compression bumps formed between the University’s observations on 5 February and 14 February. On the eastbound side of the road, a new blowup ~7-in tall formed on top of the existing transverse crack. This blowup occurred on 6 February when the longwall face was about 200-ft passed the location of the original crack. On the other side of the road, a compression bump formed on 14 February approximately 450-ft behind the longwall face. Images of these compression features were taken by the University and can be seen in Figure IIIc.5.

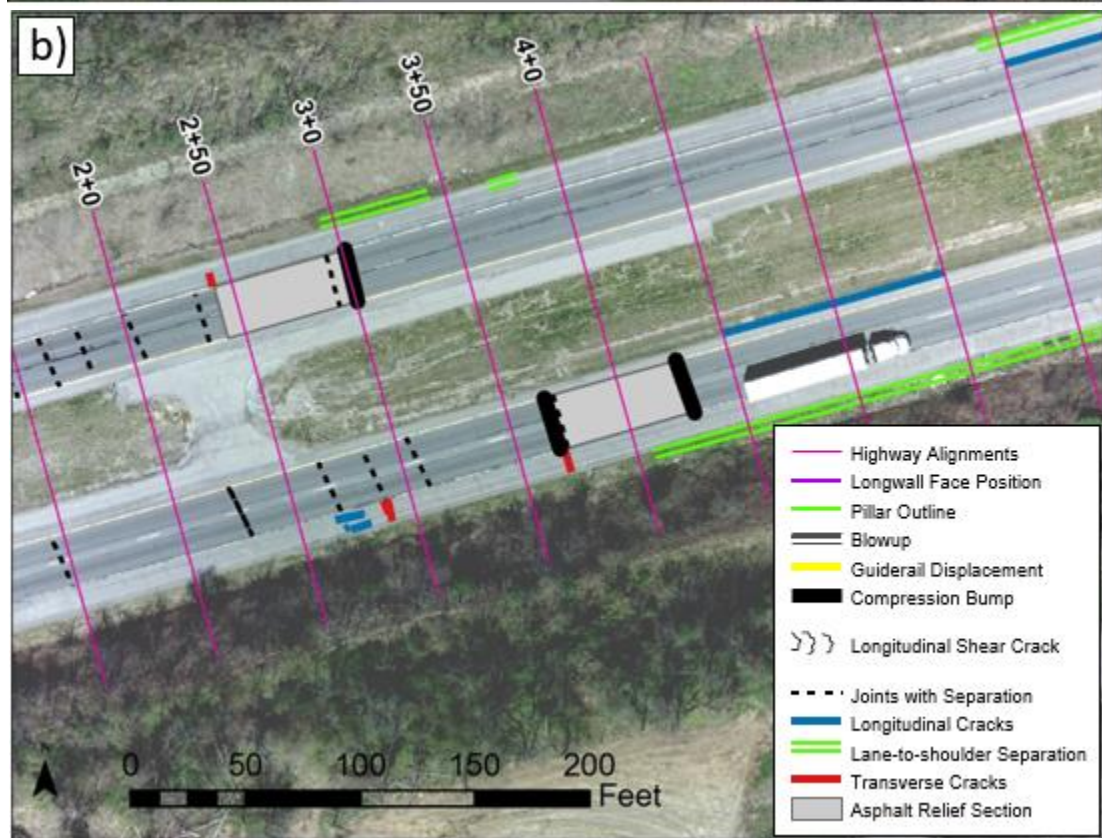
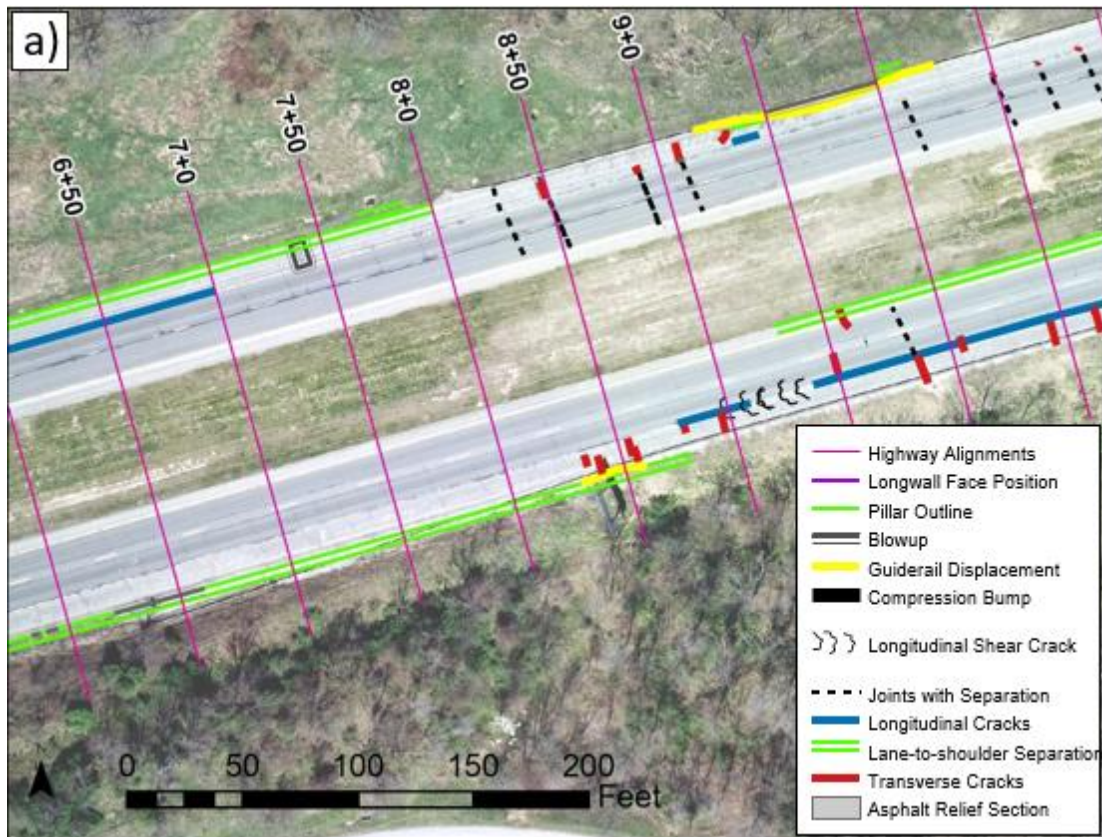
In addition to these two new compression features, significant separations between the edge of the pavement and the adjacent soil on both sides of the road, guiderrail displacements, and open expansion cracks were observed. On the eastbound side of the road, separations as much as 6-in wide were observed. Expansion joints as much as 0.75-in wide were observed on both sides of the road. These features were also photographed by the University and can be seen in Figure IIIc.5.



Figure IIIc.5 – Field images of observed features from left to right; westbound blowup, eastbound blowup 7-in tall, eastbound separation of pavement from soil, open expansion joint 0.75-in wide, sheared guiderail on westbound highway, sheared guiderail on eastbound highway

4.0 19 February 2019

The University next visited the site on 19 February. Between 14 February and 19 February 2019, the longwall face progressed approximately 275-ft. By this point in the undermining process, almost the entirety of the section of the interstate had been undermined. During this site visit, approximately 2,000-ft of the interstate had experienced damage. Like in the previous observational visit, the types of damages observed throughout the highway included transverse cracking, longitudinal cracking, longitudinal shear cracking, blowup, open expansion joints, displaced guiderails, and separations between the pavement edge and the adjacent soil. The locations of these failures observed on 19 February closest to the longwall face can be seen in Figure IIIc.6 and the remainder of the features can be seen in Appendix II.



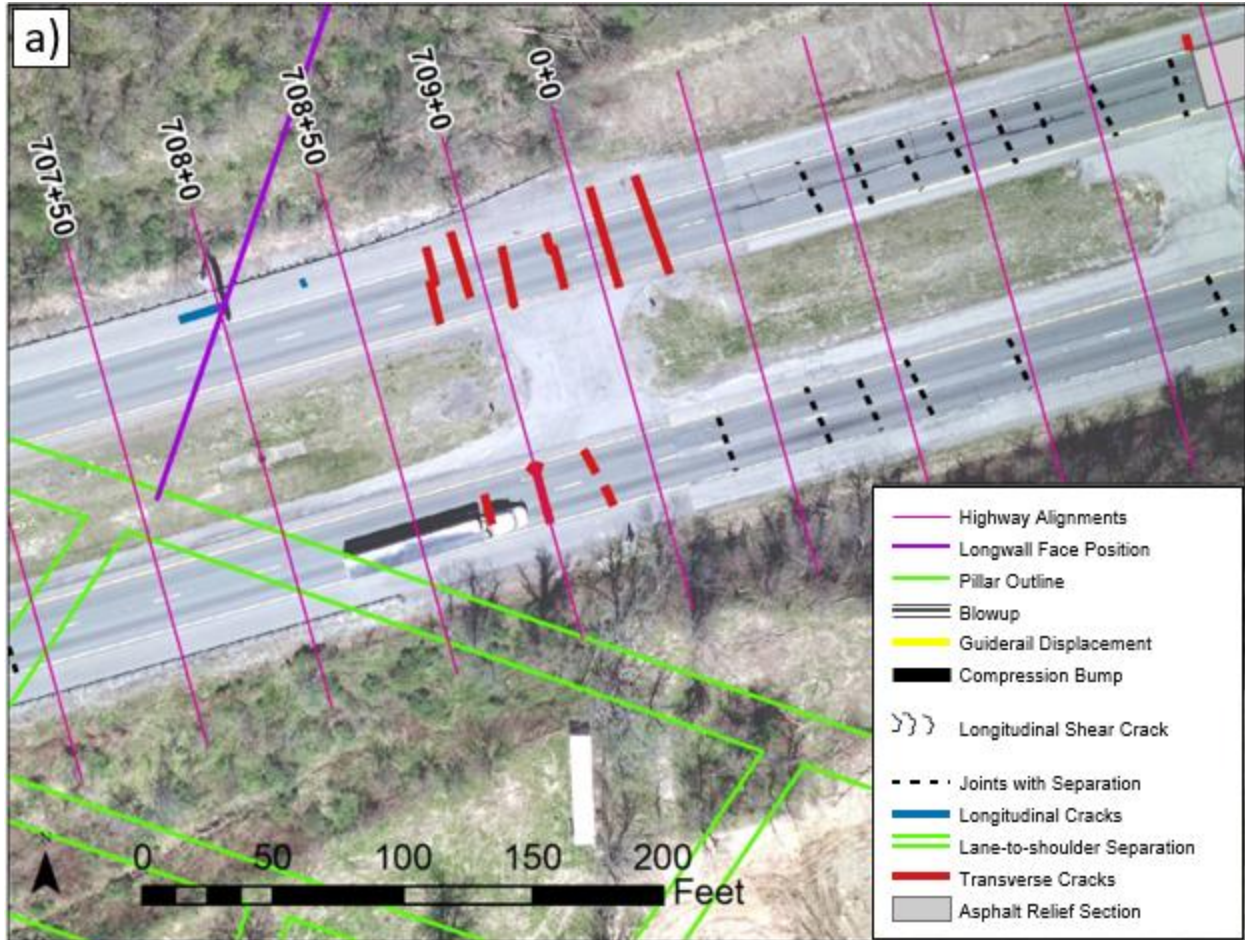


Figure IIIc.6 – Pavement features observed on 19 February

Very few new features were observed during the University’s site visit on 19 February. Some new expansion joints opened, and transverse cracks formed as much as 300-ft behind the longwall face. Additionally, new longitudinal crack opened just beyond the longwall face. The new damage observed on this site visit was not as significant as the damage observed in similar features near the center of the panel. Slight separations also occurred on the inside of the eastbound lanes between the pavement and the adjacent soil.

5.0 26 February 2019

The University returned to the site on 26 February 2019 to observe the condition of the pavement. By this date, the longwall face was approximately 465-ft beyond the extent of I-70. Various extents of damage were present throughout the entire 2,400-ft section of interstate influenced by the subsidence basin. The location of damage observed near the western edge of the panel during this site visit can be seen in Figure IIIc.7 and the remainder of the observed damage can be seen in Appendix II.

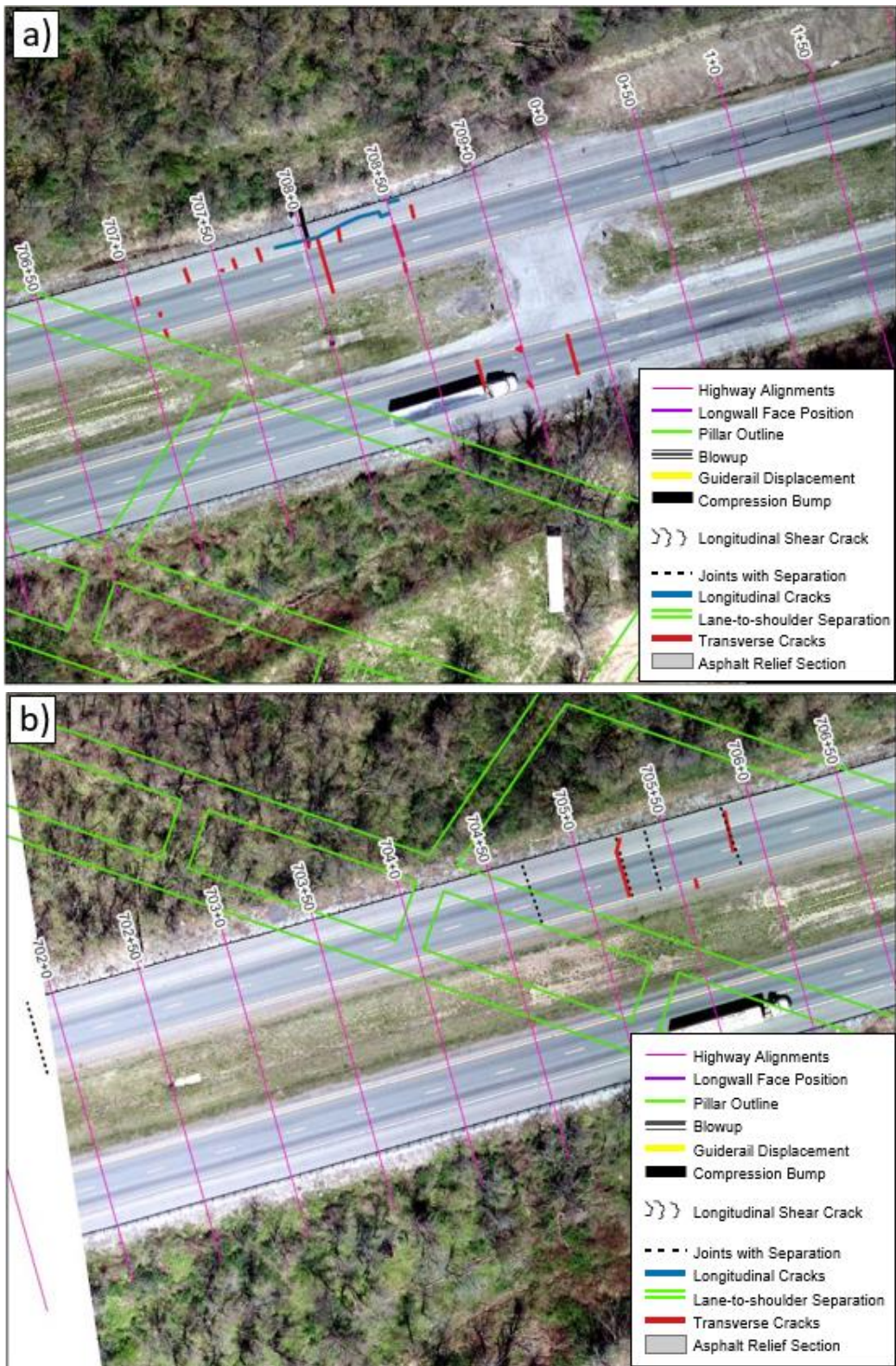


Figure IIIc.7 – Pavement features observed on 19 February

With the longwall face beyond the extent of the interstate, a small amount of new damage was observed on the West Virginia section of the highway. In this section, small transverse cracks and open expansion joints were observed on the westbound lanes. This damage was observed over the western gate road entries and just inside the panel.

6.0 5 March 2019

The University visited the site again on 5 March 2019. By this site visit, the longwall face was over 1,000-ft beyond the extent of the highway. Due to repairs made by the PennDOT maintenance team and the natural subsidence progression, the University found that the damage on the highway had been resolved by this observation.

7.0 Conclusions from Observed Failures

Reviewing the observations made during the undermining process has allowed the University to reach some preliminary inferences about the behavior of the pavement surface when subjected to longwall subsidence. As can be seen in Figure IIIc.8, the trends in the observed features show that the tensile features, such as separations and open expansion joints, tended to occur within 300-ft beyond the longwall face and 150-ft behind the longwall face. Once the longwall face was approximately 150-ft passed a point, the surface forces switched from tension to compression, causing the formation of compression features, such as blowups. These compression features tended to concentrate in the asphalt relief sections.

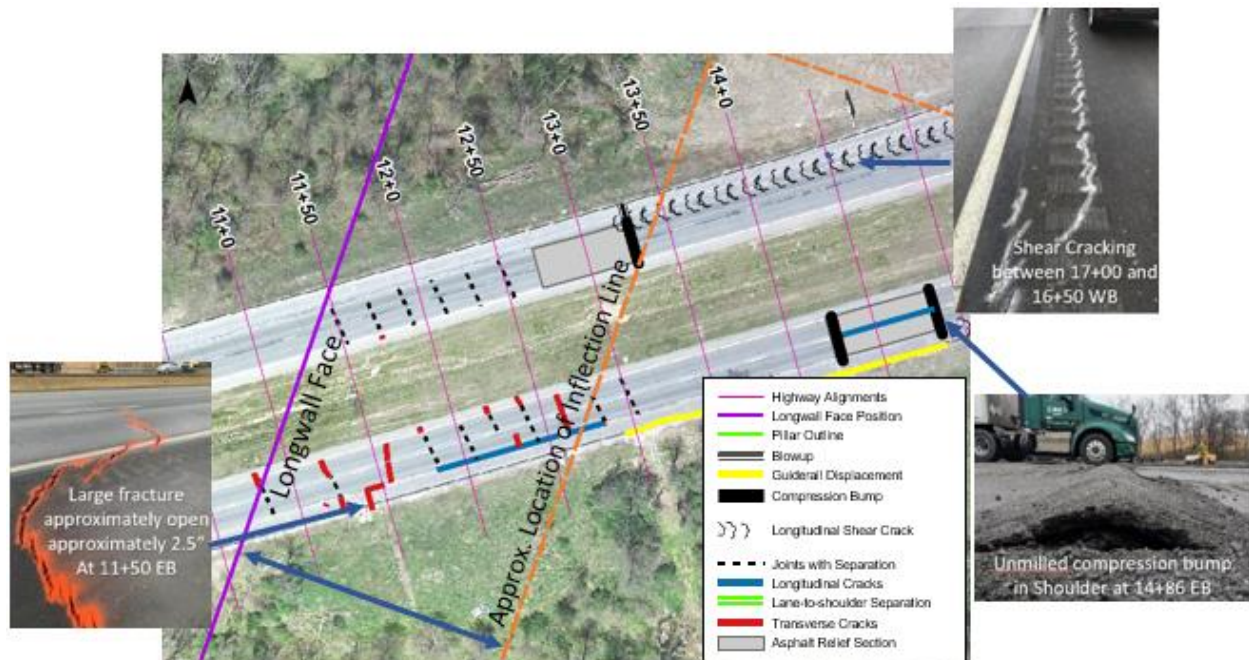


Figure IIIc.8 – Failures of the highway surface as the subsidence basin formed, demonstrating areas of tension, compression, and differential movement.

The expansion joints located throughout the pavement sections opened and closed readily throughout the undermining process. The joints opened significantly, as much as 0.75-in in places, which is three-times their original width. However, by the end of the undermining process, almost all these joints had returned to their initial widths. These features provided the highway pavement set locations to expand and contract as the subsidence basin formed.

Perhaps the most interesting observed failure is the occurrence of the large transverse crack that formed on the eastbound lanes that then transitioned into a blowup. The transverse crack that occurred in this location was 2.5-in wide, making it one of the largest that formed on the pavement surface. The section of this fracture in the shoulder transitioned into a 7-in tall blow-up, while the other sections of the initial fracture remained open as a crack. This failure occurred halfway between two expansion joints that were spaced 40-ft apart; generally, the expansion joints were placed 20-ft apart, indicating that there may be an expansion joint in the concrete that was not cut into the asphalt at the location the failure occurred, and the lack there of may have contributed to the damage that occurred there.

While this feature was of particular interest, the shear cracks that formed throughout the study area were located primarily in the rumble strip between the travel lane and the shoulder. Shear cracks are caused by shear forces that run predominately parallel to the pavement centerline resulting from differential movement between pavement slabs. All of the observed shear cracks occurred between the travel lane and the shoulder. However, these cracks occurring in the rumble strip rather than on the pavement seam indicates there may have been additional factors at work, such as the deformation and ultimate shearing of the rebar connecting the concrete slabs. A further analysis of the differential deformations observed through these shear cracks will be completed in Task 3 Report.

Subsection IIIId – Analysis of Inclinometer Data

1.0 Description of the Inclinometer Data and Setup

PennDOT installed inclinometers in six boreholes within the study area and their survey crews were to take regular readings from these inclinometers throughout the undermining process. The RST Digital Inclinometer Probe, Model No. IC 35202 was used to take readings at these locations. These probes have an accuracy of +/- 0.1-in per 100-ft and can operate within +/- 30 degrees, and in temperatures ranging from -40 to 158 degrees Fahrenheit.

1.1 Locations of the Inclinometers in the Study Area

Figure IIIId.1 illustrates the locations and orientations of the borehole casings. Notice that the orientations differ based on their locations; TB-4 and TB-2 share an orientation, while TB-6, TB-8, TB-9 and TB-13 all share a different orientation. The orientation as installed shows the A+ direction pointing down the slope of the embankments and the B+ axis clockwise from the A+ orientation. It is also important to note that the inclinometers were placed either on the top or the bottom of the embankments, so their measurements could be compared and characterized based on these locations.

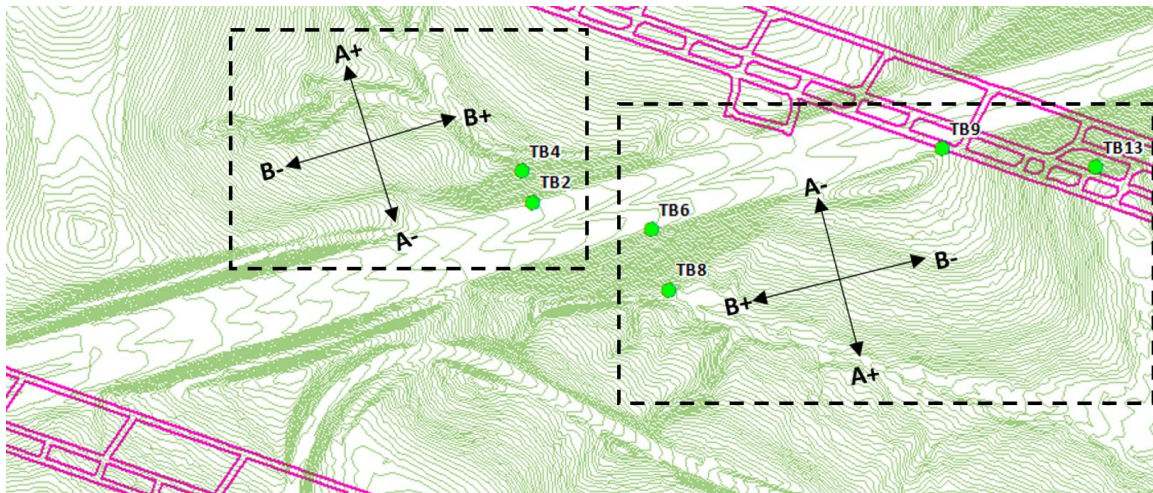


Figure IIIId.1 – Locations and orientations of the inclinometers within I-70 study area

Readings were taken twice every week during the undermining process. There dates were as follows:

- 6 January 2019
- 14 January 2019
- 16 January 2019

- 21 January 2019
- 23 January 2019
- 27 January 2019
- 30 January 2019
- 1 February 2019
- 4 February 2019
- 6 February 2019
- 11 February 2019
- 13 February 2019
- 15 February 2019
- 19 February 2019
- 27 February 2019
- 6 March 2019

Figure III d.2 shows the locations of the longwall face at the start of each of these dates.

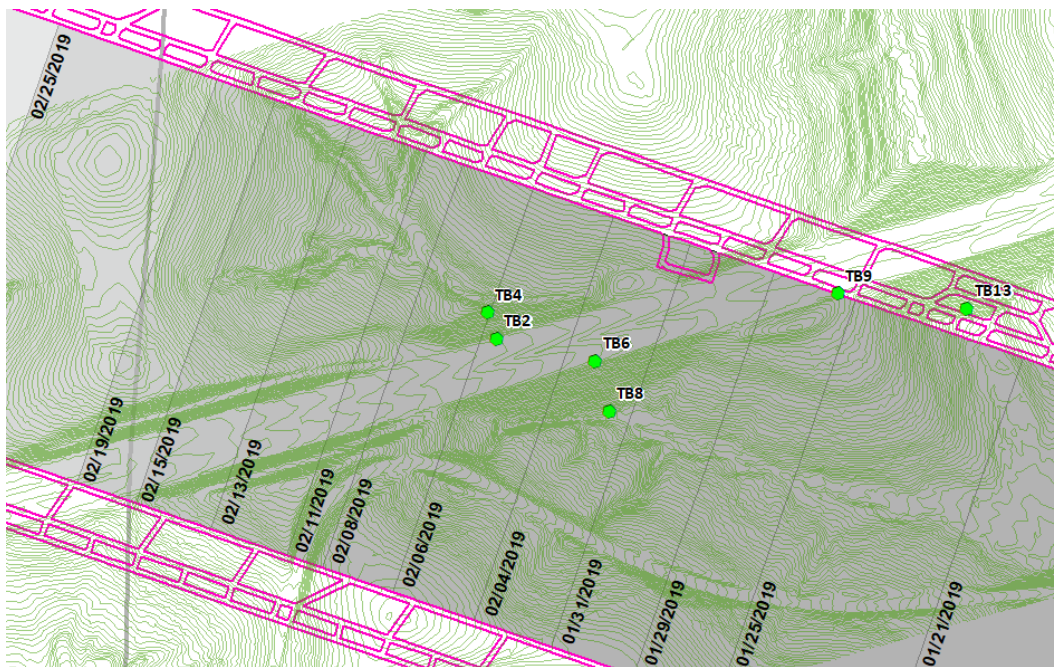


Figure III d.2 – Locations of longwall face on the dates on inclinometer surveys

2.0 Analysis of the Inclinometer Data

When the data was compiled, readings were stored at each 2-ft interval. When graphing and analyzing this data, two different methods were used. The first is the cumulative displacement method. This method adds readings together as it progresses up each interval. The second is the incremental displacement method, which strictly looks at the readings taken at each interval and

does not add them together. The graphs for the cumulative and incremental displacements are all located in Appendix III. The cumulative graphs better represent the true ground movement at each interval, while the incremental graphs are better suited for distinguishing how much movement occurred at each interval as they are independent from readings taken below them.

2.1 TB-13

TB-13 was the first inclinometer of the six that the longwall face passed. It was located over the gate road entries and at the bottom of Embankment #2, and as such was not expected to experience as much movement compared to the inclinometers that were in the subsidence basin. Refer to Figure III.d.1 for the location and orientation of TB-13. TB-13 began experience movement on 21 January, at which point the longwall face was ~200-ft from the instrument. These movement trended in the A+ and B+ directions, which indicates movement outwards from the slope and towards the longwall face. Movement kept trending in this direction as the face passed the instrument, eventually settling on 4 February when the face was approximately 1,000-ft passed the instrument. The cumulative displacement on the surface was approximately 0.7-in on the A-axis and 0.5-in on the B-axis. This again indicates slight movement towards the longwall subsidence basin. The displacement graphs for TB-13 can be viewed in Appendix III.

One note-worthy observation occurred on 30 January, when the longwall face was approximately 650-ft passed TB-13. On this day the movement indicated a large reversal in the A- direction, and a less significant increase in the B+ direction. This movement occurred at 28-ft of depth, where there was a sandstone and siltstone interface. Movement above this depth compared similarly to the other daily readings that were taken. While it could signal a misreading in the data, it could also be a sign of extraordinary movement at that depth interval at that point in time

2.2 TB-9

TB-9 was the next inclinometer that was undermined. The borehole for this inclinometer was located right on the edge of the longwall panel and at the base of the cut slope on the eastern side of the study area.

Unlike TB-13, which experienced movement prior to the passing of the longwall face, TB-9 did not experience any movement until the face had already passed its position. Movement was first recorded on 30 January, when the longwall face was approximately 300-ft passed the borehole. This movement was primarily on the A-axis, in the A+ direction. This means it moved into the basin and opposite of the direction of mining. As mining progressed, movement at each depth interval progressed in the A+ direction. For the B-axis, movement trended in the B+ direction, however, these movements were not as severe. The casing eventually settled on 4 February,

when the face was approximately 650-ft away. Movements at the surface totaled at approximately 0.8-in on the A-axis and 0.4-in on the B-axis.

2.3 TB-6 and TB-8

The boreholes for TB-6 and TB-8 were located on the south-facing slope of Embankment #1. TB-6 was placed on the top of the embankment, while TB-8 was at the bottom. For this reason, they are going to be analyzed as a group to compare movements at the top and bottom of the embankment. The south-facing slope of Embankment #1 is located close to the center of the subsidence basin, so they were subjected to much more movement than TB-9 and TB-13.

TB-8 was undermined on Thursday 31 January, and TB-6 was undermined on Friday 1 February. As such, TB-8's casing began to move at before TB-6 did. TB-8's movement was first recorded on 1 February, the day after it was undermined. Similarly, TB-6 began to move when the face progressed beyond its position on 4 February. This means that in both cases it took until the following active mining day for the data to detect measurable movements.

For TB-8, movements were more severe on the A-axis in the A+ direction. This highest amount of movement occurred at 20-ft of depth, where an interface of sandstone and siltstone met. Upward from this interval, movement steadily increased in the A+ direction. This trend increased as the longwall face continued away from the instrument. As for the B-axis, movement varied back and forth on its zero points from the bottom of the casing to the top. It eventually settled with predominant movement in the B+ direction across most intervals. The longwall face was approximately 600-ft passed borehole when it began to settle. It settled at approximately 6-in in the A+ direction, and around 1.75-in in the B+ direction. This indicated final movements pointing down the slope and toward the center of the basin.

Similarly, TB-6 also experienced a shift in the A+ direction shortly after it was undermined. Movement just below the surface shifted approximately 6.0-in in the A+ direction and 3-in in the B- direction. On 6 February, movement on the A-axis jumped to approximately 10-in, while remaining relatively equal on the B-axis. Subsequent readings showed movement on A-axis come back down to around the 6-in range just below the surface and showed that movement on the B-axis reversed in the B+ direction. The longwall face was approximately 850-ft passed borehole when it began to settle. Once settled, movement totaled at approximately 5.5-in on the A-axis and 2.5-in on the B-axis. Like TB-8, much of this total was influenced by movement near the bottom of the casing. In this case, the highest amount of movement was experienced at 68-ft of depth, where a layer of siltstone and limestone met a layer of layer of silt and gravel.

For both TB-6 and TB-8, initial movements were most pronounced in the A+ direction, which indicated movement outward from the slope and toward the middle of the basin. Movement

continued to progress this way as mining continued away from the instruments. As this occurred, movements varied back and forth on the B-axis. Finalized movements on both axes were similar between the two inclinometers with approximately 6.0-in in the A+ direction and 1.5 to 2.5-in in the B+ direction. This indicated the casings shifted towards the center of the basin. Also common amongst both inclinometers was the indication that movement was heavily influenced towards the bottom of the casing, as both experienced the highest incremental movements at different sediment interfaces. Both started to move on the first active mining day following undermining and began to settle when the face was approximately 600 to 850-ft away, or six to eight active mining days later.

2.4 TB-2 and TB-4

Located on the north facing slope of Embankment #1 were TB-2 and TB-4. Again, one was placed on the top of the slope (TB-2) while the other was placed on the bottom (TB-4). These casings are located close to the center of the basin where maximum subsidence is expected. TB-2 was undermined on 5 February, and TB-4 on the following day. As such, movement for TB-2 was detected before it was for TB-4.

Records of movement for TB-2 were first recorded on 6 February, the day after it was undermined. These initial movements were in the B+ and A- directions, with a higher degree of movement on the B-axis. This meant that the early movements pointed in the opposite direction of mining and into the subsidence basin. The subsequent readings showed the casing continued to move in these directions before it eventually reversed course on 11 February, when it was approximately 350-ft beyond TB-2. This reversal meant that it began to follow in the direction of mining, and that it began to move down the slope in the A+ direction. Just below the surface it settled with movements of approximately 3.5-in on the A-axis and -1.0-in on the B-axis. As was seen in TB-6 and TB-8, there was again the highest amount of incremental movement at 58-ft of depth, where a layer of clay and gravel met.

For TB-4, small levels of movement were detected on the B-axis on 6 February, the day it was undermined. This was followed by a much larger shift in this direction on 8 February. On this day, the movement jumped out in the A+ and B+ directions. Subsequent readings showed movements continuing in the A+ directions but settling back close to its zero point on the B-axis. Once settled, readings totaled at approximately 8.0-in on the A-axis and 0.5-in on the B-axis, which indicates movement straight down the slope. The highest levels of incremental movement were again seen in the lower portion of the borehole casing. Up to 4.5-in of movement was detected at 24-ft of depth on the A-axis. At this interval there was an interface of gravel and a sand and clay mixture. There was also significant movement at the very bottom of the casing near where a layer of claystone met a layer of limestone.

Both TB-4 and TB-2 showed records of movement either the day of undermining or on the following day. Both began to settle around 15 February, when the longwall face was approximately 750 to 800-ft passed the instruments, or seven to eight active mining days after they were undermined. As opposed to TB-6 and TB-8, which showed similar movement totals, TB-2 and TB-4 experienced a distinguishable difference in movement between the top (TB-2) and the bottom (TB-4) of the slope. The bottom of the slope ended up experiencing an increase of 4.0-in of movement outward from the slope. However, movement on the B-axis were very similar, as they initially experienced high amount of movement in the B+ direction but ended up settling close to its original point on the B-axis with some variance up and down its casing. As was true for borehole casings on the south facing slope, many movements were most severe at depth intervals near the bottom of the casing and at various sediment interfaces.

2.5 Summary of Inclinerometers Data

Several conclusions can be determined from the inclinometer data. First, noticeable shifts were not recorded until either the day of undermining or on the following day. They also did not begin to settle until the longwall face was approximately 600 to 850-ft away passed the instrument. Second, movements were highest in the A+ direction for each inclinometer, which means the slopes deformed outwards from the interstate. Movements on the B-axis were less uniform than movements on the A-axis. B-axis movements tended to move opposite the direction of mining before eventually reversing directions and following the mining direction as the subsidence basin settled. Third and final, cumulative movement was often heavily influenced by high incremental movement in the bottom portions of the inclinometer casings. Each interval with these high levels of movement was associated with an interface among two sediments. Figure III.d.3 depicts the trends of outward movement near the surface, while Figure III.d.4 represent movements both near the surface at towards the bottom of the casing. It is important to note that Figure III.d.4 depicts the inclinometers as if they are projected on the same vertical plane, which is not true. True representations of their locations are depicted in Figure III.d.3

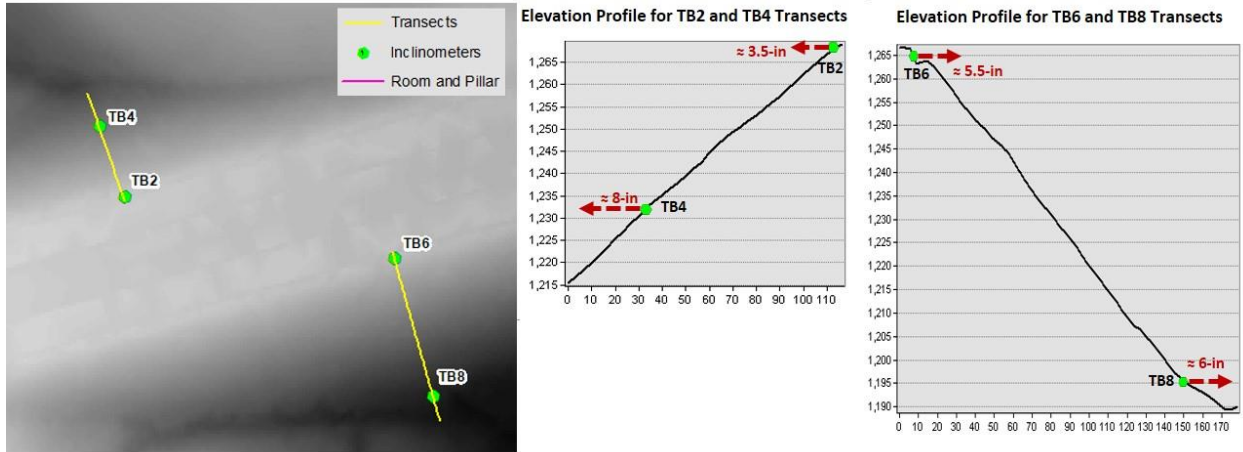


Figure III.d.3 – Depiction of the outward movements 2-ft below the surface that the inclinometer borehole casings experienced on Embankment #1. The lines represent the elevation of the transect for each inclinometer grouping

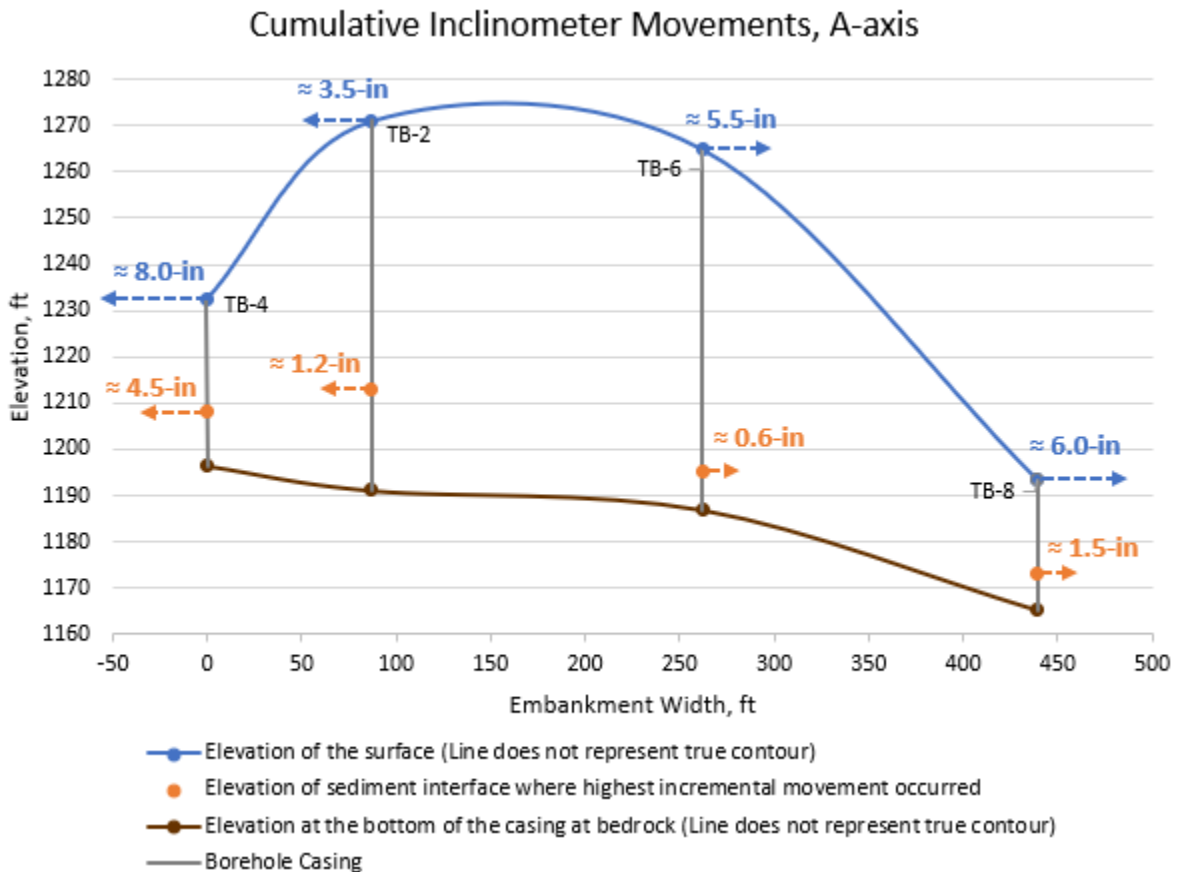


Figure III.d.4 – Depiction of outward movements that the inclinometer borehole casings on Embankment #1 experienced at the 2-ft depth interval and at the depth interval with the greatest incremental movement. This figure illustrates the inclinometers as if they are on the same vertical plane and is not meant to represent their true positions, nor do the lines represent true elevations

Subsection IIIe – Analysis of the Tiltmeter Data

1.0 Description of the Tiltmeter Data and Setup

Eight tiltmeters were installed along the eastbound lane of I-70. These tiltmeters were programmed to take a reading every ten minutes, and in those readings were several fields of data including: time, battery voltage, degrees of tilt (for both the X and Y), temperature (C), and the millivoltage (for both the X and Y). The fields that are most important to the analysis of subsidence is the degree of tilt in the X and Y planes, as this will detail the direction and the severity of ground surface's tilt as mining occurred beneath the interstate. The following section analyzes and describes the movement that the tiltmeters recorded while undermining took place.

1.1 Locations of the Tiltmeters in the Study Area

As mentioned, eight tiltmeters were installed at different locations along I-70. However, nine total borehole locations were used during the study. The University requested that the tiltmeter installed in TM-1's borehole be transferred to the bottom of Embankment #1. This transfer occurred on 24 January, and the new location was identified as TM-9. This was done with the desire to compare the tilt differences between the top and the bottom of the embankment. Figure IIIe.1 illustrates the location of each tiltmeter.

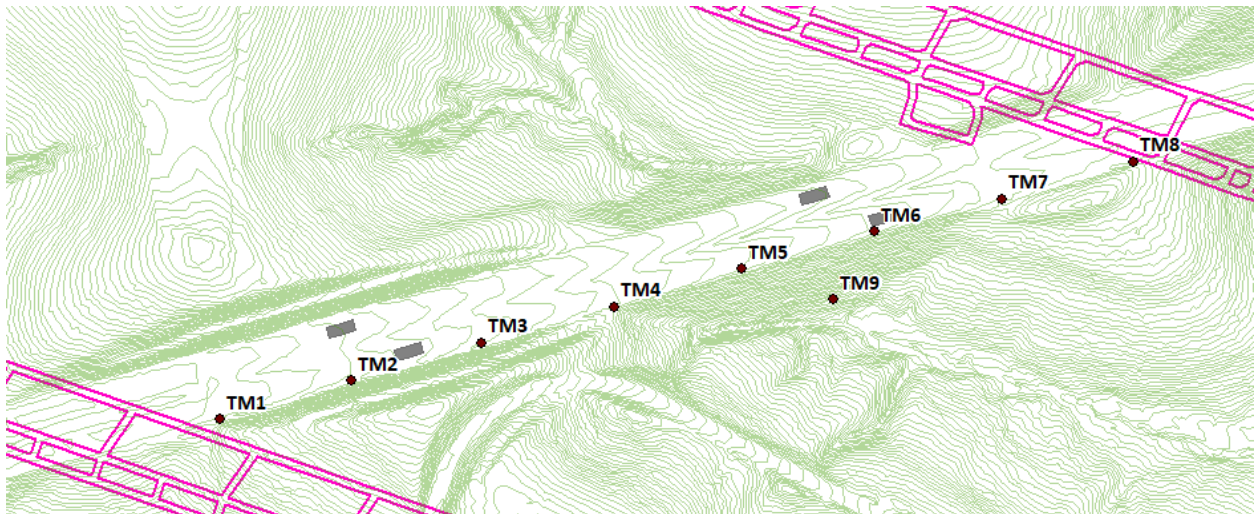


Figure IIIe.1 – Location of each tiltmeter in the study area

1.2 Tiltmeter Malfunctions

Unfortunately, due to a mishap in the tiltmeter technology, much of the data collected by the tiltmeters was lost. Tiltmeters 1-5 (TM-1/9, TM-2, TM-3, TM-4, TM-5) all experienced an override in data that led to data loss right as the longwall passed underneath these instruments.

However, TM-6, TM-7, and TM-8 did not experience this data loss as they were equipped with a different model of instrument. As such, a complete characterization of tilt can be made for TMs 6-8, whereas only pre-mining and post-mining tilt can be analyzed for TMs 1-5. Figure IIIe.2 depicts the location of TMs 6-8. As no change in tilt was expected until the longwall face approached the tiltmeter, it was only necessary to focus on the dates where the face was close in proximity to these tiltmeters. For each tiltmeter, the data was considered when the longwall face was approximately within 600-700-ft of the instrument in each direction. Figure IIIe.2 also depicts the orientation of the X and Y axes in relation to Panel 15's orientation.

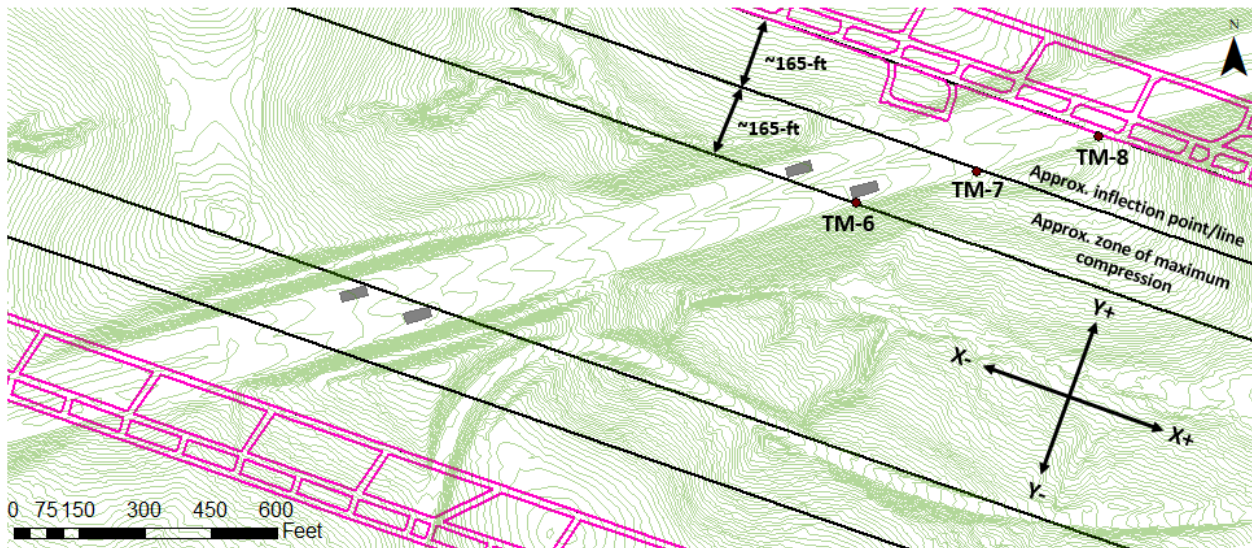


Figure IIIe.2 — Location of three tiltmeters (TM-6, TM-7, TM-8) active during undermining along the eastbound lanes of I-70 and the areas of permanent compression or extension of the surface

2.0 Analysis of the Tiltmeter Data

In this analysis, the data was viewed as cumulative tilt, meaning that each data point represents the total amount the instrument has tilted from its original, zero-point orientation. Doing so will give a representation of the positioning as undermining progressed. Figure IIIe.3 plots the movement of TM-6 on a scatterplot. Dates were used based on when movements began to occur and when they began to settle.

2.1 Tiltmeters with No Data Loss (TM-6, TM-7, TM-8)

The plot in Figure IIIe.3 depicts that the tiltmeter began to tilt in the X+ and Y- directions as the longwall face approached TM-6. In other words, as the longwall face approached the instrument, it began to tilt towards the position of the longwall face and into the center of the basin. It continued tilting in this direction until 3 February, or when the longwall face was approximately 180-ft passed the tiltmeter. At this point, the tilt reversed its direction and began to tilt in the direction of mining. The tilt continued in this direction until it began to settle on 7 February. At

that point, the longwall face was approximately 550-ft passed TM-6. It settled with very little change in tilt on the X-axis, and more dramatic change on the Y- direction. This indicates a tilt towards the center of the basin for TM-6.

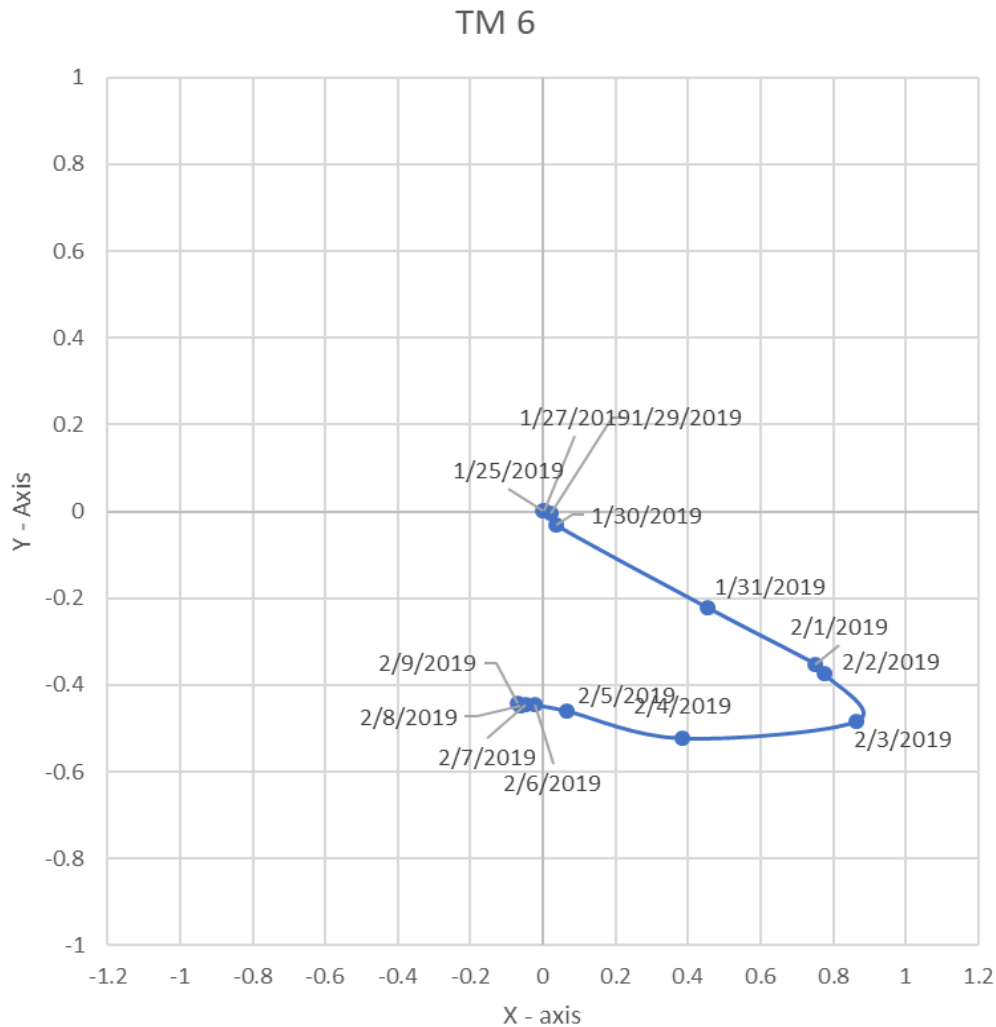


Figure IIIe.3 – Tilt measurements of TM-6 as undermining occurred

Figure IIIe.4 plots the movement of TM-7. Although the movement of TM-7 appears to differ greatly from the movement that TM-6 experienced, it has some similarities. Like TM-6, TM-7 tilts in the X+ and Y- directions, then reversed direction, tilting towards the longwall face.

One difference between the two tiltmeters, the permanent tilt change, is related to the instrument position within the subsidence basin. TM-6 is within the subsidence basin where the maximum subsidence will be achieved. In this region, minimal permanent surface slope changes are expected. Conversely, TM-7 is within the portion of the subsidence basin where permanent surface slope changes are expected. As a result, the permanent tilt change associated with the development of the subsidence basin in the area of TM-6 is approximately 50 % less than TM-7.

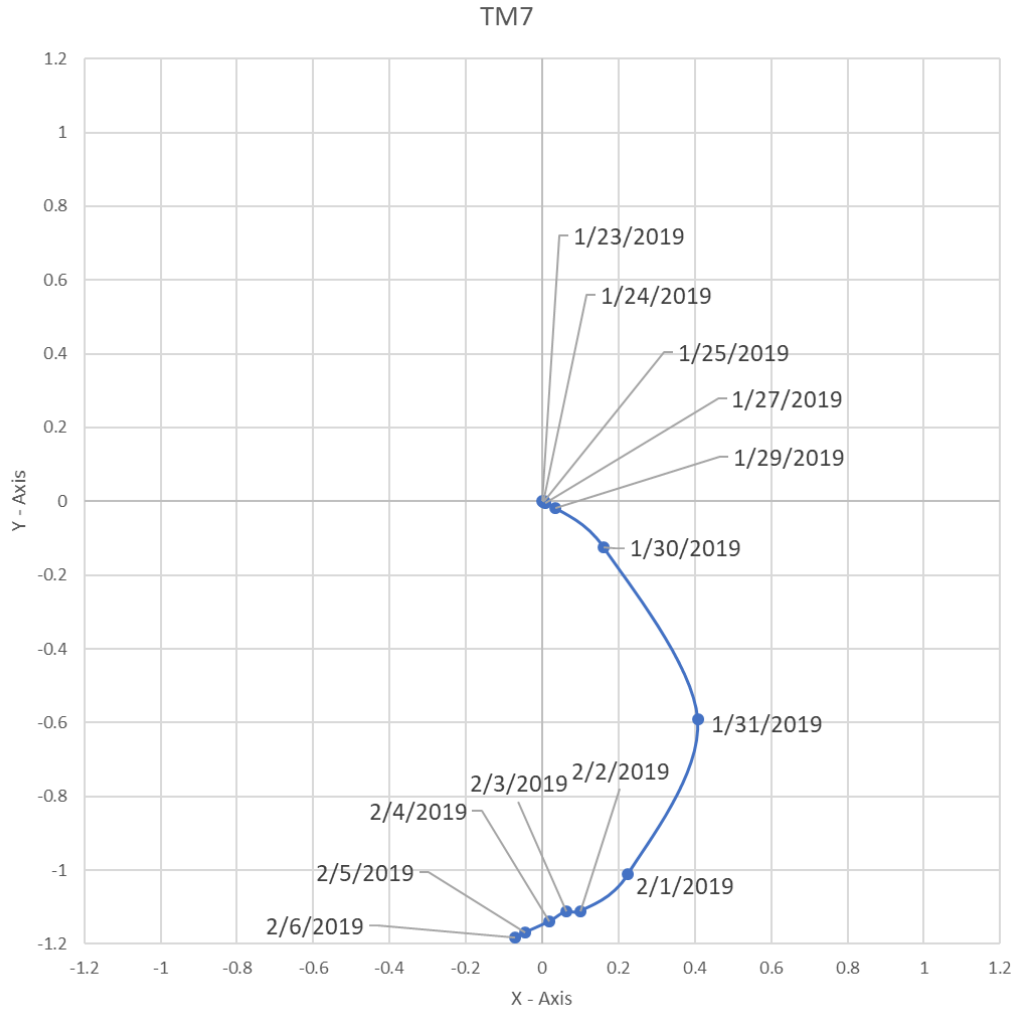


Figure IIIe.4 – Tilt measurements of TM-7 as undermining occurred

Figure IIIe.5 plots the movement of TM-8. The borehole for TM-8 is located close to the edge of the panel and therefore experienced far less dramatic tilt changes when undermining took place. It was not until 29 January, when the longwall face was approximately 300-ft passed the instrument that the tiltmeter began to move in the Y+ direction, and slightly in the X+ direction. In other words, it began to point away from the center of the basin and opposite the direction of mining. On 31 January when the face was approximately 430-ft passed the instrument, it reached its maximum in both the X+ and Y+ direction, and after this date it reversed direction. Like TM-6 and TM-7, TM-8 settled close to the same value on the X-axis and around 0.1-degrees in the Y+ direction. It settled around 3 February when the longwall face was approximately 660-ft away.

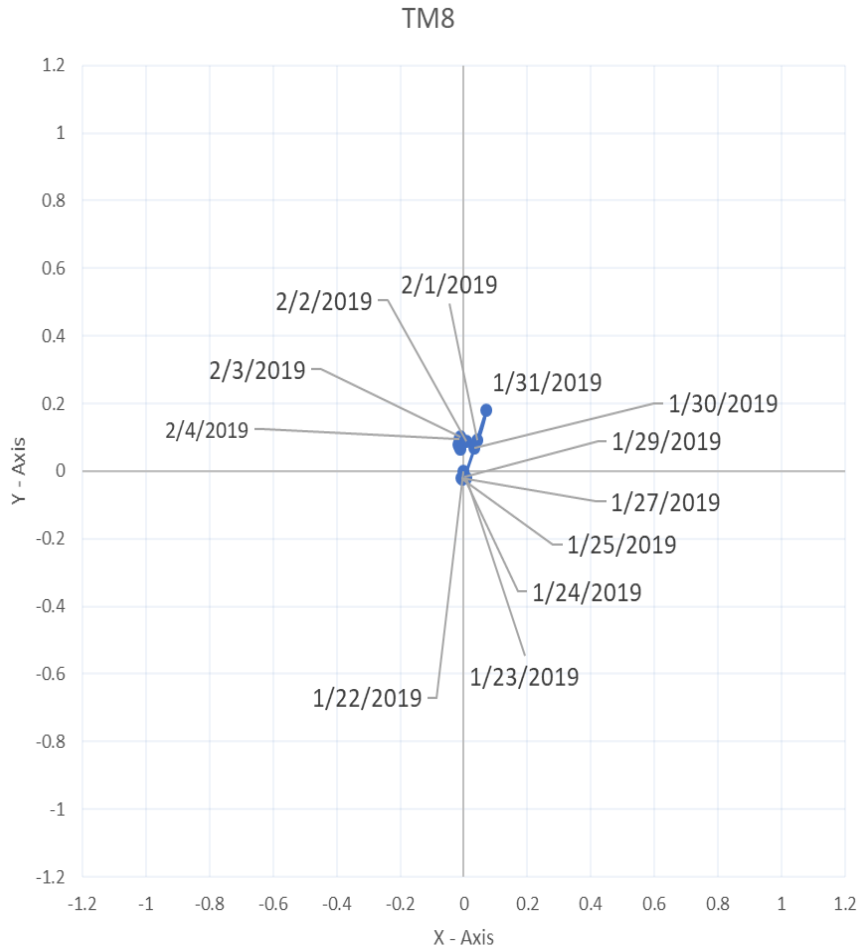


Figure IIIe.5 – Tilt measurements of TM-8 as undermining occurred

Figure IIIe.6 is depicting a map that displays the movement of the tiltmeters seen in the previous three scatterplots. The map contains vectors of the movements displayed over the tiltmeters, as well as the face positions on the dates when this section was undermined. The vectors and face positions were colorized so that it is possible to analyze when the movements were occurring and where the face position started on that day.

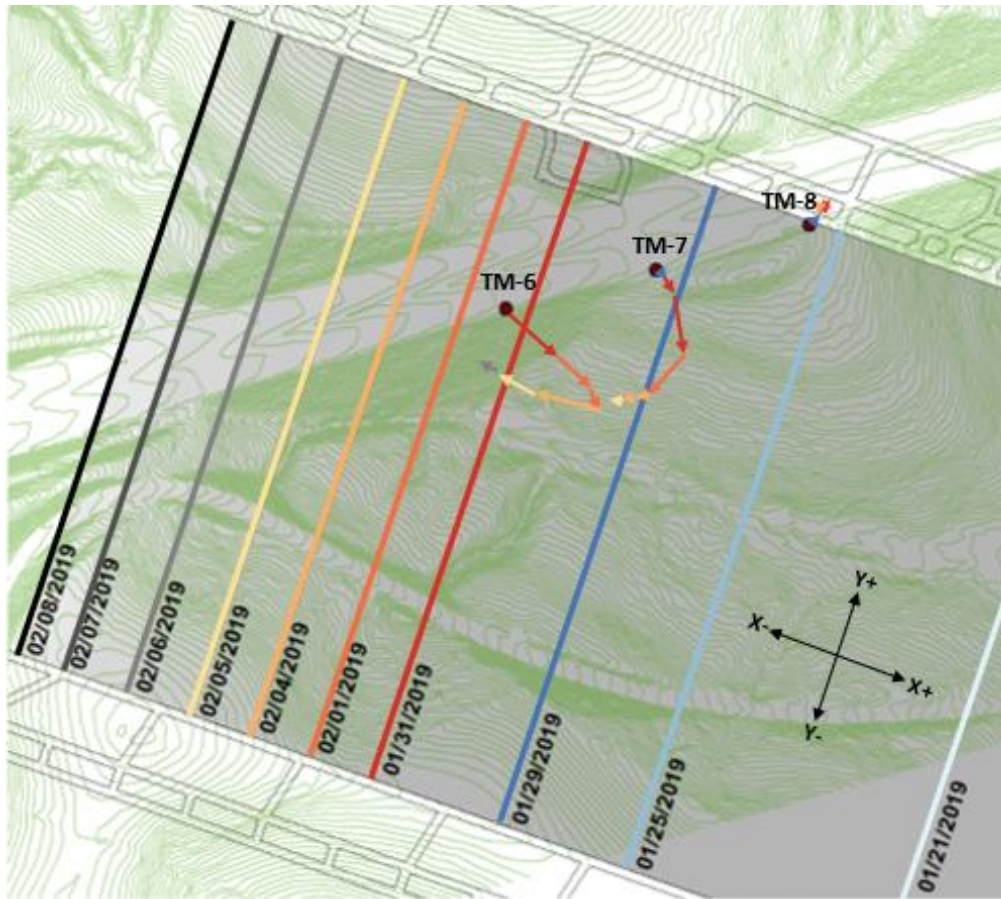


Figure IIIe.6 – TM-6, TM-7, and TM-8 vector representations of instrument tilt with respect to longwall face position

Aside from TM-8, which experienced a very small degree of tilt away from the basin, the general trend seen was tilt in the direction of the center of the basin. The severity of movement varied based on where in the basin the tiltmeter is placed. TM-7 experienced the highest degree of tilt in the Y- direction. This could be expected as it is located very close to the inflection line (Figure IIIe.2), which is where a higher degree of slope was expected. Finally, TM-6 experienced the highest degree of tilt on the X-axis, but ultimately settled with a smaller change in the Y- direction when compared to TM-7.

2.2 Tiltmeters with Data Loss (TM-2, TM-3, TM-4, TM-5, TM-9)

As has been noted, TMs 1-5 lost data during the times in which they were undermined. This means that TM-9 also lost data, as that is the same instrument that was used in TM-1. As a result, a complete analysis cannot be performed on their movements during undermining. However, it is still possible to observe the tilt positions of these instruments before and after undermining, as the data was still present at these times. Figure IIIe.7 displays the locations of each tiltmeter that lost data as well as the longwall's face position when the data was overridden.

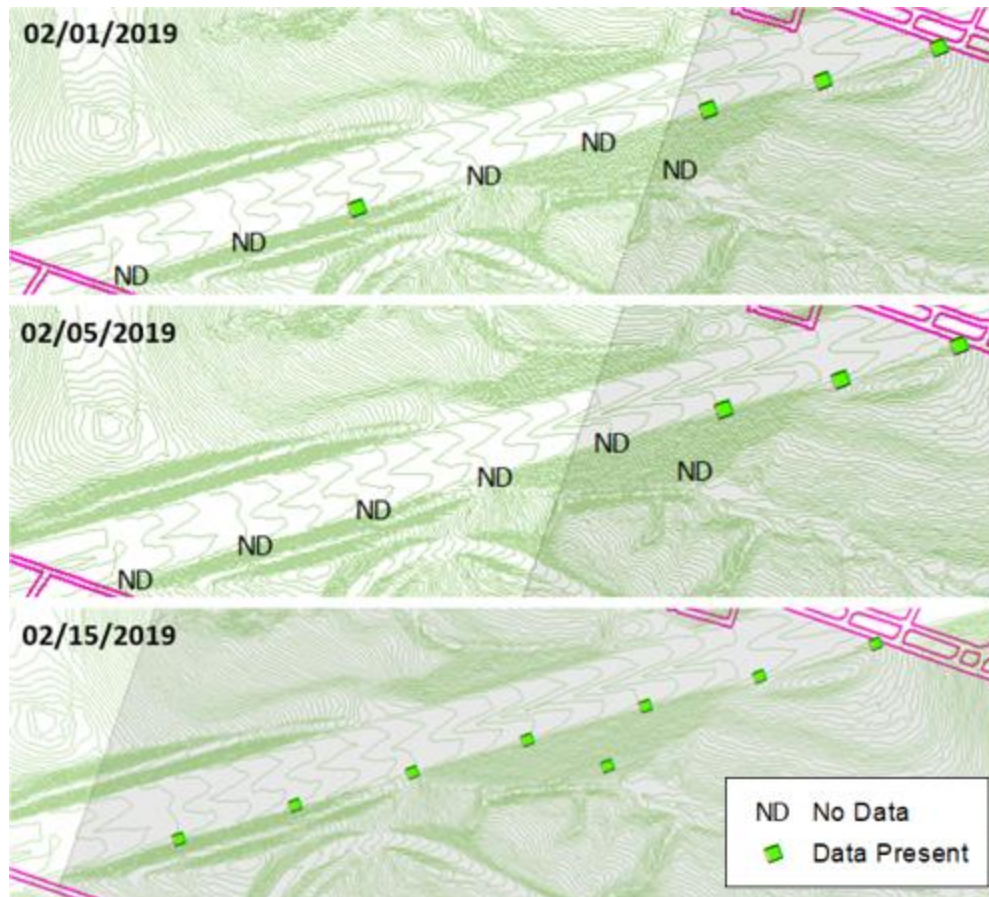


Figure IIIe.7 – Locations of tiltmeters with the timetable of when data was or was not lost

As seen above, the tiltmeters first experienced this loss of data on 1 February. On this date, the longwall face had just progressed beyond TM-9. Data was not present again until 15 February, at which point the longwall face was already approximately 230-ft past TM-2. As stated, it is still possible to analyze the tilt positions from before and after undermining for tiltmeters 1-5. Just like for TMs 6-8, their data was plotted and examined by date.

TM-9 readings were present until the day it was undermined. On this day, TM-9 began to tilt into the basin in the X+ direction. After this point, it lost its readings until 15 February. Once the readings were present again, it indicated movement had settled further in the X+ direction. Very little change in tilt was present on the Y-axis. It is unclear what movements occurred in the times that data was not present, but if it reacted similarly to the movements seen in TM-6 and TM-7, then it is possible that it moved even further in the X+ direction before reversing closer to its origin. The final tilt position indicated the slopes tilted outwards and down the slope, which would align with the expectation that the embankment slopes would shift away from the interstate. Figure IIIe.8 displays the plot for TM-9.

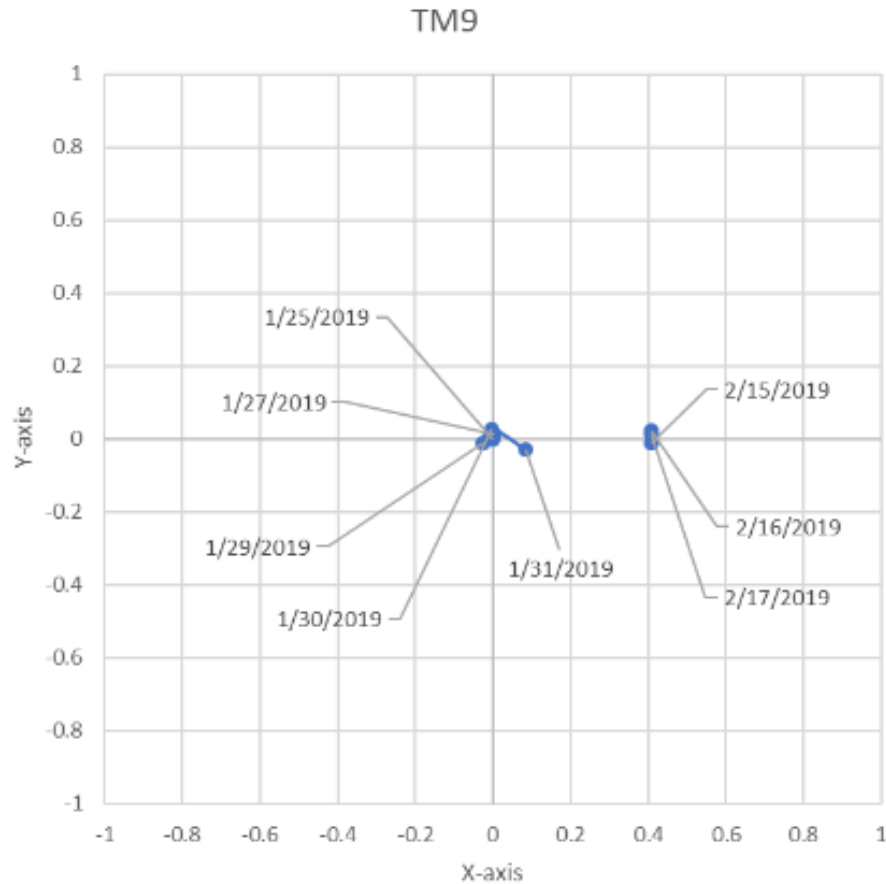


Figure IIIe.8 – Tilt measurements of TM-9 before and after undermining

Tiltmeters 2-5 each lost data during the entirety of their undermining, so only before and after tilt positions can be compared for these instruments. TM-5 was located near the center of the basin and on top of Embankment #1. No movements were present before the override. Once the readings were present again, the plot indicated movement toward the center of the basin, with predominant tilt in the Y- direction and less severe tilt in the X+ direction. The movements for TMs 2-5 are all displayed in Figure IIIe.9.

TM-4 was located very close to the center of the basin in between Embankment #1 and the cut slopes of the bedrock. The readings for TM-4 indicated little differences in tilt before and after undermining. Assuming there was movement in this location, this would indicate the tilt settled close to its zero-point reading from before undermining.

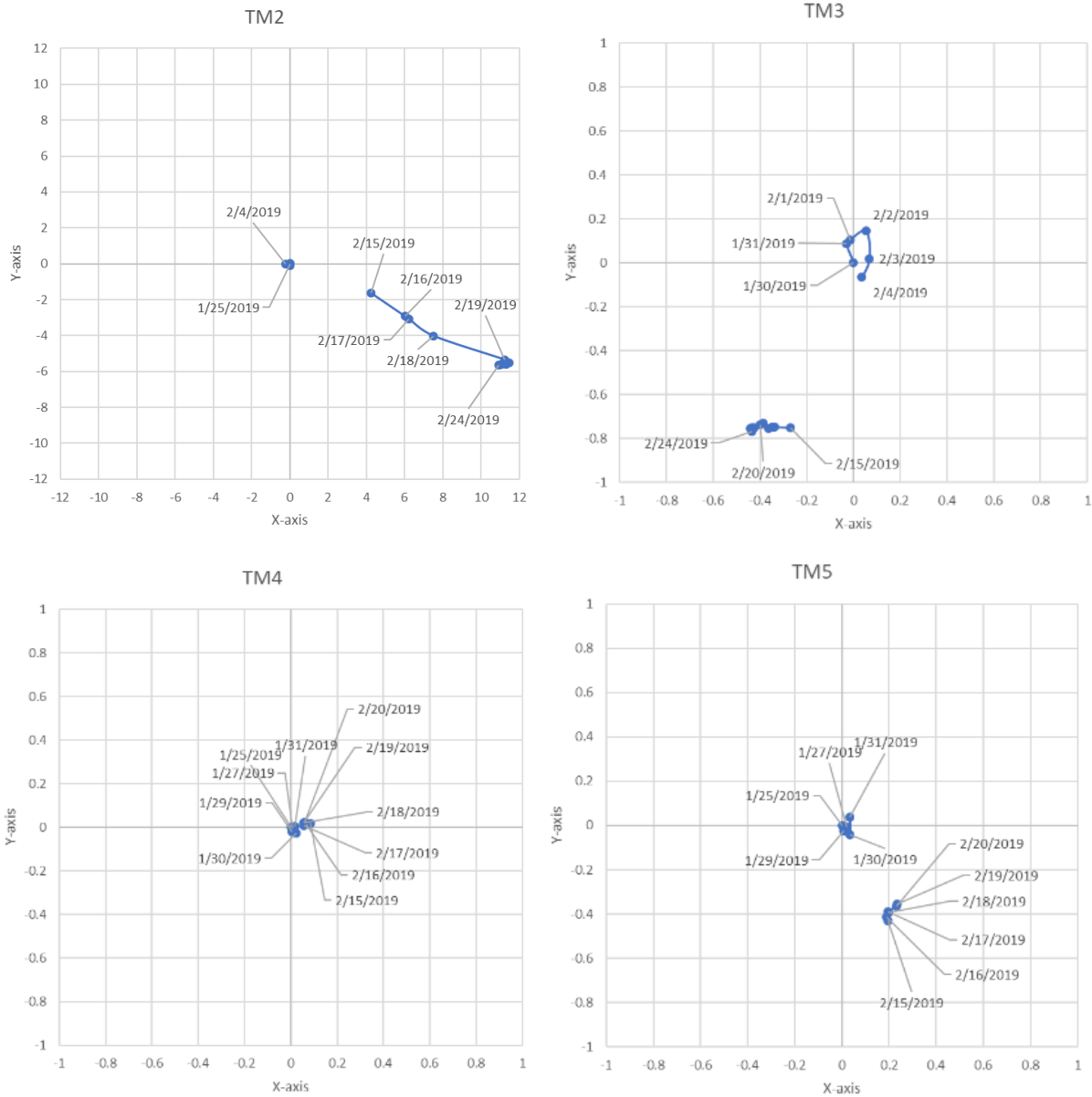


Figure IIIe.9 – Tilt measurements of TM-2, TM-3, TM-4, and TM-5 before and after undermining

TM-3 was located closer to the center of the bedrock towards the western portion of the study area. Small levels of movements were detected for TM-3 before data was lost. At this point, the longwall face was still approximately 600 to 700-ft away from its location. When the readings were present again, the tilt indicated it had moved in the Y- and X- directions. This would certainly not be expected as movement in the Y- direction at this location indicated the surface was tilting further away from the basin.

TM-2 was located in the center of the bedrock and was approximately 200-ft from the edge of the longwall panel. As expected, no movements were detected before data loss. Once the data was present again, the readings appeared to be anomalous. Tilt readings displayed differences of

approximately 10 degrees from its zero point. The University determined this was due to a miscalibration to the instruments. This determination is based on the fact that the majority of differences were within approximately one degree for the other tiltmeters.

Vector representations for TB-2, TB-3, TB-4, TB-5, and TB-9 are depicted on a map of the study area in Figure IIIe.10. The vectors and the longwall face positions were again colorized so that movements could be analyzed in relation to where the face position was on that day. The yellow lines in Figure IIIe.10 represent the direction that tilt moved before and after data was lost. TM-2's readings are not displayed as they are believed to be miscalibrations.



Figure IIIe.10 – TB-2, TB-3, TB-4, TB-5, and TB-9 vector representations of instrument tilt with respect to longwall face position

Subsection IIIf – Piezometer Data

Some variation was observed in the ground water table in Embankment #1 during the period of the mining activities of Panel 15 according to the piezometer recordings. The locations of the utilized three piezometers are shown in Figure IIIf.1.

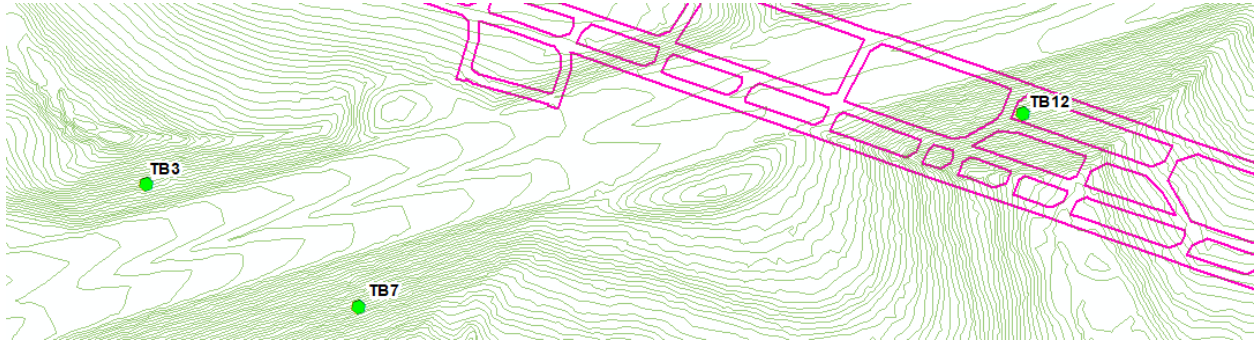


Figure IIIf.1 – Locations of three piezometers

Figure IIIf.2 indicates the piezometer measure of the elevation of the water level in TB-3, TB-7 and TB-12, which were utilized to measure the water level at the north slope of Embankment #1, south slope of Embankment #1, and south slope of Embankment #2, respectively. For the cross section 720+50, the University looked at the piezometer at TB-7. While for the cross section 720+00, the piezometer at TB-3 was analyzed.

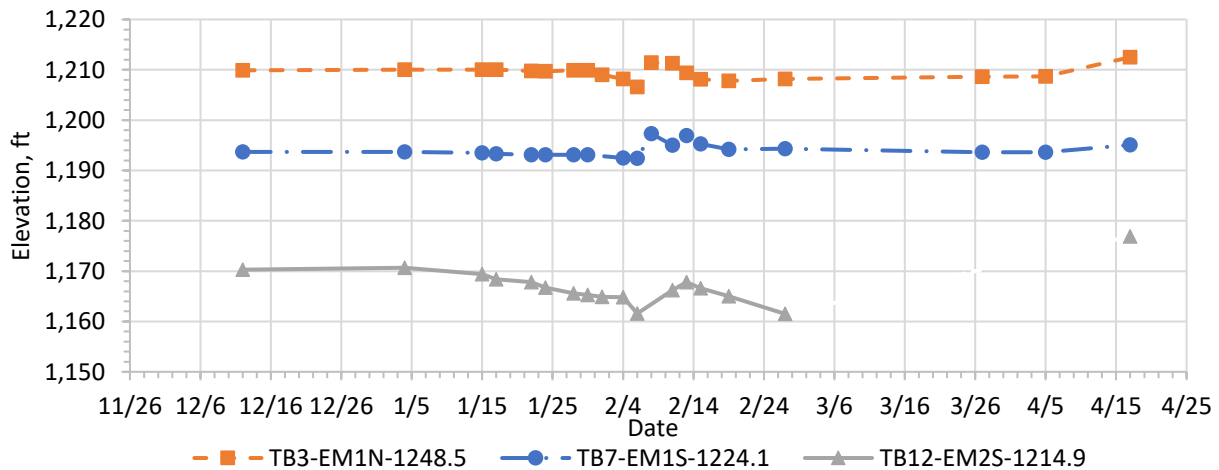


Figure IIIf.2 – Variations of the water levels due to longwall mining from 12 December 2018 to 17 April 2019

This figure demonstrates that the water level in all three boreholes drop below the typical level and then spike to greater than the normal water level before returning to the original water elevation. This movement of the water table is directly related to the passage of the longwall face and the disruption of the underground strata. An in-depth analysis of the piezometer data in

relation with the rainfall data, the longwall face position, and the behavior of the embankments can be found in Section Vd.

Subsection IIIg – LiDAR Accuracy Assessment

The University performed an accuracy assessment on the LiDAR data and its stated accuracy of 0.4-in (1-cm). The University was hesitant that this level of accuracy had been accomplished due to concerns that were raised about the movement of the control points that were used to position the LiDAR surveys. T3 Global Strategies assured the University that, despite these movements, each scan was controlled by the updated locations of each control point, so each scan should be accurate to itself to 1-cm. Despite this assurance, the University conducted an assessment to confirm the accuracy of the surveys. To conduct this assessment, the University compared the positions of the LiDAR control points to the positions of the highway alignment points that were tracked via GPS surveys. The highway alignment points are said to have an accuracy of **0.25-in**, while the accuracy of the LiDAR control points is said to have an accuracy of **0.4-in** (1-cm). This makes for a combined accuracy of **0.65-in**.

1.0 Highway Alignment Surveys

PennDOT surveyors were responsible for the GPS tracking of the pins that were placed along the shoulder of I-70. These GPS measurements were taken every week while the interstate was undermined. The exact dates of each survey are listed below:

- 15 January 2019
- 29 January 2019
- 5 February 2019
- 14 February 2019
- 19 February 2019
- 7 March 2019
- 26 March 2019

As stated, each GPS point is said to have an accuracy of 0.25-in. The highway alignment pins are located approximately 50-ft apart.

2.0 Mapping Control Survey (MCS)

PennDOT contracted T3 Global Strategies to perform LiDAR surveys over the surface of the highway. To control these surveys T3 Global set up a Mapping Control Survey (MCS). The locations of the stations in this survey were taken around the dates of every LiDAR scan. These were taken on the following dates:

- 21 June 2018
- 3 January 2019

- 15 January 2019
- 21 January 2019
- 28 January 2019
- 4 February 2019
- 12 February 2019
- 18 February 2019
- 25 February 2019
- 19 March 2019

The point clouds produced from each scan are said to have an accuracy of about 0.4-in, or 1-cm.

3.0 Control Point Movement

The MCS included stations located far beyond the outer extents of the longwall panel. It was set up this way so that it would contain points that were not expected to experience any subsidence impacts. After the undermining took place beneath I-70, T3 Global Strategies informed the University that several far-field stations experienced unexpected movements. The points that were the biggest surprise were points L171 and L173. Station L171 was located approximately 1300-ft from the eastern edge of the panel on the West Alexander bridge overpass, while L173 was located approximately 2,400-ft from the western edge on a concrete sewer structure near the West Virginia welcome center. The locations of these points relative to the study area can be seen in Figure IIIg.1. T3 Global maintained that these points converged approximately 2-in.

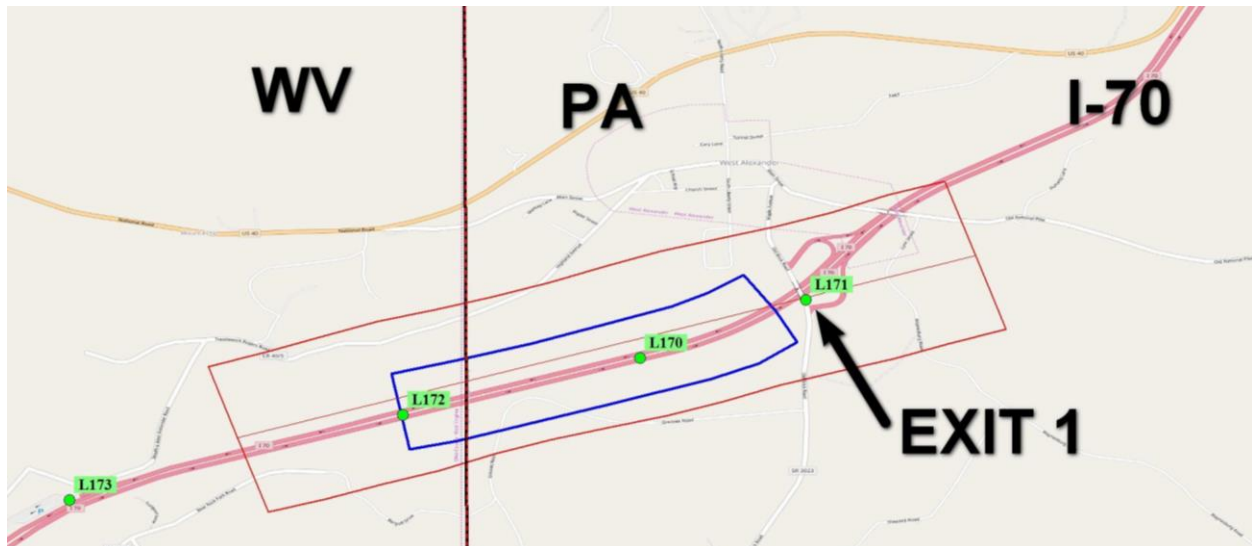


Figure IIIg.1 – Locations of LiDAR control points used for the surveys

4.0 Analysis

To properly assess the accuracy of the Mapping Control Survey used for the LiDAR surveys, the University compared points from this survey to the highway alignment points that were surveyed by PennDOT's survey team. Figure IIIg.2 shows the locations of the Mapping Control Survey station and Figure IIIg.3 shows the locations of the highway alignment points.

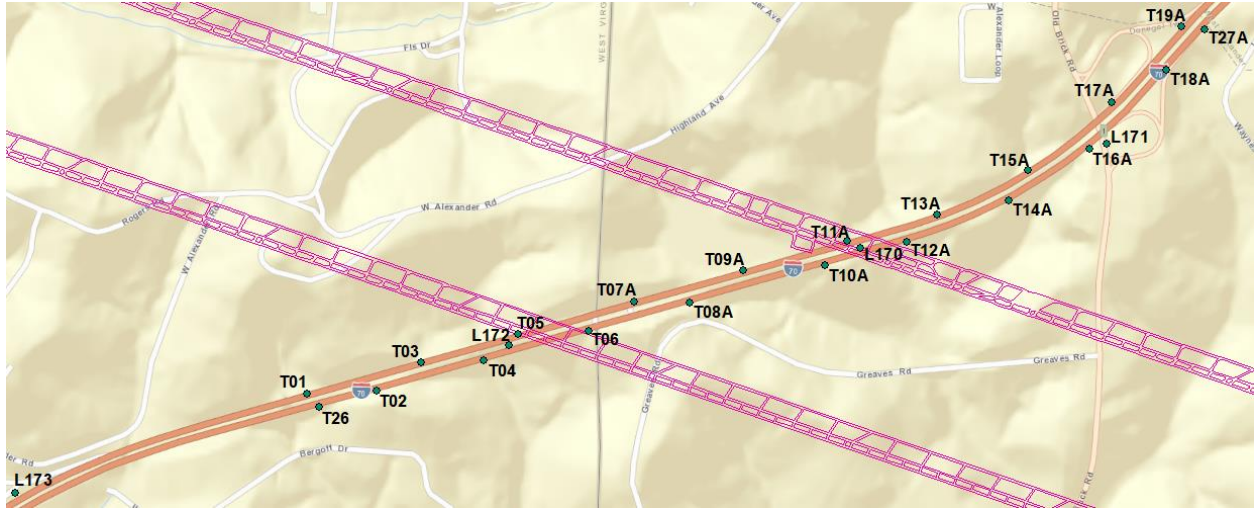


Figure IIIg.2 – Mapping Control Survey (MCS) points

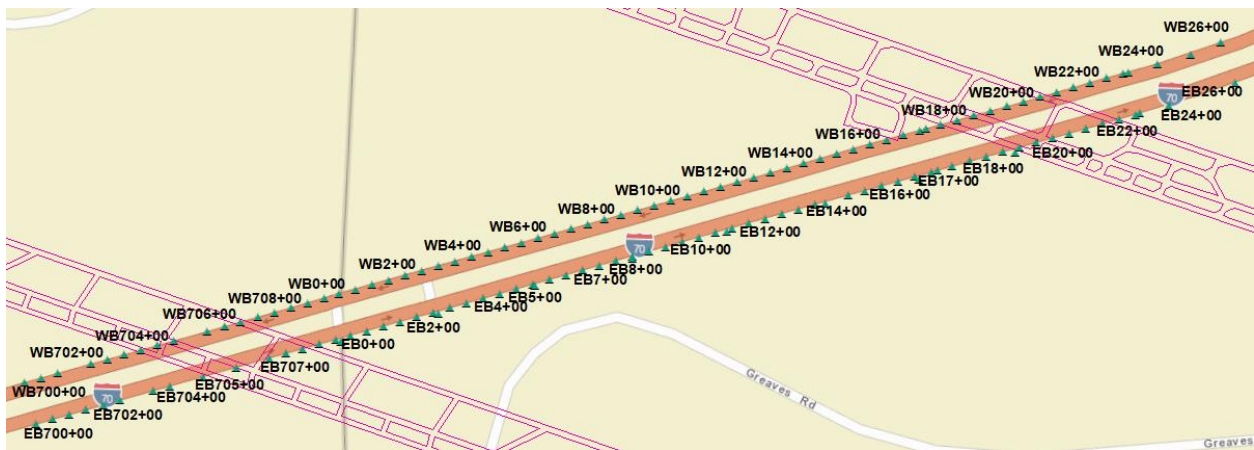


Figure IIIg.3 – Highway Alignment Points

There were four circumstances where the same station was used in both the Mapping Control Survey and the Highway Alignment Surveys. One of these stations was labeled “EB17+50BK” in the Highway Alignment Survey and “T10A” in the LiDAR control survey. The University assumed the point in both datasets were of the same station as they were only 1.1-in (2.9-cm) from each other, which is above the combined range of accuracy, but still very close. Since the same point was used in both surveys, the University was able to compare the location of the point as subsidence impacted that station.

Figure IIIg.4 depicts graphic representations of this point through time in both datasets. It also shows an image taken showing the pin and markers for the MCS. The pins and markers are color coated according to the date of the surveys; red indicates the pre-mining survey (15 January 2019) and blue indicates the post-mining survey (19/26 March 2019). The circles represent the LiDAR control points, the triangles represent the highway alignment points, and the polygons represent the station markers observed in the LiDAR point cloud. The ability to see these markers in the point clouds allowed for the digitization of the markers and for them to be compared to their control points. As the image shows, the pin is located in the center of the box marker and at the end of the arrow. In both surveys, the control points are located very close to their actual positions.

Of the four stations that were surveyed on 15 January, the average point separation was 0.65-in (1.6-cm), which is the exact number for the combined accuracy of the surveys. For the post-mining surveys, the average point separation was 1.43-in (3.6-cm). This number is considerably higher than the combined accuracy of the surveys, however, since these surveys were taken a week apart from each other, the increase in separation could be due to continued movement on the surface. Based on these results, the University can conclude that the stated accuracy of 1-cm for the LiDAR surveys was achieved and that it is now comfortable carrying on with the appropriate analysis of the LiDAR data.

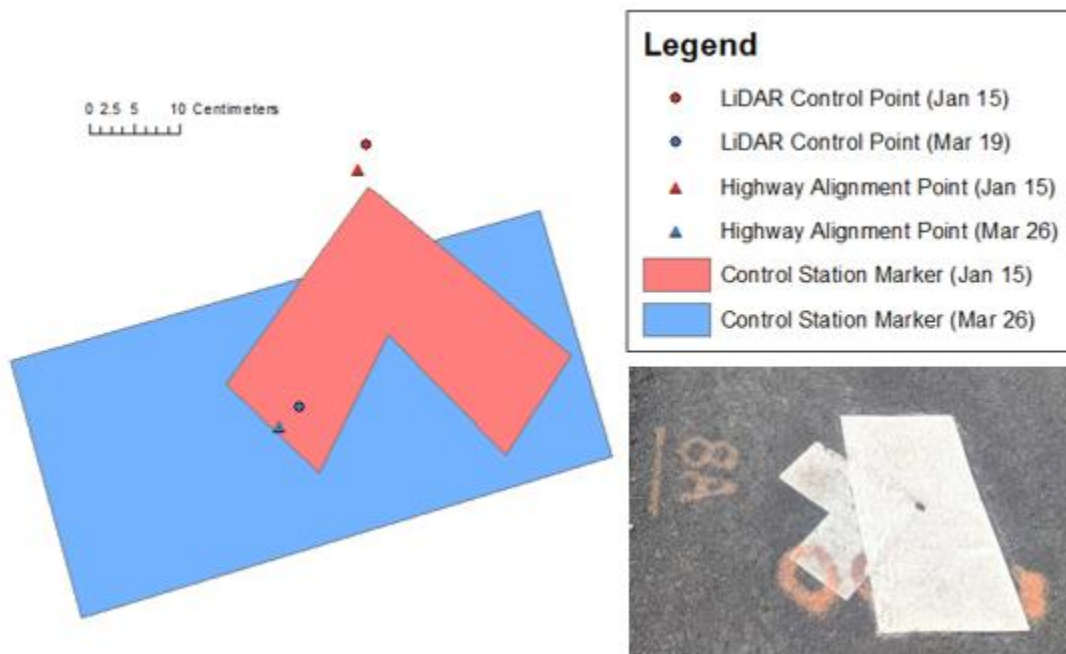


Figure IIIg.4 – Locations of station “EB17+50BK”/”T10A” before and after subsidence impacts

The analysis above focuses on the horizontal accuracy of the control network used for the LiDAR scans. A vertical accuracy assessment of the LiDAR scans was also performed for each survey. The results indicate sub centimeter accuracies, with the exception of scan on 10

February, which had a mean vertical accuracy of 1.1-cm. The vertical accuracies for each scan are depicted in Figure IIIg.5. Vertical accuracy assessments were performed by computing the distance of the control points collected in the GPS surveys to the control points as they appeared in the point clouds. The vertical accuracy assessments were performed by ESP Associates, the contractor responsible for conducting the LiDAR surveys. The results displayed in Figure IIIg.5 are derived from the results given in each LiDAR validation report that was delivered to the University.

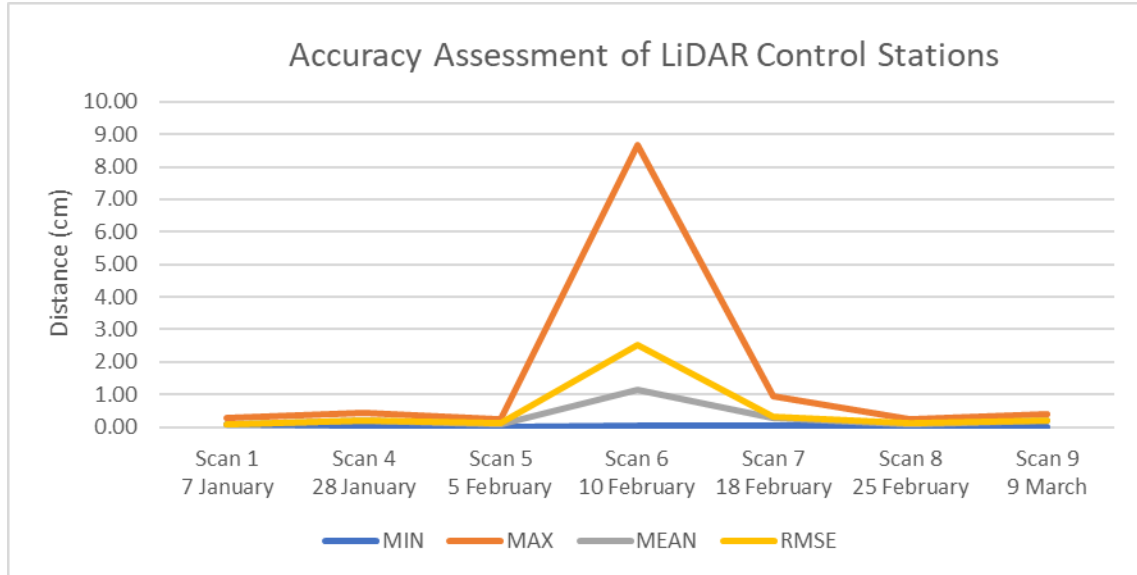


Figure IIIg.5 – Results of the Vertical Accuracy Assessments

SECTION IV – CHARACTERIZATION OF SUBSIDENCE BASIN

Subsection IVa – Subsidence Movement Explained Through Survey Data and Observations

Panel 15 in the Tunnel Ridge Mine undermined a section of I-70 adjacent to the West Virginia border. Data was collected throughout the undermining process and can be used to explain the movement of the ground surface from the subsidence event.

1.0 Final Subsidence Basin Movement

Traditionally, a longwall subsidence basin is bathtub shaped. The panel subsides symmetrically along the long and short axis. The ground surface elevation drops by the maximum vertical subsidence in the center of the panel and then slopes up to the original ground elevation beyond the longwall panel. As a result of this extension and bending of the ground surface, the points on the surface move on the horizontal plane towards the center of the longwall panel.

1.1 Vertical Subsidence

Survey data was compiled from the highway alignment points and the slope points. These points can be analyzed to determine the final subsidence of the highway surface and the adjacent slopes. Figure IVa.1 shows the final subsidence throughout the study area.

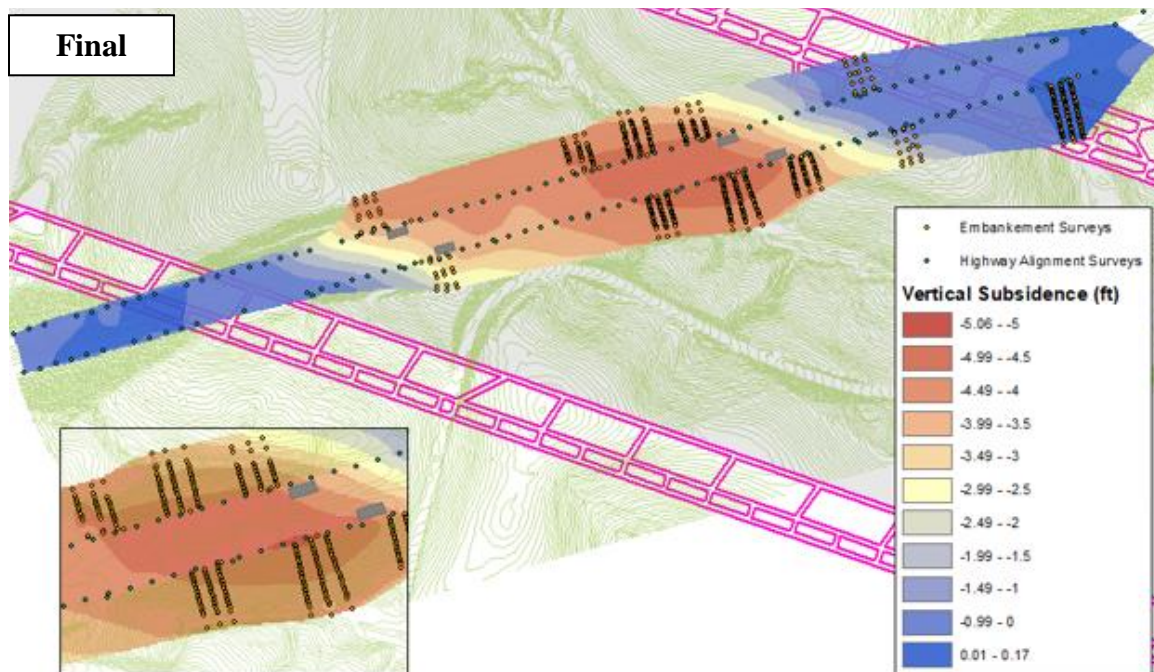


Figure IVa.1 – Final vertical movement of I-70 caused by Panel 15 subsidence

As can be seen in this figure, the majority of subsidence occurred over Embankment #1 on the highway surface.

1.2 Horizontal Movement

The highway alignment points and slope points can also be combined to analyze the movement of the highway surface and the adjacent slopes in the horizontal plane. Figure IVa.2 shows the final horizontal movement throughout the study area.

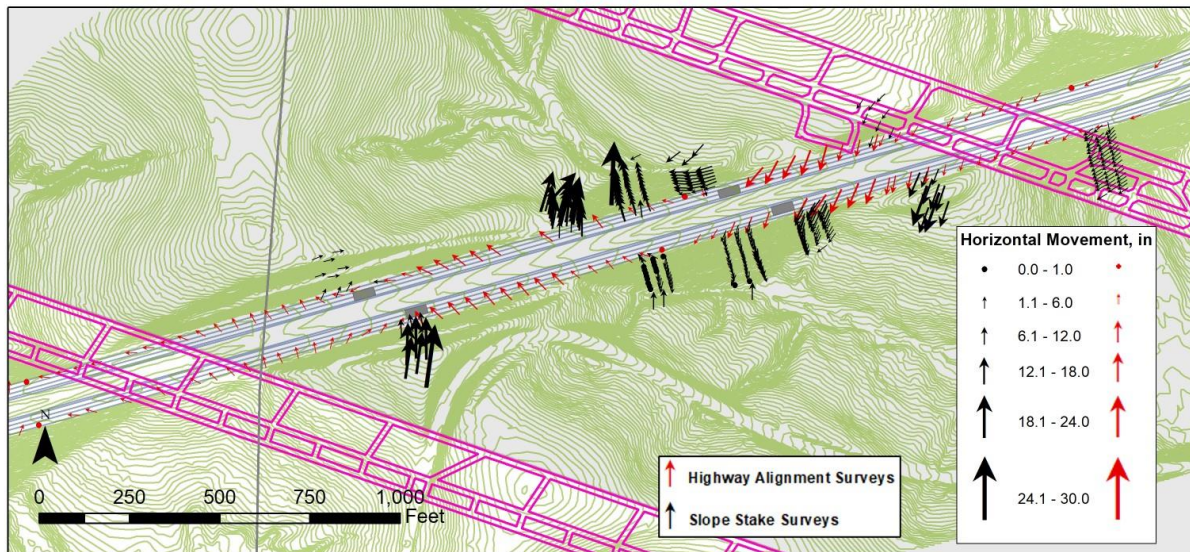


Figure IVa.2 – Final horizontal movement of I-70 caused by Panel 15 subsidence

This figure shows the magnitude and direction of horizontal movement of all of the points surveyed during the undermining. The maximum horizontal movement was observed at the bottom of the northern slope of Embankment #1. The point at this location moved over 2-ft north in the horizontal plane, which indicates movement out from the slope.

Overall, more horizontal movement was observed on the slopes than on the highway surface. The western side of northern slope of Embankment #1 moved primarily in the north-northeast direction at large magnitudes, showing that this the embankment slope is moving outwards from the core of the embankment. Though this movement is not towards the center of the basin, it can be explained by a spreading phenomenon of the embankment when subjected to subsidence. The opposite side of the embankment also show movement primarily moving outward from the core of the embankment, but at significantly lower magnitudes. This indicates that more spreading occurred on the northern slope than the southern slope of the embankment.

Unlike the central embankment, the movement of the cut slopes and Embankment #2 are more typical of a traditional subsidence basin. These points moved horizontally towards the center of longwall panel. The point on the southern cut slopes move at larger magnitudes, between 1.5-ft and 2-ft, due to the ground surface sloping from the original elevation to the final subsidence elevation at these locations. This indicates that without the presence of the embankment, the ground likely would've performed as a typical, well-behaved subsidence basin.

The highway surface experienced less horizontal movement, with the maximum movement observed around 1.5-ft. The eastern side of highway surface experienced the most horizontal movement, which was oriented primarily towards the center of the subsidence basin. This direction of movement is typical of a traditional subsidence basin. This movement dissipated at the eastern asphalt relief sections at the edge of embankment #1, which served to absorb the excess movement. The movement over the embankment was minimal and in no specific orientation. The highway surface adjacent to cut slope #1 to the east of the western asphalt relief sections also experienced significant movement. These points moved primarily in a north-west orientation at a magnitude between 0.5-ft and 1-ft. The western asphalt relief sections also dissipated the horizontal movement, causing minimal movement at the western most edge of the study area.

The direction of movement of the highway surface adjacent to cut slope #1 is not typical for subsidence basins. When looking at the magnitudes and directions of all of the movement of the highway surface, it appears that the pavement structure is twisting throughout the study area. Rather than both extents of the highway moving towards the center of the panel, the eastern side of the highway moved towards the center of the panel and the western side of the highway moved parallel to the gate roads towards the longwall face. The pivot point appears to be over the central embankment, meaning that the granular fill material may have absorbed movement and facilitated the twisting.

2.0 Ground Movement caused by Dynamic Subsidence

As longwall mining occurs over time, the subsidence basin forms gradually as a dynamic wave. The dynamic subsidence wave subjects the ground first to tension beyond the face and between the longwall face and the inflection line and then to compression behind the inflection line. This gradual change causes the surface to experience horizontal stresses and strains at different magnitudes and locations than represented by the final subsidence event.

Panel 15 was mined at an average rate of 115-ft/day. The longwall operated on a standard schedule, meaning it did not extract coal on the weekends. There was one unscheduled shutdown day when the panel was underneath I-70.

2.1 Vertical Subsidence over Time

As the longwall face progresses, the ground surface subsides vertically. The ground surface moves gradually as the longwall basin forms. The surveys collected weekly show the progression of the vertical subsidence basin as the longwall face progresses, which can be seen in Figures IVa.3 through IVa.6.

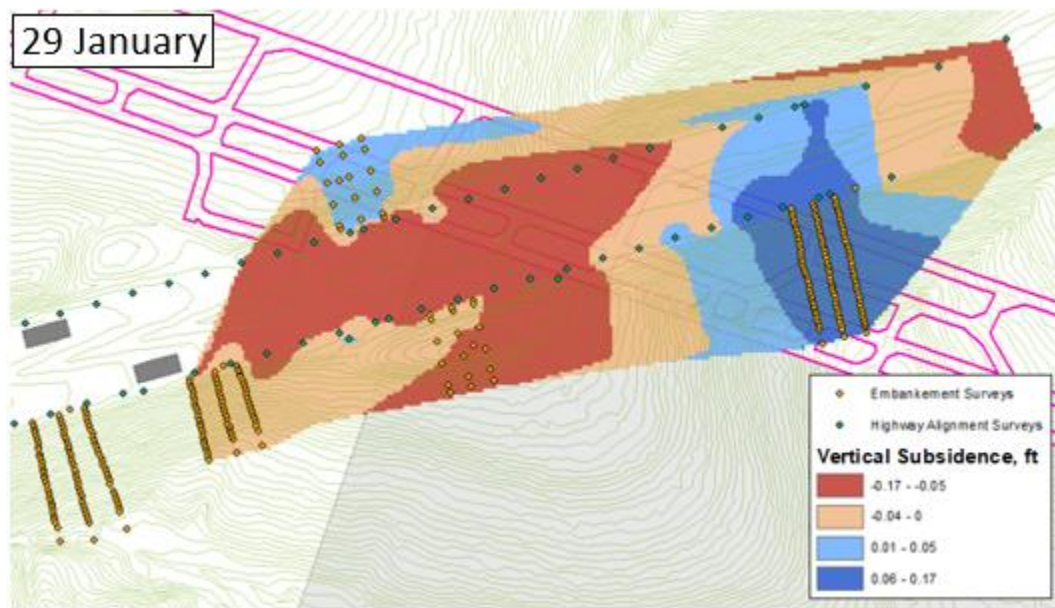


Figure IVa.3 – Vertical subsidence on 29 January 2019

Figure IVa.3 shows very small movements as the longwall face begins to influence the interstate. Up to 0.17-ft of heave was observed over Embankment #2 and up to 0.17-ft of vertical subsidence was observed on the eastern-much portion of the highway alignment. The majority of the movement observed is likely due to noise in the surveys.

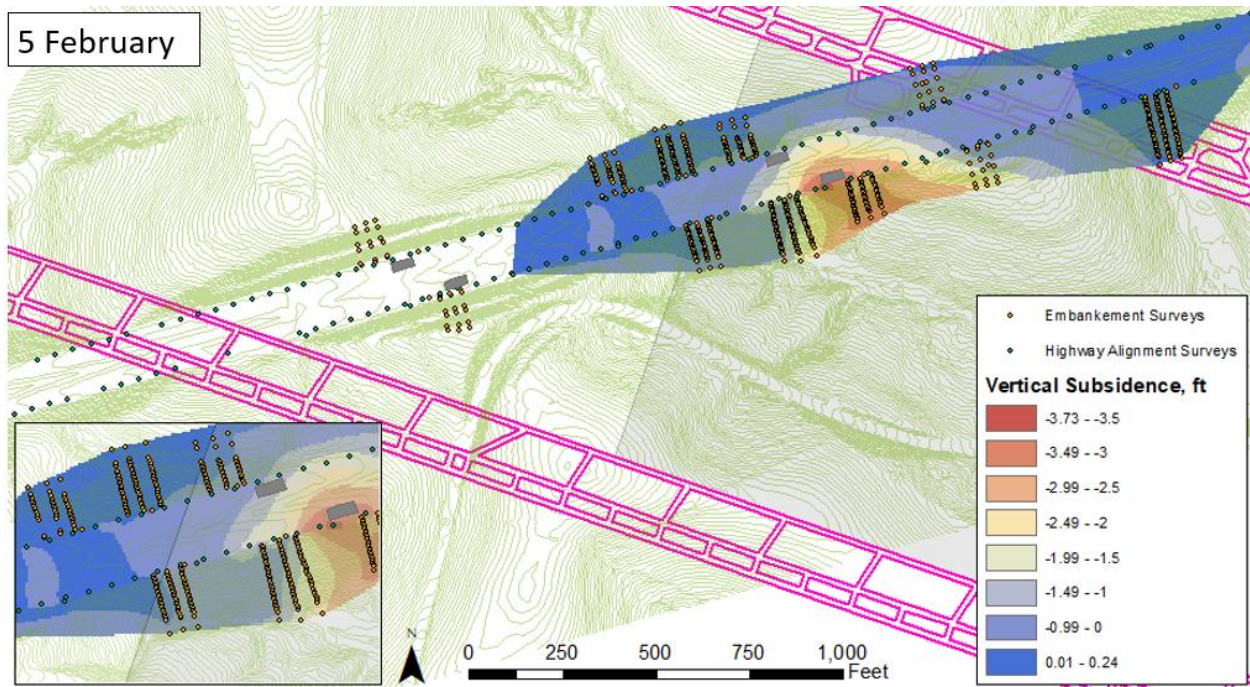


Figure IVa.4 – Vertical subsidence on 5 February 2019

Figure IVa.4 shows the vertical subsidence when the longwall face was below embankment #1. This shows the maximum subsidence of about 3.75-ft at the top of the south slope of embankment #1, occurring about 300-ft behind the longwall face. No point in the study area has reached the maximum predicted subsidence at this point in time. This is due to the fact that the points far enough behind the longwall face to drop to the maximum allowable subsidence are too close to the gate road entries to experience this maximum drop in surface elevation.

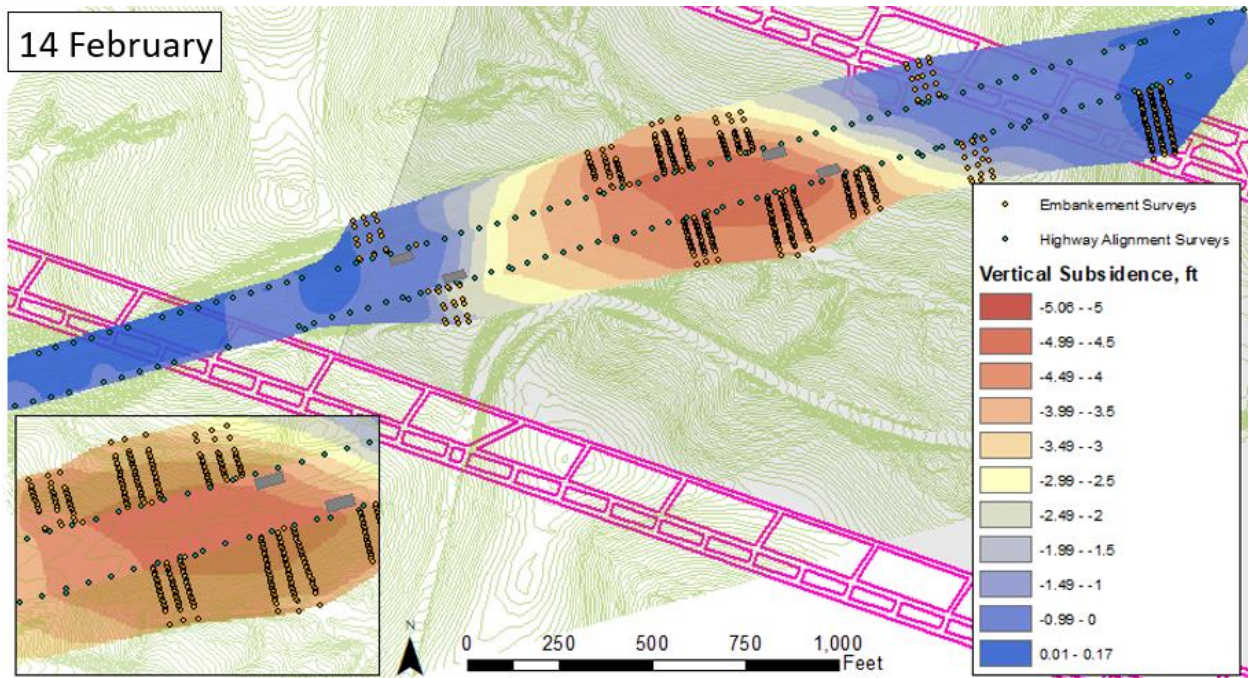


Figure IVa.5 – Vertical subsidence on 14 February 2019

Figure IVa.5 shows the vertical subsidence when the longwall face was just beyond the western asphalt relief sections. At this point in time, a maximum subsidence of about 5-ft was observed over the center of the embankment. The embankment was approximately 650-ft behind the longwall face on 14 February. The entire embankment subsided over 4.5-ft. It can also be seen that the change in surface drop between the gate road and the maximum subsidence occurs in a shorter distance on the eastern side of the study area than the western, meaning the slope is steeper on the eastern half of the study area.

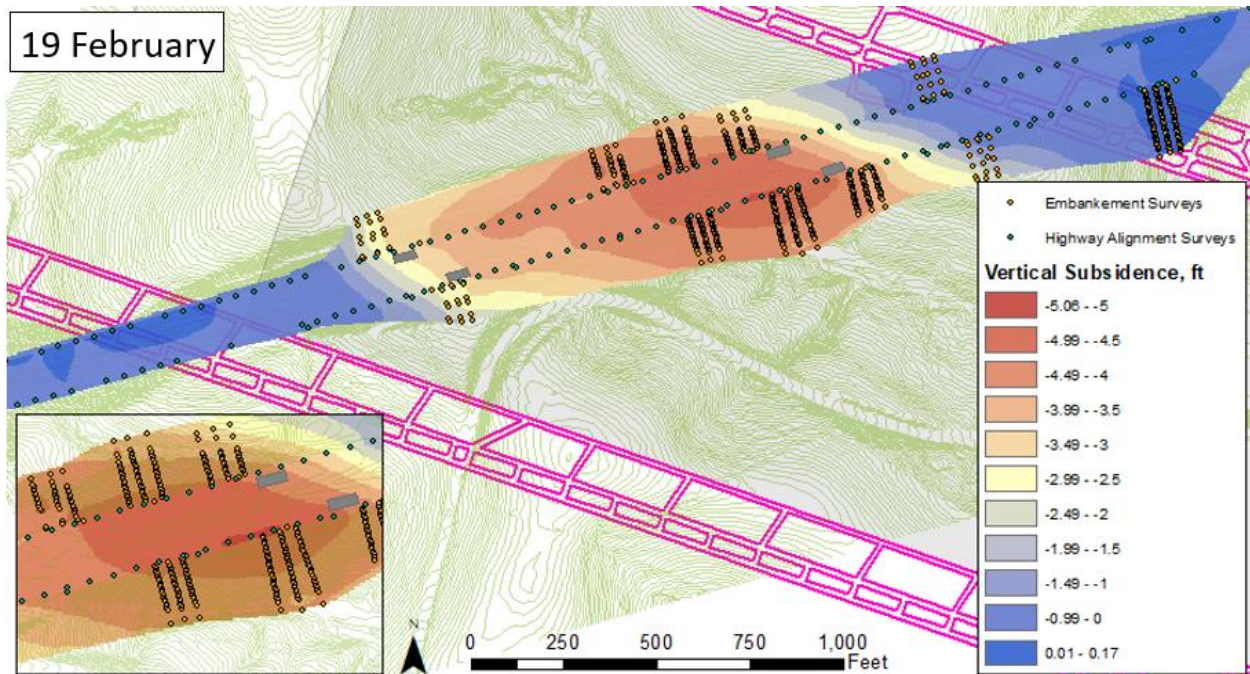


Figure IVa.6 – Vertical Subsidence on 19 February 2019

Figure IVa.6 shows the vertical subsidence when the longwall face was at the end of the highway section. This shows a small area of maximum subsidence of just over 5-ft at the top of the south slope of embankment #1, occurring about 1,200-ft behind the longwall face. By this point in time, the slope on the western side of the study area is closer to that on the eastern side, making the subsidence basin closer to symmetrical throughout the panel. It is also worth noting that small amounts of heave were observed over the gate road entries of the panel.

2.2 Horizontal Movement over Time

As the longwall face progresses, the ground surface also moves horizontally. The ground surface moves gradually as the longwall basin forms. The surveys collected weekly show the progression of the horizontal movement of the subsidence basin as the longwall face progresses, which can be seen in Figures IVa.7 through IVa.10.

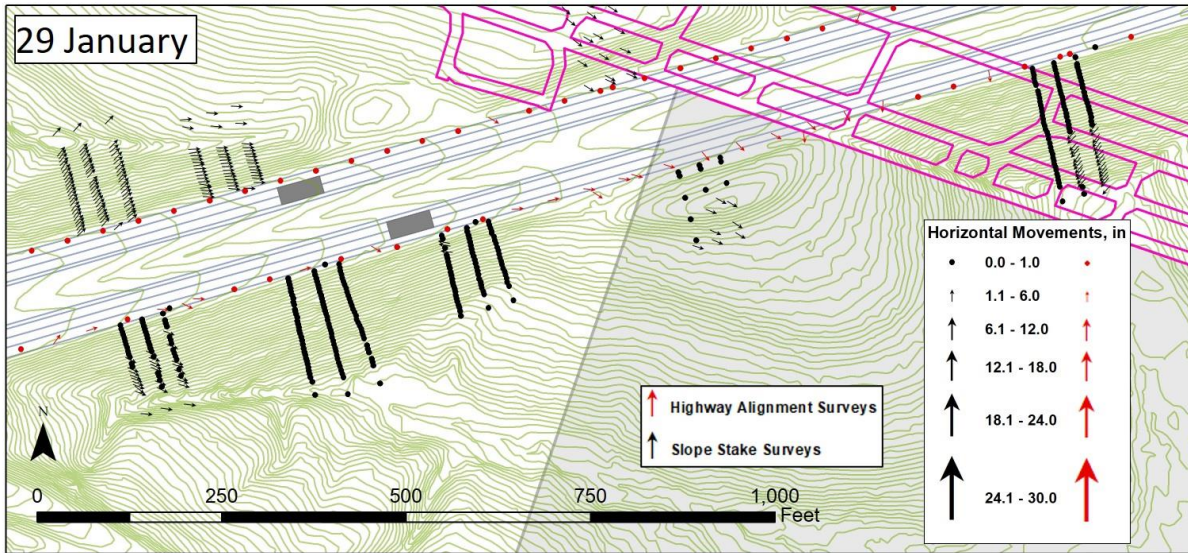


Figure IVa.7 – Cumulative horizontal movement on 29 January 2019

Figure IVa.7 shows the horizontal movement on the eastern portion of the study area on 29 January 2019. As the longwall face is just starting to influence the interstate at this point, the horizontal movements are very small, less than 0.5-ft in any direction. The movement is generally oriented towards the longwall face.

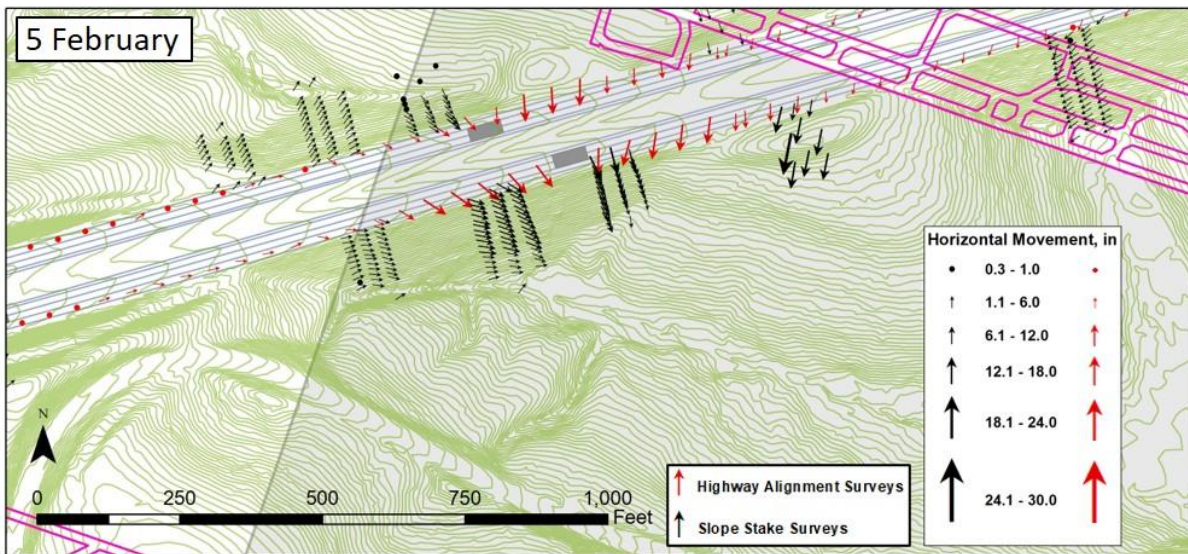


Figure IVa.8 – Cumulative horizontal Movement on 5 February 2019

Figure IVa.8 shows the cumulative horizontal movement of the ground surface on 5 February 2019, when the longwall face was beneath the central embankment. At this point in time, most of the points along the embankments experienced minimal movement, with magnitudes of less than

1-ft. The cut slope nearest to the gate road entries experienced larger movements, with magnitudes of almost 2-ft, oriented towards the center of the longwall panel. This section of highway also experienced significant horizontal movement, with magnitudes around 1.5-ft, oriented towards the center of the longwall panel. These movements on the highway surface are dissipated at the asphalt relief section, causing there to be minimal movement beyond the longwall face.

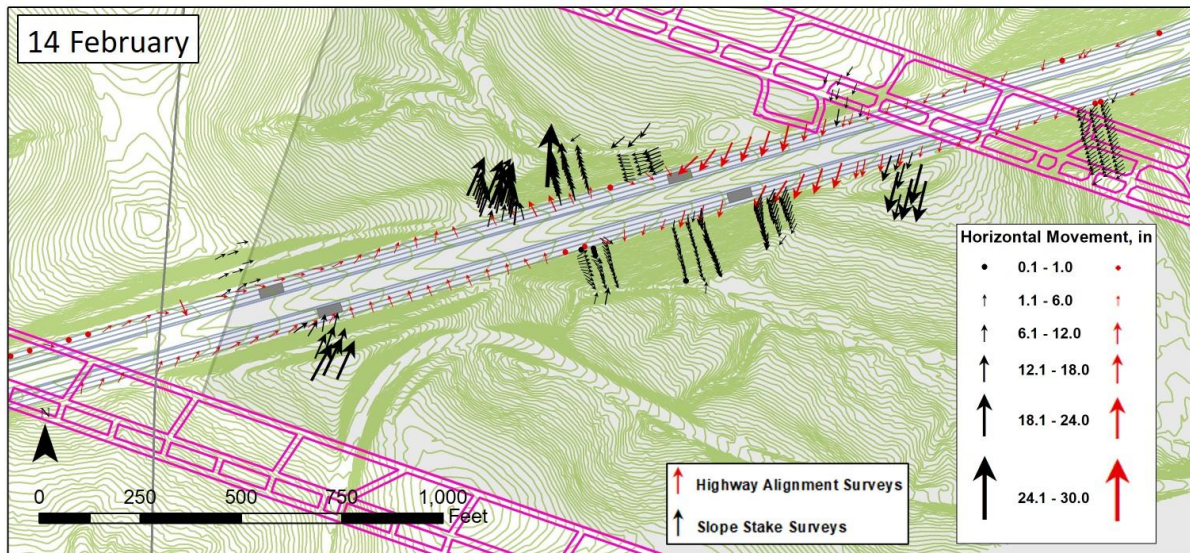


Figure IVa.9 – Cumulative horizontal Movement on 14 February 2019

Figure IVa.9 shows the cumulative horizontal movement of the ground surface on 14 February 2019, when the longwall face was just past the western asphalt relief sections. At this point in time, some of the slopes within the study area had begun to experience significant movement. The northern slope of embankment #1 moved away from the center of the embankment, with magnitudes as high as 2.5-ft. These movements are larger than and in a different orientation than that which would be typically be expected on a longwall panel, but this is likely due to spreading of the embankment. Like on 5 February, the eastern side of the highway surface experienced horizontal movements with magnitudes around 1.5-ft that are oriented towards the center of the longwall panel. These movements are dissipated at the asphalt relief sections, causing there to be very minimal movement west of these relief sections.

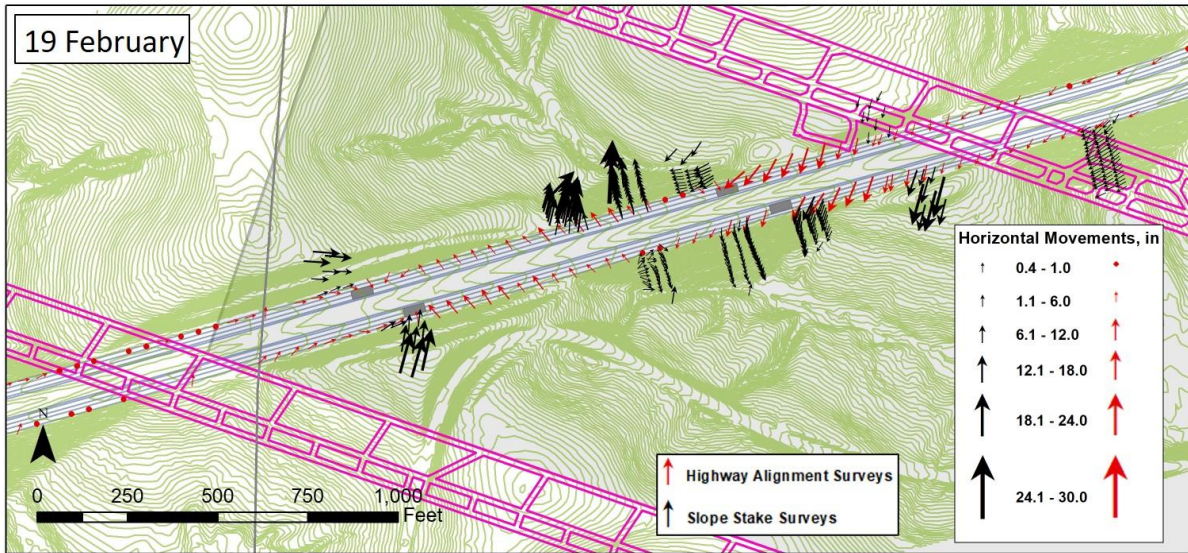


Figure IVa.10 – Cumulative horizontal Movement on 19 February 2019

Figure IVa.10 shows the cumulative horizontal movement within the study area on 19 February 2019 when the longwall face was at the end of the area of highway influence. At this point in time, most of the slopes within the study experienced significant movement. The northern western cut slope moved away from the longwall face with magnitudes of movement up to 1.5-ft. The movement of the remainder of the slopes remained mostly unchanged from that observed on 14 February. The movement observed on the highway surface had magnitudes of up to 1.5-ft on the eastern side of the study area oriented towards the center of the basin and up to 1-ft on the western side of the study area oriented towards the longwall face. These movements were dissipated at the asphalt relief sections, causing the areas just west of the asphalt relief sections to experience minimal horizontal movement.

The horizontal movements can also be examined incrementally between surveys. The incremental movements can be seen in Figure IVa.11. As this figure shows, the eastern side of the highway surface experienced the majority of movement between 29 January and 5 February, when it was about 150-ft behind the longwall face. The western side of the highway surface experienced the majority of movement weeks later between 19 February and 7 March, when the longwall face was far beyond the movement area. It is also worth noting that between 5 and 14 February, there was significant change in the direction of the horizontal movement adjacent to the southern slope of embankment #1. Embankment #1 experienced the majority of movement between 5 and 14 February, when the longwall face was approximately 550-ft beyond the embankment. The western cut slopes each experienced the majority of movement when the longwall face was approximately 250-ft past the points. By looking at the movements of the surface incrementally, it is evident that the progression of the longwall face has a significant impact on the horizontal surface movements.

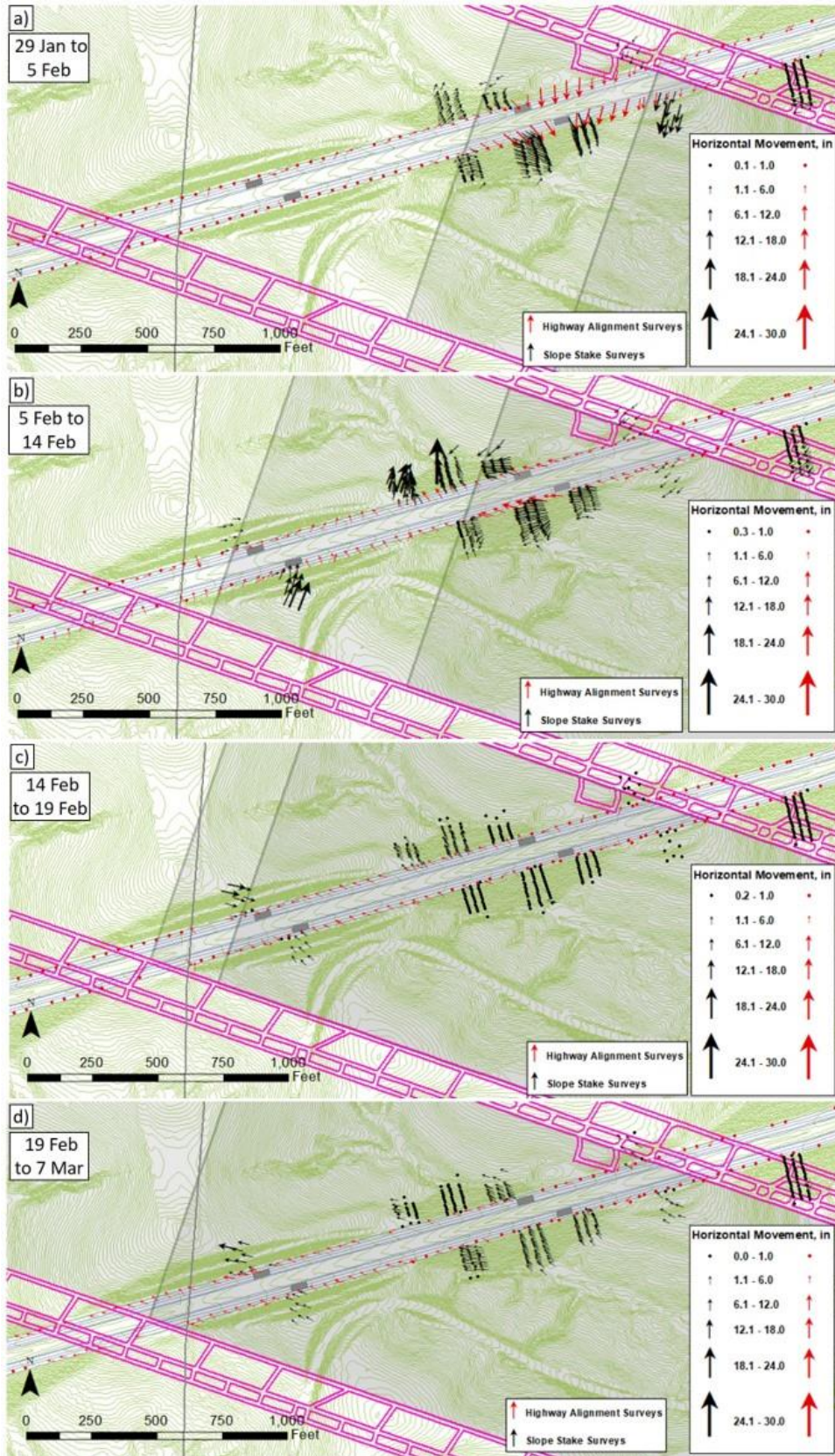


Figure IVa.11 – Incremental horizontal movement throughout study area influenced by undermining

2.3 Highway Observations compared with Horizontal Movements

The horizontal movements on the ground surface have the largest impact of the damage observed. As such, reviewing the damage that occurred on the highway in areas of large horizontal movement may reveal important relationships. The damage to the highway observed by the University in the locations of greatest horizontal movement at various times throughout the undermining process can be seen in Figures IVa.12 through IVa.14.

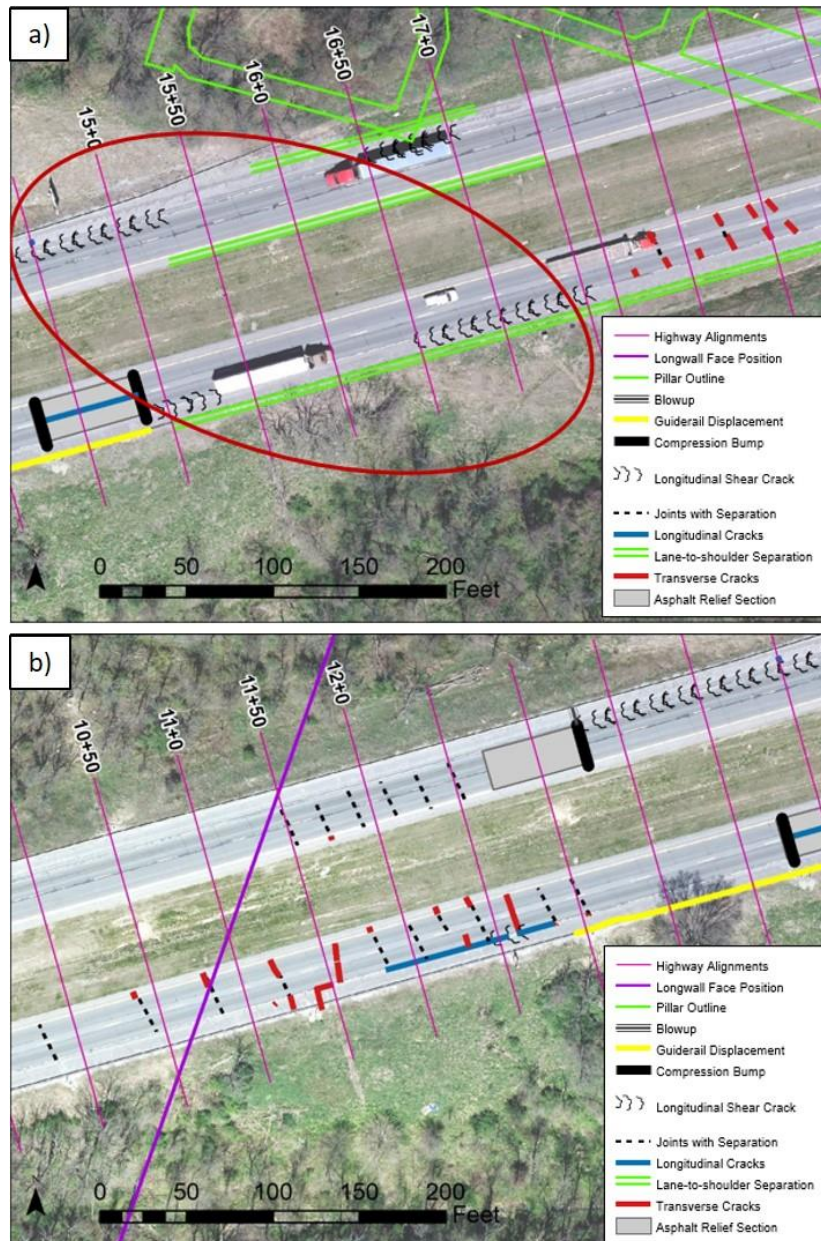


Figure IVa.12 – Highway observations in areas of large horizontal movements on 5 February 2019: a) 14+50 to 19+00; and b) 10+00 to 14+50

Figure IVa.12 shows the distresses observed on the highway in the areas of high horizontal movement on 5 February. These areas of large horizontal movement are circled in red. Damage observed in this region on this day included three compression bumps in the asphalt relief sections and extended shear cracks on both sides of the highway. Significant lane-to-shoulder separations and guiderail displacements were also observed on the eastbound lands.

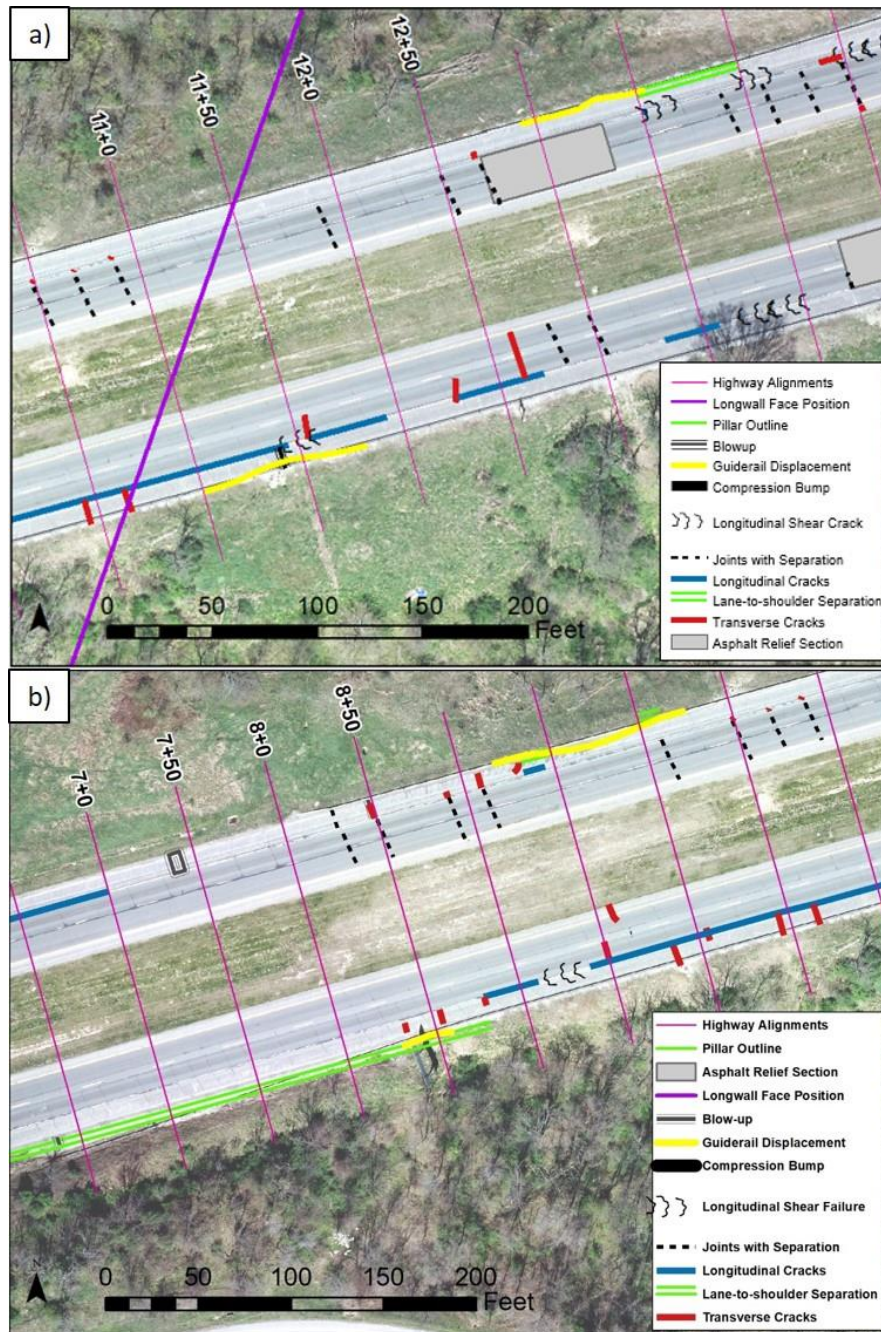


Figure IVa.13 – Highway observations in areas of large horizontal movements on 14 February 2019: a) 10+50 to 14+50; and b) 6+50 to 10+50

Figure IVa.13 shows the distresses observed on the highway in the areas of high horizontal movement on 14 February. The area of large horizontal movement are circled in red. Damage observed in this region on this day included the formation of a large blowup on top of an existing transverse crack, the opening of joints, transverse cracking, and the formation of longitudinal cracks in the rumble strip. It is also worth noting that there was a significant guiderail displacement just west of this area of large horizontal movement.

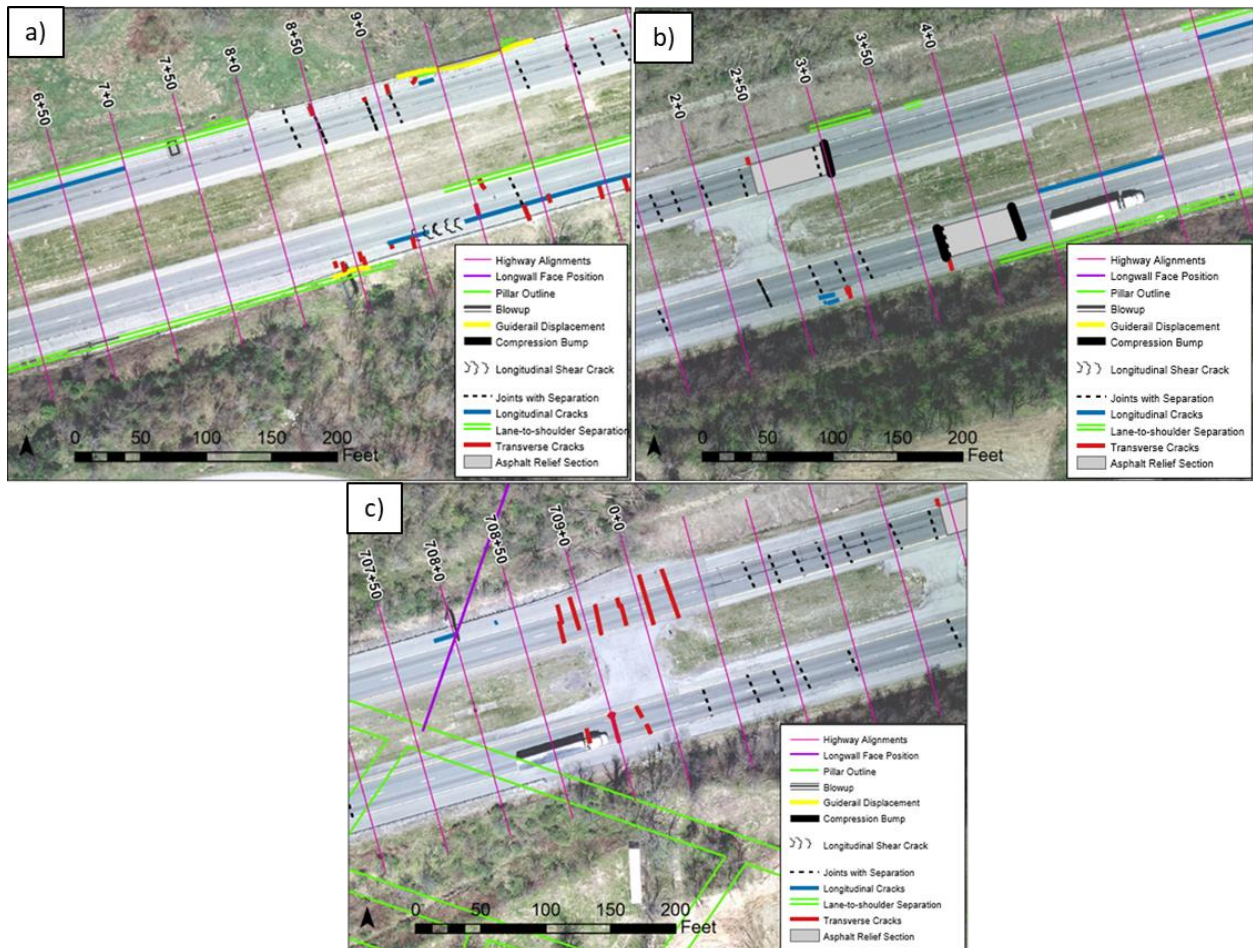


Figure IVa.14 – Highway observations in areas of large horizontal movements on 19 February 2019: a) 6+00 to 10+50; b) 1+50 to 6+00; and c) 707+00 to 2+50

Figure IVa.14 shows the distresses that occurred west of the central embankment on 19 February. The horizontal movement between 14 and 19 February was relatively consistent at a moderate magnitude along the entire extent of the highway within the study area, dissipating slightly to the west of the western asphalt relief sections. Despite the moderate magnitude of horizontal movement, most of the damage to the western side of the highway was observed at this time. Damage observed in this region included lane-to-shoulder separations, open joints, and transverse cracks.

Based on the review of the damages observed in relation to horizontal movements, it is evident that there is a relationship between the large horizontal movements and the occurrence of highway distress on the eastern side of the study area. This is demonstrated by the formation of large compression bumps and blowups, shear cracks, and longitudinal cracks in areas that were subjected to horizontal movements greater than 1-ft.

However, on the western side of Embankment #1, the highway surface did not experience incremental horizontal movements greater than 1-ft, meaning that the relationship between the horizontal movement and damage is less evident. This section of the study area moved horizontally gradually and in smaller increments between 14 February and 7 March. It can also be observed that the western side of the highway experienced less damage than the eastern side. This indicates that the gradual movements may have given the pavement structure a chance to adapt to the movement rather than causing immediate failure, which would suggest a relationship between the magnitude of horizontal movement and the amount of damage that occurs on the highway surface.

Subsection IVb – Calibration of SDPS Model Using Survey Data

1.0 Initial Analysis of Panel 15 Subsidence in SDPS

An initial analysis of Panel 15 in the Tunnel Ridge Mine was developed using the Surface Deformation Prediction System (SDPS) modeling software to consider the effects of undermining on I-70. This initial analysis considered only the final subsidence basin that may impact the highway and the embankments. Based on the mine maps received from the Tunnel Ridge Mine, the panel has a width of approximately 1,200 feet and a length of approximately 14,500 feet. The layout of Panel 15 and the highway intersection can be seen below in Figure IVb.1.



Figure IVb.1 – Orientation of I-70 alignment crossing panel 15

The following assumptions were made for this initial analysis:

- Extraction thickness is approximately 7.25-ft (typical for Pittsburgh coal bed)
- Supercritical Subsidence Factor = 64.2pct
- Average overburden thickness is 675-ft
- Average percentage of hard rock is approximately 30-pct (this was changed from the Task 1 Report to better replicate conditions in Panel 15)
- All pillars will remain rigid, minimizing vertical subsidence over the gate roads and creating an edge effect of 175-ft
- Surface is at a constant elevation
- The longwall face progresses at an average rate of 115-ft/day

This analysis was completed in the SDPS program and predicted deformation and strain over the extent of the longwall mining operation. The results were displayed using graphs. The models can be generated for the entire panel and displayed as a 3D graph or can be generated for points

and displayed as a 2D cross-sectional graph. Using the SDPS final predictive model, the vertical subsidence, horizontal displacement, horizontal strain, and ground strain that could affect the ground surface as a result of mining panel 15 were predicted. The visual representations of some of these factors for a cross section through the highway alignment can be seen below in Figures IVb.2 through IVb.4.

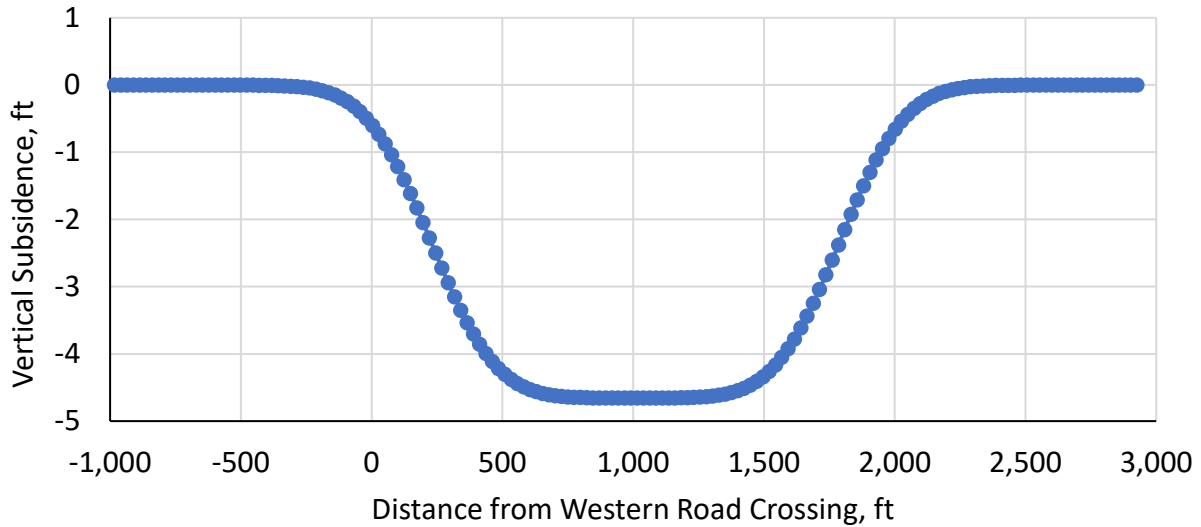


Figure IVb.2 – Initial model of vertical subsidence on I-70 alignment from undermining of Panel 15

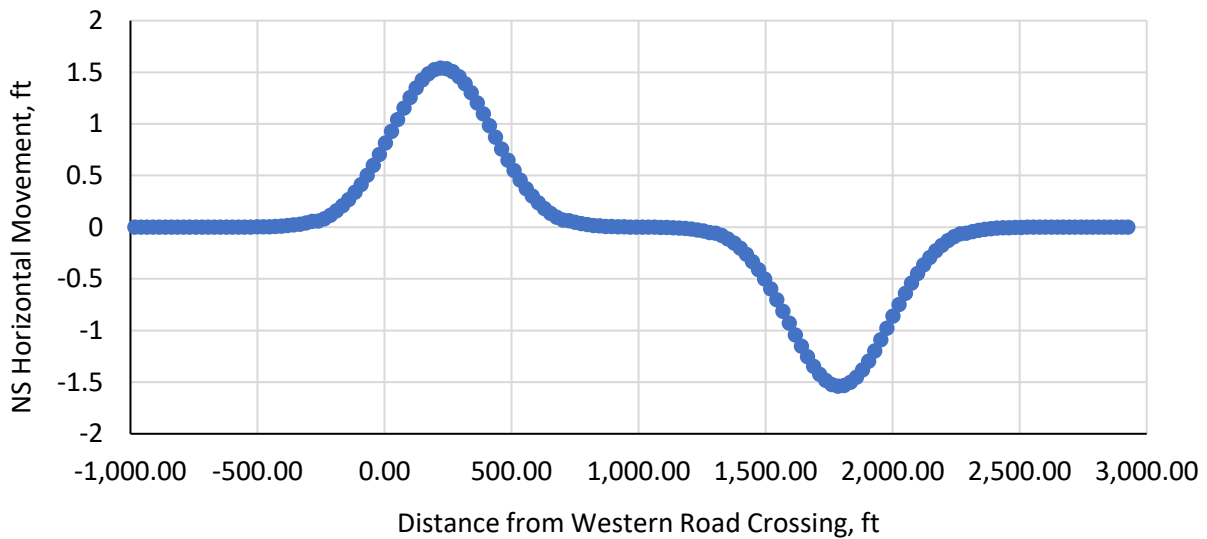


Figure IVb.3 – Initial model of north-south horizontal displacement on I-70 alignment from undermining of Panel 15

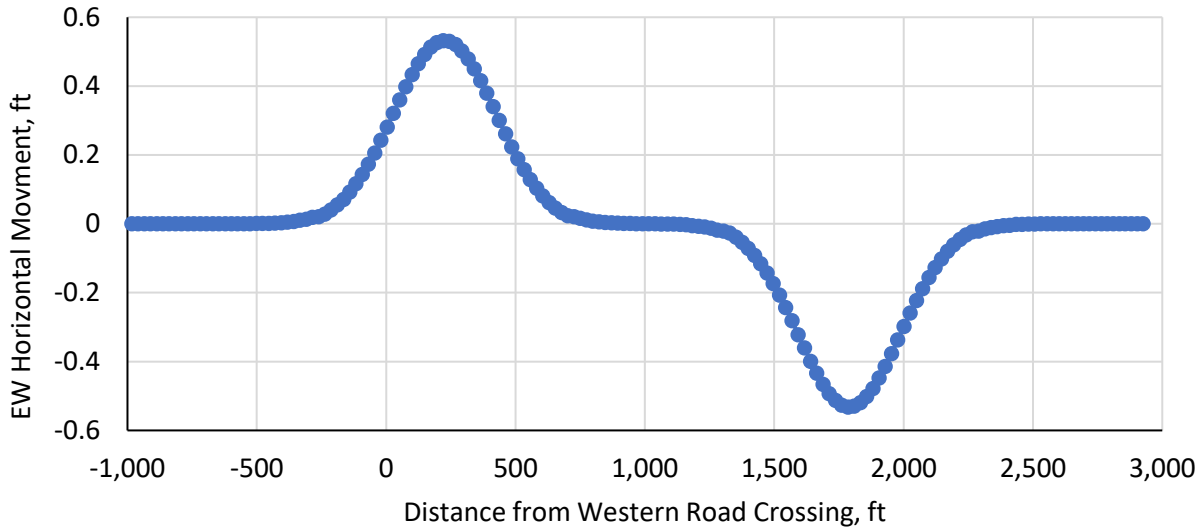


Figure IVb.4 – Initial model of east-west horizontal displacement on I-70 alignment from undermining of Panel 15

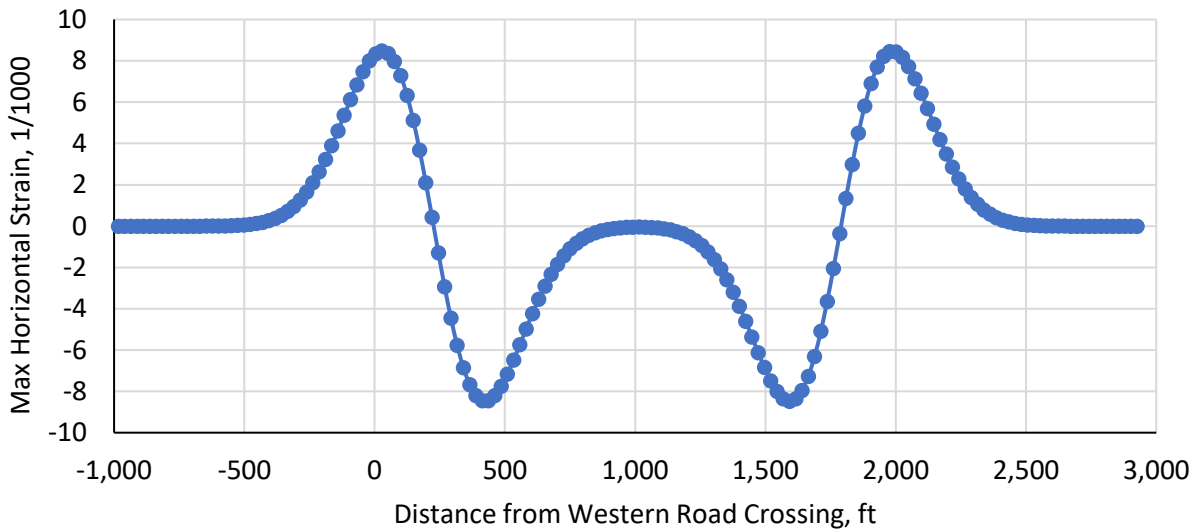


Figure IVb.5 – Initial model of maximum horizontal strain on I-70 alignment from undermining of Panel 15

An analysis of this model shows that, under the aforementioned parameters, the maximum amount of vertical subsidence expected is -4.66-ft. The horizontal deformations are expected to be a maximum of 1.53-ft in the north-south plane and 0.52-ft in the east-west plane.

2.0 Calibrated Analysis of Panel 15 Using SDPS

During the undermining of I-70, a total the highway alignment was surveyed on six different occasions. An analysis of the survey data showed a significant difference in the predicted subsidence values from the initial SDPS model and the survey data. As a result of these differences, this survey data was used to calibrate the SDPS model of Panel 15 to show the real subsidence behavior of the roadway.

The following factors were used for the calibrated analysis:

- Extraction thickness is approximately 7.25-ft (typical for Pittsburgh coal bed)
- Supercritical Subsidence Factor = 59.5%
- Average overburden thickness is 675-ft
- Average percentage of hard rock is approximately 30%
- All pillars will remain rigid, minimizing vertical subsidence over the gate roads and creating an edge effect of 175-ft
- Surface points are at the initial topographic elevation
- The longwall face progresses at an average rate of 115-ft/day

2.1 Calibrating the Data to Surveys

Based on these new parameters, the vertical subsidence and horizontal deformations were modeled and compared to the final survey data. Due to the irregular nature of survey data, no model will be able to match the data perfectly. Figures IVb.6 through IVb.8 show the correlation between the SDPS model data and the survey data.

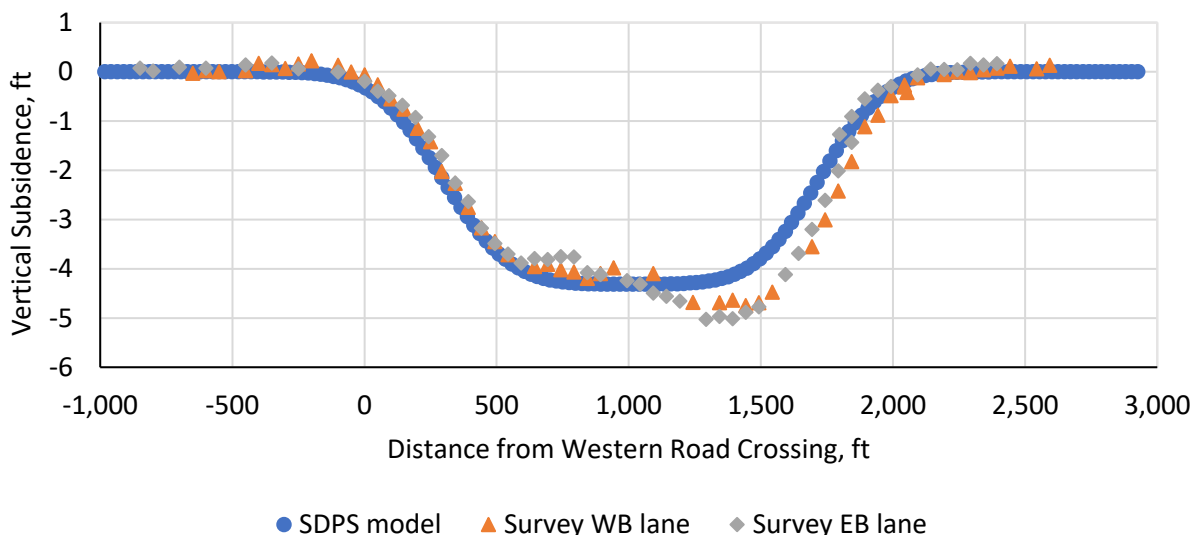


Figure IVb.6 – Vertical subsidence relationship between SDPS model and highway alignment survey data

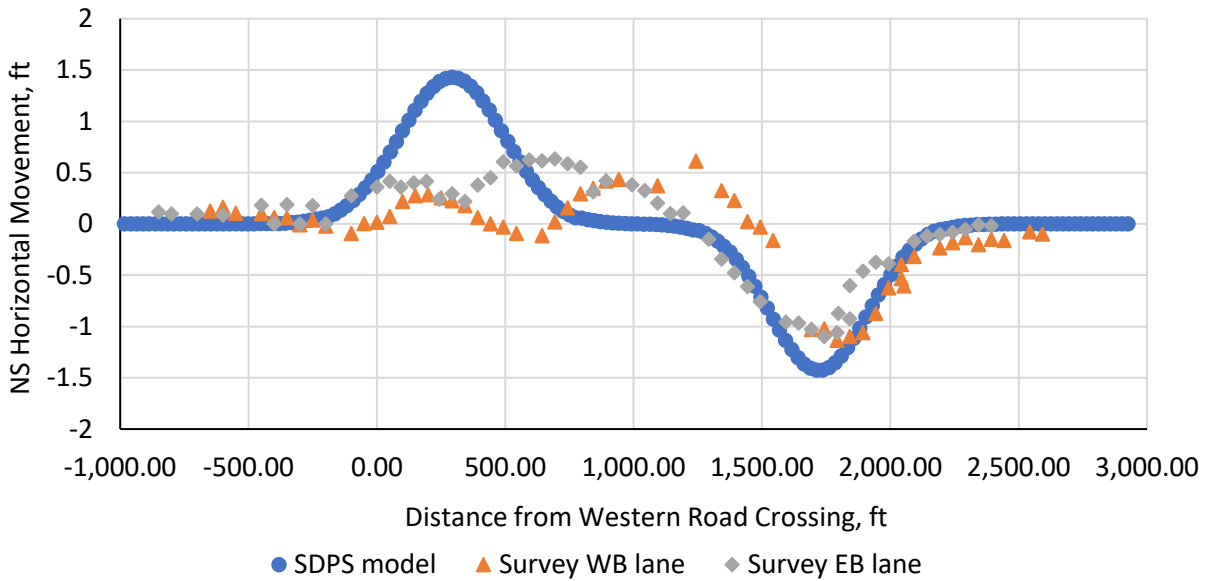


Figure IVb.7 – North-south horizontal movement relationship between SDPS model and survey data

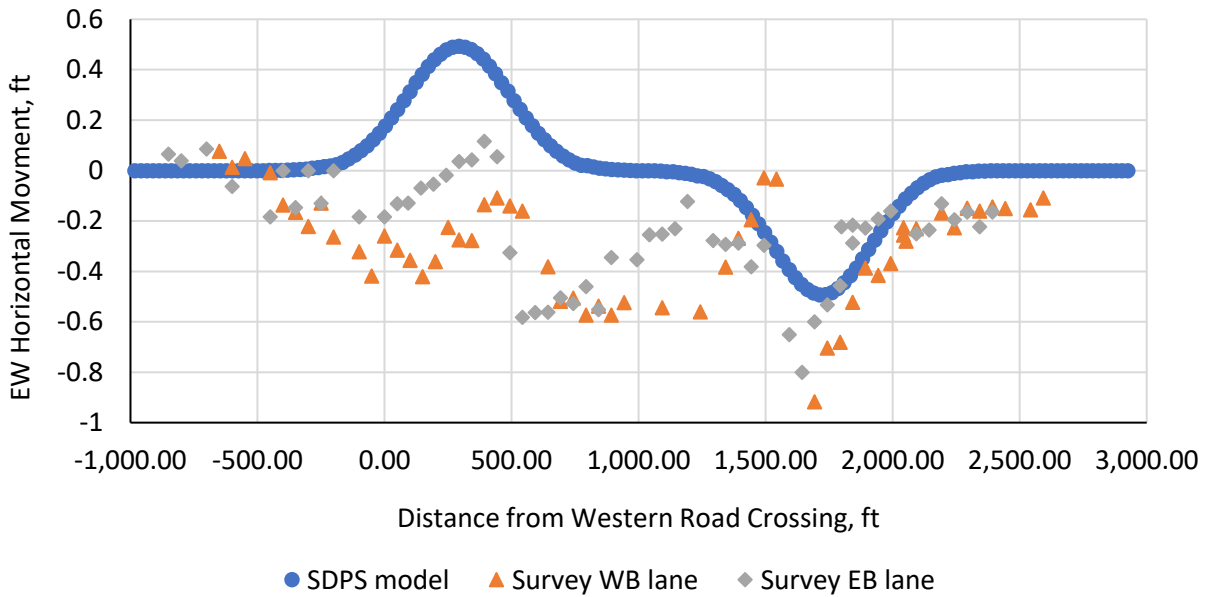


Figure IVb.8 – East-west horizontal movement relationship between SDPS model and survey data

These figures show the relationship between the model predictions and the survey data. Looking at Figure IVb.6, it is evident that the model is well calibrated to the observed highway movement; the area in the figure that shows subsidence greater than the model is the location of Embankment #1, which experienced additional vertical movement due to consolidation and spreading of the fill. Unfortunately, the horizontal deformations observed did not match those

predicted by the model. The inconsistencies displayed in Figures IVb.7 and IVb.8 are likely due to the variation in the fill and cut materials on the surface.

2.2 Analysis of 2D Calibrated SDPS Model

Using SDPS, graphs were generated to represent the subsidence basin that formed over the extent of the longwall mining operation. The vertical subsidence, horizontal displacement, horizontal strain, and ground strain that could affect the ground surface as a result of mining Panel 15 were predicted. The visual representations of these factors for a cross section through the highway alignment can be seen below in Figures IVb.9 through IVb.12.

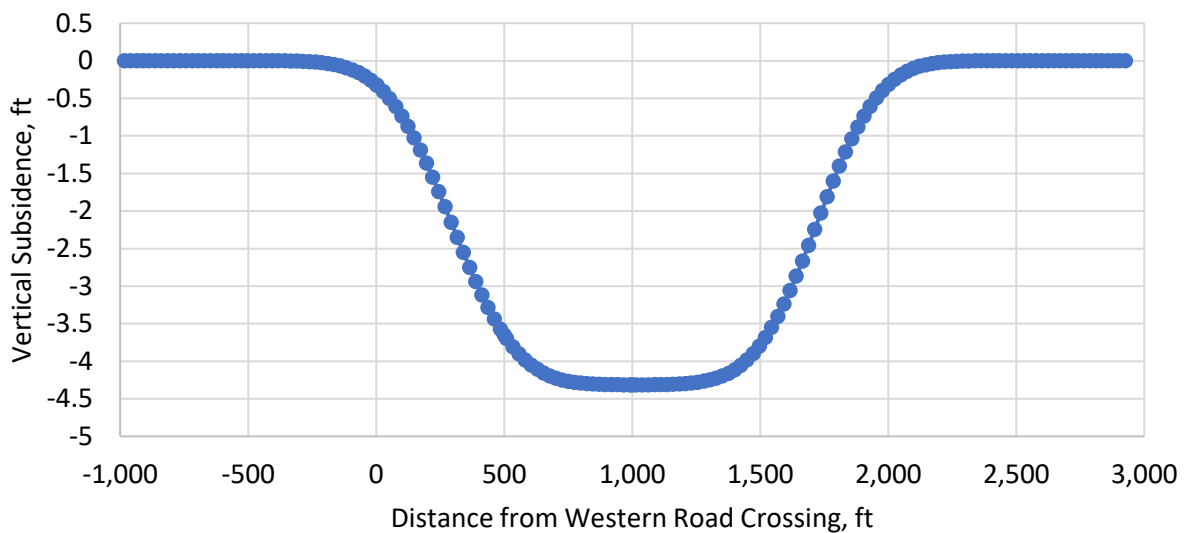


Figure IVb.9 – Calibrated model of vertical subsidence on I-70 alignment from undermining of Panel 15

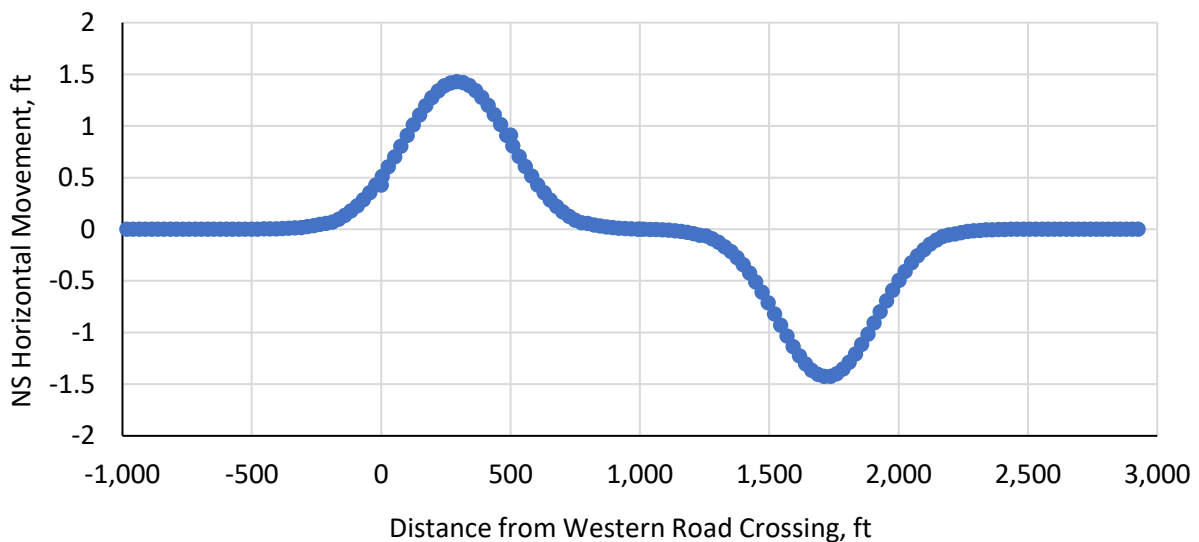


Figure IVb.10 – Calibrated model of north-south horizontal displacement on I-70 alignment from undermining of Panel 15

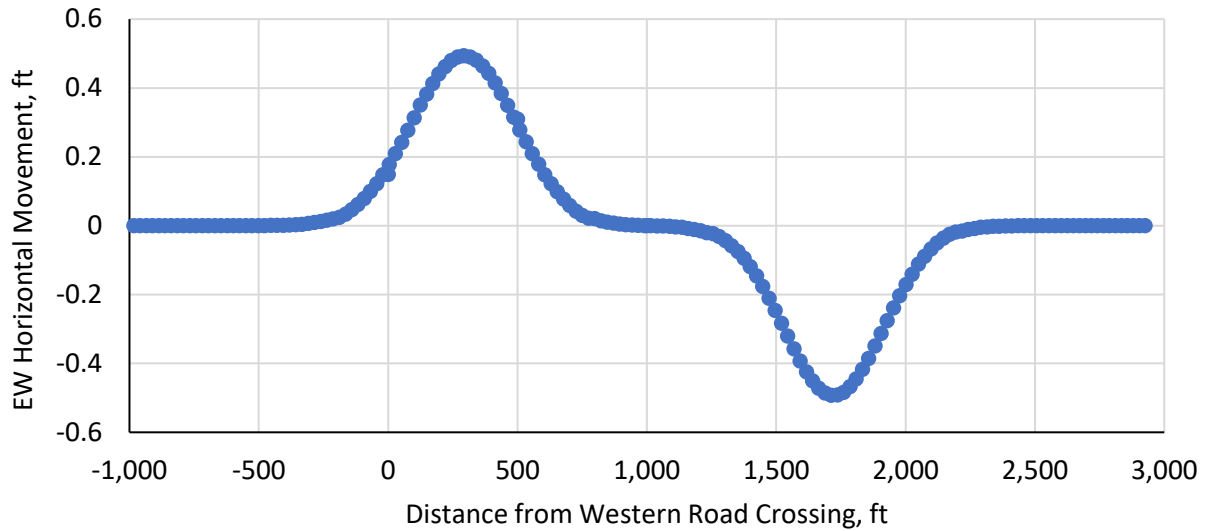


Figure IVb.11 – Calibrated model of east-west horizontal displacement on I-70 alignment from undermining of Panel 15

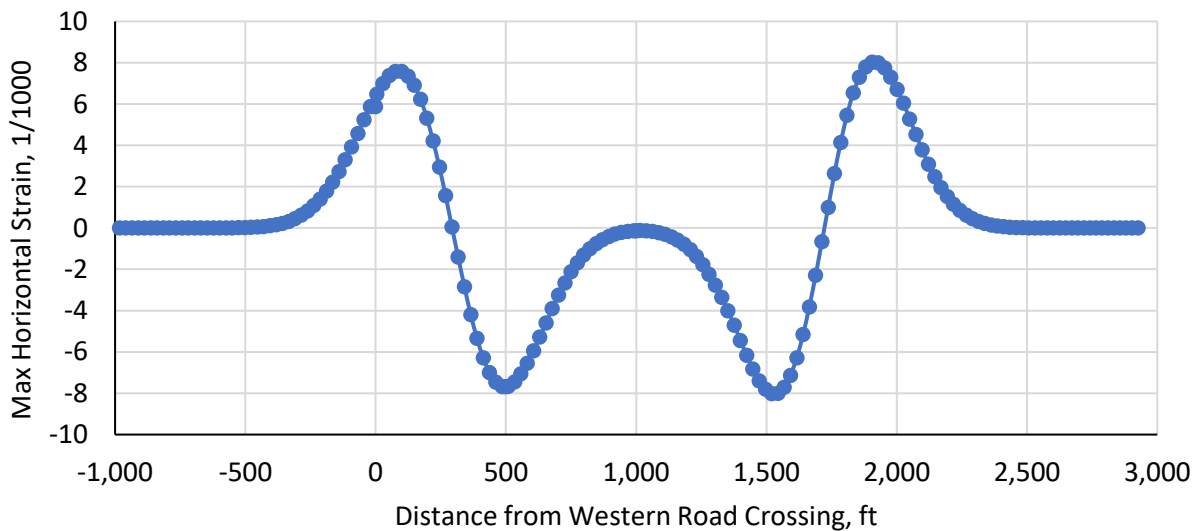


Figure IVb.12 – Calibrated model of maximum horizontal strain on I-70 alignment from undermining of Panel 15

An analysis of this model shows that, under the calibrated parameters, the maximum amount of vertical subsidence expected is -4.31-ft. The horizontal deformations are expected to be a maximum of 1.43-ft in the north-south plane and 0.49-ft in the east-west plane.

2.3 Comparison of SDPS Models and Highway Alignment Survey Data

Table IVb.1 shows the relationships between the initial SDPS model, the calibrated SDPS model, and the observed data at a variety of points throughout the subsidence basin. Comparing the initial model and the calibrated model, it can be seen that the calibrated model predicts 0.34-ft less vertical subsidence, 0.04-ft less east-west horizontal deformation, and 0.11-ft less north-south horizontal deformation. This shows that the increased percentage of hard rock in the overburden lessens the effects of subsidence on the surface.

Comparing the results of the calibrated model and the observed results, it can be seen that the model fits the data well. The percent error between the vertical profile and the observed data is about 14.5%, which indicated a good correlation. Contrarily, the horizontal deformations don't fit the model profiles as well. This may indicate a possibility of error in the horizontal observed data, inaccuracy in the model, or the influence of slopes and colluvium in the surface behavior.

Table IVb.1 – Comparison of subsidence values between SDPS models and the highway alignment survey data

| | | Distance from Western Panel Edge, ft | Vertical Subsidence, ft | EW Horizontal Deformation, ft | NS Horizontal Deformation, ft | Maximum Horizontal Strain, 1/1000 |
|---------------------------------|-------|---|--------------------------------|--------------------------------------|--------------------------------------|--|
| Initial Model | POI 1 | 0 | -0.59 | 0.28 | 0.80 | 8.29 |
| | POI 2 | 500 | -4.27 | 0.20 | 0.59 | -7.40 |
| | POI 3 | 1000 | -4.66 | 0.00 | 0.00 | -0.04 |
| | Max | -- | 0.00 | 0.53 | 1.54 | 8.48 |
| | Min | -- | -4.66 | -0.53 | -1.54 | -8.48 |
| Calibrated Model | POI 1 | 0 | -0.32 | 0.17 | 0.50 | 6.38 |
| | POI 2 | 500 | -3.65 | 0.29 | 0.85 | -7.66 |
| | POI 3 | 1,000 | -4.32 | 0.00 | 0.00 | -0.13 |
| | Max | -- | 0.00 | 0.49 | 1.43 | 8.03 |
| | Min | -- | -4.32 | -0.49 | -1.43 | -8.02 |
| Highway Alignment Survey | POI 1 | 0 | -0.26 | -0.32 | 0.07 | -- |
| | POI 2 | 500 | -3.73 | 0.39 | -0.04 | -- |
| | POI 3 | 1,000 | -4.07 | -0.54 | 0.39 | -- |
| | Max | -- | 0.22 | 0.63 | 0.39 | -- |
| | Min | -- | -5.03 | -1.14 | -0.92 | -- |

Subsection IVc – Comparison of Subsidence Observations with Empirical Models

Empirical relationships were employed to characterize the subsidence basin of Panel 15 in the Pittsburgh Coalbed. The Department of Mining Engineering at West Virginia University collected ~40 case studies from longwall mines in the Pittsburgh Coalbed to develop these relationships. For supercritical panels, the maximum vertical subsidence, inflection point location, and influence radius are provided below:

$$a = 0.6760821 * 0.9997678^h = 0.6760821 * 0.9997678^{675} = 0.578 \quad [\text{Eq. IVc.1}]$$

$$S_{max} = a * m = 0.578 * 7.25 \rightarrow S_{max} = 4.19 - ft \quad [\text{Eq. IVc.2}]$$

$$d = 0.45439 * h * e^{-0.000914 * h} = 0.45439 * 675 * e^{-0.000914 * 675} \rightarrow d = 165.5 - ft \quad [\text{Eq. IVc.3}]$$

$$r = \frac{h}{\tan(\beta)} = \frac{675}{\tan(67)} \rightarrow r = 286.5 - ft \quad [\text{Eq. IVc.4}]$$

With the aid of these empirical relationships and the profile function method, a generalized picture of the final subsidence basin can be constructed (Figure IVc.1).

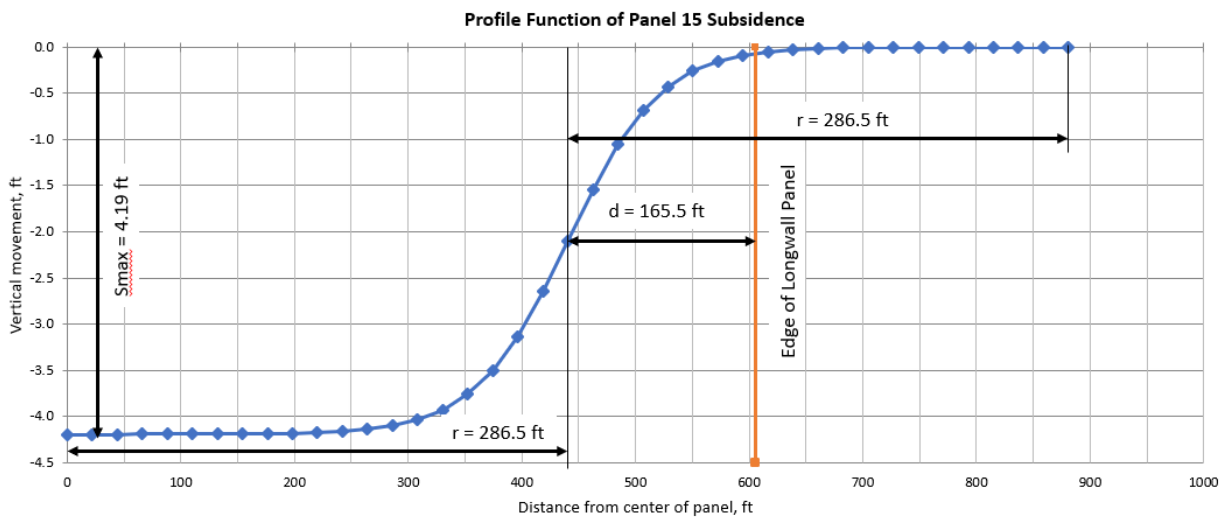


Figure IVc.1 – Generalized final subsidence basin sketched utilizing the profile function method and empirical relationships derived from Pittsburgh Coalbed data

This empirical/profile function model can be compared with the calibrated SDPS model to determine the validity of using it to estimate future subsidence. Figure IVc.2 shows a comparison between the two models for half of the longwall panel. As can be seen in this figure, the

empirical/profile function model predicts slightly less subsidence than the SDPS model. The empirical/profile function model also shows a more abrupt slope change than the SDPS model, meaning that it will predict less area to experience permanent slope changes. However, it is worth noting that the subsidence profiles from these two models intersect at a subsidence value between 2-ft and 2.5-ft, meaning that they reach the inflection point at about the same distance of 165-ft from the gate roads.

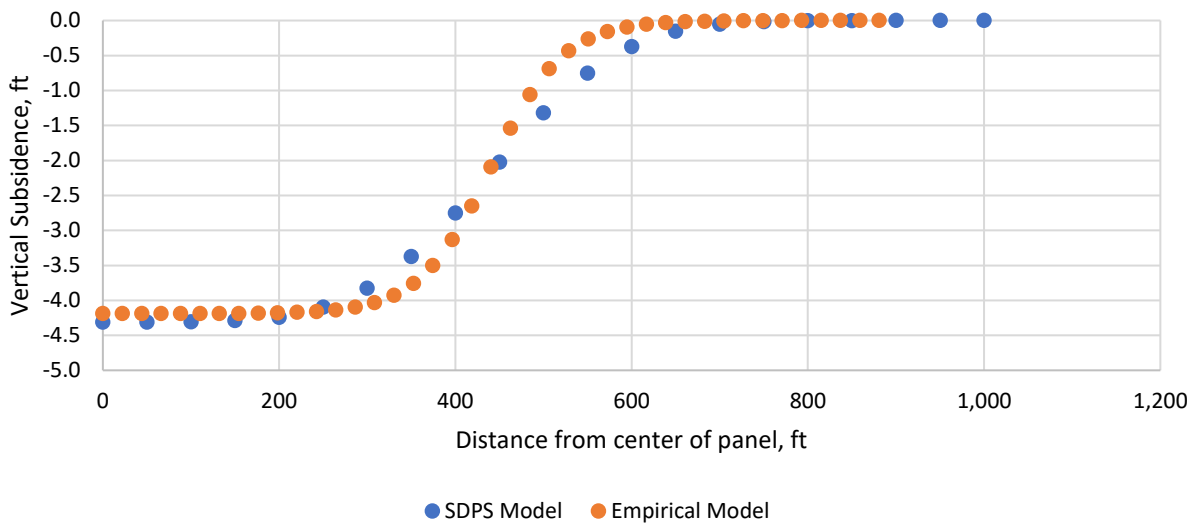


Figure IVc.2 – Comparison of vertical subsidence predicted by the calibrated SDPS and empirical/profile function models for one-half of Panel 15

The empirical/profile function model can also be compared with the final survey data collected on the highway alignment (Figure IVc.3). This comparison shows that this model would also be effective to be used to predict the vertical subsidence on the highway surface. The maximum amount of subsidence predicted by this model matches the maximum subsidence observed in areas of cut along the highway. The curvature of the model also matches very well with the data observed on the eastern side of the highway; however, the curvature does not match as well with the data observed on the western side of the highway. The empirical/profile function cannot predict heave like that which was observed over the gate road entries when mining Panel 15.

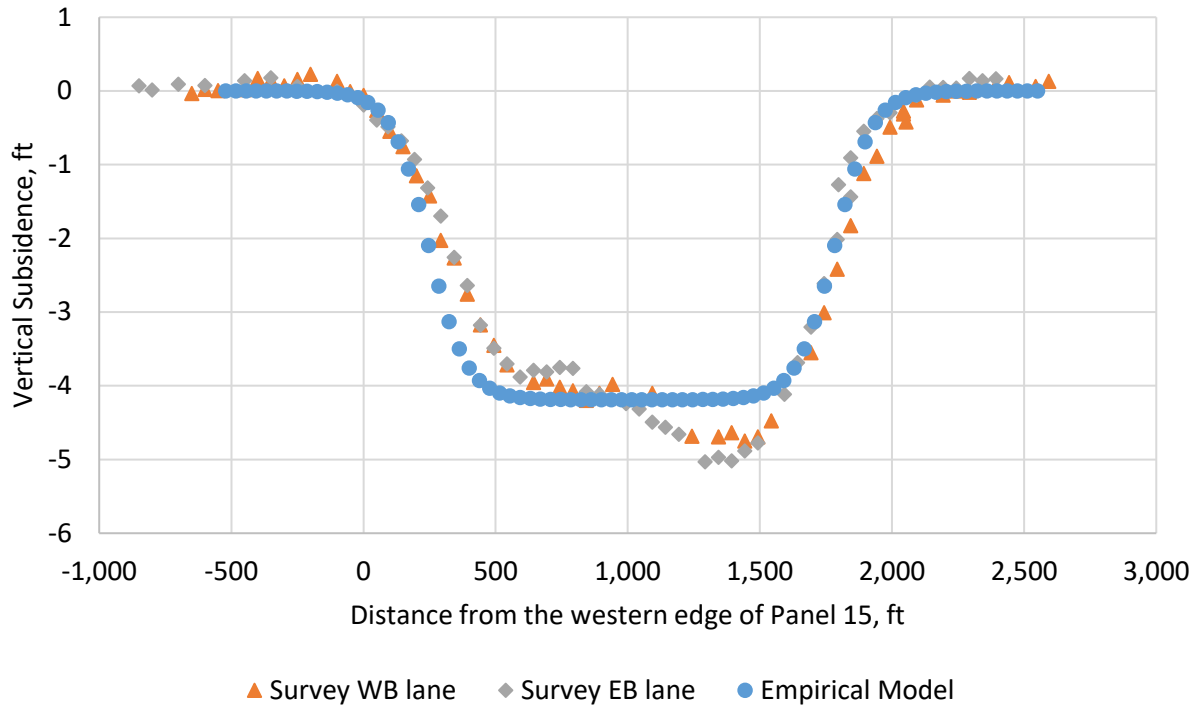


Figure IVc.3 – Vertical subsidence relationship between empirical/profile function model and highway alignment survey data

Based on the empirical relationships set forth previously, the distance from the edge of the longwall panel to the inflection line should be about 165-ft. Assuming that the inflection line remains the same distance away from the active mining as it does from the edges of the longwall panel, the location of the inflection line can be monitored throughout mining. The inflection line is the location that stress that mining induces on the ground surface transfers from tension to compression. Based on this principal, the University expected to see tension features between the longwall face and the inflection line and then compression features after the inflection line. The relationship between the longwall face, the inflection line, and the observed distresses is shown in Figures IVc.4 and IVc.5.

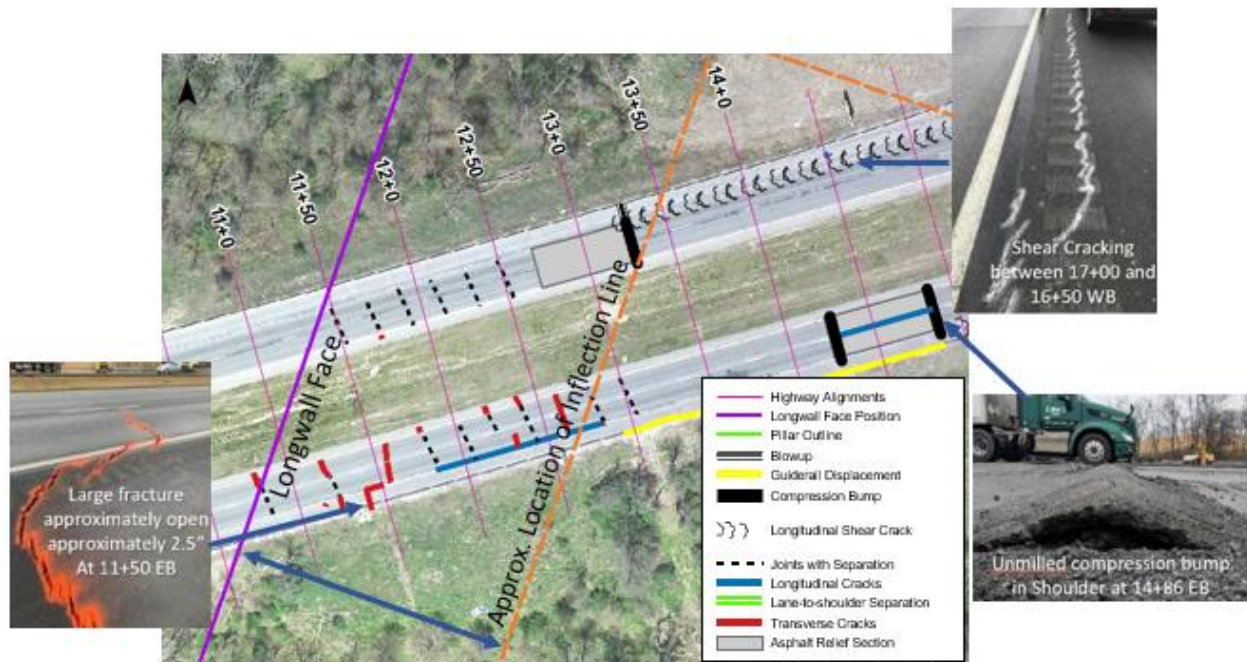


Figure IVc.4 – Failures of the highway surface as the subsidence basin formed on 5 February 2019, demonstrating areas of tension and compression



Figure IVc.5 – Failures of the highway surface as the subsidence basin formed on February 14th, demonstrating areas of tension and compression

As can be seen in Figures IVc.4 and IVc.5, the trends in the observed features show that the tensile features, such as separations and open expansion joints, tended to occur within 300-ft beyond the longwall face and 150-ft behind the longwall face. Once the longwall face was approximately 150-ft passed a point, the surface forces switched from tension to compression,

causing the formation of compression features, such as blowups. These figures help to confirm that the empirical relationships were accurate in predicting the zones of compression and tension for the mining of Panel 15. The survey data collected through the mining of Panel 15 beneath I-70 verifies the validity of the empirical/profile function model for the Pittsburgh coalbed, meaning that these relationships can also be utilized to predict future mining operation.

SECTION V – EMBANKMENT BEHAVIOR

Subsection Va – Stress-Strain Response of the Soil Samples from Embankment #1

Panel 15 in the Tunnel Ridge Mine undermined a section of I-70 adjacent to the West Virginia border. Soil samples were collected from boreholes located in Embankment #1 (Figure Va.1). Surface samples were also obtained from Embankment #1.

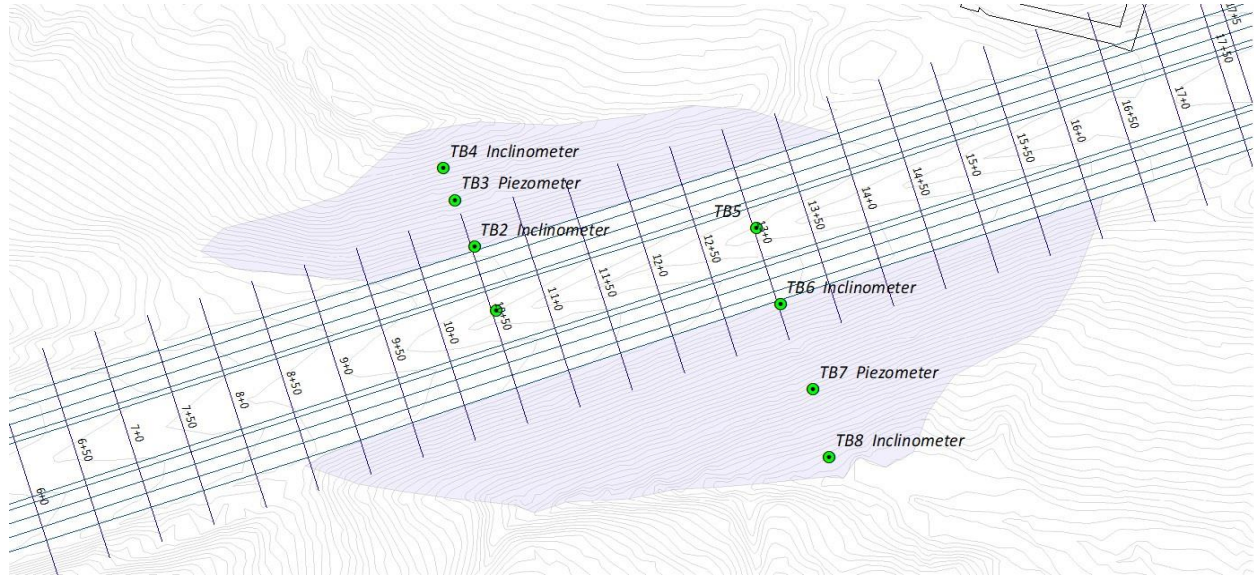


Figure Va.1 – Borehole drilled into Embankment #1 along the 720+00 and 720+50 profiles

The samples from the boreholes as well as the surface samples were subjected to triaxial compression tests in order to obtain the stress-strain response under tri-axial conditions as well as to obtain the effective shear strength parameters (cohesion = c' ; and angle of friction = ϕ') for the stability analysis of the embankment. The testing was performed by the company Earth Inc.

Tri-axial compression tests were performed on the soil samples taken from boreholes TB-1 to TB-8 as well as on soil samples collected from the surface of the embankment and named as HS-1, HS-2 and HS-3. The tri-axial compression tests were of the CU (Consolidated-Undrained tests with pore pressure measurements) type. From the CU tri-axial compression tests, plots can be obtained relating the value of the deviator stress ($\Delta\sigma = \sigma_1 - \sigma_3$) with the axial strain (ϵ) (Figures Va.2 and Va.3). Also, from these plots the values of the Young's Modulus of Elasticity, E , can be obtained. The value of E is used in the stability and deformation analysis of the embankment using the finite element method. The stress-strain plots shown in Figures Va.2 and Va.3 indicated that the soil samples behaved as a strain hardening soil (Figure Va.2) or as an elastic-plastic material (Figure Va.3). The strain hardening response represent a soil that becomes stronger as its deformation (strain) progresses.

CONSOLIDATED-UNDRAINED TRIAXIAL COMPRESSION TEST ON COHESIVE SOILS ASTM D4767-11

| | | | |
|-------------------|---------------------------------------|----------------|-------------|
| Client | Earth, Inc. | Boring | TB-8 |
| Client Project | SR 0070 Longwall Mining - Panel 15 | Depth | 6.5' - 8.5' |
| Project No. | 41068 | Sample | ST-1 |
| Test Conditions: | Undisturbed - Side And Double Drained | Lab Sample No. | 41068013 |
| USCS Description: | BROWN ELASTIC SILT WITH SAND | | |

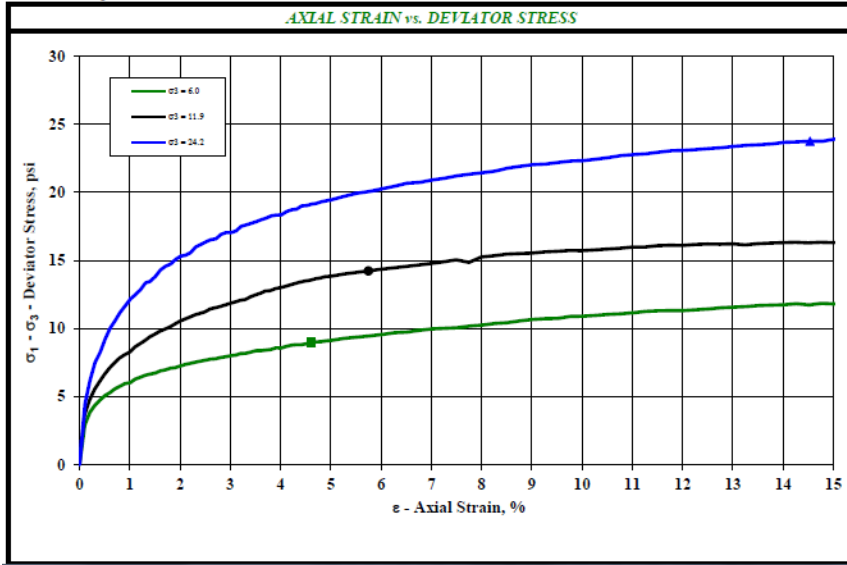


Figure Va.2 – Stress-strain plot from a CU tri-axial test on soil sample from borehole TB-8 (Figure IIIb.2, Task 1 Report)

CONSOLIDATED-UNDRAINED TRIAXIAL COMPRESSION TEST ON COHESIVE SOILS ASTM D4767-11

| | | | |
|-------------------|------------------------------------|----------------|-------------|
| Client | Earth, Inc. | Boring | HS-2 |
| Client Project | SR 0070 Longwall Mining - Panel 15 | Depth | 0.0' - 2.0' |
| Project No. | 41076 | Sample | B-1 |
| Test Conditions: | Remolded - Side And Double Drained | Lab Sample No. | 41076002 |
| USCS Description: | REDDISH BROWN SANDY FAT CLAY | | |

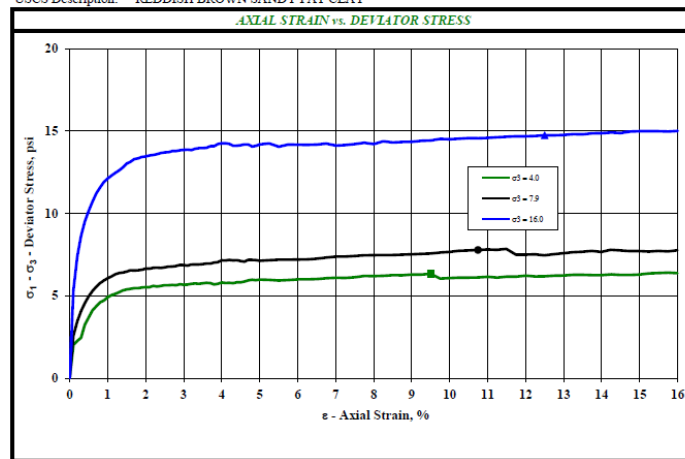


Figure Va.3 – Stress-strain relationships for sample H-2 from surface of Embankment #1 (Figure IIIb.3, Task 1 Report)

1.0 Influence of the Stress-Strain Response on Slope Stability

Newmark (1960) has analyzed the effect of the stress-strain response of a soil to the stability of a slope or embankment of which the soil forms part. This effect was illustrated by Newmark (1960) and is shown in Figure Va.4.

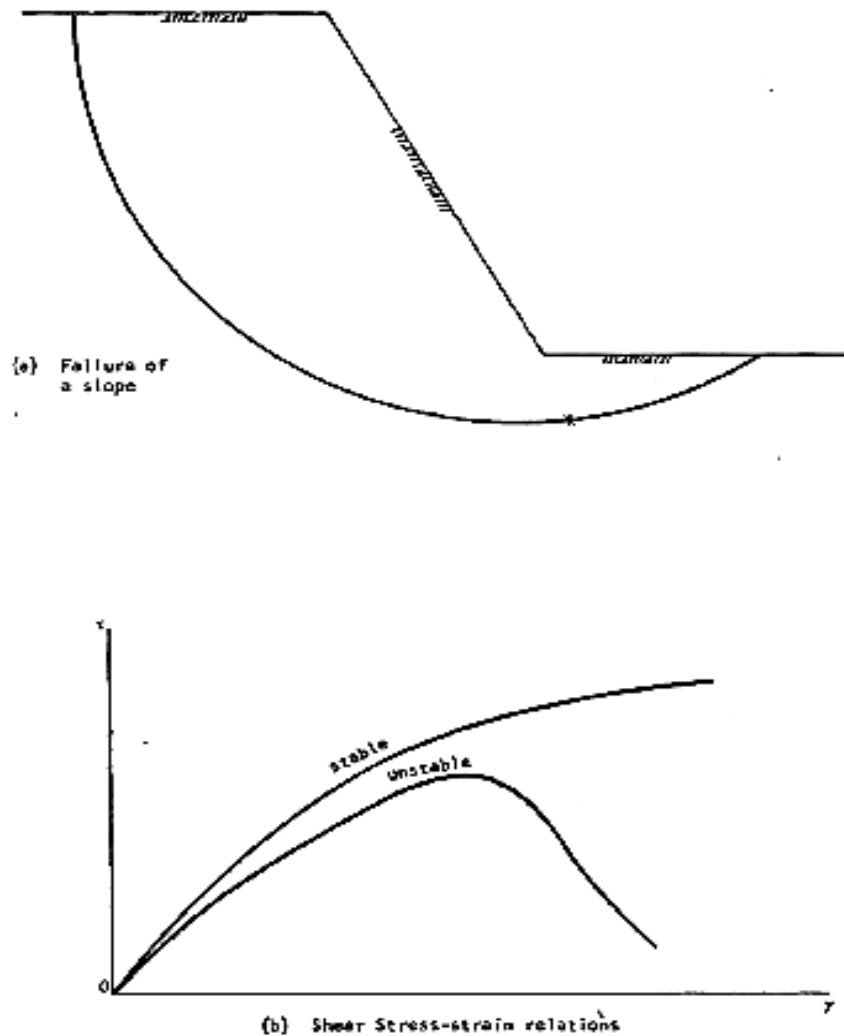


Figure Va.4 – Effect of the shear stress-strain of a soil on the stability of a slope of which it forms part (Newmark, 1960).

If the slope is made of a soil with a strain hardening behavior [top curve in Figure Va.4]. The slope will be stable. If the soil forming the slope respond to shear as a strain softening soil [bottom curve in Figure Va.4], the slope will fail as deformation progresses. The Embankment #1 is made of a soil that is a strain hardening soil (Figure Va.2). Thus, under deformation caused

by subsidence, the embankment will become stronger and will not fail. The deformations experienced by the embankment as a result of subsidence will be vertical as well as horizontal.

2.0 The Role of Dispersed Gravel on the Stress-Strain Response of a Soil-Rock Mixture

2.1 When Subjected to Shear

The soil forming part of Embankment #1 was found by the engineering company (Earth Inc.) that conducted the laboratory tests on the soils forming Embankment #1 to be made of a mixture of fine-grained soil and gravel. The gravel was dispersed in the fine-grained matrix.

Tri-axial compression tests conducted by Zhao and Liu (2018) (Figure Va.5) on soil-rock mixtures indicated that the resulting stress-strain response of these type of soils was similar to the ones shown in Figures Va.2 and Va.3.

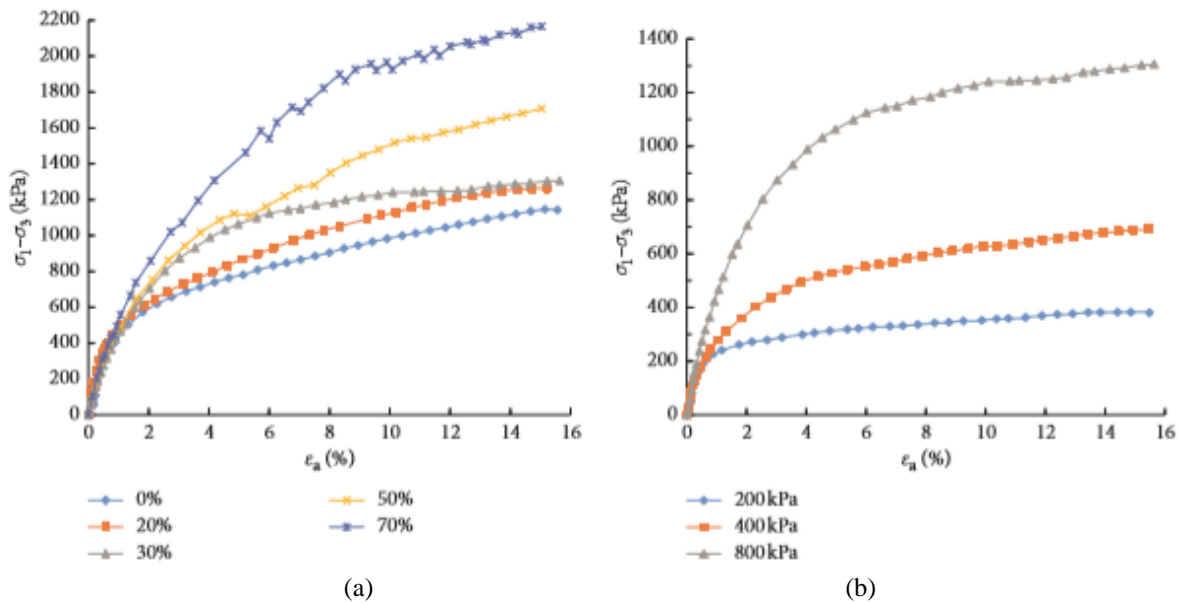


Figure Va.5 – (a) Stress-strain curves obtained from tri-axial tests on different soil-rock mixtures with different rock concentrations (0 to 70%) and cell pressure $\sigma_3 = 800$ kPa; (b) Stress strain curves for different values of the cell pressure σ_3 (200, 400, and 800 kPa) and rock concentration equal to 30% (Zhao & Liu, 2018)

Thus, the strain hardening behavior of the soils forming part of Embankment #1 seems to be the result of the presence of gravel in the soil.

3.0 Vertical and Horizontal Displacements of Embankment #1

The sections of Embankment #1 that will be considered for a deformation analysis are shown in Figure Va.6.

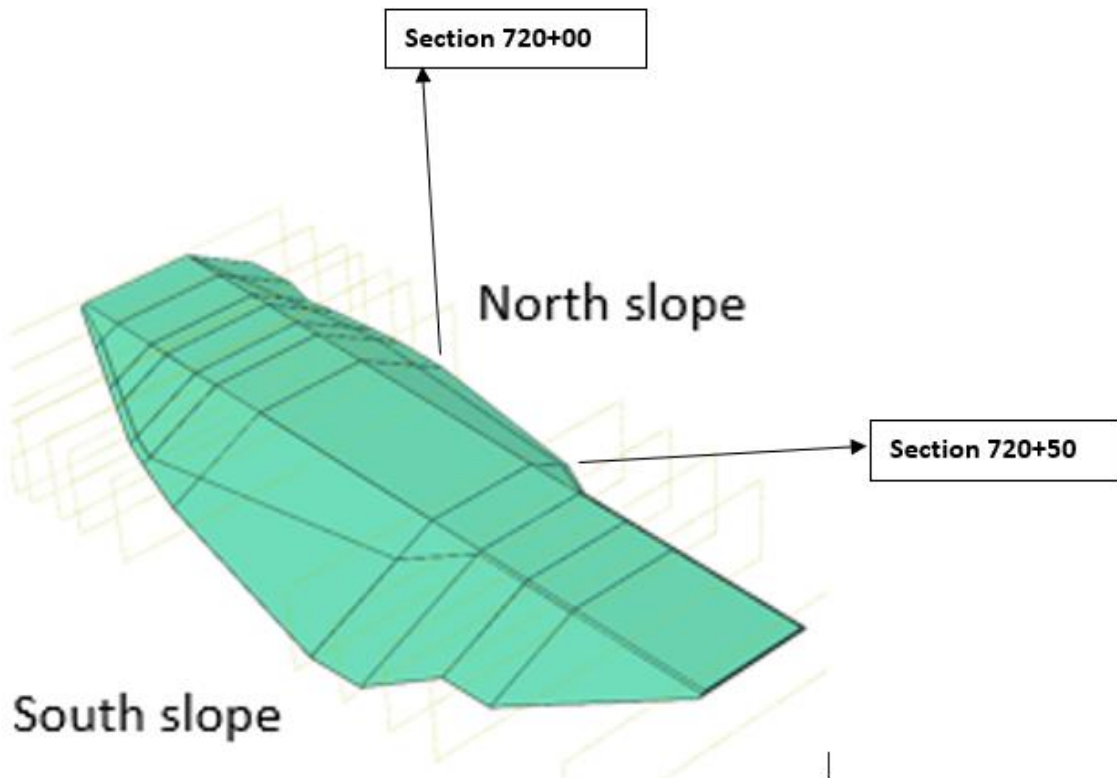


Figure Va.6 – Location of slopes in Embankment #1 for deformation analysis

3.1 Photographic, Field Measurements and Numerical Analyses of Vertical and Horizontal Displacements

Figures Va.7 and Va.8 shows photographic records taken on 19 February 2019 of the surface deformations on the north slope forming part of the cross-sectional area located at 720+00 and at 720+ 50 on the south slope (Figure Va.).

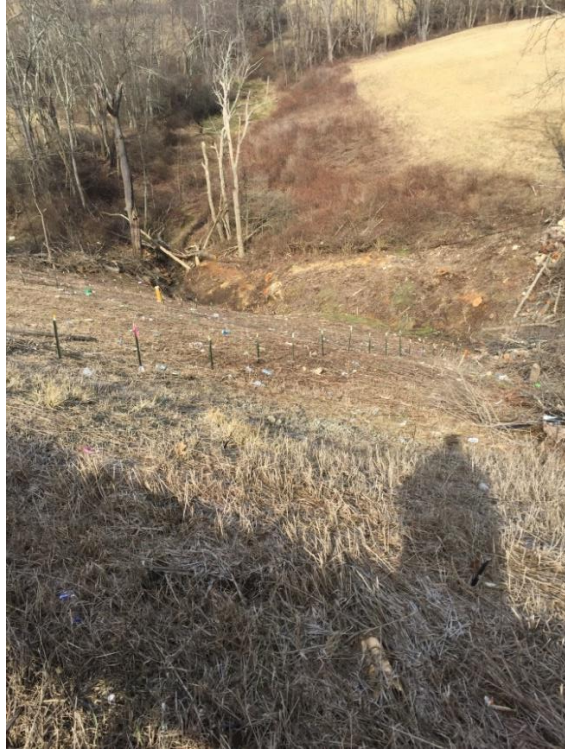


Figure Va.7 – Photograph taken on 19 February 2019 of the surface of the north slope in section 720+00



Figure Va.8 – Photograph taken on 19 February 2019 of the surface of the south slope in section 720+50

Analyses of the photographs show evidence that the slope, at section 720+00 (Figure Va.7) experience lateral displacement on the lower portion of the slope (see possible bulge at the lower part of the slope). Also, the embankment at section 720+50 experienced small lateral deformations at the top of the slope.

Section IIIb provides information on vertical subsidence along the I-70 highway alignment within the study area. Figure Va.9 shows vertical subsidence contours in the area of Embankment #1. The maximum subsidence (-5.5-ft) occurred on the top surface of the embankment. Measurably less subsidence occurred along the bottom portions of Embankment #1, ranging from 3.9 to 4.2-ft. The difference of more than 1-ft and suggests that portions of the embankment consolidated as a result of the subsidence.

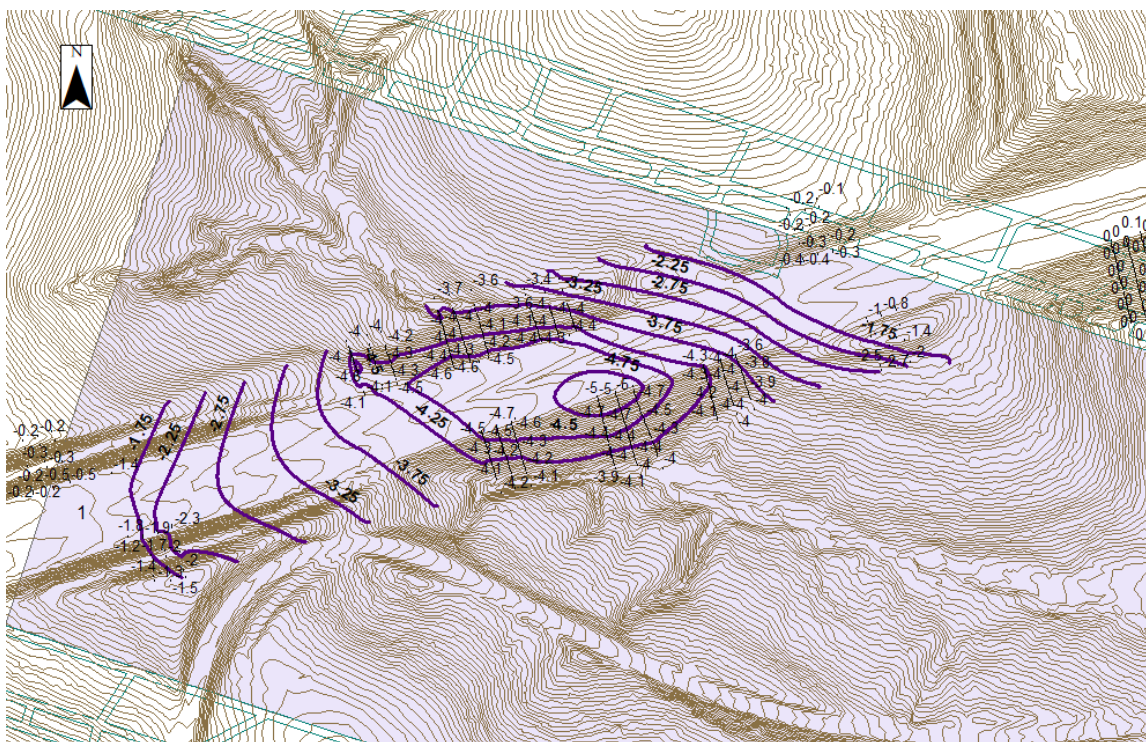


Figure Va.9 – Vertical surface subsidence contours along the I-70 highway alignment in the study area

A numerical study was carried out to analyze the vertical deformations experienced by the Embankment #1. This numerical analysis uses the University's previously discussed FEM. The results of the numerical analysis is shown in Figure Va.10. The vertical deformation experienced by Embankment #1 using the numerical analysis was -5.9 ft.

Lateral deformations of Embankment #1 was previously discussed in Section IIIId. The results of the lateral deformations are shown with the borehole TB-4 inclinometer (Figure Va.11). This data confirms the lateral spreading within the embankment during subsidence. Using the SDPS

method, the vertical and horizontal deformations effective in Embankment #1 were determined to be -4.31-ft while the maximum horizontal deformations are calculated to be a maximum of 1.43-ft.

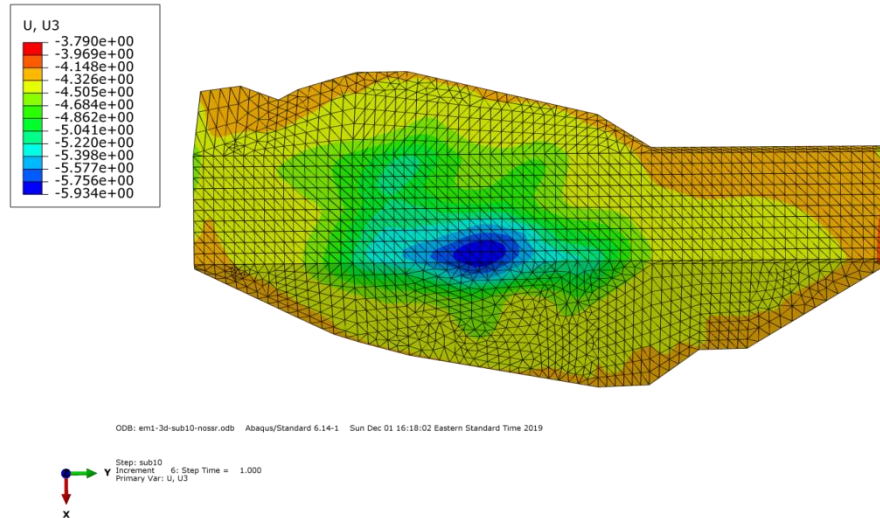


Figure Va.10 – FEM vertical displacements of Embankment #1 after subsidence

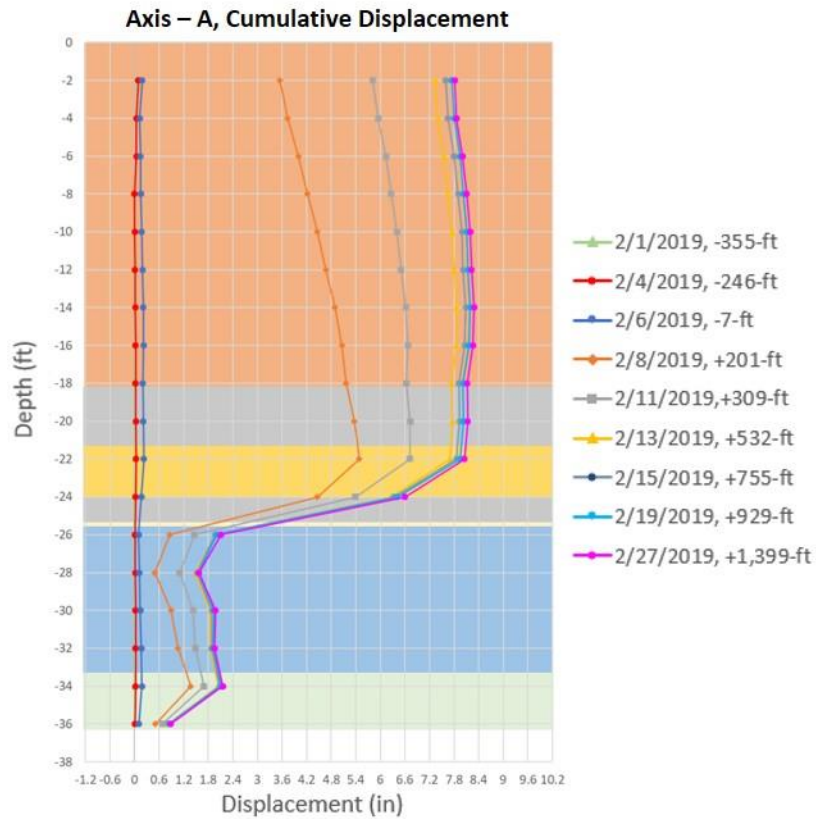


Figure Va.11 – Lateral deformations in an inclinometer located in borehole TB-4 in the south slope located in section 720+50 (see Figure Va.1)

This maximum subsidence within the FEM (Figure Va.10) took place at approximately the same location in Embankment #1 as that measured by slope survey (Figure Va.9). These similar locations indicate that the FEM is adequately predicating the actual subsidence measured within the study area. The numerical results of vertical subsidence (-5.9-ft.) are greater than the field subsidence using the SDPS approach (-4.3-ft), and the subsidence measured at the surface of Embankment #1 using the slope surveys (-5.5-ft.). The extra-subsidence (5.5-ft.- 4.3-ft) = 1.2-ft likely represents the amount of consolidation experienced by Embankment #1 during subsidence.

3.2 Mobilized Shear Strength in the Soils Forming Part of Embankment #1

The Embankment #1 experienced large vertical and large lateral deformations as a result of the longwall mining of Panel 15 (Figures Va.9, Va.10, Va.11 and Va.12). When modeling large strain behavior, deformations take place in shear bands (Vallejo, 1982). The width of the shear band within the FEM is estimated to be a few feet thick. The large lateral deformations zone observed from inclinometer TB-4 was measured to be about 3-ft thick (Figure Va.11). A simulated shear band in a soil containing dispersed gravel is shown in Figure Va.13.

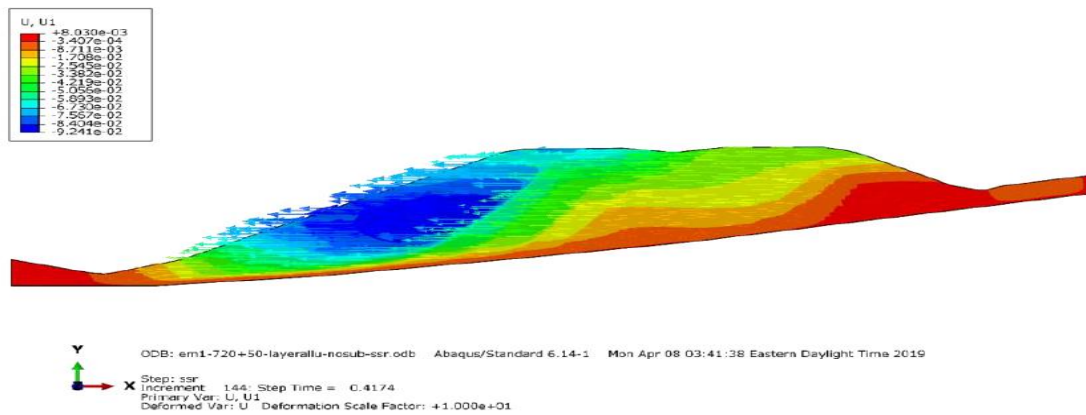


Figure Va.12 – Lateral deformations from numerical analysis at Section 720+50 of Embankment #1

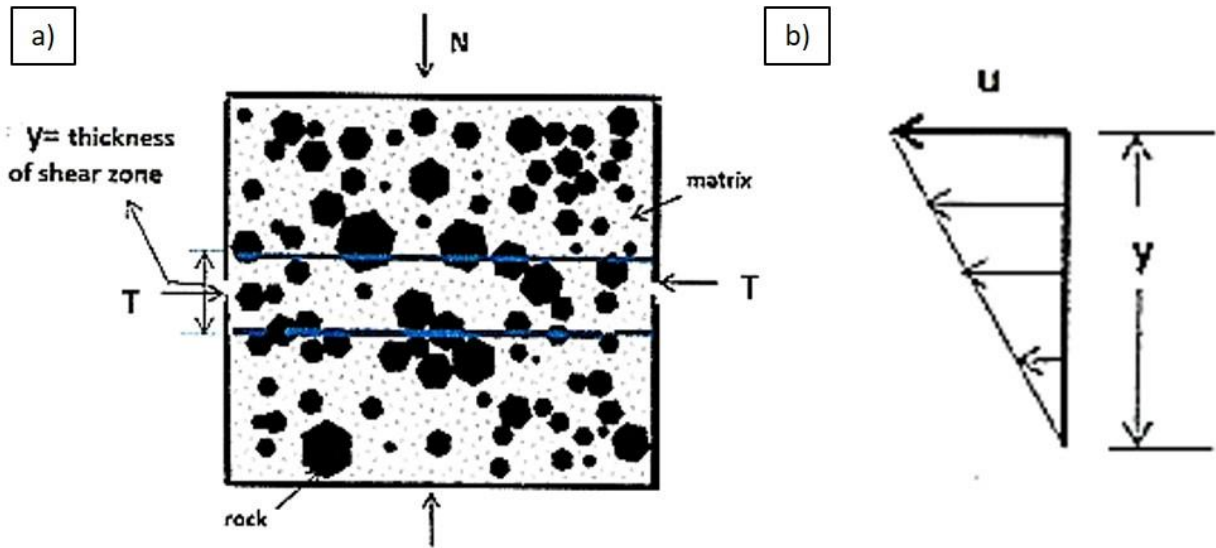


Figure Va.13 – Simulated shear band subjected to simple shear conditions

In the shear band under simple shear conditions (Figure Va.13), the following equation is effective for the shear strength, s , of the soil-rock mixture under large deformations (Johnson, 1970),

$$s = c + \sigma_n \tan \phi + \eta \left(\frac{du}{dy} \right) \quad [\text{Eq. Va.1}]$$

In Equation Va.1, c is the cohesion of the soil-rock mixture, σ_n is the normal stress at a point in the failure surface, ϕ is the friction angle of the soil-rock mixture, η is the viscosity of the soil-rock mixture, and (du/dy) is the velocity gradient (Figure Va.13). For soils in the Appalachian region, Scovazzo (1999) determined that the value of their viscosity, η , to be in the range between 1.12×10^{11} and 2.34×10^{11} lbs-sec/ft². The value of the velocity gradient can be obtained from inclinometer data (Figure Va.11).

3.3 Shear strength of sand-gravel mixtures under direct shear conditions

Vallejo et al. (2014) have carried out direct shear tests on mixtures of sand and gravel. The results of these tests are relevant to the proposed project since Embankment #1 is made of a mixture of a fine-grained soil and gravel. The sand used in the tests has an average diameter of 0.4 mm, and the gravel had a diameter of 5-mm. The shear strength of the samples was measured at different volume concentrations, c_v , of the gravel in the mixtures. The results of the tests are shown in Figure Va.14.

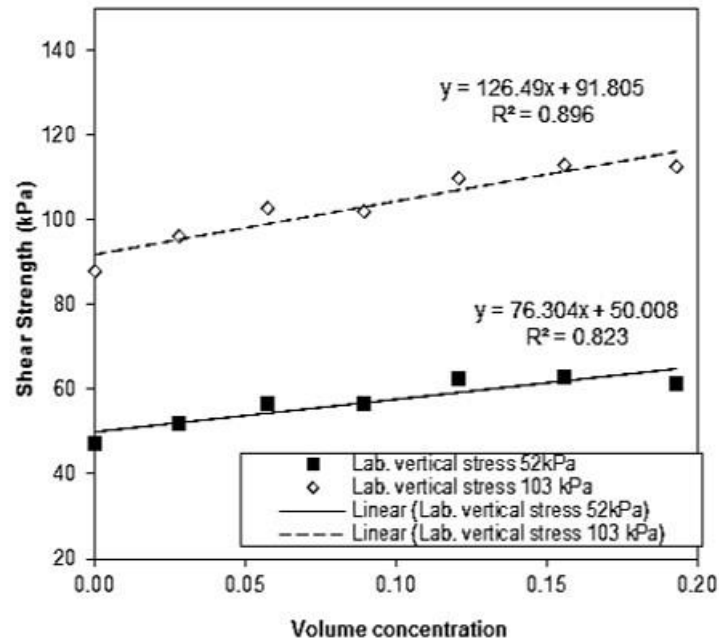


Figure Va.14 – Results of direct shear tests on samples made of sand with different volume concentrations, c_v , of dispersed gravel (Vallejo et al., 2014)

An analysis of the results of the direct shear tests on the sand-gravel mixtures shown in Figure Va.14 indicates that the presence of the gravel in the mixture, enhances the shear strength of the mixtures. Thus, the presence of the gravel in the fine-grained soils forming part of Embankment #1 is beneficial for its stability.

Subsection Vb – Embankment Observations during Subsidence

1.0 Observation Strategy

While the University's field observation was primarily interested in the subsidence impacts to the pavement, the characteristics of the two embankments within the initial study area could potentially represent the greatest risk. If one of the embankment slopes failed, it could disrupt traffic flow and force re-routing traffic onto other nearby highways. To monitor the conditions of the two embankments during undermining, the University routinely examined the four slopes (Figure Vb.1).

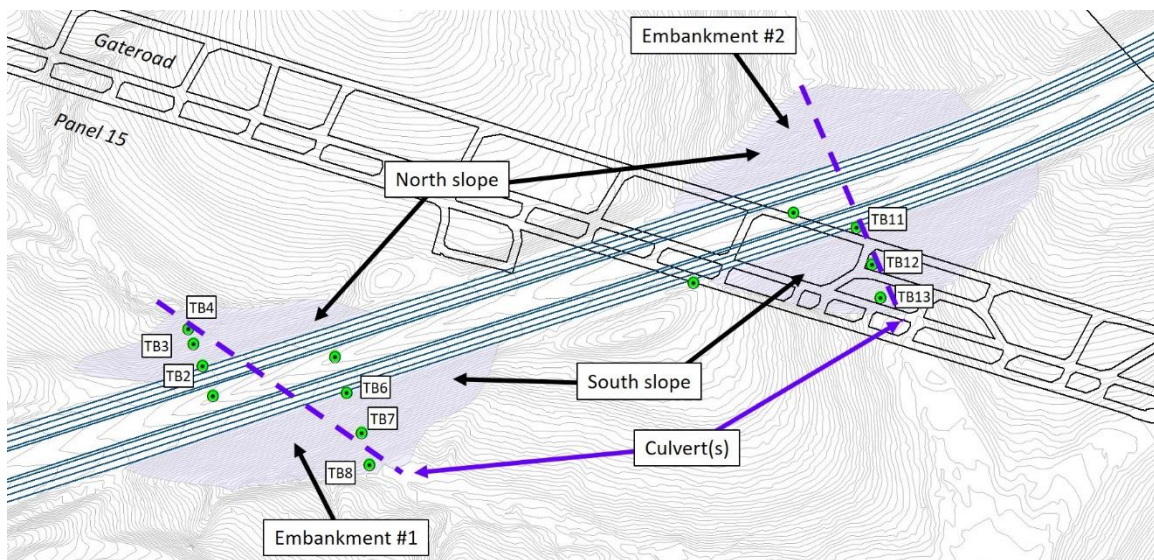


Figure Vb.1 – The location of the two embankments that were expected to be within the Panel 15 subsidence basin

The average slope of Embankment #1 and #2 are 24-deg. To assist in field observations, ropes were added to slopes at three key locations. These locations follow the three borehole trends (Figure Vb.1):

- Embankment #1 South Slope – boreholes number TB-6, TB-7, and TB-8
- Embankment #1 North Slope – boreholes number TB-2, TB-3, and TB-4
- Embankment #2 South Slope – boreholes number TB-11, TB-12, and TB-13

The boreholes contained instruments including inclinometers and piezometers that were read on a regular basis. All three observational slope survey lines encompassed the entire height of the embankment, terminating at the culverts. On occasion, the entire slope was walked to validate trends along the slope survey lines.

2.0 Embankment Examination Schedule

Observations of embankment conditions were made 12 times during the undermining of I-70 by Panel 15 (Table Vb.1). Photographs were taken and relevant features were identified and logged. The longwall face positions during these 12 slope observation field visits are shown in Figure Vb.2.

Table Vb.1 – Important dates associated with the undermining of I-70 by Panel 15

| Dates | Comment |
|------------------|---|
| 19 December 2017 | First site visit to examine conditions of the highway and adjacent slopes |
| 11 December 2018 | Examined conditions within the study area |
| 8 January 2019 | Examined conditions within the study area |
| 15 January 2019 | Examined conditions within the study area |
| 18 January 2019 | Examined conditions within the study area |
| 22 January 2019 | Mapped water discharging from Embankment #1 south slope |
| 29 January 2019 | Examined conditions within the study area |
| 5 February 2019 | Examined conditions within the study area |
| 13 February 2019 | Examined conditions within the study area |
| 14 February 2019 | Light mass wasting west of culvert Embankment #1 lower north slope |
| 19 February 2019 | Examined conditions within the study area |
| 26 February 2019 | Examined conditions within the study area |

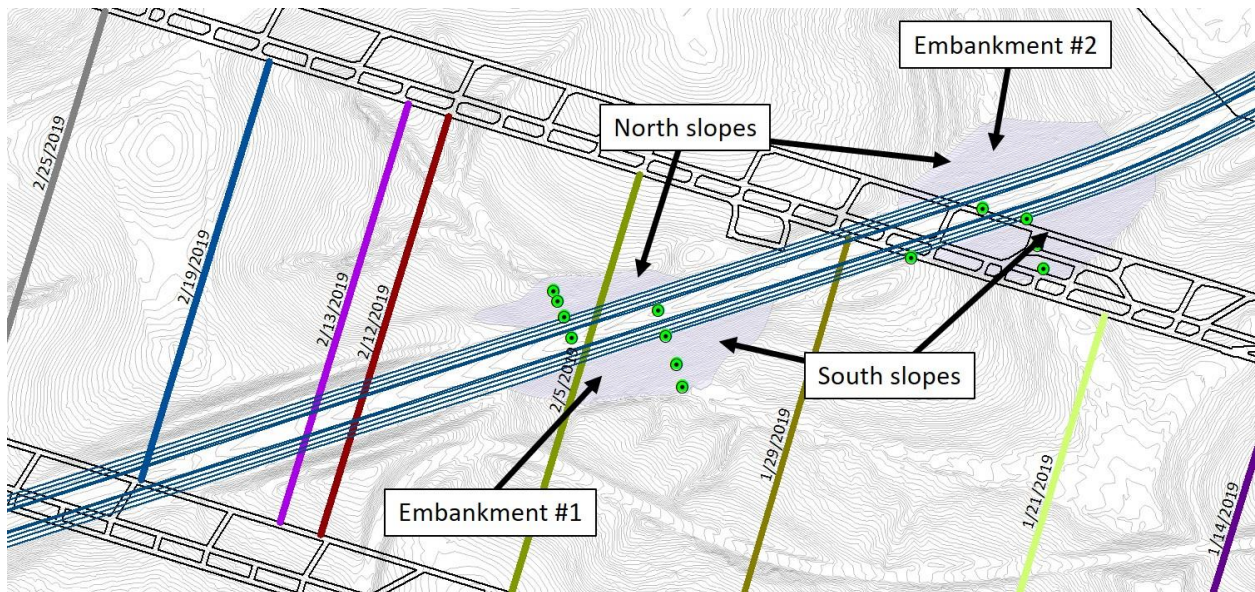


Figure Vb.2 – Location of Embankment #1 and #2, the observation slope survey lines, and longwall face positions

3.0 General Characteristics of Embankment #1 and #2

The two initial study area embankments were first visited on 19 December 2017. At that point in time, the 13 study area boreholes were drilled but the trees on the slopes had not been removed (Figure Vb-3).



Figure Vb.3 – Photographs of the north (a) and south (b) slopes of Embankment #1 prior to tree removal

While inspecting a small fill area on the north side of the alignment, two deep holes were discovered (Figure Vb.4). The cause of these structures is not known but it is speculated that differential movement and erosion may have occurred over the years. The trend of these holes is towards the highway. It is possible that these holes are part of a larger linear void. The character of these two holes was monitored throughout the study and no notable changes were observed.



Figure Vb.4 - a) One of two sinkholes found along the north side of the west bound lanes adjacent to Embankment #1

Several inclinometers and piezometers had already been installed across the highway alignment (Figure Vb.1) and extended down the north and south slopes of Embankment #1 (Figure Vb.5). As is evident from the photographs, the slopes were impacted by the drilling of the boreholes.

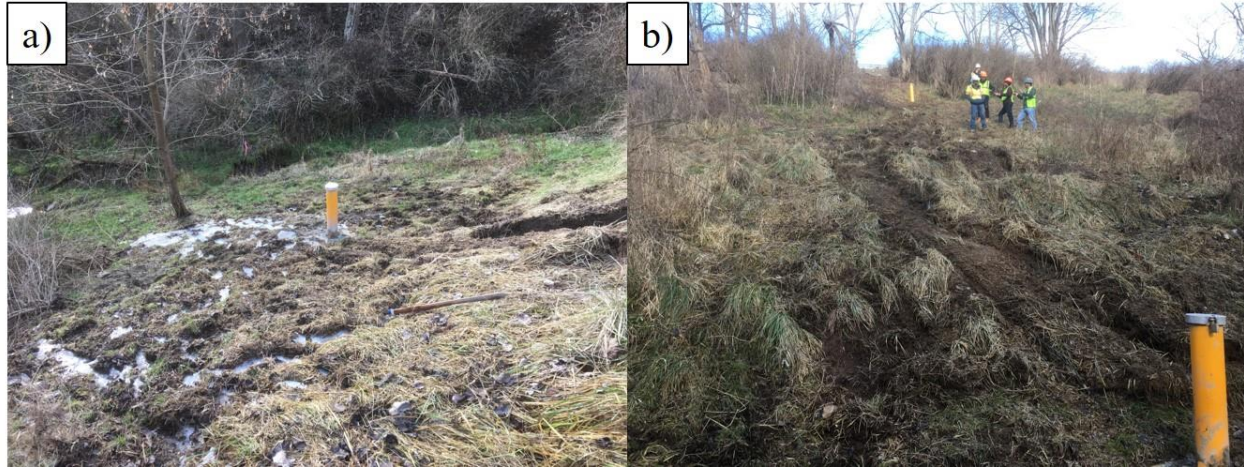


Figure Vb.5 – Tiltmeters and piezometers installed in 2017 along the slopes of Embankment #1 showing the conditions of the south slope around TB-7 and 8: a) looking down on TB-8; and b) looking up the slope from TB-8 to TB-7.

There are culverts that pass through the base of both Embankment #1 and #2 (Figure Vb.1). The culverts remained open on both ends during the mining of Panel 15. The concrete facing on Embankment #1 south slope was cracked or fractured and part of the wall rotated out of position (Figure Vb.6a).



Figure Vb.6 - a) the culvert pipe and concrete facing on Embankment #1 south slope, and b) the culvert pipe on Embankment #1 north slope

Embankment #2 was on the very margins of the subsidence basin. No significant observable changes occurred to either the north or the south slopes of Embankment #2. The following observations are confined to Embankment #1.

4.0 Embankment Conditions just Prior to Undermining

On Tuesday 22 January 2019, the longwall face was still several hundred feet from the I-70 alignment (Figure Vb.2), approaching Embankment #2 south slope. Slope survey stations were in place and were used to identify location of slope features (Figure Vb.7). No obvious changes in slope conditions were observed.

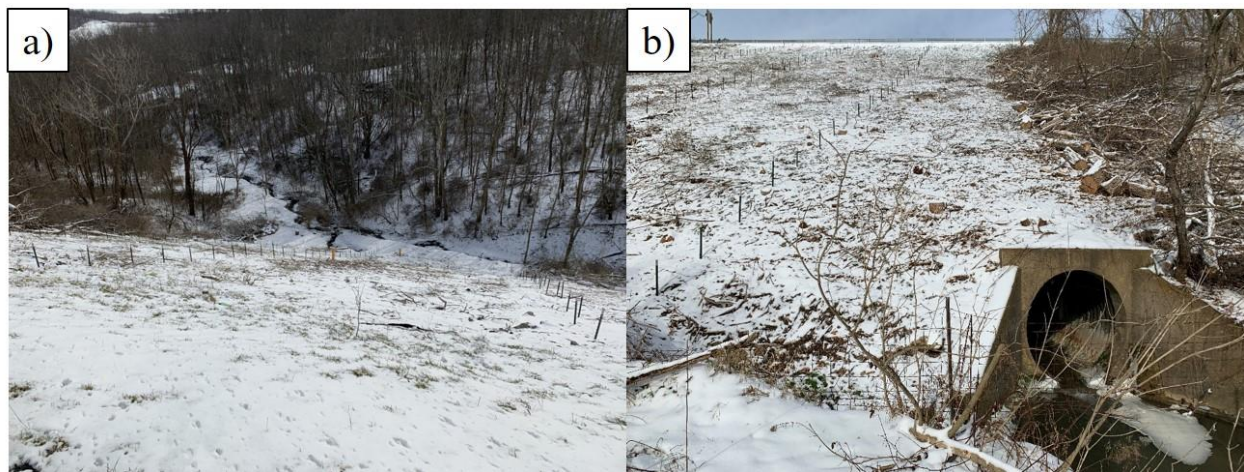


Figure Vb.7 – a) Embankment #1 south slope showing survey lines; b) Embankment #2 south slope showing survey lines and culvert.

A detailed inspection of the Embankment #1 south slope was made. Due to the very cold temperatures (overnight 5 to 15 degrees Fahrenheit), water seeping from the embankment froze rapidly forming ice sheets (Figure Vb.8). These ice sheets typically formed stair step patterns down the slope in ribbons 2 to 4-ft wide. In addition, several wet areas where walking was difficult were observed. All ice sheets and wet areas were located within the bottom quarter of the south slope.



Figure Vb.8 – Photographs were all taken from the approximate elevation between 1,210 and 1,216-ft (estimated for surface topographic contour maps) along Embankment #1 south slope. The approximate location and direction of the three photographs are shown in Figure Vb.9; a) western side; b) center; and c) eastern side

The highest occurrence of ice sheets is thought to represent the highest elevation of discharge from the south facing slope of Embankment #1 (Figure Vb.9). Using the surface contours from the Pennsylvania Spatial Data Access (PASDA) online database for this area, the University estimated the elevation to be between 1,210 and 1,216-ft.

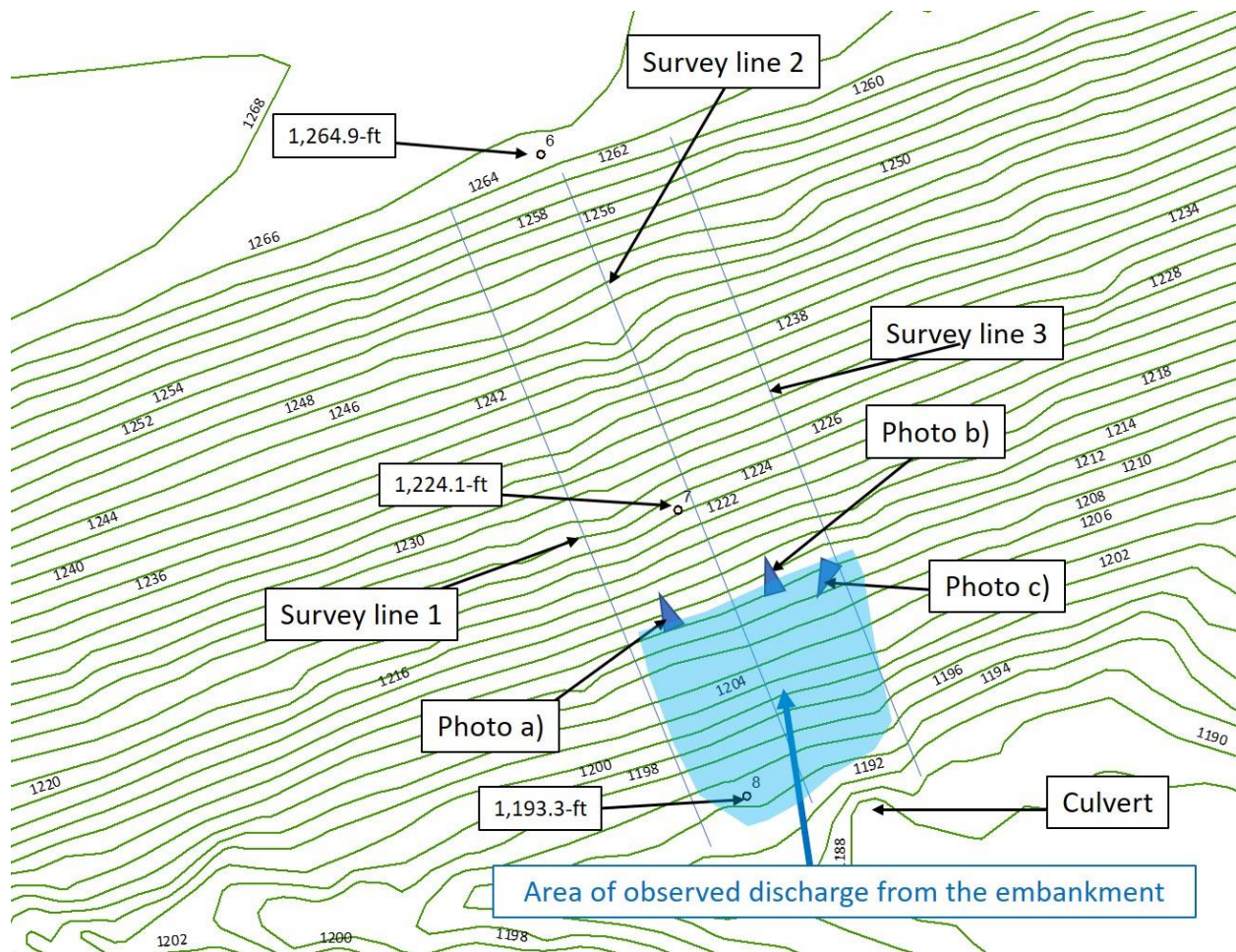


Figure Vb.9 – Surface topographic contour on 2-ft intervals showing the east-bound lane of I-70 and the south facing slope of Embankment #1. Of particular note are the location of the photographs from Figure Vb.8 as well as the general area of observed discharge.

The material properties of the fill are discussed in other sections of this document (Section Vd). The fill is underlain by bedrock comprised of siltstone, sandstone, limestone and thin claystone. The bedrock will be generally impervious to the flow of water, except where fractures and beddings planes provide adequate flow paths. The fill is generally a cohesionless material (comprised mainly of fine-grained material) with varying concentrations of clay, silt, and sand. There are also boulders of varying size, especially near the base of the fill. The constructed fill comprising the embankment appears to be pervious to flow. As discussed in the Task 1 Report, the construction method used to construct the embankments is unknown. It is possible that the colluvium (surface soil) which previously covered the bedrock may not have been removed and could had been reworked into the fill. This data suggests that water entering the embankment from the highway alignment flows down-dip along the relatively impervious contact with the bedrock (Figure Vb.10). The zone of soil saturation measured along the south slope surface is ~50-ft.

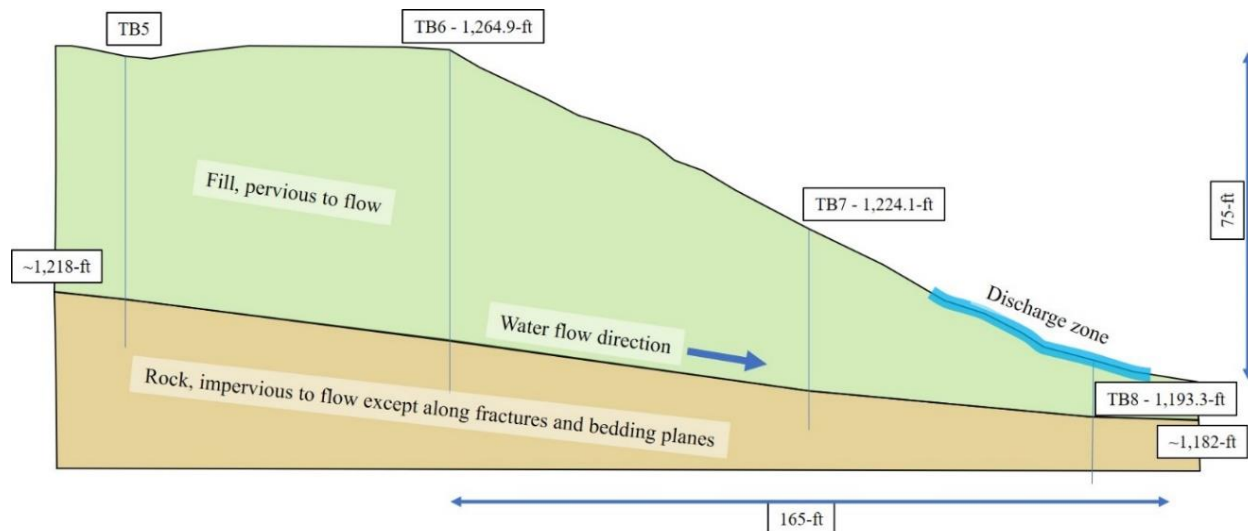


Figure Vb.10 – Cross-section of the Embankment #1's south slope constructed from borings and indicating the most likely direction of flow

Borehole TB-7 is located close to the projected saturated fill zone (Figure Vb.10). After drilling, this borehole was repurposed to act as a piezometer. Water levels within the borehole ranged in elevation from 1,192.7 to 1,196-ft (Table Vb.2). The small changes in the elevation of the water table are likely due to seasonal effects and variation in precipitation. The elevation of the highest water discharge estimated on the southern slope of Embankment #1 contradicts the water level measured with the piezometer in TB-7 to define the top of the phreatic surface. It should be noted that the condition of the piezometer was never verified, which may be the cause of such disagreement.

Table Vb.2 – Location of the water table within TB-7

| Date | Feet below surface | Elevation, ft | Comment |
|-------------|--------------------|---------------|---------|
| 30-Nov-2017 | 31.2 | 1192.9 | |
| 21-Dec-2017 | 30.5 | 1193.6 | |
| 9-Feb-2018 | 28.1 | 1196 | |
| 22-Mar-2018 | 31.4 | 1192.7 | Mud |
| 24-Aug-2018 | 31 | 1193.1 | |
| 23-Oct-2018 | 30.3 | 1193.8 | Mud |
| 12-Dec-2018 | 30.4 | 1193.7 | Mud |
| 4-Jan-2019 | 30.4 | 1193.7 | Mud |
| 15-Jan-2019 | 30.6 | 1193.5 | Mud |
| 17-Jan-2019 | 30.8 | 1193.3 | |
| Average | 30.5 | 1193.6 | |

5.0 Undermining Embankment #1

Because of south slope conditions and the position of the longwall face in early February 2019, PennDOT decided to drill another tiltmeter within Embankment #1 (Figure Vb.11a). This borehole was located between TB-7 and TB-8 within an area of highly saturated fill (Figure Vb.11b). The amount of water that emitted from this area seemed higher than at any other time. The Embankment #1 north slope did not show the same magnitude of water saturation as the south slope (Figure Vb.11c). This could be a result of the general slope of the bedrock/fill contact, allowing water to flow to the south. The north slope to the west of the culvert did not yet show signs of distress (Figure Vb.11d).



Figure Vb.11 – a) new borehole (BH14) added to Embankment #1 south slope; b) highly-saturated conditions of Embankment #1 lower south slope; c) Embankment #1 observation north slope survey line; and d) conditions of Embankment #1 lower north slope

During the weeks of 7 February 2019, several of the inclinometers within Embankment #1 began to show significant movement (Section III d). At this same time, vertical subsidence of over 4-ft occurred on Embankment #1's south slope. Conversely, portions of the north slope were only beginning to experience vertical subsidence (Figure Vb.12).

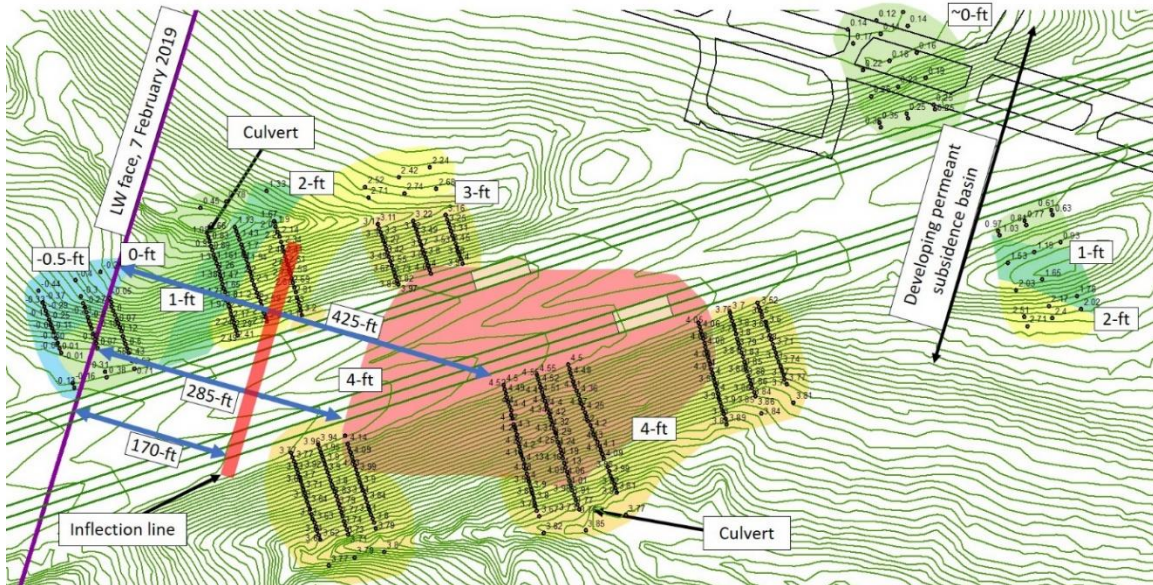


Figure Vb.12 – location of survey stakes monitored by SPK within the study area and vertical subsidence contours between 7 January (no mining related subsidence) and 7 February 2019 (subsidence related to the longwall face position on 7 February). Of particular note is the distances (170, 285, 425-ft) from the longwall face to the 4-ft and 4.5-ft vertical subsidence and to the inflection line.

The culverts are critical structures within the embankments. If stream flow is disrupted, the embankment could become distressed. That being said, no visual changes occurred to the culvert on Embankment #1's north slope from 13 November 2018 to 14 February 2019 (Figure Vb.13). The crack at the apex of the culvert has remained ~0.5-in wide and no new cracks have been observed.



Figure Vb.13 - Two photographs of the culvert at the base of Embankment #1's north slope three months apart. Both photos show very similar features.

On 14 February 2019, minor mass wasting was present at the base of Embankment #1's north slope approximately 30-ft west of the culvert (Figure Vb.14). The longwall face was estimated to be approximately 400-ft from the culvert. Approximately 4-ft of vertical subsidence would have occurred in this area of the north slope by 14 February. No further mass wasting was observed.



Figure Vb.14 – Two photographs of the slope directly to the west of the culvert on the north side of Embankment #1. Some minor mass wasting appears in the 14 February 2019 picture. The Vertical subsidence of survey stakes near this slope on 7 February show ~1-ft of movement. On 14 February the longwall face was more than 400-ft from this area and the vertical subsidence is ~4-ft.

The Embankment #1 south slope culvert was observed twelve times. An effort was made to photograph the culvert from multiple angles. One of these angles is shown in Figure Vb.15. As is confirmed from these photographs, no significant deformation occurred to the Embankment #1 south slope culvert during the undermining by Panel 15.

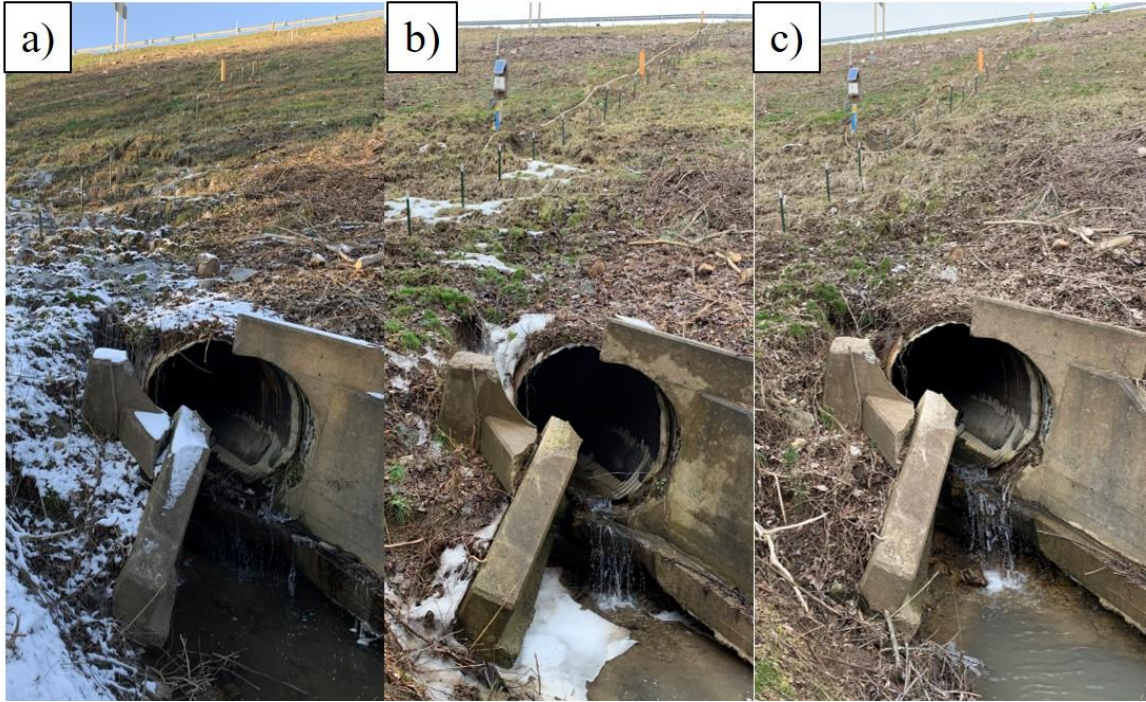


Figure Vb.15 – Embankment #1 south slope culvert: a) 8 January 2019; b) 5 February 2019; and c) 26 February 2019

Subsection Vc – Consolidation and Lateral Spreading

According to the highway alignment and the slope stake surveys, the Embankment #1 which was impacted by longwall mining Panel 15 experienced extra vertical displacement compared to the other highway segments without embankments. In addition, lateral movements along the slope direction was observed through the inclinometers installed in the two critical cross sections of the Embankment #1.

1.0 Consolidation

The vertical displacement along the highway was measured by monitoring the movement of pins on the two sides of the highway in the shoulders, using the highway alignment surveys. The vertical displacement at each pin was measured through time. For the embankments, the vertical movement was monitored by the slope stakes installed on the two sides of slope surface on the embankment. All the vertical movement data from both the highway alignment surveys and the embankment slope stake surveys was imported to ArcGIS in order to make the vertical displacement contours along the highway and on the embankment through dates. One of these contours was shown in Figure IVa.6 in the Section IV.

This figure shows the vertical displacement along the highway segment and on the embankment when the working face is just passed the embankment. According to the contours, higher vertical displacement happened in the region with embankment which is represented by red color compared to that in the region of highway only represented by blue color. In addition, the vertical displacement is different in the embankment when the thickness of the embankment fill differs. It is found that the maximum consolidation was located at the crest of the south-facing slope. And the length of the slope reached the largest value in that location. It seems that the consolidation caused by the successive subsidence had a positive relationship with the thickness of embankment fill. The embankment presented a higher vertical displacement in the region of higher thickness of fill while a lower displacement in those areas with less embankment fill. In other words, more embankment fill resulted in a higher degree of consolidation and consequently a larger vertical displacement.

2.0 Lateral Spreading

The embankment presented lateral spreading through analyzing the inclinometer data. The inclinometer was installed in the boring cases upon the boring hole was set up. It measured the movement of slopes on the north and south sides of the embankment. Referring to Figure III d.1 in Section III d, the instruments measured the displacement in two orientations, along the highway direction and perpendicular to the highway direction pointing down to the slope. Referring to Figure III d.3 in Section III d, the inclinometers measured the movement along A+

axis, which means that the embankment moved outward and lateral spreading happened due to the subsidence.

The lateral spreading represented in Figure III d.3 based on the inclinometer data was summarized in Figure Vc.1 with an overview of the simulated 3D model.

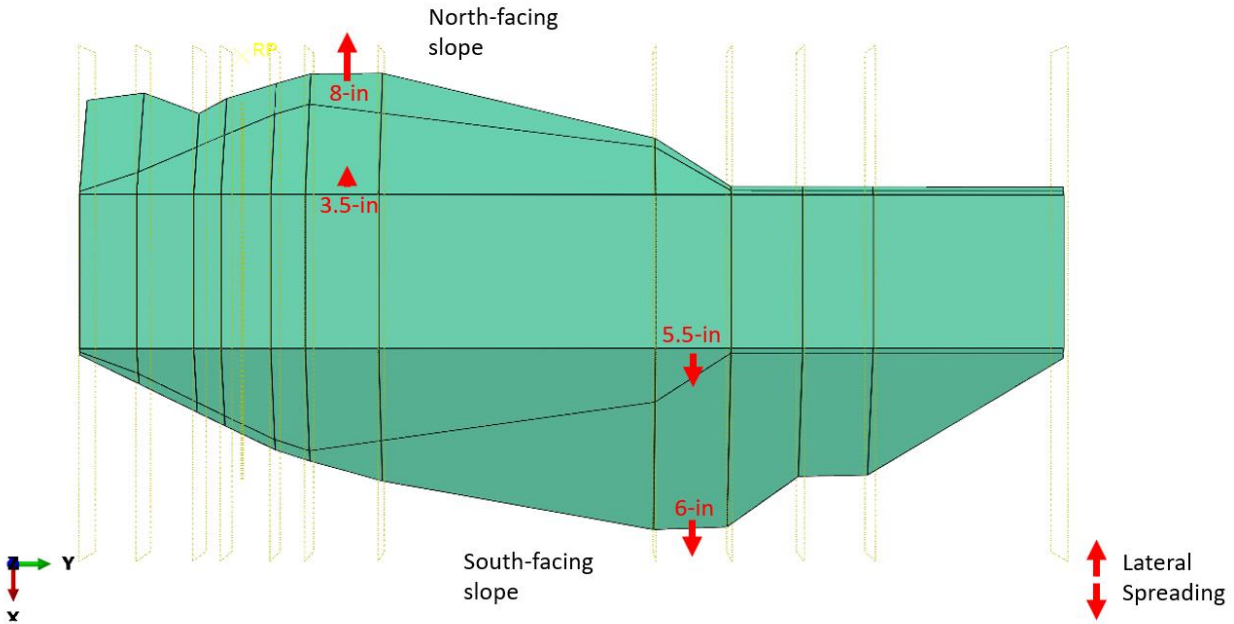


Figure Vc.1 – Lateral spreading on Embankment #1 after subsidence

The maximum magnitude of the outward movement happened at the toe area. It indicates that the toe area experienced larger deformation than that on the crest of the embankment. More deformation was observed on the surface than on the bottom of the embankment. For instance, the lateral spreading on the surface is two to three times to the bottom deformation on the north-facing slope. On the south-facing slope, the surface spreading is nine times to the bottom spreading at the crest, and at the toe, the surface spreading is four times to the bottom spreading. In addition, the lateral spreading on the south-facing slope is larger than that on the north-facing slope, which means that the south-facing slope experience more sliding deformation due to subsidence.

3.0 Correlation between the Consolidation and the Lateral Spreading

When comparing the consolidation and lateral spreading in different areas in a certain slope, consolidation was more likely on the crest, while larger lateral spreading took place at the toe area according to the field measurement.

When comparing different slopes (north-facing slope and south-facing slope), the consolidation was higher on the south-facing slope than on the north-facing slope, which means that the south-facing slope is more critical than the north-facing slope impacted by subsidence in terms of the consolidation. The lateral spreading is more serious on the north-facing slope, which means that the north facing slope is more critical with respect to the lateral spreading.

Subsection Vd – Analysis of Piezometer Data

1.0 Description of piezometer data

Some variation was observed in the ground water table in Embankment #1 during the period of the mining activities of Panel 15 according to the piezometer recordings. The locations of the utilized three piezometers are shown in Figure Vd.1. Figure Vd.2 indicated the piezometer measure of the water level in TB-3, TB-7 and TB-12, which were utilized to measure the ground water table at the north slope of Embankment #1, south slope of Embankment #1, and south slope of Embankment #2, respectively. For the cross section 720+50, the University looked at the piezometer at TB-7. While for the cross section 720+00, the piezometer at TB-3 was analyzed.

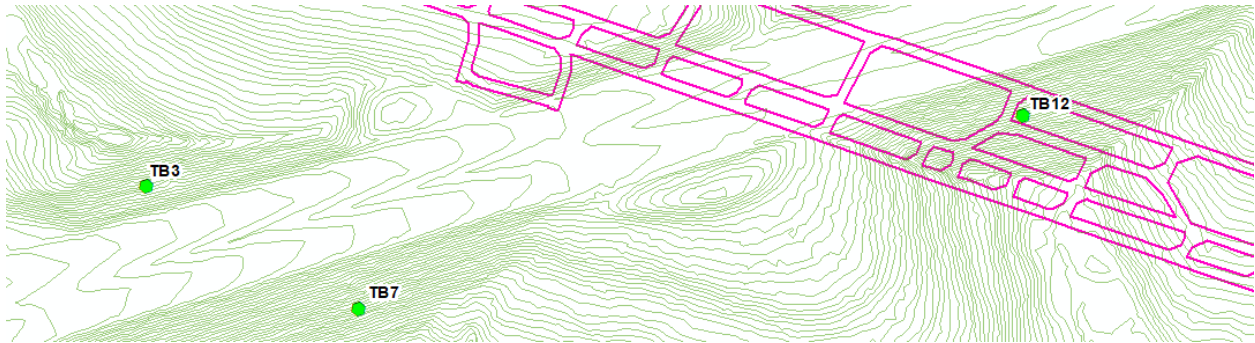


Figure Vd.1 – Locations of three piezometers

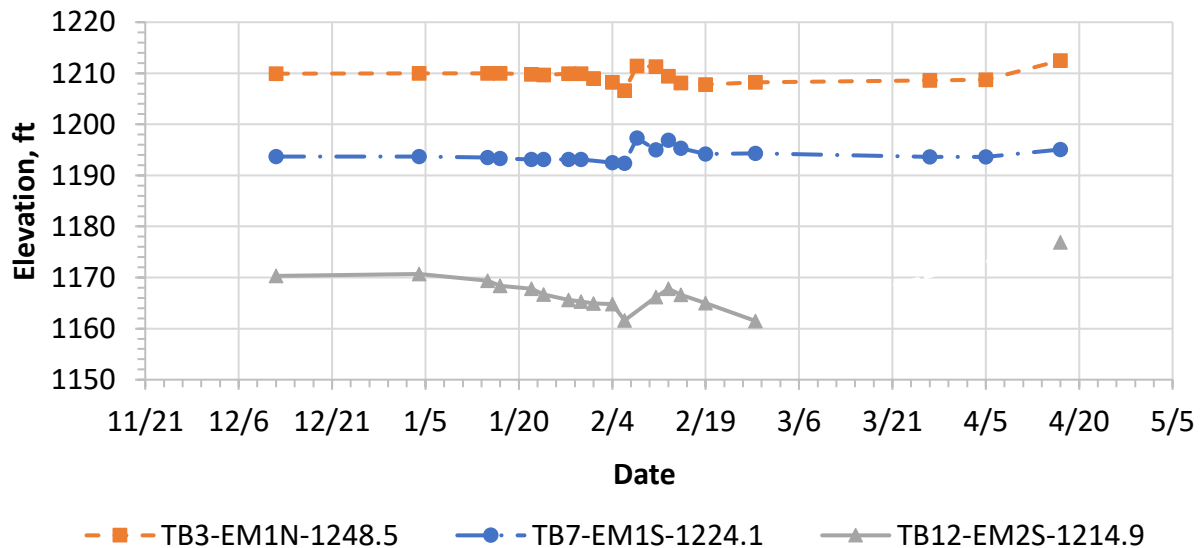
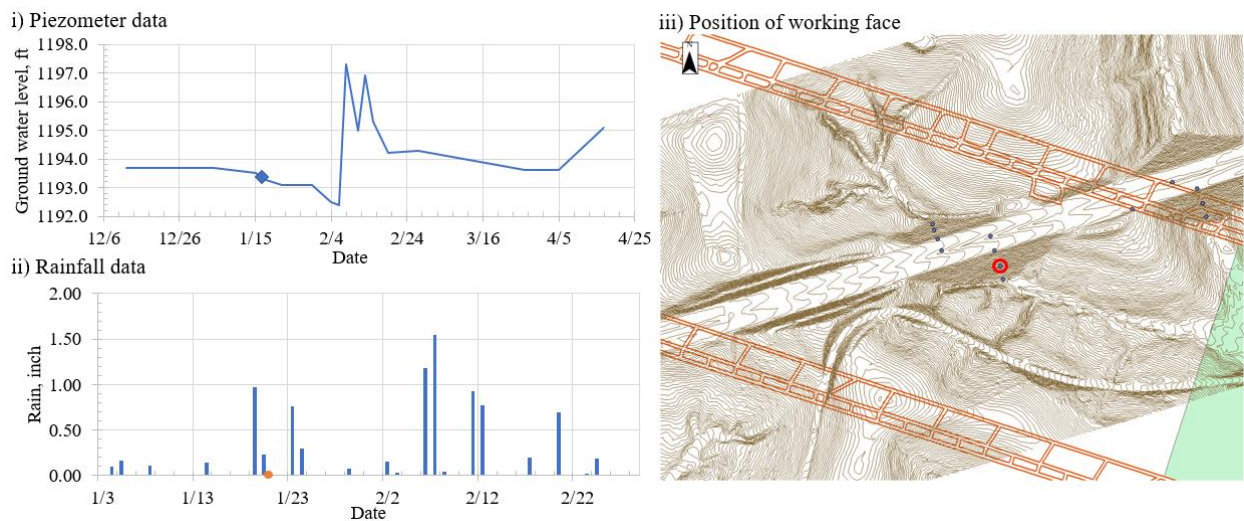


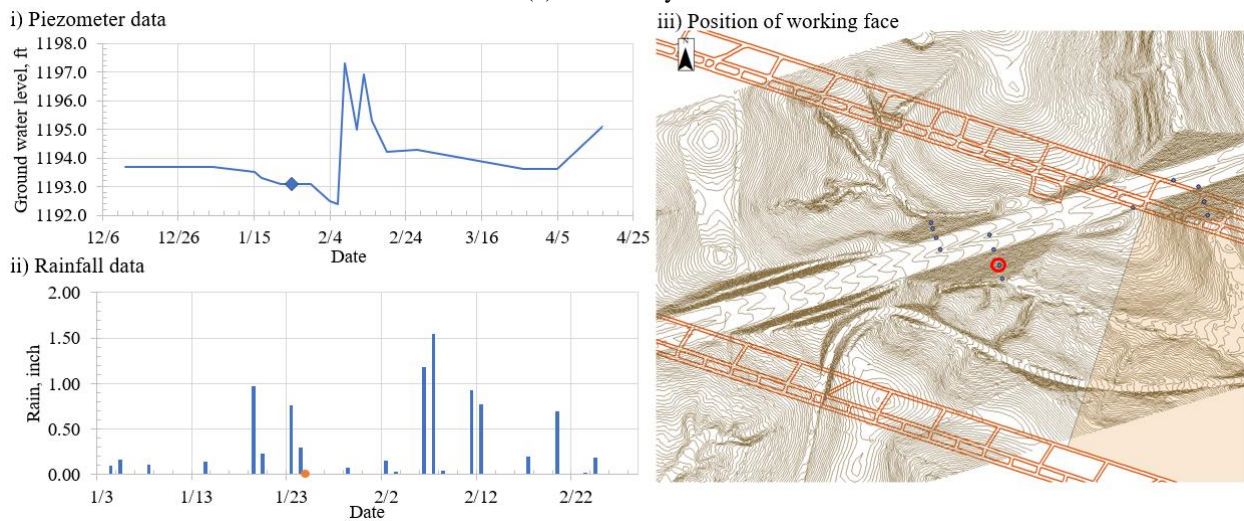
Figure Vd.2 – Variations of the water levels due to longwall mining from 12 December 2018 to 17 April 2019

2.0 Correlation among piezometer, rainfall, and face position

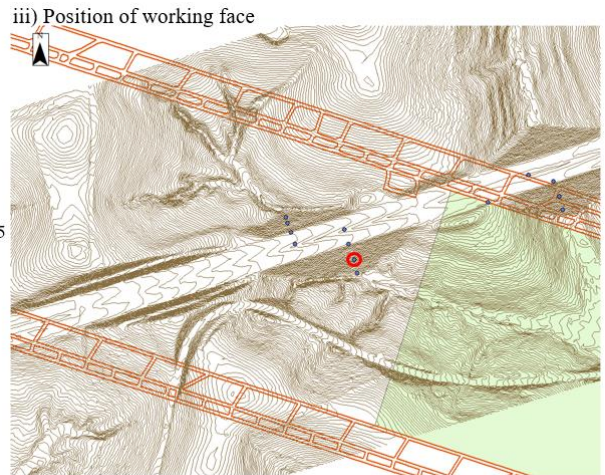
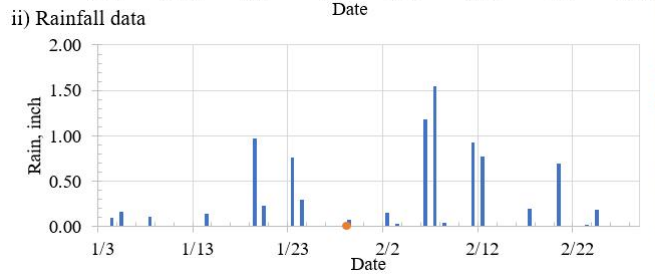
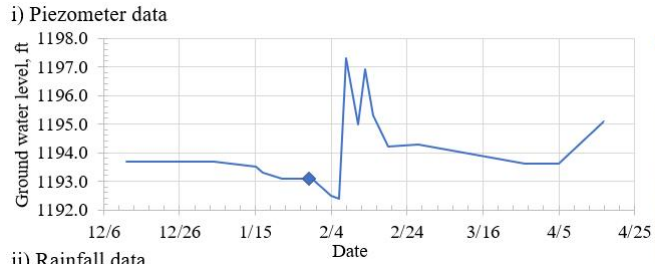
The rainfall at night before the recording date of piezometer will have a dramatic influence on the readings. As such, it is helpful to analyze the rainfall data when utilizing the piezometer to observe the changes in the ground water table elevations. In addition, it is good to know where the working face was located to better understand the influence of the longwall mining on the ground water table variation. Figure Vd.3 indicates the piezometer data (TB-7), rainfall data, and the position of working face on several dates when the longwall mining was beneath the embankment.



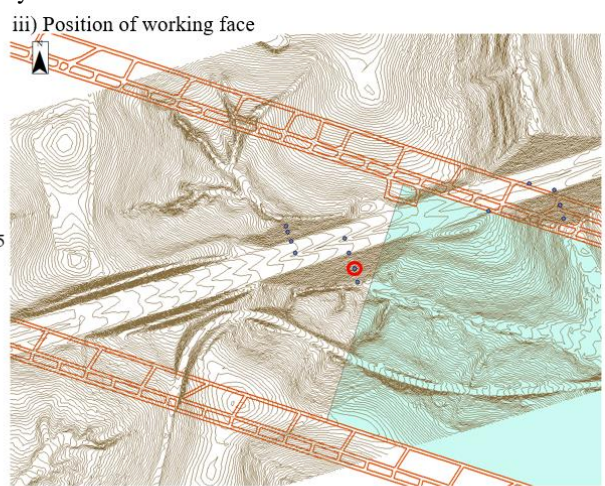
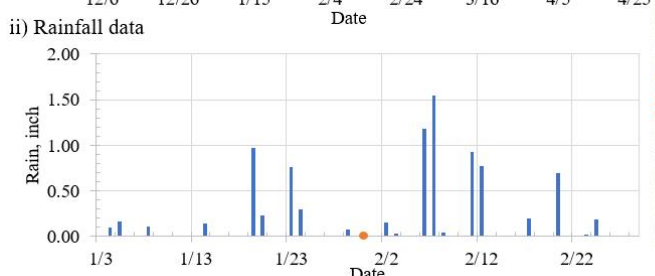
(a) 21 January 2019



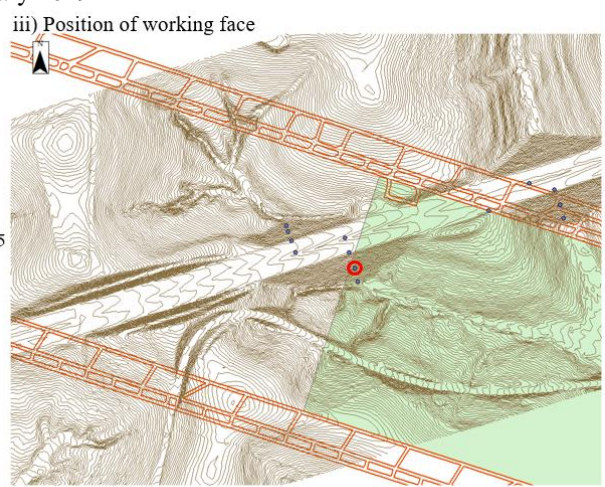
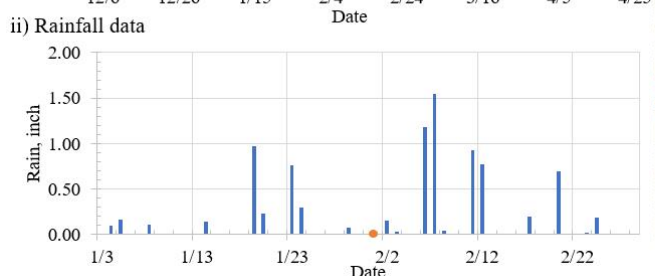
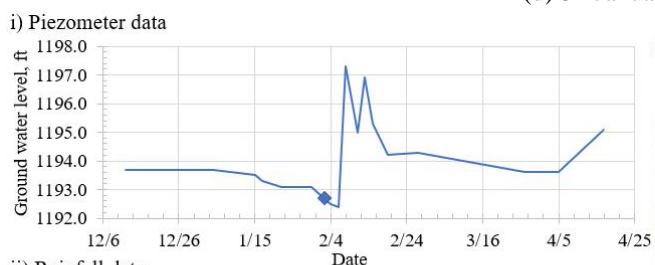
(b) 25 January 2019



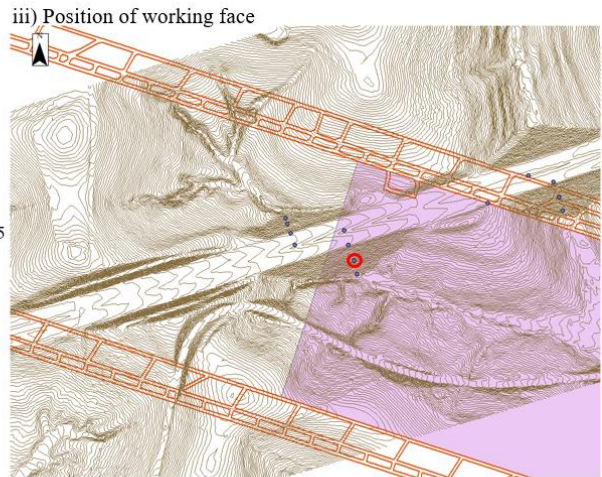
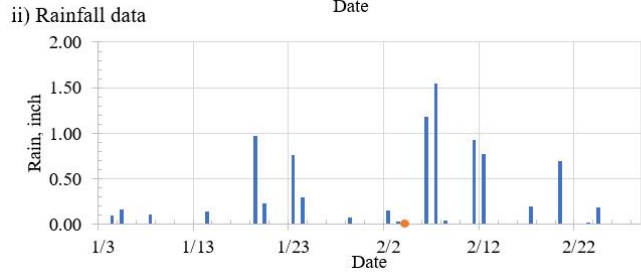
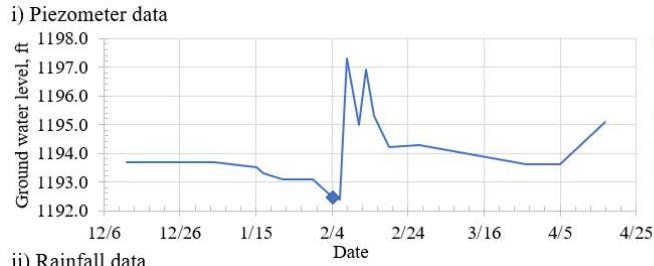
(c) 29 January 2019



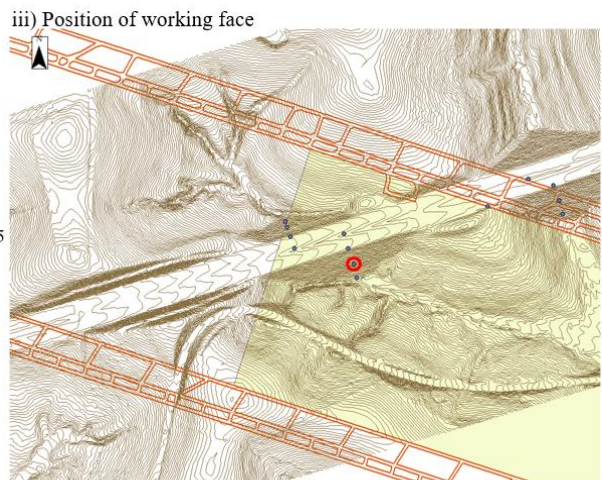
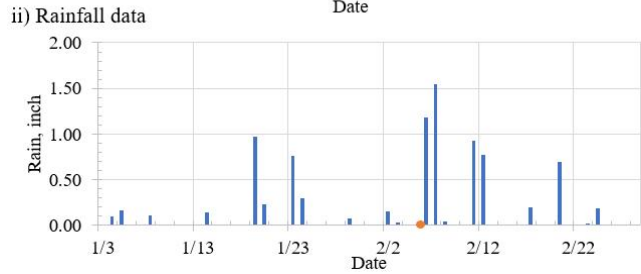
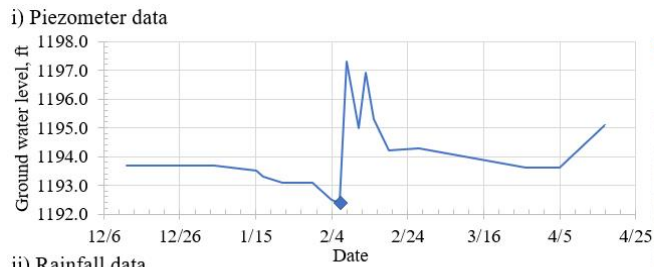
(d) 31 January 2019



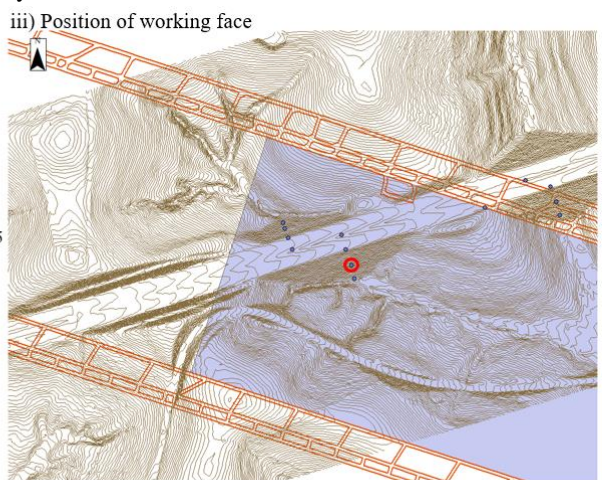
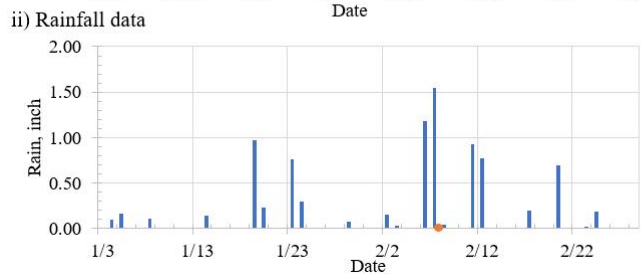
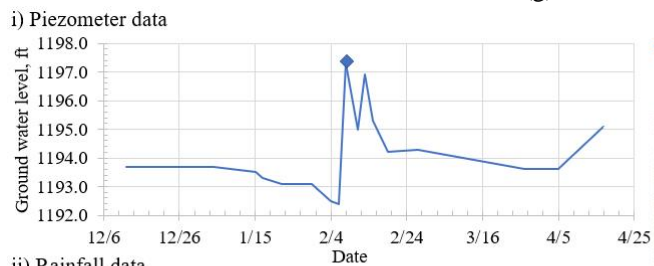
(e) 1 February 2019



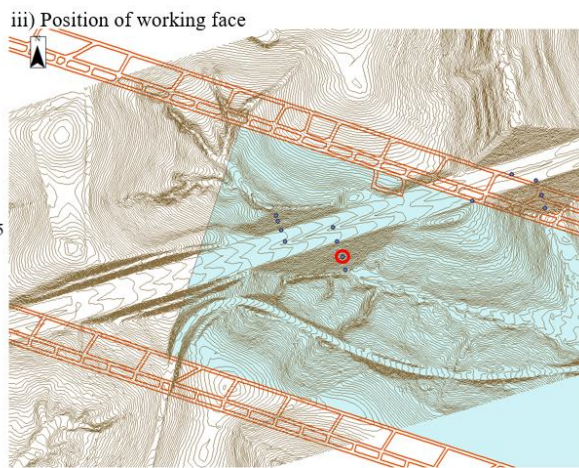
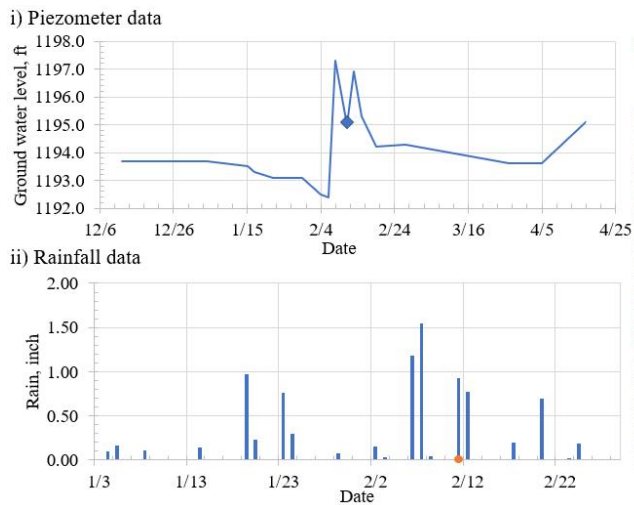
(f) 4 February 2019



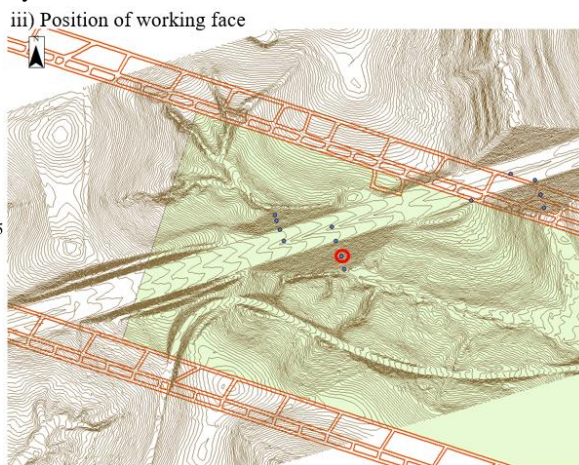
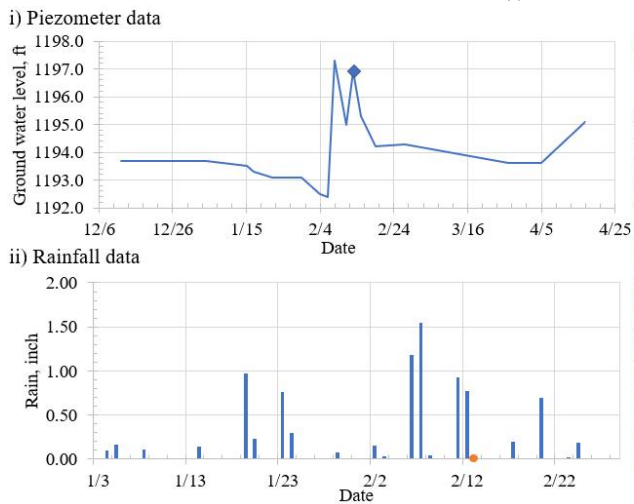
(g) 6 February 2019



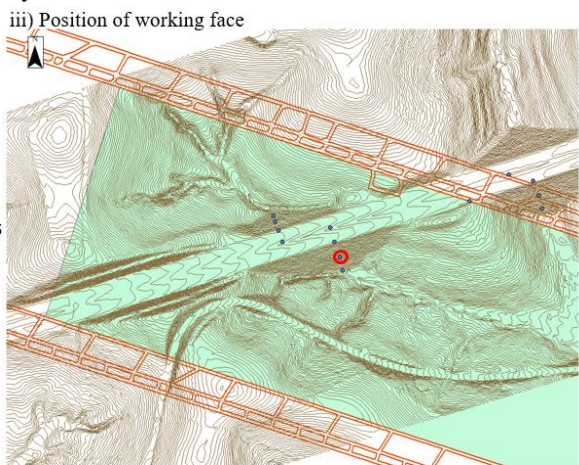
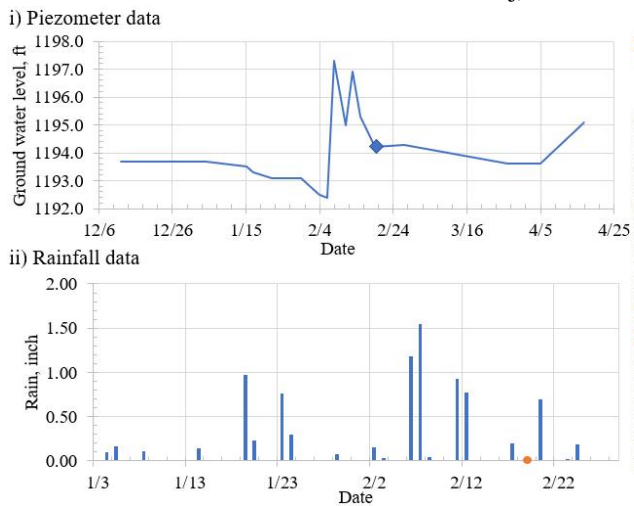
(h) 8 February 2019



(i) 11 February 2019



(j) 13 February 2019



(k) 19 February 2019

Figure Vd.3 – Plot of piezometer data (TB-7) and rainfall data when the working face of longwall mining went through the Embankment #1 on different dates

The water table first dropped when the working face was approaching the embankment, which means that the embankment was located at the tension zone (Figure Vd.4). Cracks were produced in the bedrocks and the water leaked through these cracks.

When the working face just passed the embankment, water table increased. This indicated that the embankment was located in the compression zone. On 8 February, water level increased to the highest magnitude. This was caused not only by the movement of the ground but also by the rain. Cracks closed on this date and rain fall could not penetrate through the compacted earth and accumulated in the lower part of the embankment. The ground water table rose quickly when the embankment was located on the compressive zone of a subsidence profile in the condition of raining. After the working face was far away from the embankment, the water level decreased to the original level.

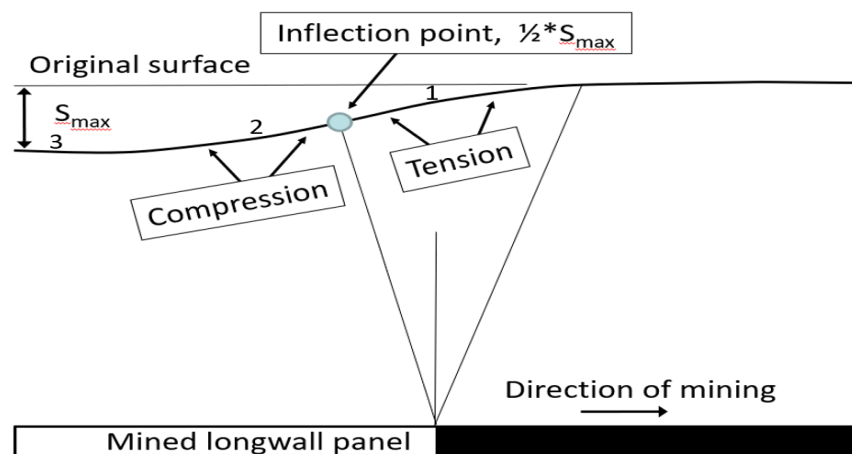


Figure Vd.4 – Cross section of dynamic subsidence along the longitudinal axis of the panel (Peng, et al. 1992)

3.0 Numerical Analysis of Partially Saturated Soils Using FEM

3.1 Coupled Analysis

The FEM ABAQUS is able to consider two fields, soil field and stress field in one step, meaning that it can conduct coupled pore fluid diffusion and stress analysis. Typically, there are three conditions where this technique will be applied.

- Saturated flow: Generally involved in the soil mechanics problem when solid is fully saturated with ground water, that is, the soil is saturated or dry. In this case, no absorption is included.
- Partially saturated flow: The water is absorbed into or escaped from soil due to the capillary behavior when the flow is partially saturated.

- Combined flow: For instance, in the case of the seepage through an earth dam, the fully saturated flow happens on the lower level of water, and partially saturated flow happens on the surface of the water.

In the combined case, there will be an interface between the saturated soil and unsaturated soil, known as the phreatic surface. Pore pressure is positive below the phreatic surface and negative above the phreatic surface.

3.2 Flow through Porous Media

A conventional approach that involved the multiphase material and the effective stress principle is adopted in ABAQUS to describe the behavior of the porous media. Two fluids are considered when modeling the porous medium as a multiphase material, wetting liquid and the gas. The wetting liquid was assumed incompressible while the gas was comparatively compressible.

Soil containing the ground water is an example of such porous medium. When the medium is partially saturated, meaning that partially saturated flow is involved, both two fluids, water and gas exist at a node. When the medium is fully saturated, the voids are completely filled with the wetting liquid, so there is no gas, only the wetting liquid and the solid.

Generally, the elementary volume, dV , in such multi-phase porous media is composed of a volume of grains of solid material, dV_g , a volume of voids, dV_v , and a volume of wetting liquid, $dV_w < dV_v$ that is free to move through medium. In some systems (for instance, systems that absorb the wetting liquid), there could also be a volume of trapped wetting liquid, dV_t . The porous medium is modeled by attaching the finite element mesh to the solid phase and fluid can flow through this mesh.

3.3 Effective Stress Principle

The mechanical part of the multi-phase model is based on the effective stress principle. The total stress acting at a point, σ , is assumed to consist of an average pressure stress in the wetting liquid, u_w , called the wetting liquid pressure, that is, pore water pressure, an average pressure stress in the gas, u_a , and an effective stress, σ' . The composition was explained in Equation Vd.1.

$$\sigma' = \sigma + [\chi u_w + (1 - \chi)u_a]\mathbf{I} \quad [\text{Eq. Vd.1}]$$

Where: χ is a parameter that depends on saturation of the porous media and the surface tension of liquid/solid system (Wu and Kraft, 1970). χ is 1.0 when the medium is fully saturated and between 0.0 and 1.0 in unsaturated systems depending on the degree of saturation of the medium. In ABAQUS, this parameter is assumed to be equal to the

saturation of the medium due to the lack of data of its dependence on saturation. Remember in ABAQUS, the tensile stress is positive, compressive stress is negative, and u_w and u_a are pressure values, which accounts for the sign in the equation above.

The model is simplified by assuming that the pressure applied to the gas is constant throughout the domain. Also, it does not vary with time and is small enough that it can be neglected. The precondition for this simplification is that the dry fluid can diffuse through the medium sufficiently freely so that its pressure, u_a , never exceeds the pressure applied to this fluid at the boundaries of the medium, which remains constant throughout the process. This assumption allows the dry fluid pressure, u_a to be removed from the original effective stress equation for the reason that the u_a is small enough so that its influence on the deformation of the multi-phase medium is inconsequential. Therefore, the effective stress principle can be expressed as Equation Vd.2.

$$\boldsymbol{\sigma}' = \boldsymbol{\sigma} + \chi u_w \mathbf{I} \quad [\text{Eq. Vd.2}]$$

3.4 Pore Water Pressure

The basic equation utilized for the pore water pressure u_w is calculated using Equation Vd.3.

$$u_w(y) = \gamma_w (y_{top} - y) \quad [\text{Eq. Vd.3}]$$

Where: water pressure at an elevation y is related to the vertical elevation from that point to the top of the water surface, that is, $y_{top} - y$. Specific weight of water, γ_w is defined using Equation Vd.4.

$$\gamma_w = \rho_w g \quad [\text{Eq. Vd.4}]$$

Where: ρ_w denotes the density of water, and g the gravitational acceleration.

In this problem, the unit system was based on ‘ft’ system in ABAQUS, hence, the unit for the specific weight of the liquid is lbf/ft³, and if it is the water, the specific weight is 62.4-lbf/ft³.

This illuminated the reason we need to specify the specific weight of the liquid in the property set-up in ABAQUS whenever utilizing the soil field, that is, to calculate the pore water pressure.

4.0 **Analysis of Results**

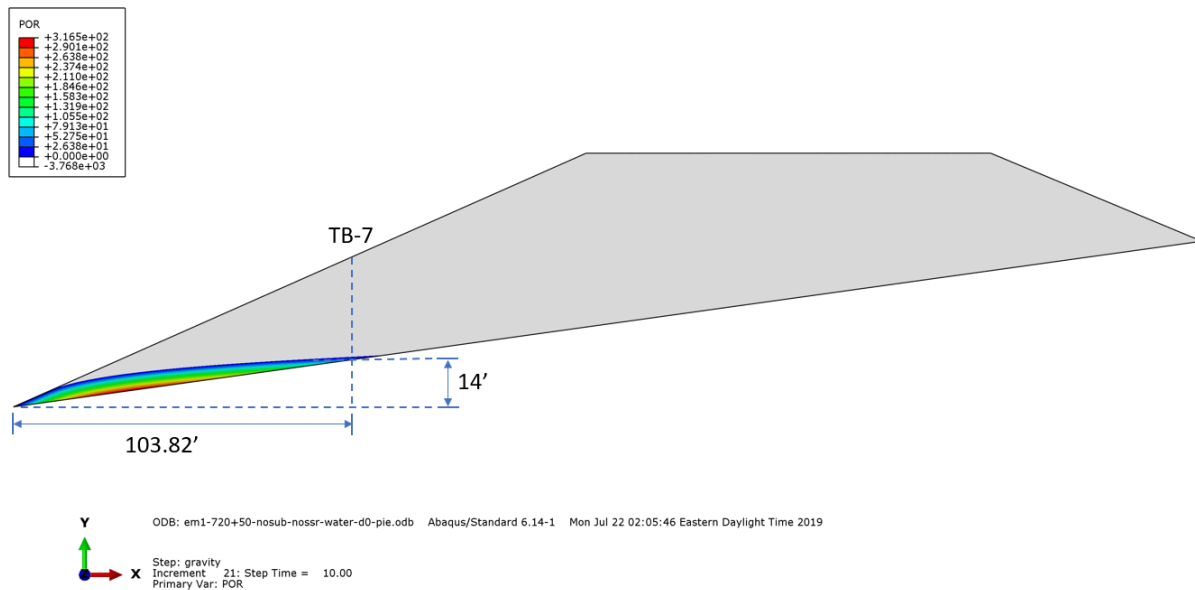
4.1 Cross Section 720+50

The water table at this cross section varied from 1192.4-ft to 1197.3-ft. The elevation of the lower toe is 1190-ft. Besides, looking through the previous readings of the piezometer data at

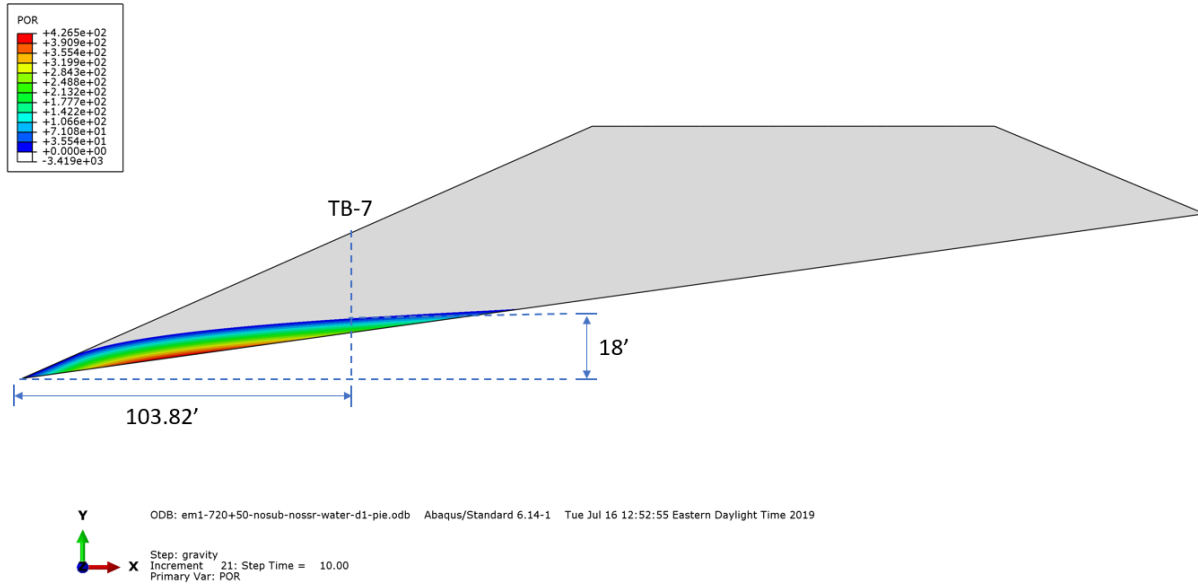
TB-7, the highest record was 1204-ft on the date of 9 February 2017. From the boring log provided from PennDOT, the water level was 1208-ft at TB-7 which was recorded 17 hours after the installation of the boring hole was finished.

4.1.1 Phreatic Surface

The University compared the influence of such difference in the water table on the slope stability of embankment at cross section 720+50. The resulting phreatic surface is shown in Figure Vd.5. The elevation of the phreatic surface in the location of TB-7 at cross section 720+50 in Embankment #1 was 1204-ft (from piezometer data in Feb, 2017) and 1208-ft (from piezometer data recorded after installation of the boring hole). Below the phreatic surface, the soil is saturated and the pore water pressure turns out to be positive. From the contour, the phreatic surface did not go straight to the toe forming a discharge zone, which corresponded to the field observation that the water came out of the slope.



(a) Water level = 1204-ft



(b) Water level = 1208-ft

Figure Vd.5 – Two elevations of the phreatic surface at TB-7 indicated by the positive pore water pressure

However, this resulted discharge zone is much smaller than that observed in field. According to the field observation on 17 December 2018, the distance from the top of the saturated zone to the lower toe is around 50-ft with a vertical distance of 18-ft. Hence, another model was constructed by defining the saturated zone on the slope corresponding to the field observation. Based on this boundary condition, FEM calculated the resulted water level at TB-7 as 1206.3-ft shown in Figure Vd.6, which is in the range of the piezometer data at the installation of the boring hole.

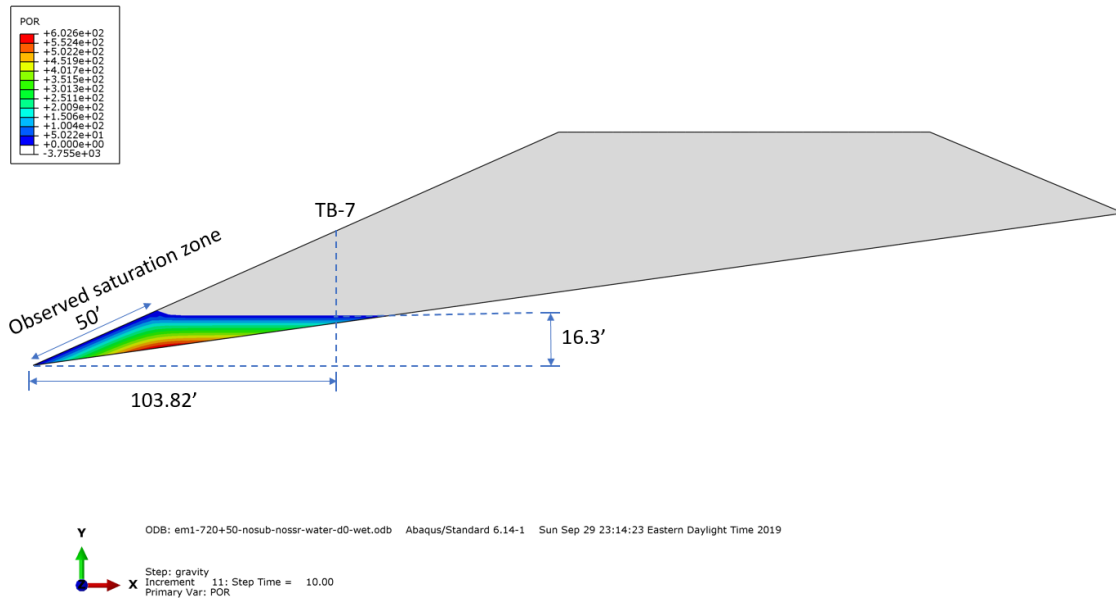
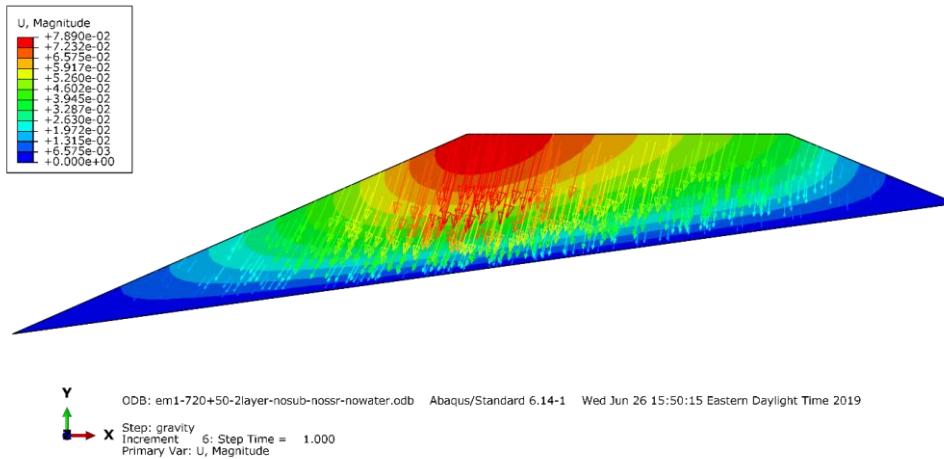


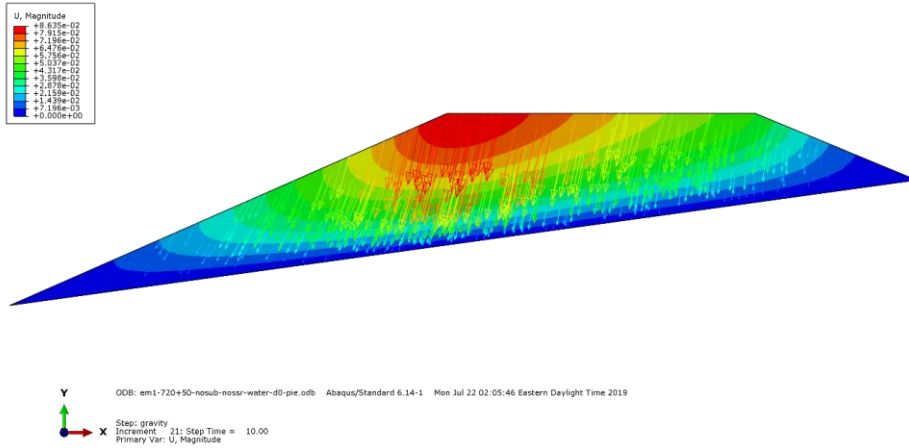
Figure Vd.6 – The elevation of the phreatic surface at TB-7 resulted from the observed saturation zone

4.1.2 Total Displacement

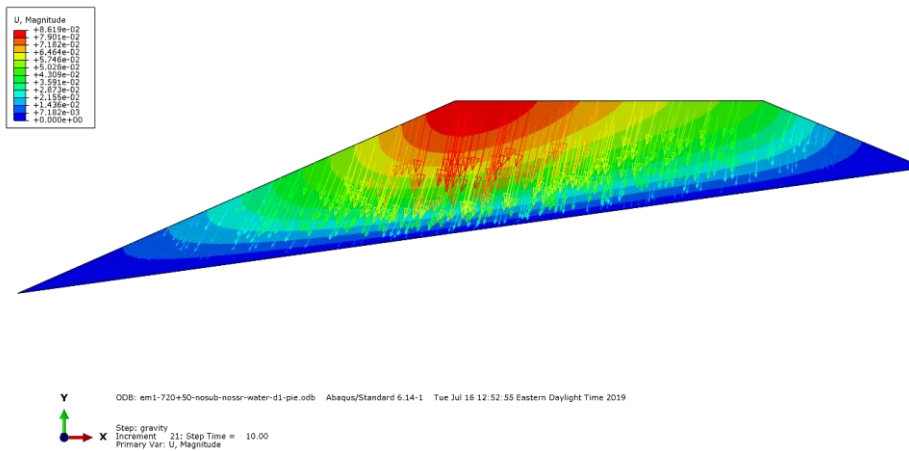
Figure Vd.7 indicated the total displacement at cross section 720+50 with different elevations of the water table. The magnitudes of the total displacement under these four conditions were plotted against the vertical distance between the phreatic surface and the lower toe of the slope in Figure Vd.8. The slope with water presented a 7.6% higher displacement at the crest than that without water.



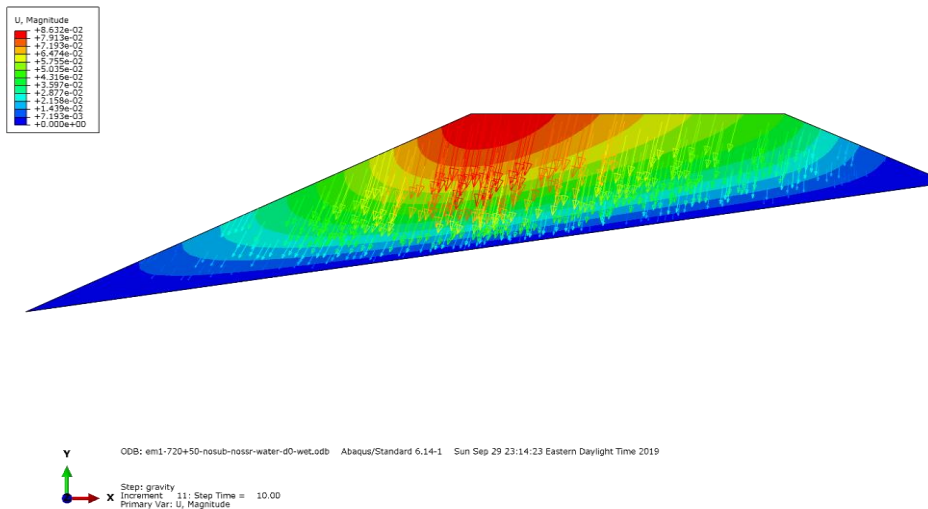
(a) no water



(b) 1204-ft



(c) 1208-ft



(d) 1206-ft resulted from field saturated zone

Figure Vd.7 – Total displacement in the Embankment #1 at cross section 720+50 with (a) no water and with phreatic surface at an elevation of (b) 1204-ft; (c) 1208-ft and (d) 1206-ft with field saturated zone

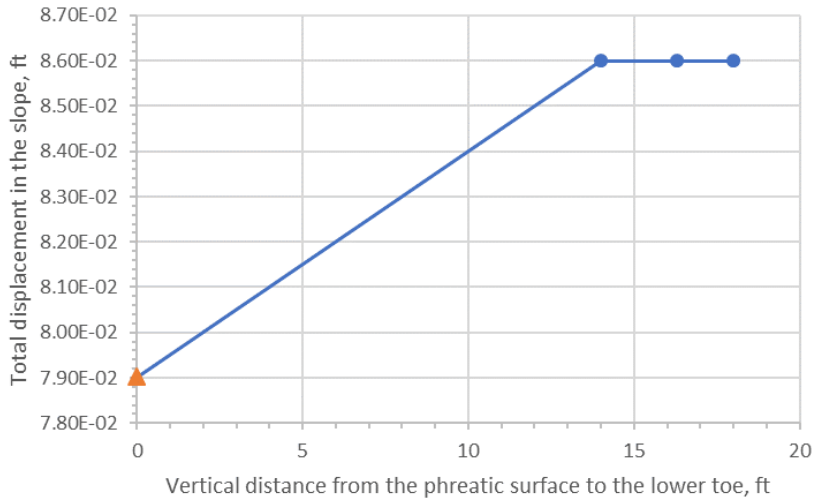
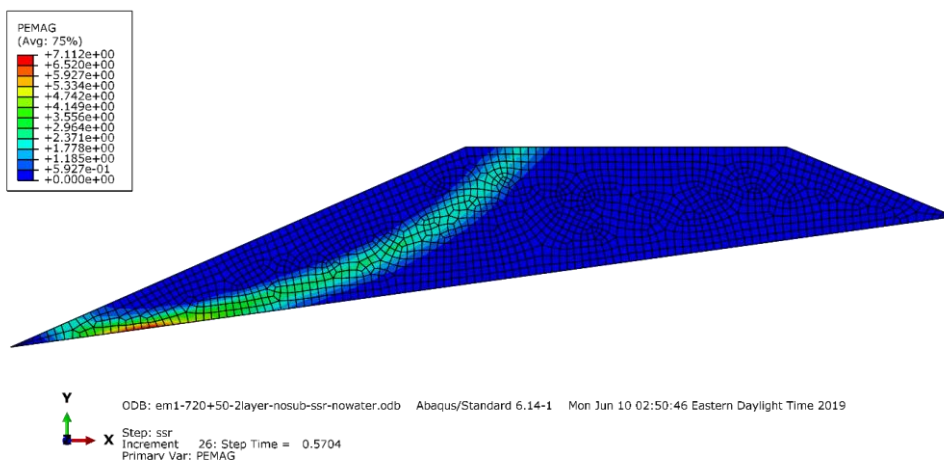


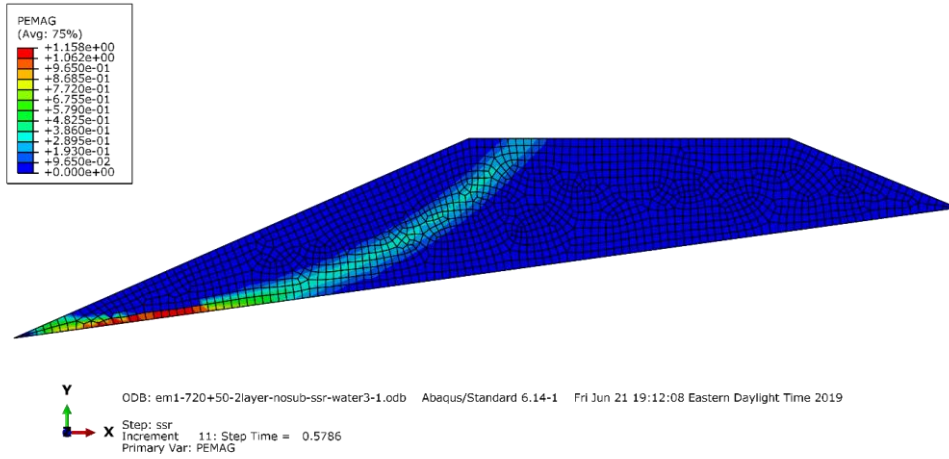
Figure Vd.8 – Total displacement versus the vertical distance between the phreatic surface and the lower toe

4.1.3 Potential Rupture Surface at Failure

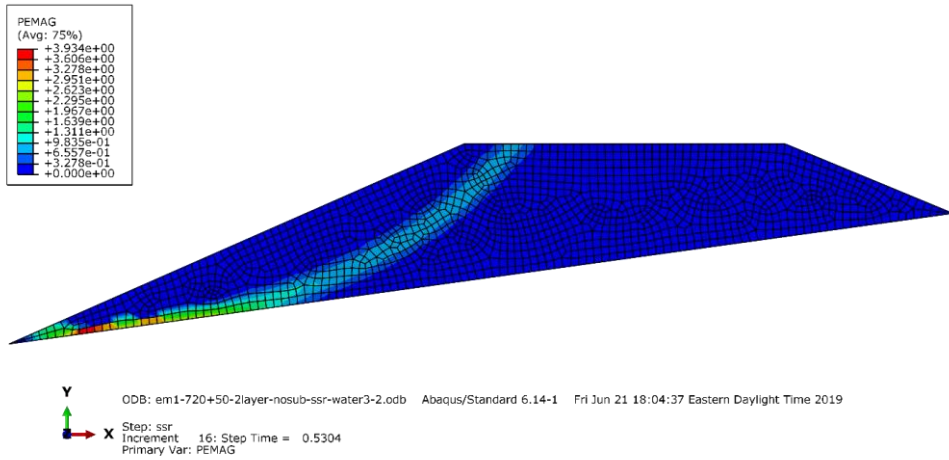
The rupture surface at failure was tracked by the development of plastic shear strain. Figure Vd.9 indicates the magnitude of the plastic strain at cross section 720+50 with different elevations of water table. A large difference was observed in the potential plastic zone between no water and in different elevations of water table. The magnitude of plastic strain reached the maximum on the bottom of the embankment near the toe area. For the conditions with water, the plastic zone is more concentrated in the area near the toe. The majority of the plastic zone remains in the lower part of the slope where there was water, while on the upper part of the slope, the magnitude of the plastic strain was much lower. Besides, the slope with a higher water level presented the plastic strain with more intense concentration on the bottom.



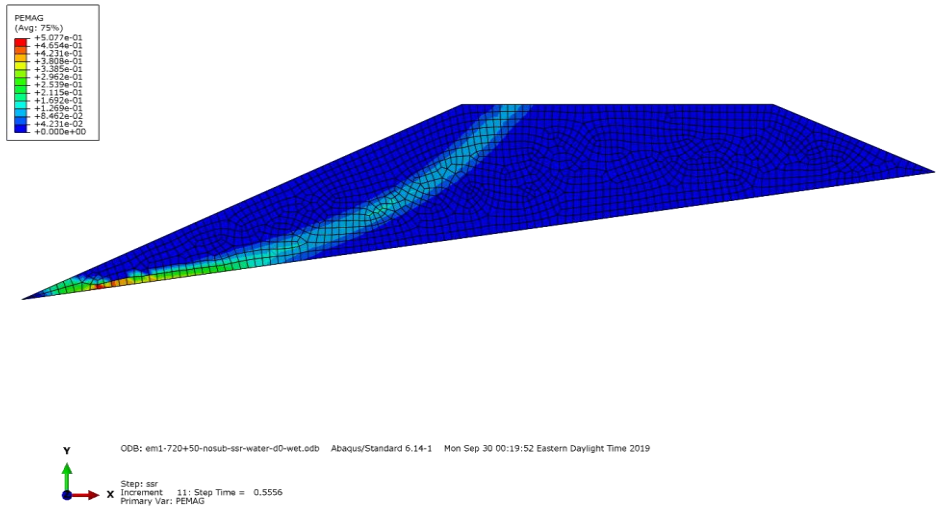
(a) no water



(b) 1204-ft



(c) 1208-ft



(d) 1206-ft with field saturated zone

Figure Vd.9 – Potential plastic strain at failure in the Embankment #1 at cross section 720+50 with (a) no water and with phreatic surface at an elevation of (b) 1204-ft; (c) 1208-ft and (d) 1206-ft with field saturated zone

4.1.4 Factor of Safety

The determination of the factor of safety in four different conditions of water content was summarized in Figure Vd.10. The total displacement was plotted against the strength reduction factor in this process. The field value at the inflection point represented the factor of safety. The resulted factor of safety was plotted versus the vertical distance between the phreatic surface and the lower toe in Figure Vd.11. The factor of safety was the lower when there was water compared to the dry conditions, but still above one, indicating that the embankment was safe. However, the increase of the water level contributed to the decrease of the factor of safety. When the water level increased from 1204-ft to 1208-ft, factor of safety decreased from 2.3 to 2.16.

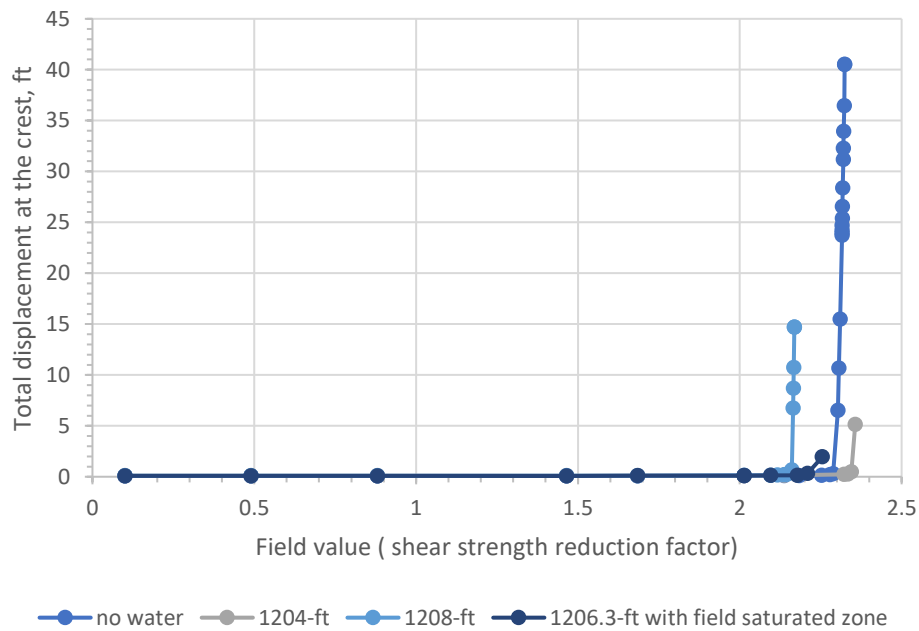


Figure Vd.10 – Determination of the factor of safety by plotting the total displacement at the crest versus the shear strength reduction factor

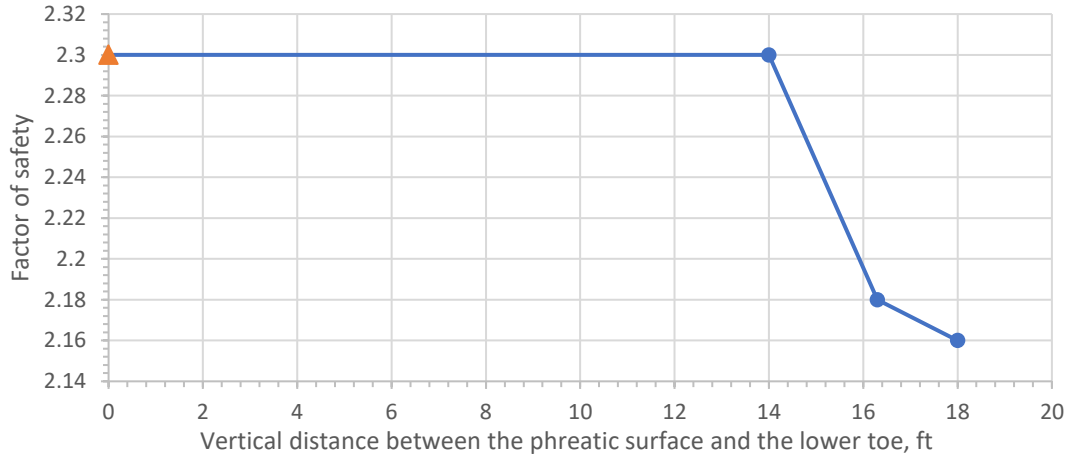
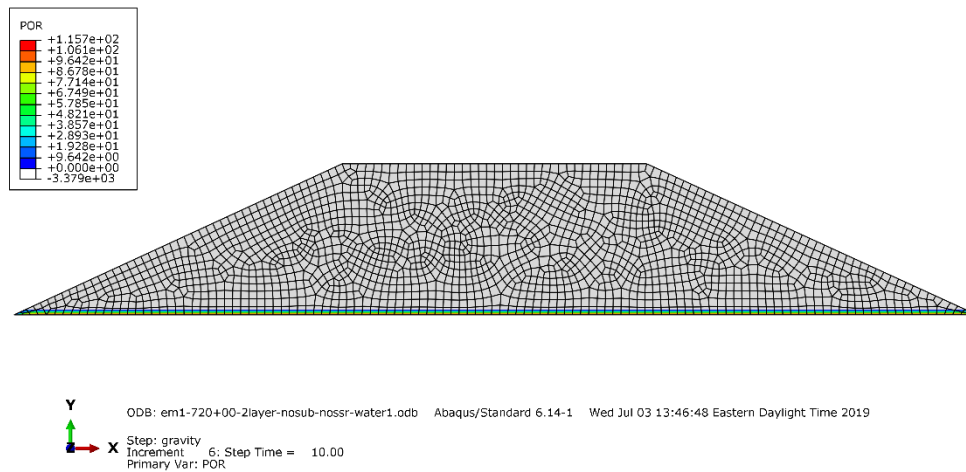


Figure Vd.11 – Factor of safety of Embankment #1 at cross section 720+50 with different ground water tables

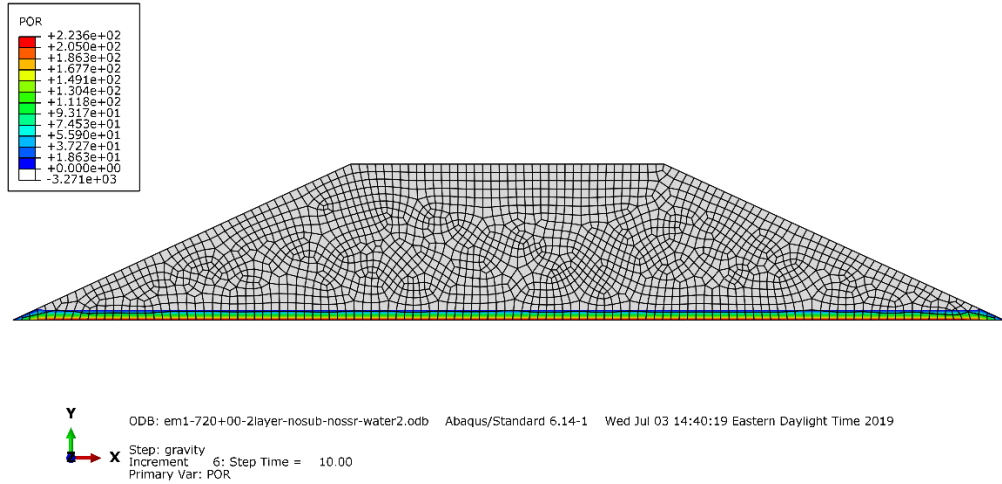
4.2 Cross Section 720+00

4.2.1 Phreatic Surface

The water table varied from 1206.6-ft to 1214.0-ft from the piezometer readings at cross section 720+00. This indicated that the water table was below the bottom of the embankment, which was at 1216-ft. However, considering the growing trend in the latest readings of April, there is a possibility that the water table will reach the elevation which is above the bottom of the embankment. Two elevations were selected to analyze the influence of the potential water level, 1218-ft and 1220-ft, which were 2-ft and 4-ft above the toe, shown in Figure Vd.12.



(a) water level = 1218-ft

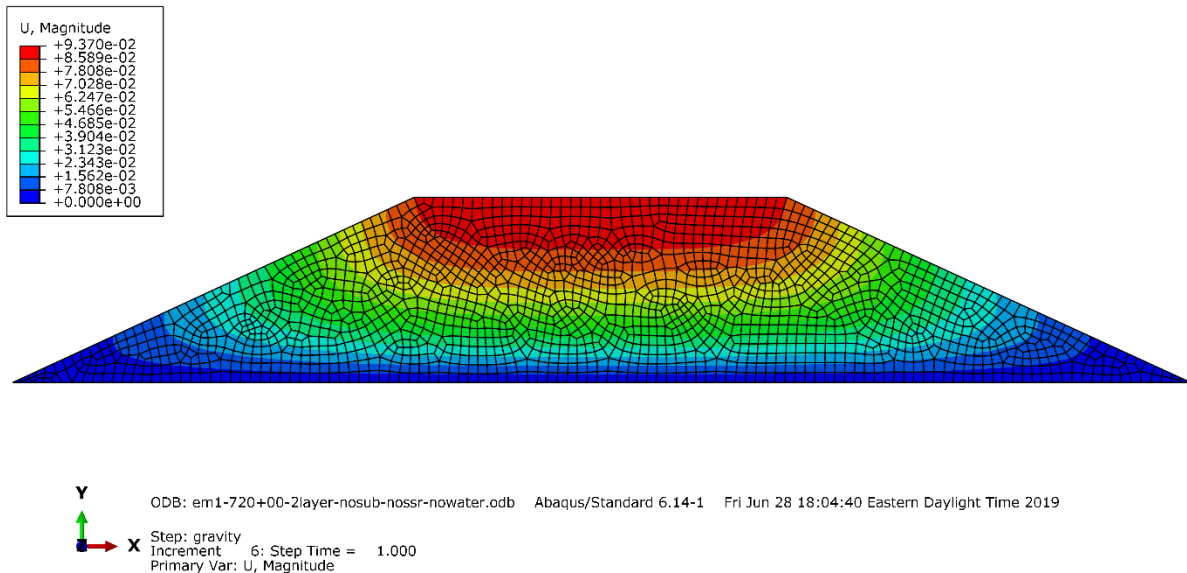


(b) water level = 1220-ft

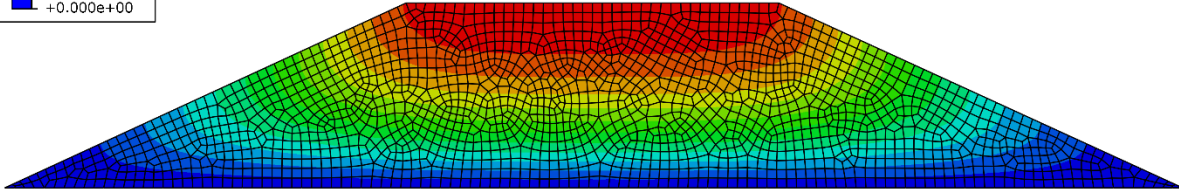
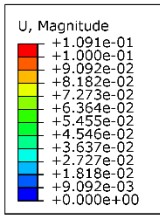
Figure Vd.12 – Two elevations of the phreatic surface indicated by the positive pore pressure

4.2.2 Total Displacement

Figure Vd.13 indicated the total displacement at cross section 720+00 with different elevations of water table. The total displacement was plotted against the vertical distance between the phreatic surface and the lower toe in Figure Vd.14. The total displacement increased when the water level rose from 0-ft to 2-ft from the toes.

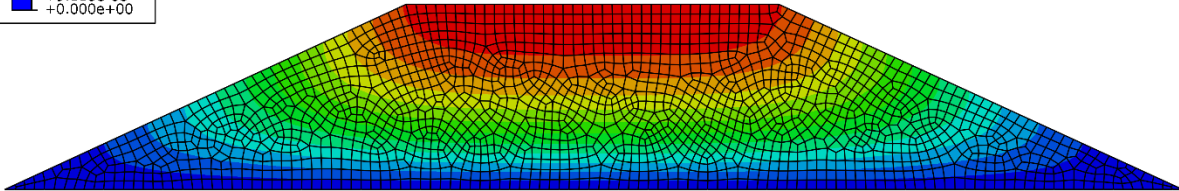
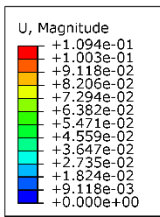


(a) no water



Y
 X
 ODB: em1-720+00-2layer-nosub-nosr-water1.odb Abaqus/Standard 6.14-1 Wed Jul 03 13:46:48 Eastern Daylight Time 2019
 Step: gravity
 Increment 6: Step Time = 10.00
 Primary Var: U, Magnitude

(b) 1218-ft



Y
 X
 ODB: em1-720+00-2layer-nosub-nosr-water2.odb Abaqus/Standard 6.14-1 Wed Jul 03 14:40:19 Eastern Daylight Time 2019
 Step: gravity
 Increment 6: Step Time = 10.00
 Primary Var: U, Magnitude

(c) 1220-ft

Figure Vd.13 – Total displacement in the Embankment #1 at cross section 720+00 with (a) no water as well as with phreatic surface at an elevation of (b) 1218-ft and (c) 1220-ft

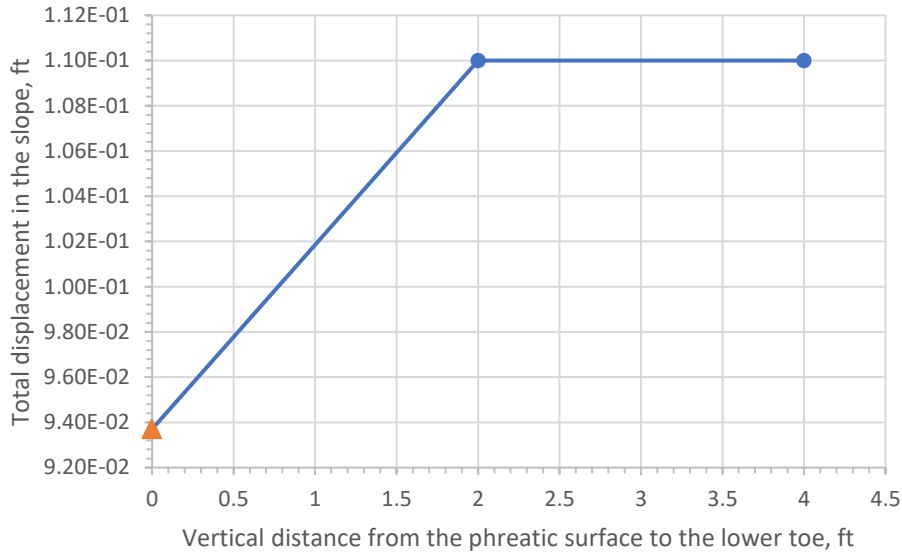
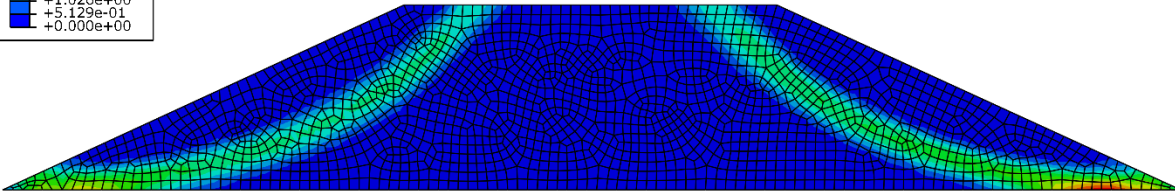
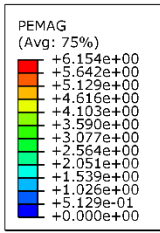


Figure Vd.14 – Total displacement versus the vertical distance between the phreatic surface and the lower toe at cross section 720+00

4.2.3 Potential Rupture Surface at Failure

The rupture surface at failure was tracked by the development of plastic shear strain. Figure Vd.15 indicates the magnitude of the plastic strain at cross section 720+00 with different elevations of water table. A large difference was observed in the potential plastic zone in different water contents. Without water, both slopes present the plastic strain zone which indicated that the slipping surface will happen at both sides. When the water level was 2-ft above the toe, the left side was the critical one for the reason that the water level is still very low and the left side, which is the lower side, will take more influences from water than the higher side, the right side. However, when the water level reached 4-ft, the right side becomes the critical one because the water level has covered both sides, and due to the right side has a higher slope, and water will enlarge such difference, making the weaker side much weaker.

In addition to the locations, the plastic zone itself was different. When there was water, the plastic zone more concentrated on the lower part, and the concentration at the bottom of the slope became more intense.

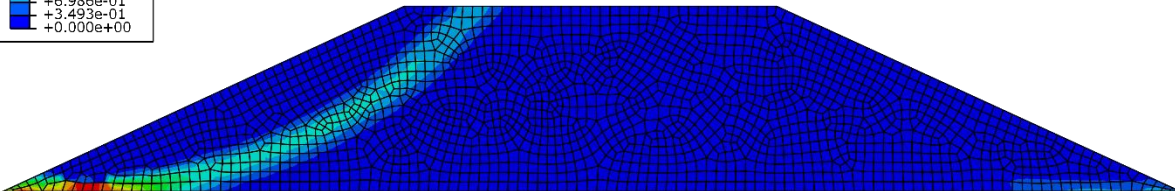
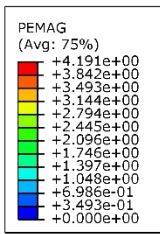


Y ↑
 X →

ODB: em1-720+00-2layer-nosub-ssr-nowater.odb Abaqus/Standard 6.14-1 Sun Jun 30 23:37:18 Eastern Daylight Time 2019

Step: ssr
 Increment 144: Step Time = 0.6016
 Primary Var: PEMAG

(a) no water

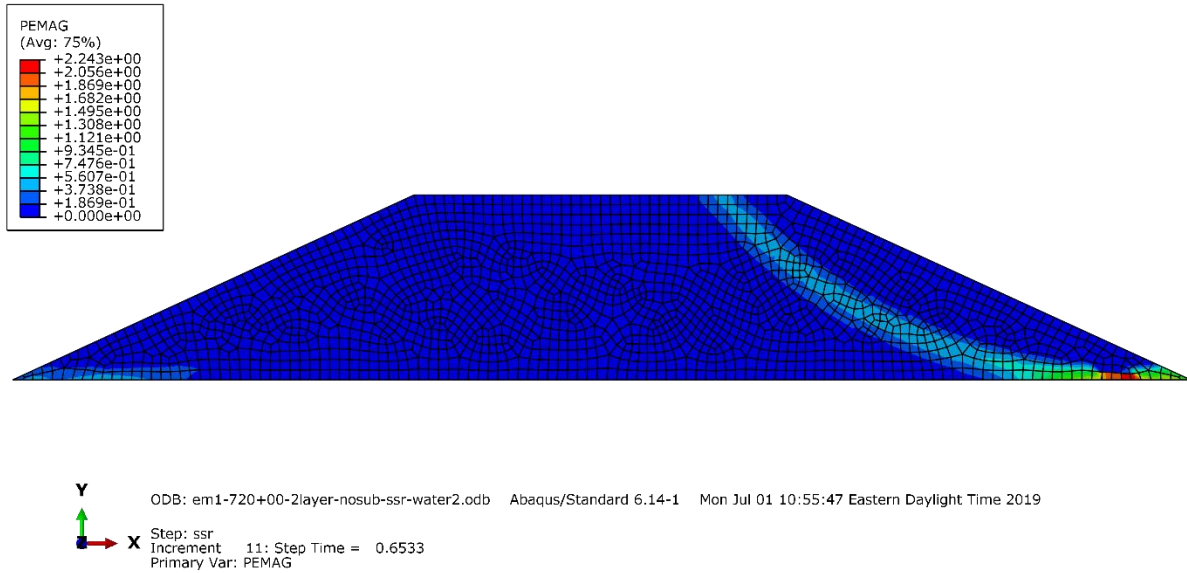


Y ↑
 X →

ODB: em1-720+00-2layer-nosub-ssr-water1.odb Abaqus/Standard 6.14-1 Mon Jul 01 10:58:18 Eastern Daylight Time 2019

Step: ssr
 Increment 78: Step Time = 0.6706
 Primary Var: PEMAG

(b) 1218-ft



(c) 1220-ft

Figure Vd.15 – Potential plastic strain in the Embankment #1 at cross section 720+00 with (a) no water as well as with phreatic surface at an elevation of (b) 1218-ft and (c) 1220-ft

4.2.4 Factor of Safety

The determination of the factor of safety in three different conditions of water content was summarized in Figure Vd.16. The total displacement was plotted against the strength reduction factor in this process. As the water level increased, the factor of safety decreased a little bit, but the embankment was still safe as shown in Figure Vd.17.

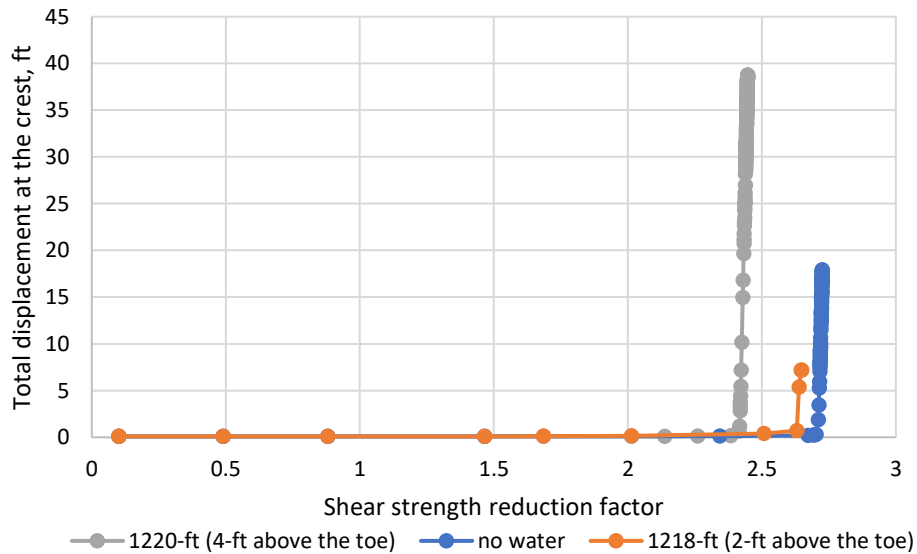


Figure Vd.16 – Determination of the factor of safety by plotting the total displacement at the crest versus the lower point of the slope

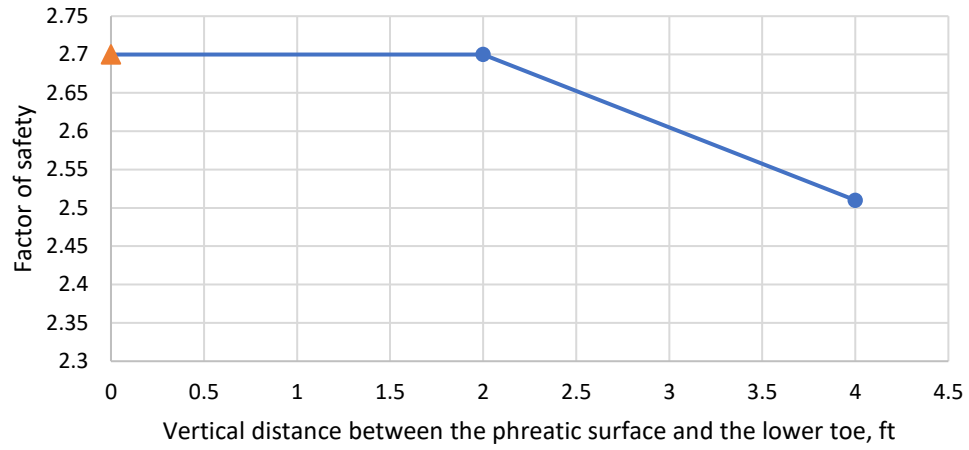


Figure Vd.17 – Factor of safety of Embankment #1 at cross section 720+00 with different ground water tables

Subsection Ve – FEM Analysis of Embankment #1 Subjected to Limited (2D) Simulated Subsidence

1.0 Introduction

This report presented the work from the University on building the numerical regression function of the vertical subsidence basin generated from the University's SDPS model and subjecting the three-dimensional Embankment #1 to the limit subsidence wave. Progress has been made by applying the limit subsidence wave to the bottom of the 3D Embankment #1 Finite Element model to accurately simulate the behavior of the embankment including the deformation and slope stability. The SDPS model assumes a flat ground surface.

2.0 Numerical Regression of the SDPS Model

The successive subsidence profiles at the bottom of the embankment is needed for the Finite Element models. The University utilized the Richard Model (Graybill and Iyer, 1994; Gutierrez, 2010; Vallejo and Lin, 2010) to conduct the numerical fitting of the vertical subsidence basin generated from the SDPS model. The regression function is shown in Equation Ve.1.

$$\frac{S}{S^*} = \frac{1}{\left[1 + e^{-\left(a_1 + a_2 \frac{x}{H}\right)}\right]^{a_3} \left[1 + e^{-\left(a_4 + a_5 \frac{y}{H}\right)}\right]^{a_6}} \quad [\text{Eq. Ve.1}]$$

Where:

- S^* = the maximum subsidence;
- H = overburden;
- S = subsidence at point (x, y);
- $a_1 a_2 a_3 a_4 a_5 a_6$ = constant parameters.

The six parameters were determined by utilizing a Genetic Algorithm (GA) so that the function could be fitted to the SDPS data. When utilizing GA in this problem, a fitness function is defined as the square error of the regression profile compared to the SDPS model shown in Equation Ve.2.

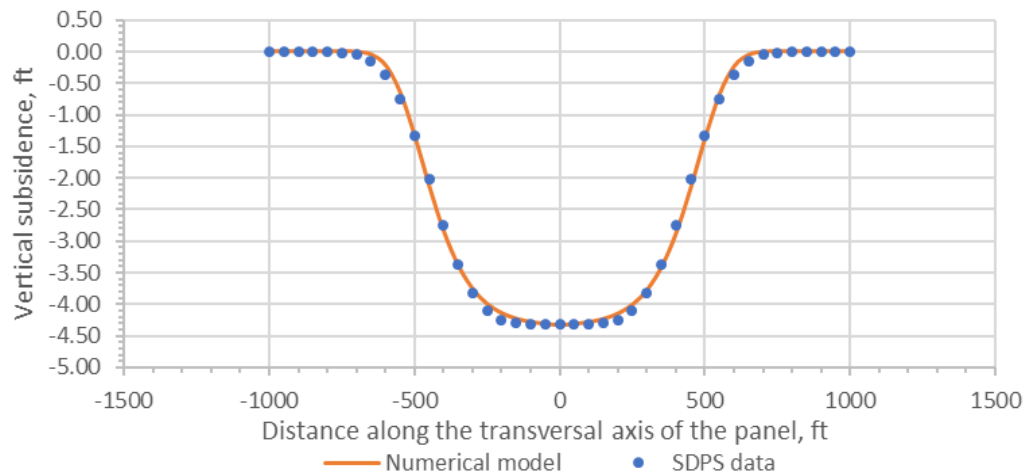
$$\text{Fitness function} = \frac{\sum_{i=1}^n [S_i - S(x_i)]^2}{n} \quad [\text{Eq. Ve.2}]$$

Where:

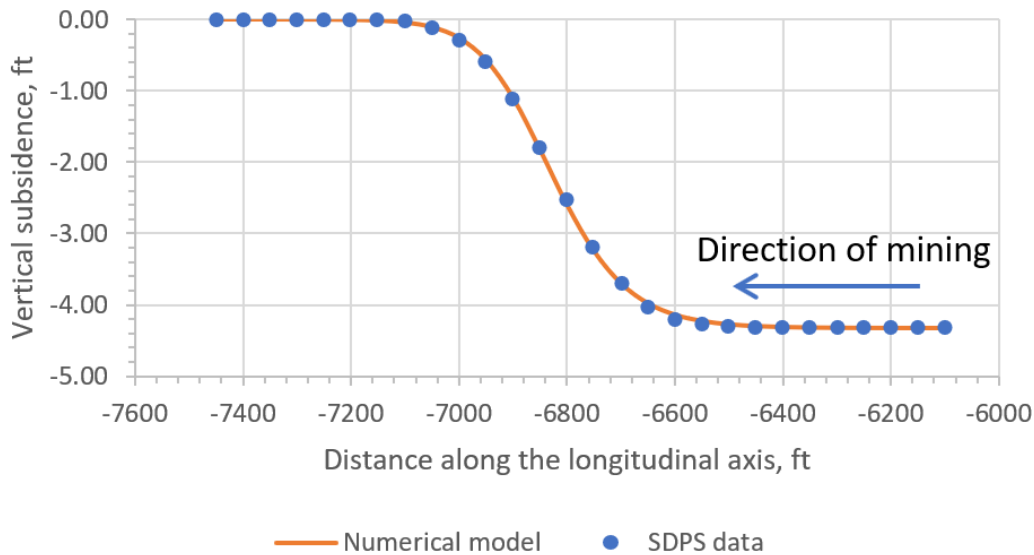
- n = the number of points;
- S_i = the subsidence from SDPS;
- $S(x_i)$ = the subsidence from the numerical fitting.

The optimization toolbox in MATLAB was utilized to conduct the procedure and find the six constant parameters. The resulting regression fitting functions were plotted along the transversal and longitudinal axis of the mining panel in two dimensions as well as in three dimensions shown in Figure Ve.1a, b and c respectively. The figures indicate that the numerical fitting functions can accurately simulate the actual formation of the subsidence basin.

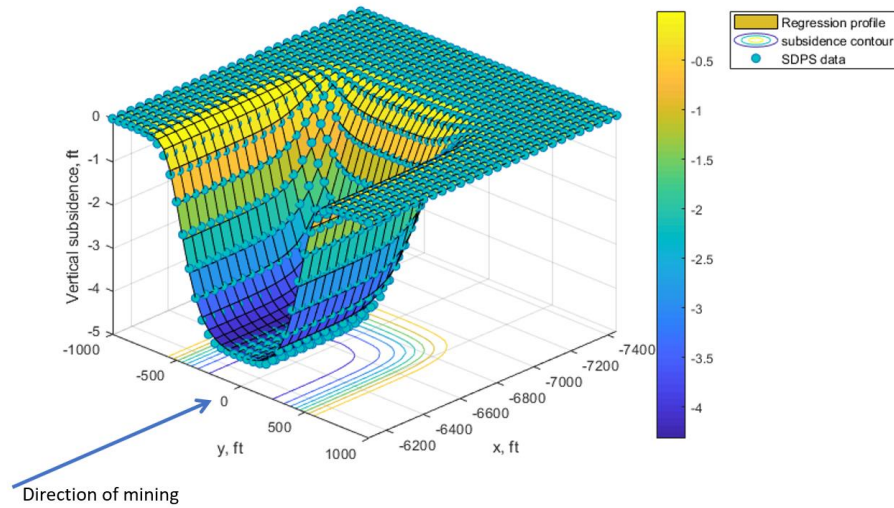
It should be mentioned that the subsidence basin was simplified as a uniform subsidence wave considering that Embankment # 1 is in the center of the panel. Only vertical subsidence showed good match to the field measurement and only vertical subsidence was considered in this study.



(a) Numerical regression model of SDPS data for 2D vertical subsidence along the transversal axis of panel



(b) Numerical regression model of SDPS data for 2D vertical subsidence along the longitudinal axis of panel



(c) Numerical regression model of SDPS data for 3D vertical subsidence

Figure Ve.1 – Numerical regression results (a) along the transversal axis, (b) along the longitudinal axis and (c) in three dimensions

3.0 Implementation of the Fitting Function into the FEM

In order to simulate the behavior of the embankment subjected to the dynamic subsidence basin, the fitting function needed to be applied to the FEM. The User Defined Displacement was utilized to implement the subsidence profile functions in the form of vertical displacement applied on the bottom of the Finite Element model of Embankment #1.

Considering that Embankment #1 was located in the middle of the panel, a limited subsidence was assumed and applied on the bottom of the embankment in this preliminary analysis. The limited subsidence profile was obtained by expanding the 3D subsidence along the transversal axis that is perpendicular to the direction of mining. There were no lateral boundaries in this limited subsidence shown in Figure Ve.2.

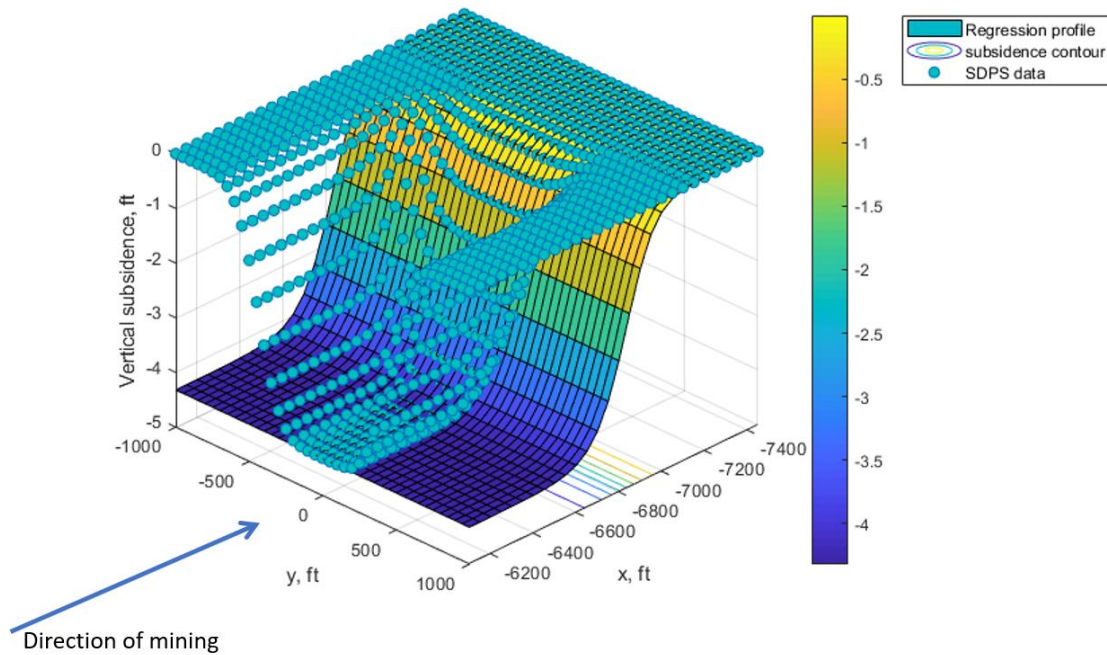


Figure Ve.2 – Numerical regression model of a limit (2D) subsidence

Figure Ve.3 indicates two coordinate systems involved in the procedure of implementation. The coordinates of points on the highway embankment are x' and y' . The points on the ground are x and y . The University correlated these two coordinate systems using the transformation equations for the rotation. The final basin was moved ahead along the direction of negative X axis (Figure Ve.3) to simulate the successive subsidence.

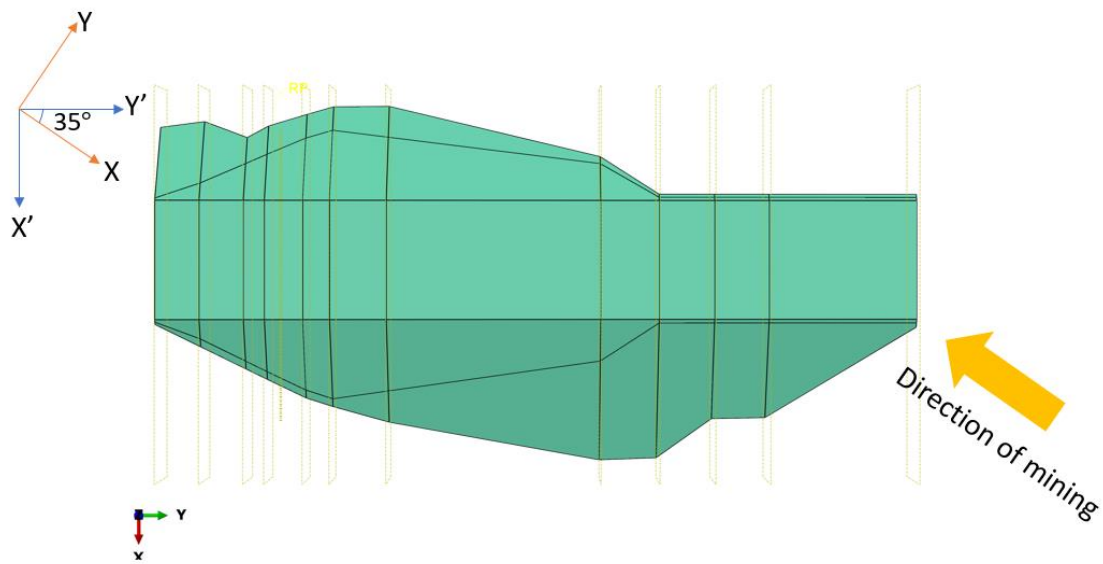


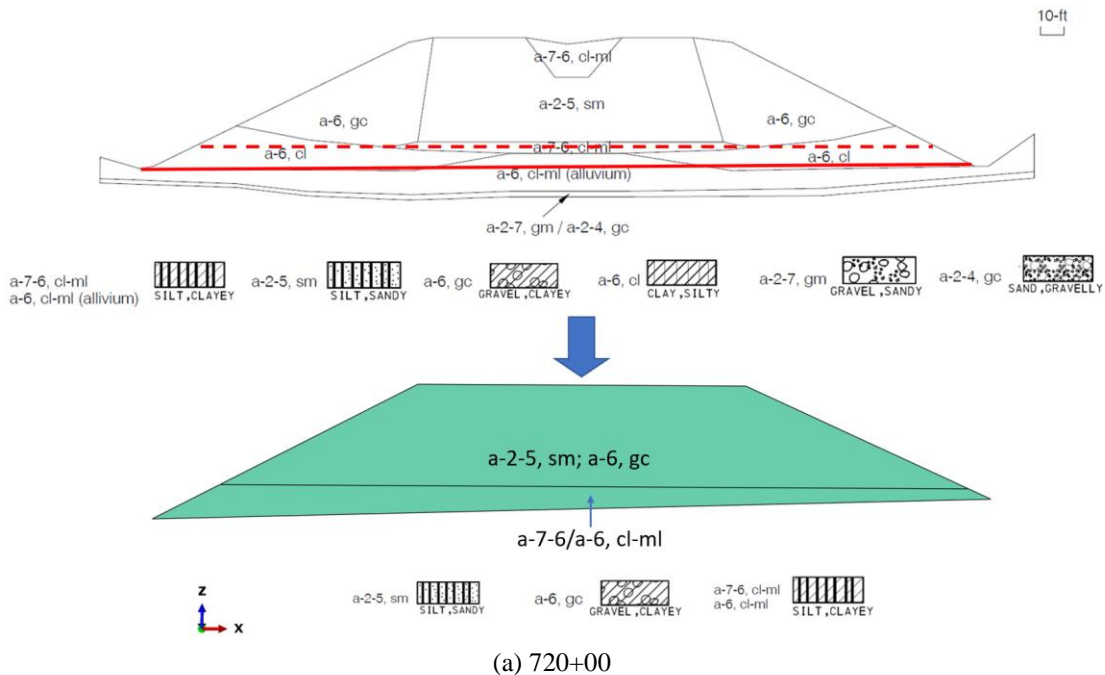
Figure Ve.3 – Two coordinate systems involved in the implementation of the profile function into the FEM

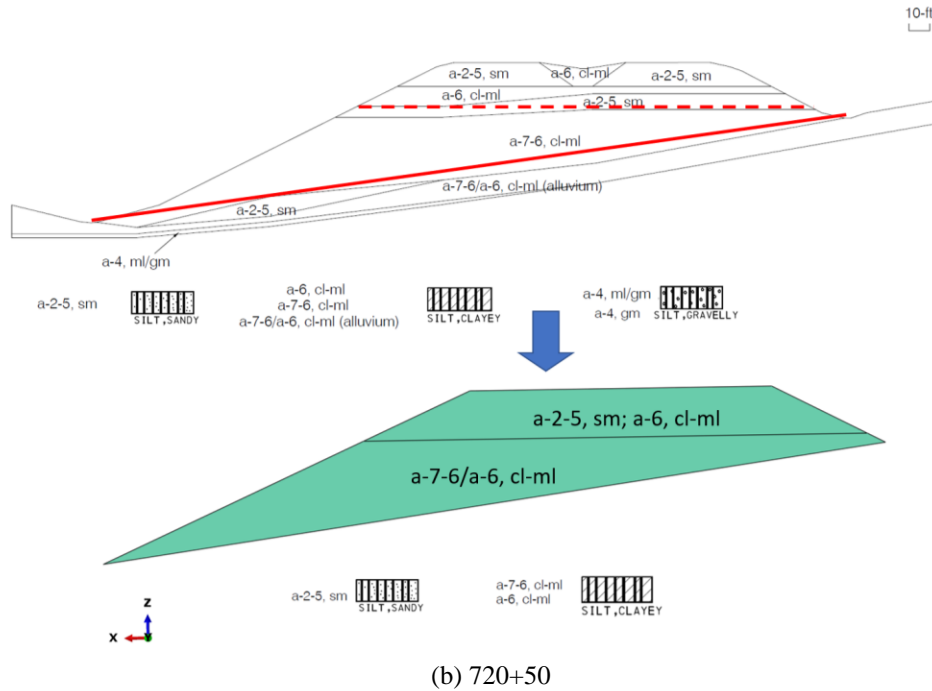
The implementation of the successive subsidence into FEM consists of the following steps:

1. The point of zero subsidence is found from the SDPS model and the X' coordinate of that point is -7250 ;
2. Move the regression profile along X axis so that the zero-subsidence point lied on the original point;
3. Move the regression profile along X axis so that the zero-subsidence point lied on the point at which the subsidence basin first touched the embankment;
4. Move the regression profile along Y axis so that the embankment lied on the correct location in the panel;
5. Switch the coordinate system from $X - Y$ to $X' - Y'$ using the transformation equations; and
6. Add the distance of each step of subsidence to the magnitude after X in order to move the final subsidence basin ahead until the embankment settled down completely.

4.0 Material Properties

According to the Task 1 report, a 3D FEM was constructed based on a generalized two layered model shown in Figure Ve.4. The upper part consists of sandy silt, clayed silt, and gravelly clay. The lower part is mainly composed of clayed silt.





(b) 720+50

Figure Ve.4 – Generalized two-layered cross sections in the Finite Element model originated from the field observed boring log at cross section (a) 720+00 and (b) 720+50

Clayey gravel is located at the lateral parts of embankment at cross section 720+00 shown in Figure Ve.5. According to the laboratory test results, friction angle for sand clay gravels increases from 34° to 36° as the gravel ratio rises from 20% to 40%, which is similar to what was found in the previous research shown in Figure Ve.6. This validated that previous research can be utilized to determine the friction angle of similar materials in the embankment. As the friction angle at a depth of 6 to 10-ft was determined to be 34° through laboratory tests of TB-1, previous findings allow the University to derive the shear parameters of the soil in the area of the lateral part where the rock ratio is as high as 50% (Figure Ve.6).

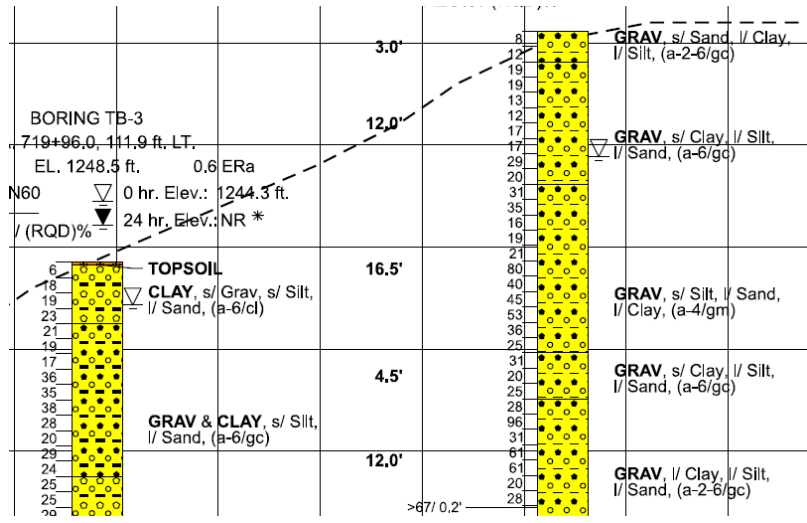


Figure Ve.5 – Clayey/Silty gravel in the lateral region of embankment at cross section 720+00

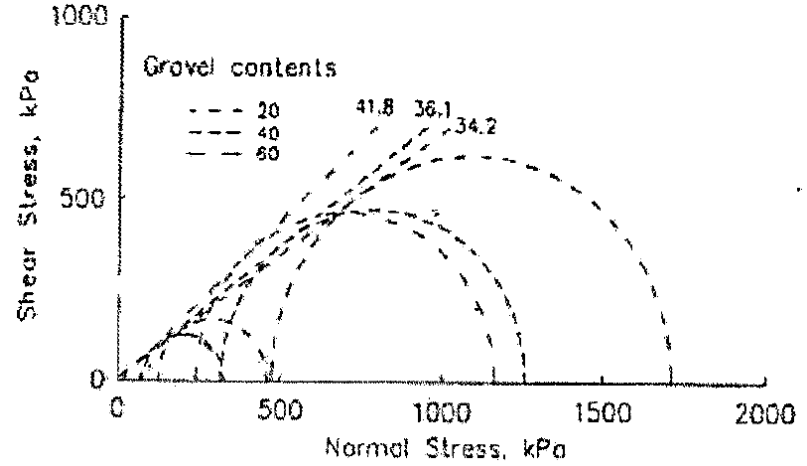


Figure Ve.6 – Variation of shear strength of sand-clay gravels with changes of rock ratios (Graph: Iannacchione and Vallejo, 2000; Data: Donaghe and Torrey, 1979)

During the subsidence event, the embankment experienced the consolidation according to the highway alignment monitoring and slope stake surveys conducted by Penn DOT. The particles in the soil become closer to each other and the rock ratio of the gravel will increase in the process. By utilizing the findings from previous research (Miller and Sowers, 1958; Donaghe and Torrey, 1979; Iannacchione and Vallejo, 2000) and conducting the sensitivity tests, the friction angle is increased according to the rock ratio. The material properties that gave the reasonable results are found and summarized in Table Ve.1.

Table Ve.1 – Material properties of the two-layered Finite Element model of Embankment #1 considering the effects of gravels and consolidations

| Layer name | Soil name | AASHTO | Approximate Depth(ft) | c (p.s.f.) | ϕ | E (p.s.f.) | Rock ratio |
|------------|--|-----------|-----------------------|------------|--------|------------|------------|
| Upper | Sandy silt/ Clayey Silt/ Gravelly clay | a-2-5/a-6 | 0-40 | 753 | 42° | 1211356.47 | 40-60% |
| Lower | Clayey silt | a-7-6 | 40-60 | 771 | 40° | 1211356.47 | 40% |

5.0 Result Analysis

In this section, the University analyzed the behavior and the stability of Embankment #1 subjected to the successive flat subsidence in the following steps:

- 1) Analyzed the vertical displacement in the embankment under gravity and with successive flat subsidence and compare the results with field data;
- 2) Obtained the Critical areas in the embankment using Shear strength reduction method (SRM)
- 3) Plotted the total displacement at the critical cross section versus the strength reduction factor (SRF)
- 4) Found the factor of safety ranges under gravity and with successive limit subsidence

5.1 Vertical Displacement

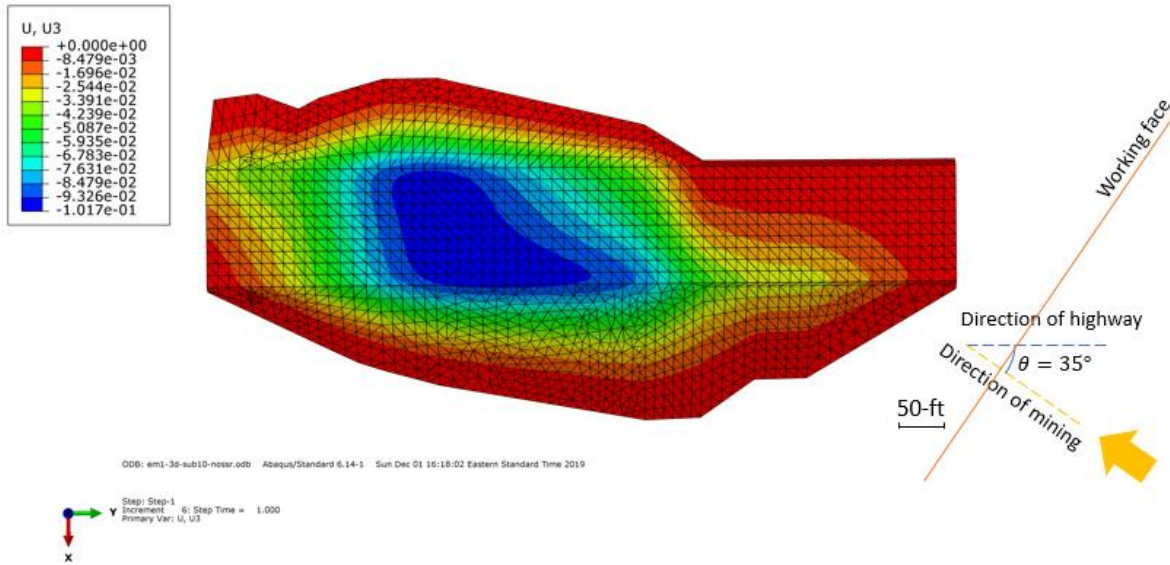
Figure Ve.7 indicates the vertical displacement on the surface of Embankment #1 when subjected to the dynamic subsidence. The maximum vertical subsidence after mining will happen on the east bound lane in the middle of the highway segment shown in Figure Ve.7k. In these figures, the letters denoted the distance from the current working face to the initial working face when the subsidence first touched the embankment shown in Equation Ve.3.

$$s(n) = 135 * n \tag{Eq. Ve.3}$$

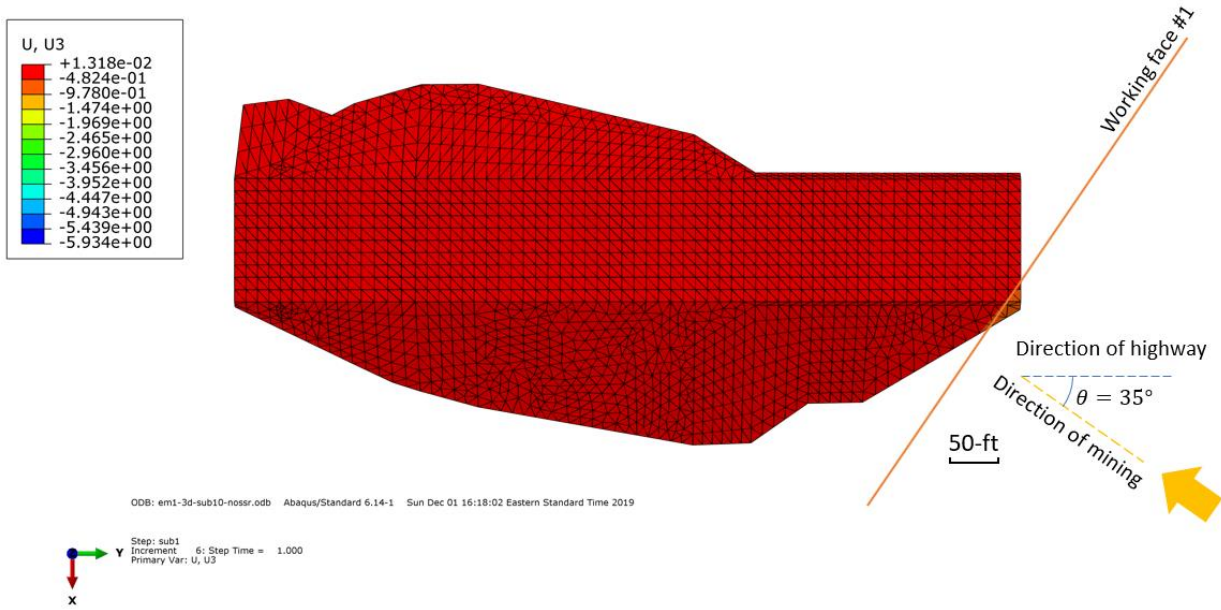
Where:

- $s(n)$ = the distance from the #n working face to the initial working face;
- n = 1:10

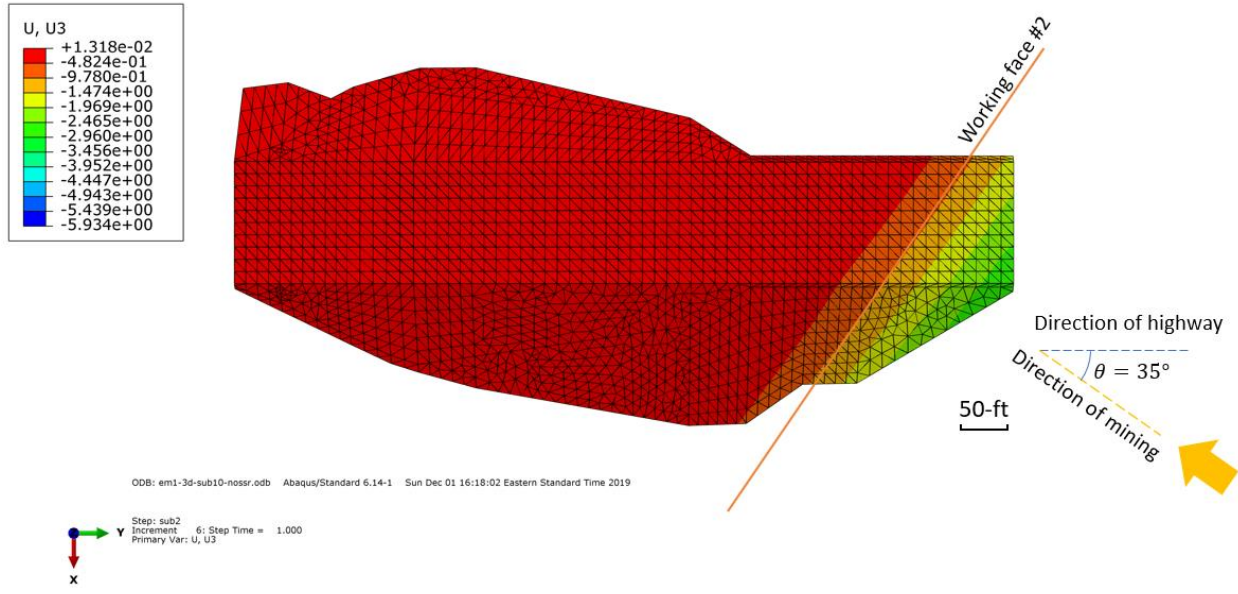
It should be noticed that the legend for the contours with subsidence is specified to be same in each step. The legend for the contours without subsidence under gravity is automatic calculated in order to show the amount of displacement that occurred due to gravity upon completing the construction.



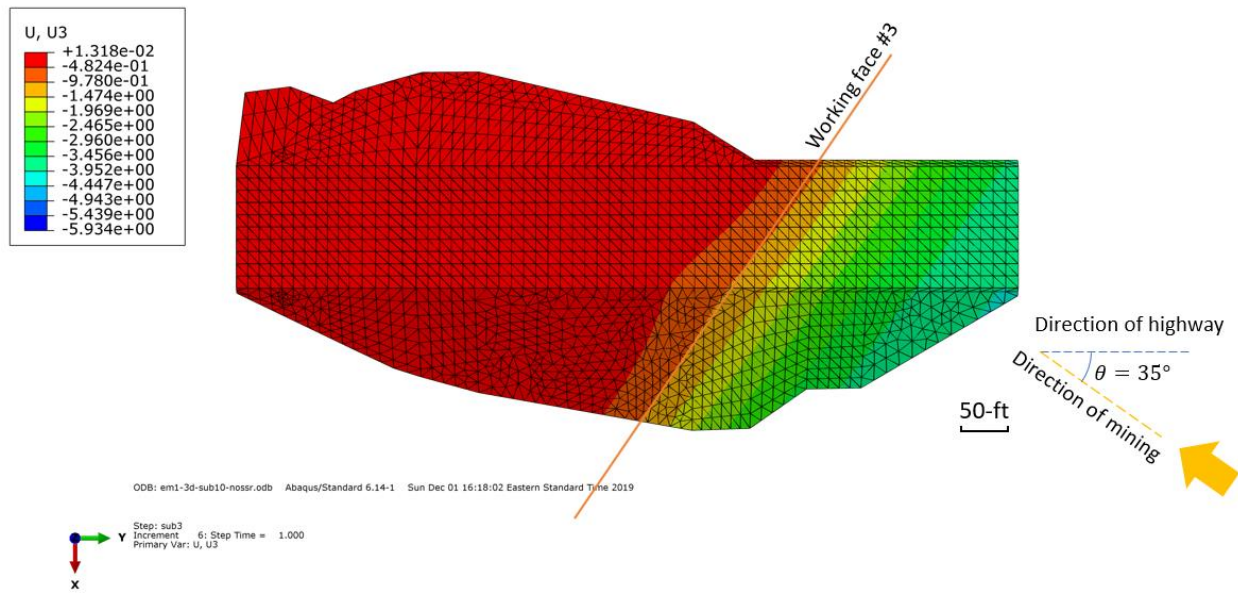
(a) Subsidence has not touched the embankment, initial position of the working face



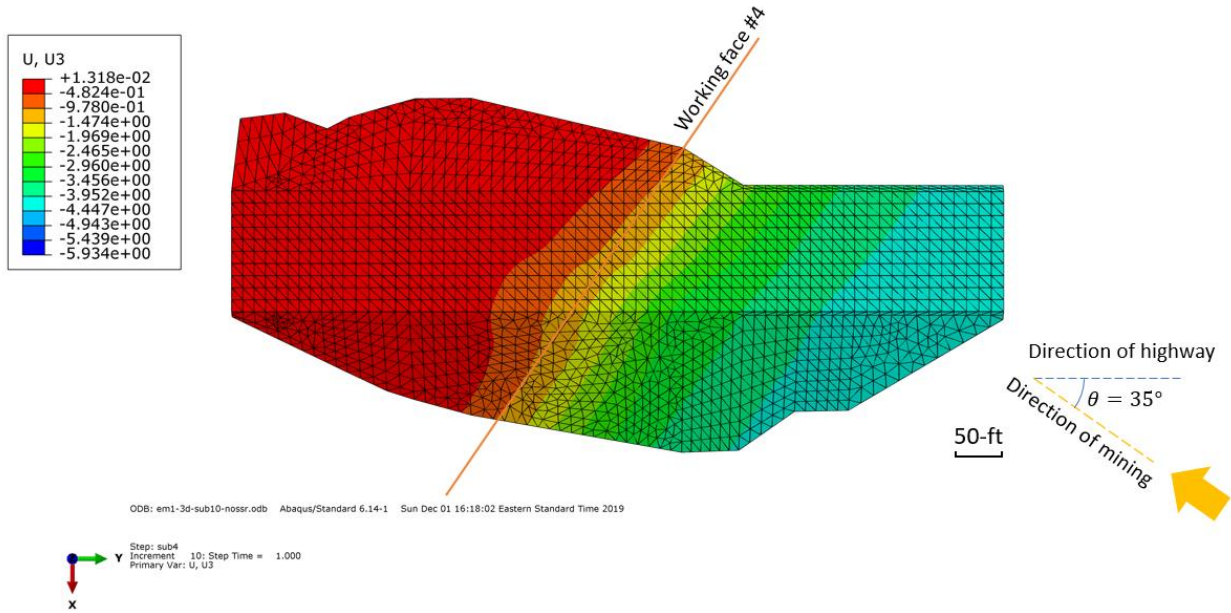
(b) $s(1) = 135\text{-ft}$



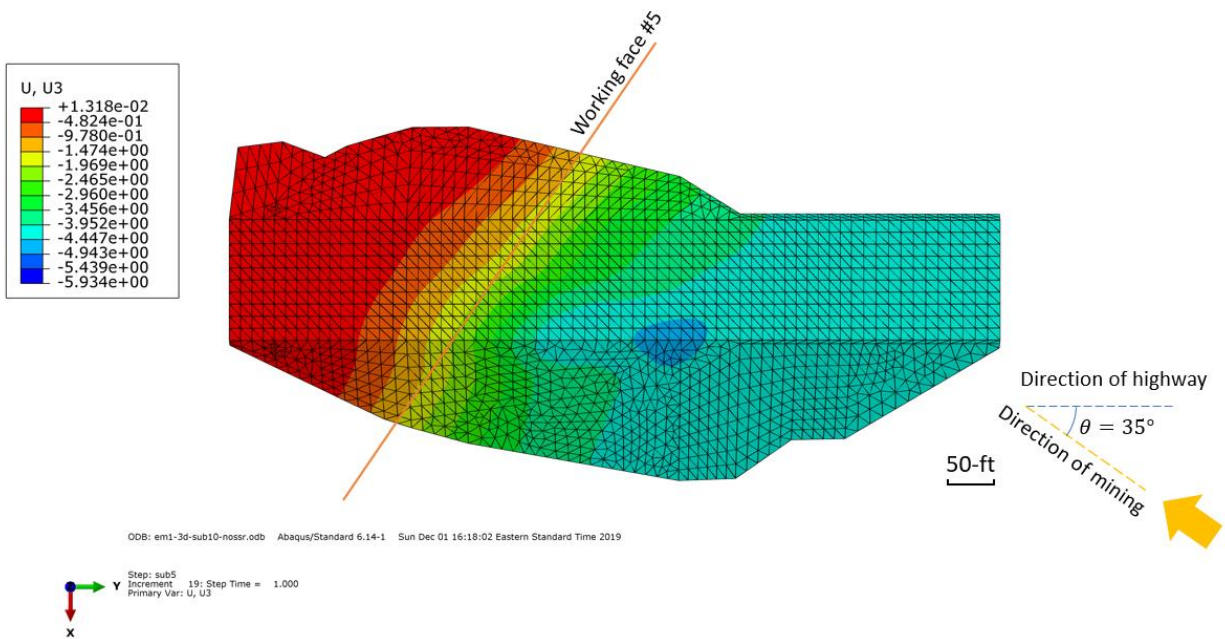
(c) $s(2) = 270\text{-ft}$



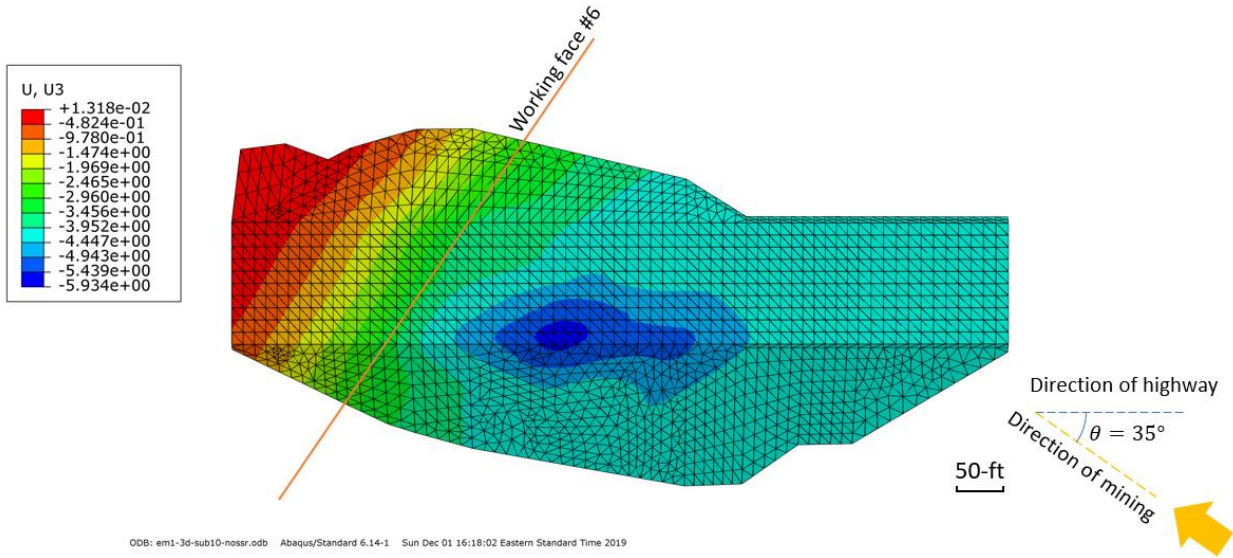
(d) $s(3) = 405\text{-ft}$



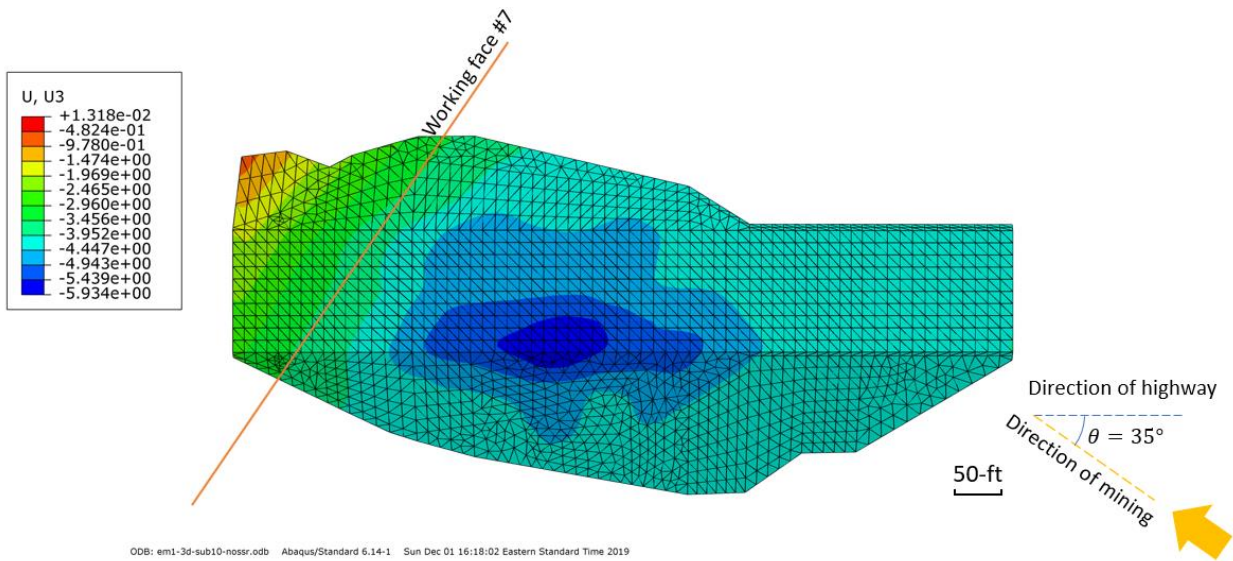
(e) $s(4) = 540\text{-ft}$



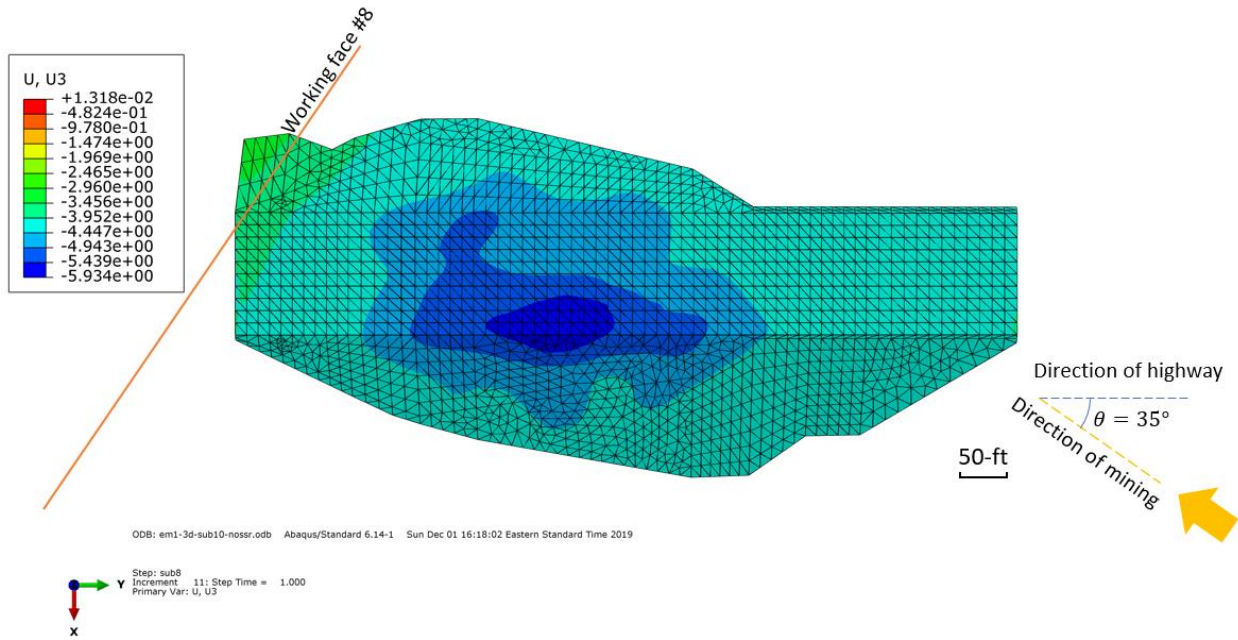
(f) $s(5) = 675\text{-ft}$



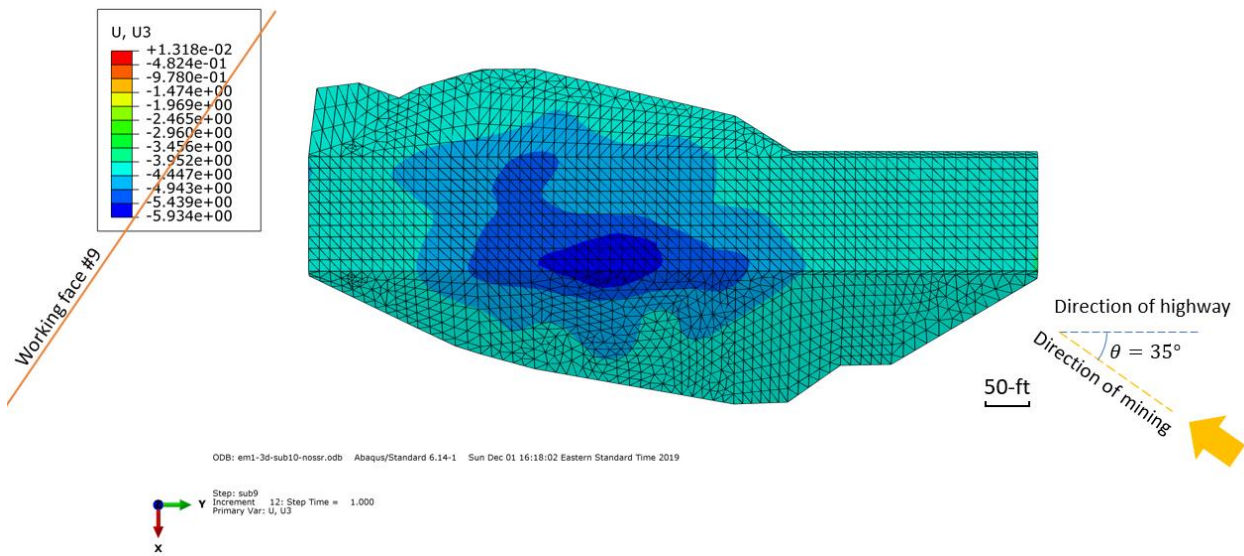
(g) $s(6) = 810\text{-ft}$



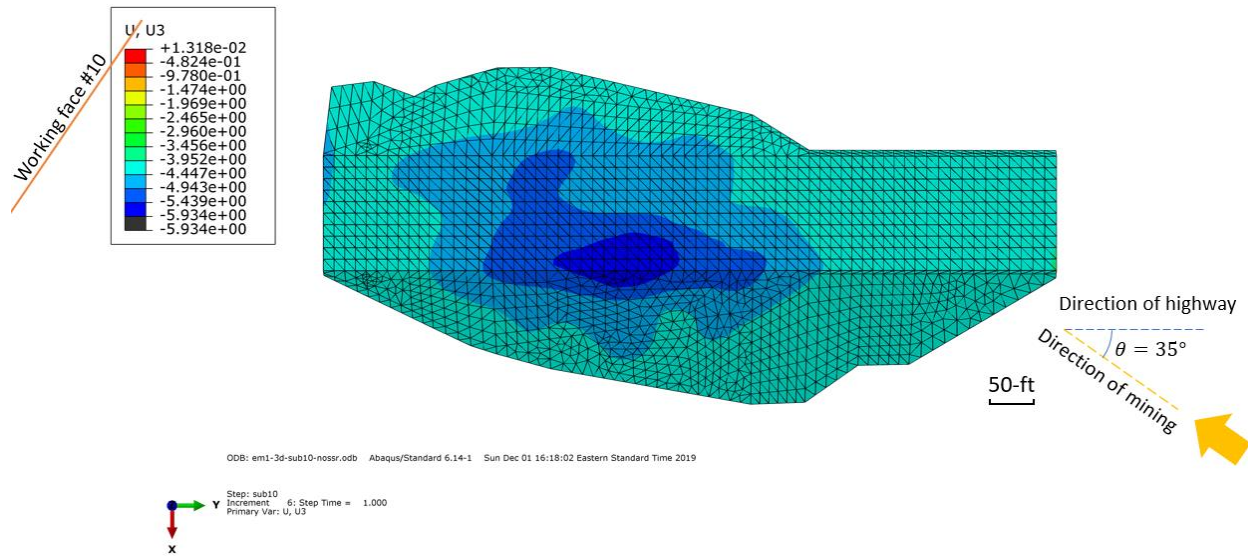
(h) $s(7) = 945\text{-ft}$



(i) $s(8) = 1080\text{-ft}$



(j) $s(9) = 1215\text{-ft}$

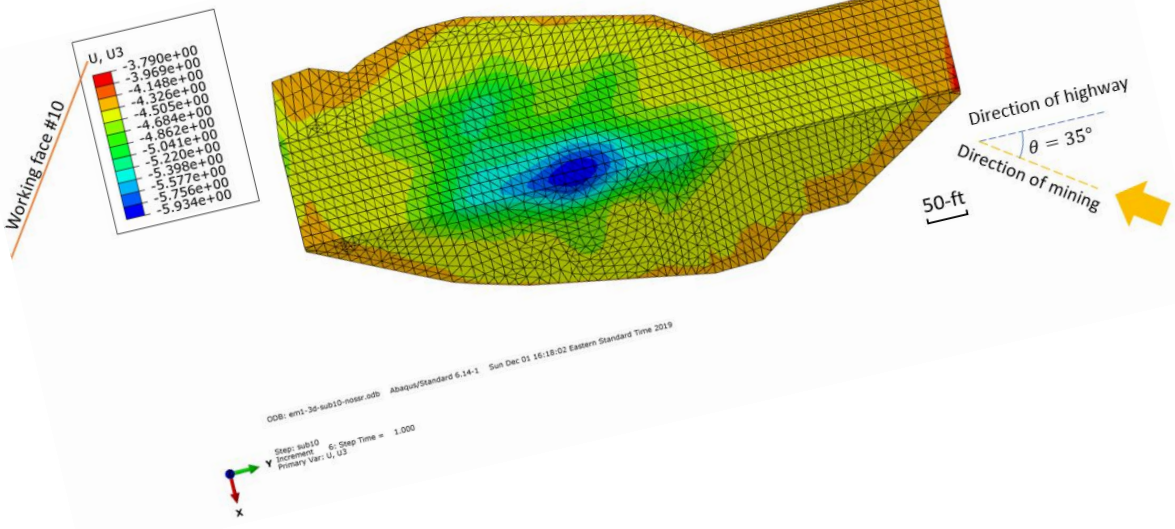


(k) $s(10) = 1350\text{-ft}$

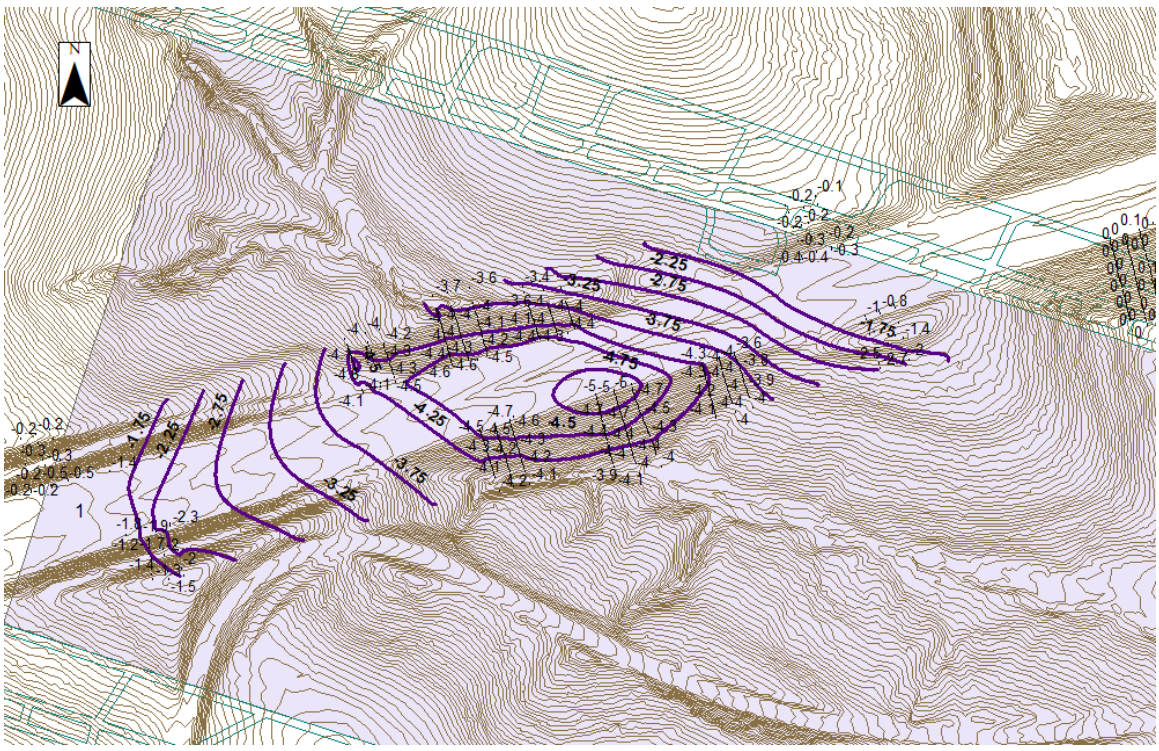
Figure Ve.7 – Vertical displacement on the surface of the Embankment # 1 subjected to successive subsidence

The final vertical displacement from the FEM was then compared to what was measured in the field shown in Figure Ve.8. The vertical component of the displacement was obtained from the slope stake survey and was plotted using ArcGIS.

Both figures show that the region with the maximum displacement was located in the center of the highway segment on the east bound lane. The magnitude of the maximum displacement from the FEM was 5.9-ft, which was larger than the field measurement of 5-ft. The possible the reason for this difference is that the FEM embankment was subjected to a flat subsidence in this preliminary result. In Task 3, a 3D subsidence basin will be applied to the FEM of the embankment to get a more accurate representation of the subsidence effects on the embankment.



(a)



(b)

Figure Ve.8 – Vertical subsidence contour on the highway Embankment #1 from (a) Finite Element model and (b) field measurement with the working face as shown (also see Figure Va.9)

5.2 Shear Strength Reduction Method

Shear strength reduction method (SRM) was utilized to find the potential critical part in the embankment as well as the factor of safety of the embankment. Strength reduction method (SRM) is widely utilized in the slope stability analysis (Zienkiewicz et al., 1975; Matsui and San, 1992; Dawson, 1999; Griffiths et al., 2001; Zheng et al., 2005).

In the SRM, in order to obtain the factor of safety (FS) equivalent to Limit Equilibrium Method (LEM), a strength reduction factor (SRF) was utilized. The factor was employed to reduce the cohesion c and $\tan\phi$ until the slope failed. The original shear strength parameters are divided with this factor to obtain the reduced shear strength parameters c_r and ϕ_r shown in Equation Ve.4.

$$c_r = \frac{c}{SRF}, \tan \phi_r = \frac{\tan \phi}{SRF} \quad [\text{Eq. Ve.4}]$$

Where:

c = cohesion;

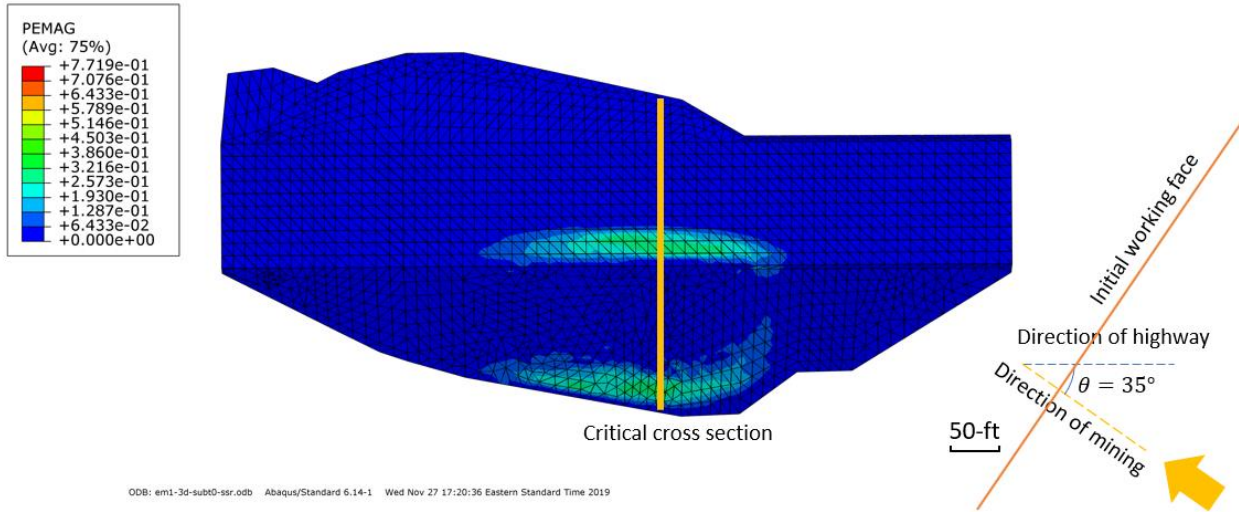
ϕ = friction angle;

SRF = shear strength reduction factor.

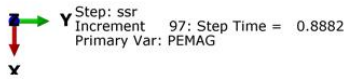
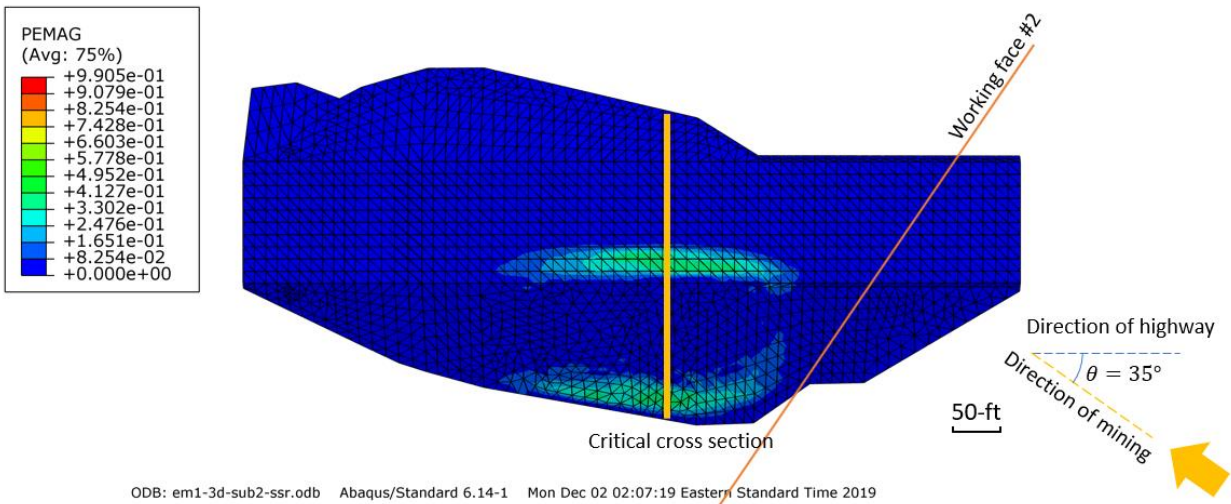
When applying the SRM in FE analysis, increasing SRFs are applied successively on the model to reduce the shear strength of the model until the solution runs out of convergence. In ABAQUS, the method is implemented by creating a field value to represent SRF applied on the FEM. The field value is set less than one before the SMR step in order to make the slope is stable in the gravity and deformation steps. Then, in the SMR step, the value increases until the solution diverges. Previous research found that the shear strength reduction ratio (SRF) of a slope at failure is approximately equivalent to the factor of safety using Bishop's limit equilibrium method (LEM). The failure pattern can be traced from the shear strain development.

5.3 Potential Critical Area in the Embankment Using SRM

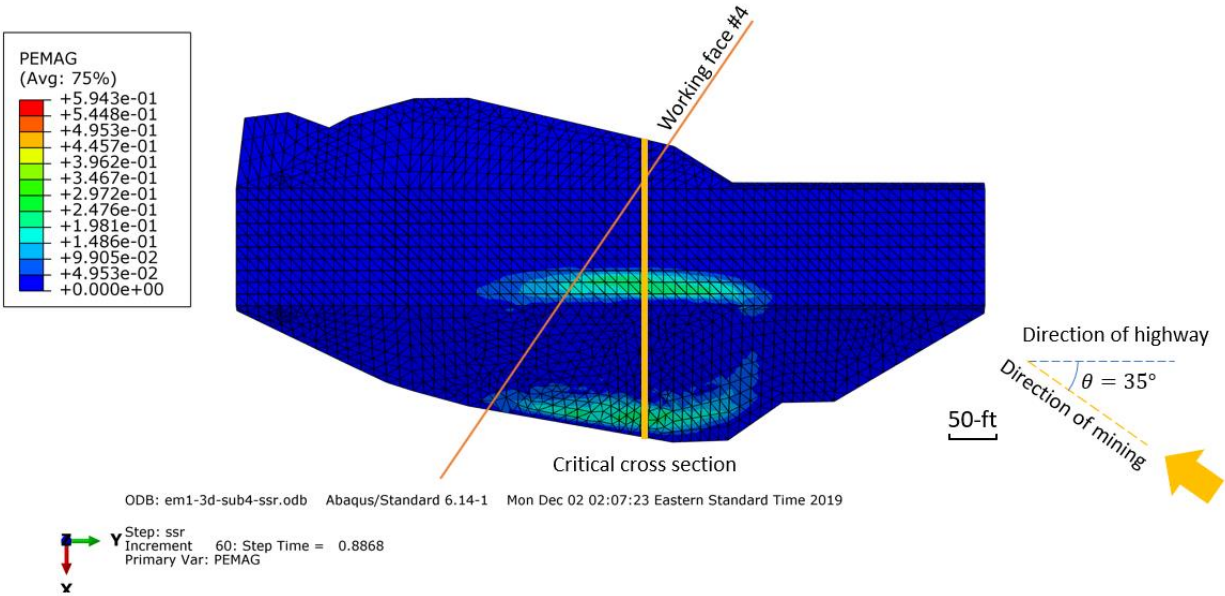
Centrifuge tests have indicated that the plastic shear strain zone in unstable slopes coincided with rupture surface (Roscoe, 1970). The SRM can be utilized to make the embankment collapse and identify the critical area with the higher plastic strain. The critical area was utilized to conduct the factor of safety analysis in the next section. Figure Ve.9 indicates the magnitude of the plastic strain in the embankment at the final point of SRM when a complete sliding failure happened. The contours resulted from four steps of successive subsidence wave. The critical cross section was located on the south facing slope in the middle of the longitudinal length of the embankment.



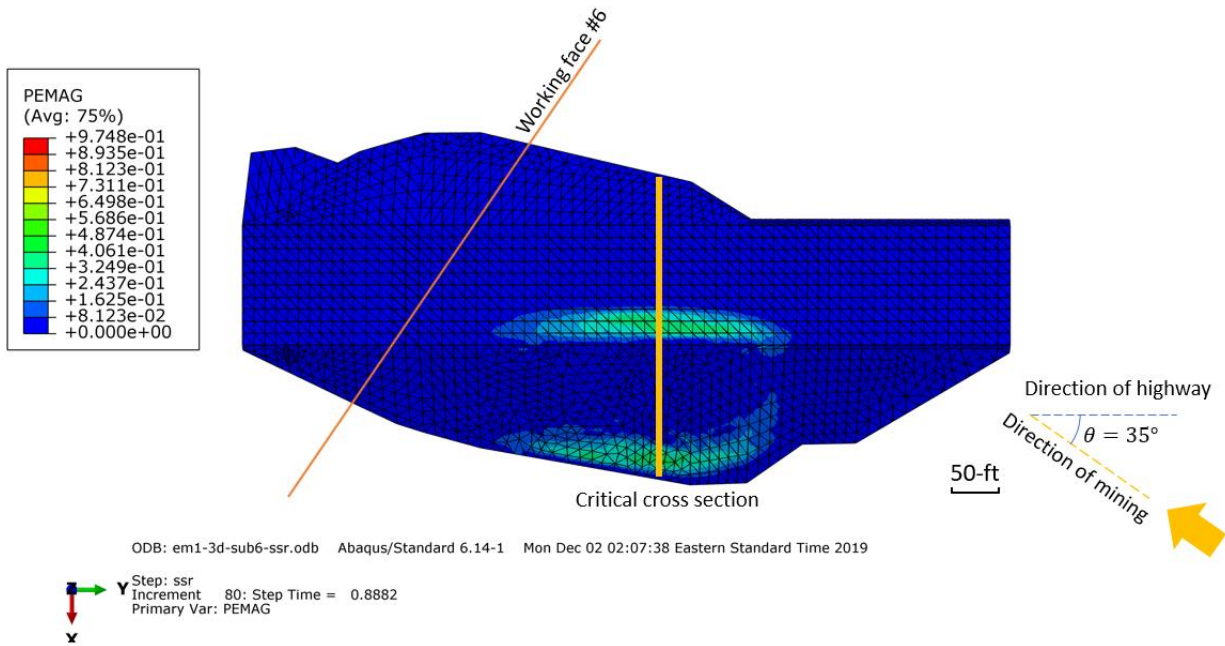
(a) no subsidence



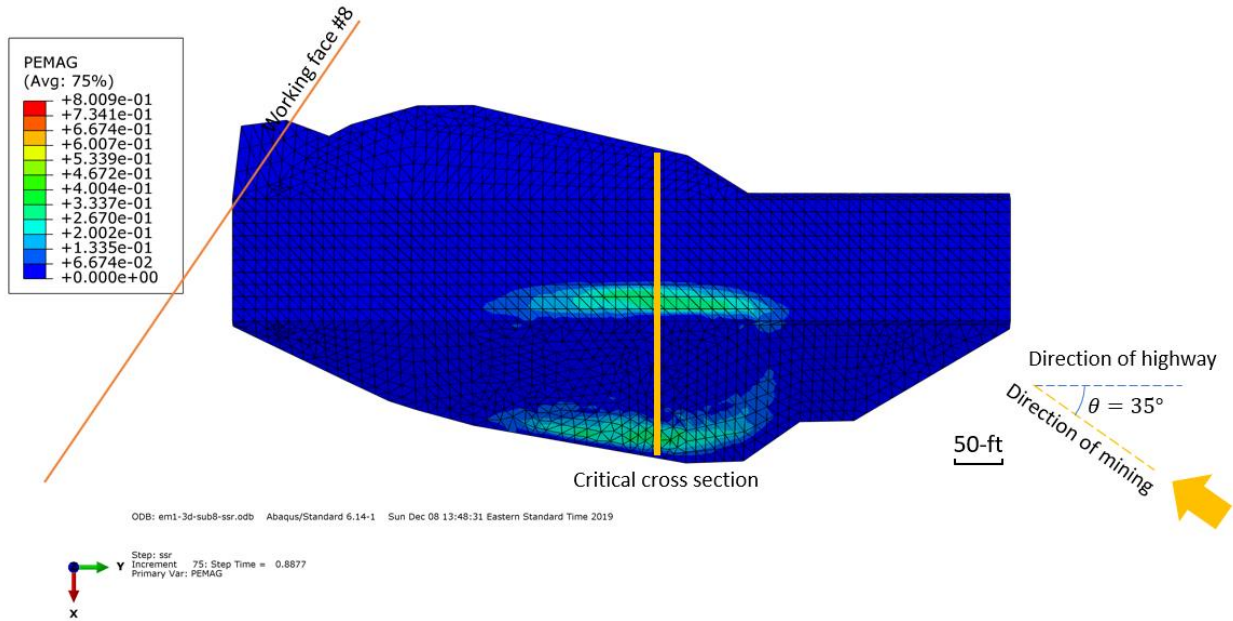
(b) $s(2) = 270\text{-ft}$



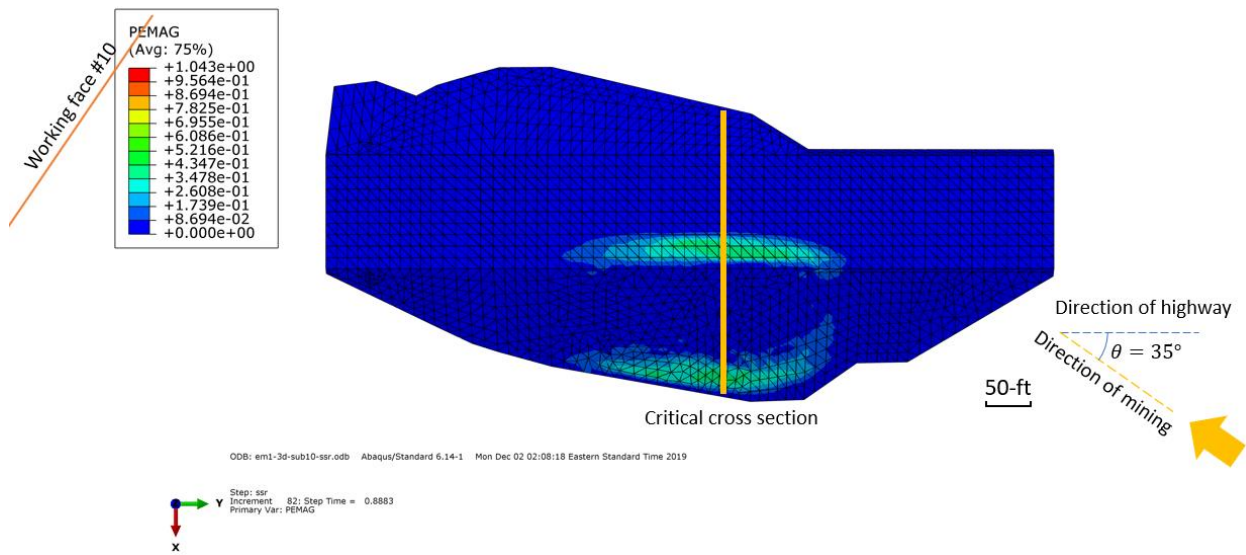
(c) $s(4) = 540\text{-ft}$



(d) $s(6) = 810\text{-ft}$



(e) $s(8) = 1080\text{-ft}$



(f) $s(10) = 1350\text{-ft}$

Figure Ve.9 – Critical cross section for the factor of safety analysis when the working face is (a) 0-ft; (b) 270-ft; (c) 540-ft; (d) 810-ft; (e) 1080-ft and (f) 1350-ft away from the initial position

5.4 Factor of Safety

Factor of safety was obtained using shear strength reduction method (SRM) as illustrated in the previous sections. The shear strength reduction factor (SRF) was utilized to reduce the cohesion and $\tan\phi$ until the embankment failed. Total displacement was plotted against SRF to conduct the factor of safety analysis. The knee point, which represents failure of the slope is identified

and previous research found that the SRF at this point, is equal to the factor of safety using the limit equilibrium approach.

The factor of safety analysis of the embankment without subsidence was conducted first. Figure Ve.10 indicates the plastic strain inside the embankment at the critical cross section. This state of plastic strain happened when the analysis reached the knee point of the factor of safety plot (Figure Ve.11). The shear band has reached the top of the embankment and a complete rupture face was formed.

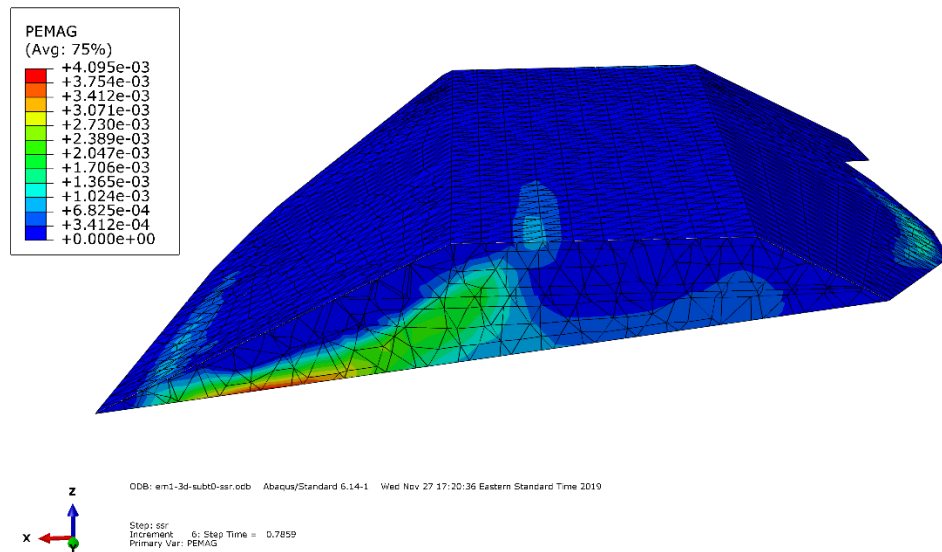


Figure Ve.10 – Magnitude of plastic strain inside the Embankment #1 at the critical cross section

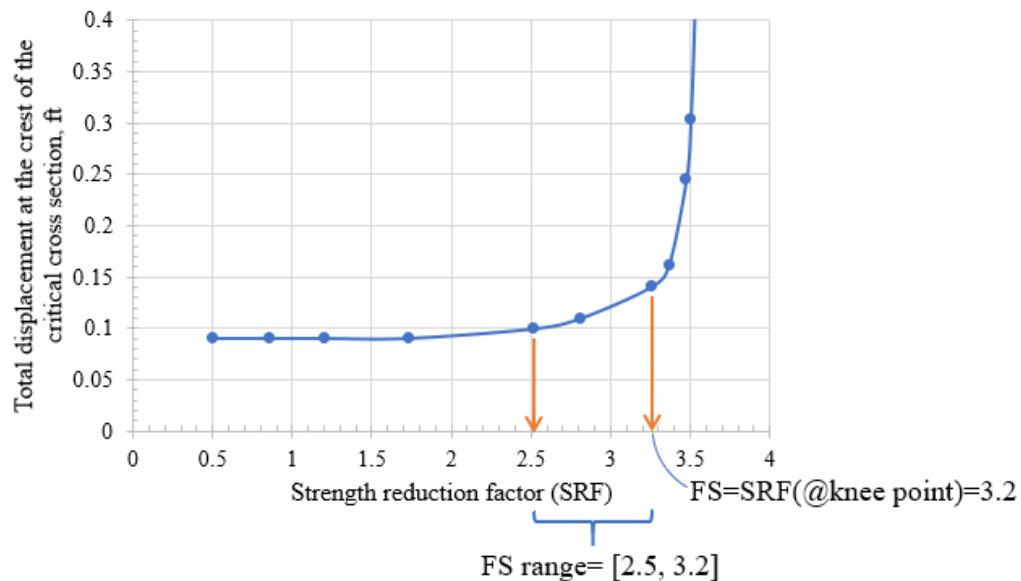


Figure Ve.11 – Total displacement at the crest of the critical cross section versus the shear strength reduction factor for the case without subsidence

However, before the displacement started to increase exponentially (which means the embankment collapsed), the plot was not horizontal but an inclined curve, indicating that the embankment already experienced sliding deformation before the total collapse. The factor of safety range is introduced here to better describe the stability of the embankment. It started from the point when the displacement started to increase and ended at the knee point. The lower bound of this range can be utilized to identify if the embankment will experience sliding deformation. And the upper bound helped us determine if the embankment will collapse and experience large deformation. For this case, without subsidence, the upper bound and lower bound are close to each other. The embankment started to slide at an SRF of 2.5 and failed at an SRF of 3.2.

For the case when the embankment was subjected to the subsidence, it was more difficult to identify the knee point because more deformation appeared before the knee point. Consequently, the factor of safety range is more reasonable than using a single factor of safety. The case when the Embankment #1 was subjected to the subsidence with the working face reached the middle of the highway segment (Subsidence #6 in Figure Ve.12) was chosen to explain how the factor of safety was determined.

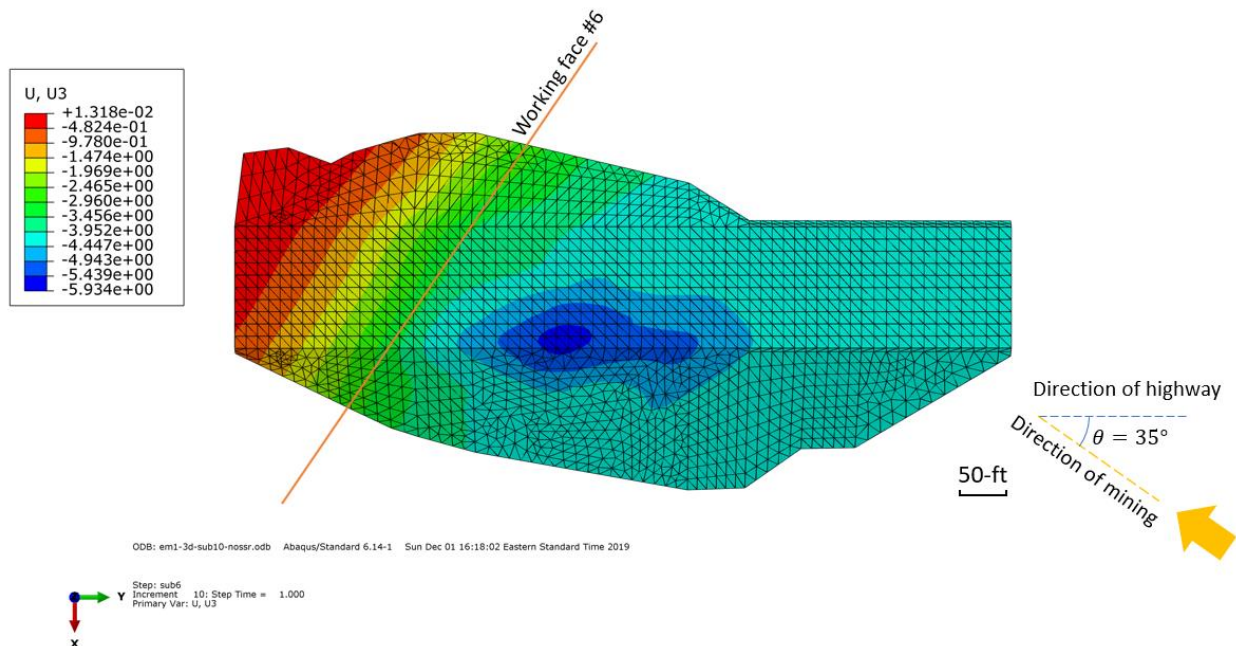


Figure Ve.12 – Embankment #1 subjected to subsidence #6

As shown in Figure Ve.13, the upper bound of the factor of safety range is 2.7, which means that the embankment was safe and would not collapse. However, the plot before this point presented more movement compared to that without subsidence. In addition, the embankment started to slide at 1.0. The movement increased at a greater rate from this point. Before this point (SRF=1), the displacement increased at a rather low rate and the plot is almost horizontal. The lower bound of the factor safety reflected that the embankment will experience some sliding deformation

though it is safe and stable. In this way, the factor of safety range better describes the stability and behavior of the embankment, especially when subjected to subsidence.

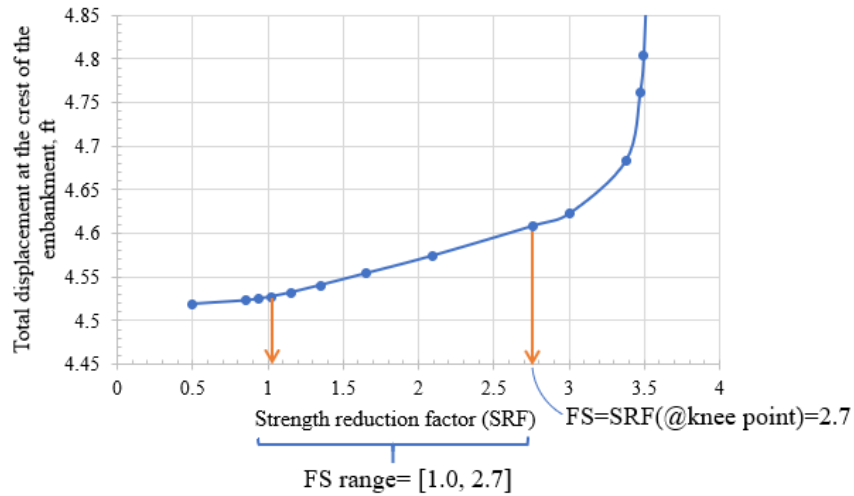


Figure Ve.13 – Total displacement at the crest of the critical cross section versus the shear strength reduction factor for the case with subsidence of #6

The same procedure was conducted to determine the factor safety range of the Embankment #1 when subjected to subsidence with the working face at different locations. The resulting factor of safety ranges as well as the average were plotted versus the number of the steps of successive subsidence shown in Figure Ve.14.

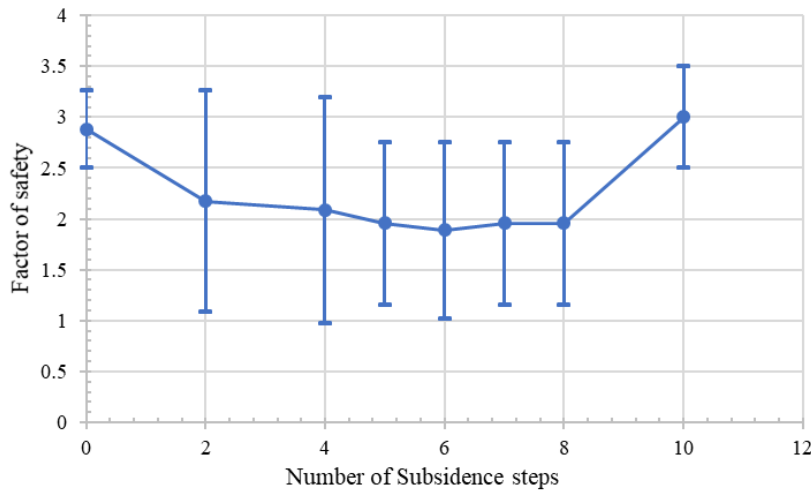


Figure Ve.14 – Plot of factor of safety versus the longwall face positions or subsidence steps

The factor of safety of the embankment decreased when subjected to subsidence and reached the lowest value at step #6 where the working face is around the middle of the embankment. After the subsidence passed the highway segment and the embankment settled down, the factor safety increased and even became higher than the factor of safety before subsidence. The position of working face at each step and the vertical displacement contour was shown in Figure Ve.9.

Subsection Vf – Discussion of Challenges in Utilizing the SDPS Subsidence Numerical Regression within the Embankment #1 FEM

A regression model is fits a defined, mathematical curve to a data set. As mathematical curves assume perfect conditions and collected data is inherently flawed, it will be difficult to make the regression match the data closely. The regression model utilized in Section Ve fits a mathematical curve to a theoretical SDPS model. As both models are mathematical in nature, the fit of the curves is very close.

The curve fitting will only become more challenging when additional factors are considered. In Task 3, the regression model will be defined for a three-dimensional SDPS model. By adding the additional factor of surface topography, fitting the numerical regression to the SDPS curve will be more challenging and likely less precise. However, the addition of new factors will hopefully make the model more accurate in explaining the subsidence that occurred on the Panel 15 embankment (Embankment #1), which will make it better equipped to predict the behavior of the embankments subjected to future mining.

The various angles of the longwall face to the overlying I-70 highway alignment within the study area has the potential to produce a wide range of surface impacts. Figure VIa.1 indicates a range of possible angles, producing an assortment of surface impacts. The influence of these longwall face to highway alignment angles will be evaluated as part of Task 3.

Section VIb - Overburden Influence

Longwall mining in the Pittsburgh Coalbed first occurred within Pennsylvania around 1971 (Iannacchione et al., 2013). Since that time, over 600 longwall panels of various sizes, shapes, orientations and overburdens have been mined (Bain et al., 2019). The spatial reference of these panels is provided by the PADEP and available on the PASDA site as a shape file. The University determined the overburden associated with the Pittsburgh Coalbed in southwestern Pennsylvania by comparing surface topography with coalbed elevation (Figure VIb.2). The Tunnel Ridge Mine property outline was provided by PennDOT at the initiation of the contract. Its accuracy could not be validated.

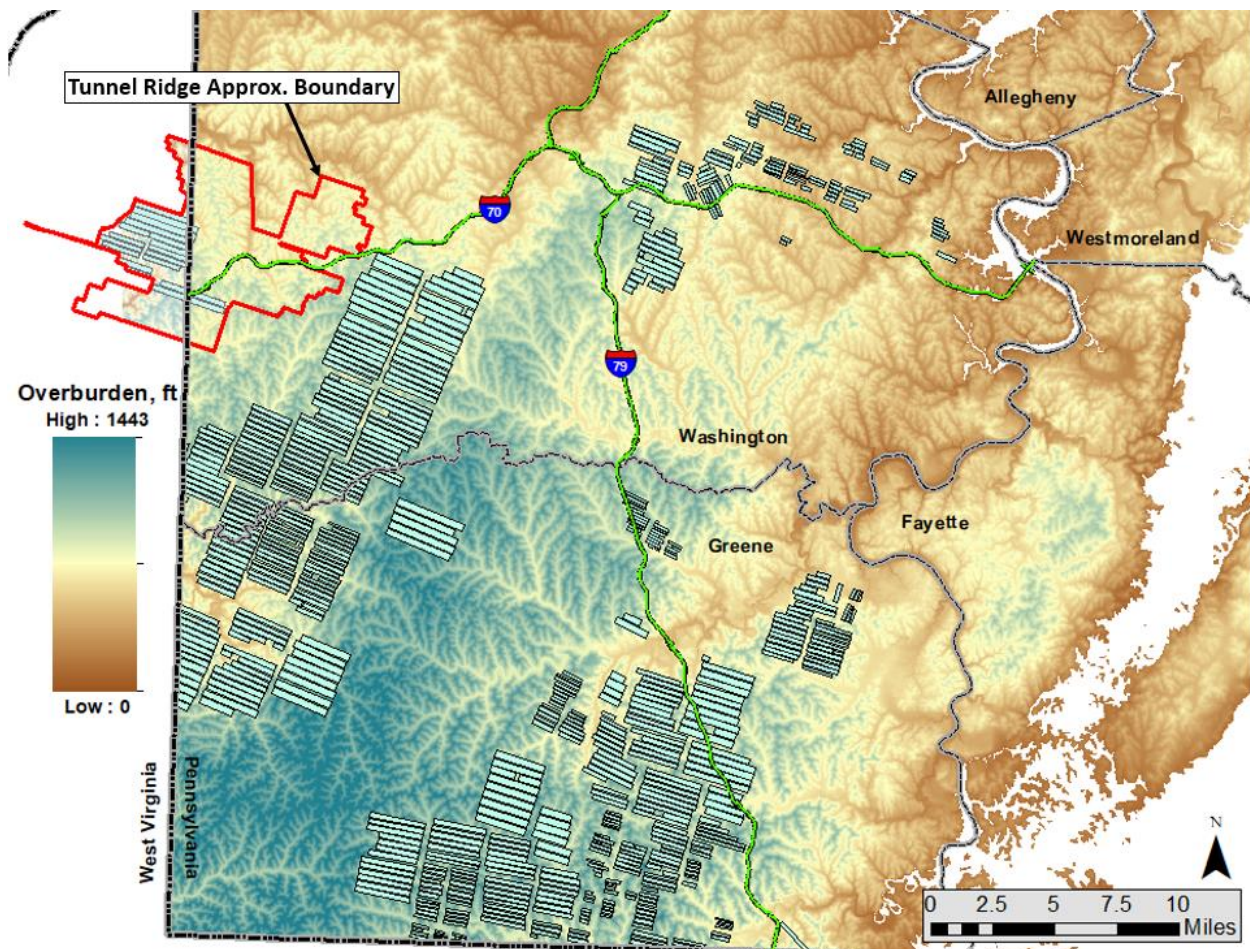


Figure VIb.1 – Pittsburgh Coalbed overburden and the location of mined longwall panels. The estimated 2018 Tunnel Ridge property extent is outlined in red

Overburden within the extended study area (Figure VIb.1), i.e. along the I-70 highway alignment within the Tunnel Ridge Mine property, has been determined as part of the University’s Task 3 objectives. The longwall panel layouts within the extended study area, are currently not known as a permit for this area has not yet been submitted to the PADEP. Figure VIb.2 is the

University’s attempt to provide the most likely location of longwall panels under the I-70 highway alignment between the West Alexander and Claysville Interchanges. An assumption is made that the orientation and widths of the longwall panels will follow the same pattern as those used in Panel 15, i.e. 1,200-ft wide panels oriented N 71° W. The University theorizes that a set of main entries will separate Tunnel Ridge’s future reserves from the current longwall mining district. These main entries will likely split the future reserves into two parts. Please note that this is the University’s best estimation; the actual position of the panels and location of the supporting main entries is likely to change when the permit request is submitted to the PADEP for approval.

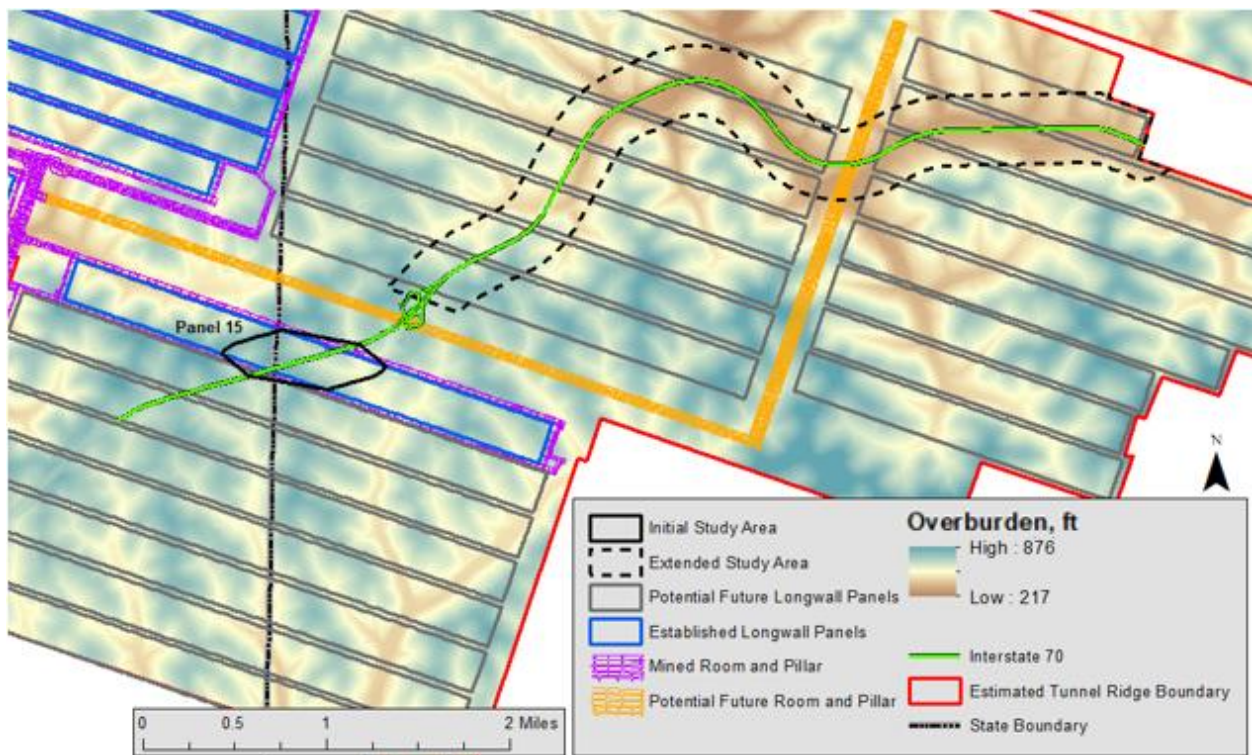


Figure VIb.2 – Overburden map showing the location of existing and potential future longwall panels at the Tunnel Ridge Mine. Also shown are the initial and extended study areas

All projected mining shown in Figure VIb.2, represents mining after the spring of 2019. It is presented to assist in understanding the risk associated with future coal extraction beneath I-70 in Pennsylvania. It should be noted that information concerning existing room-and-pillar developments, as well as extracted longwall panels, were provided to the University by the Tunnel Ridge mining company.

Overburden characteristics for both the initial and extended study areas is presented in Table VIb.1. The initial study area average overburden is 658-ft. The initial study area extends 3,300-ft along I-70 (Figure VIb.2), spanning the subsidence basin developed by the extraction of Panel 15 (see page 3, Section I for a description of the initial study area). The average overburden for

the extended study area is 474-ft. The extended study area comprises a 1,000-ft buffer on either side of I-70 from the West Alexander to Claysville Interchanges (Figure VIb.2).

Table VIb.1 – Overburden conditions within the initial and extended study areas within 1,000-ft of I-70

| | Min, ft | Max, ft | Range, ft | Mean, ft | Median, ft | STD, ft |
|---------------------|---------|---------|-----------|----------|------------|---------|
| Initial Study Area | 546 | 771 | 225 | 658 | 658 | 51 |
| Extended Study Area | 332 | 777 | 446 | 474 | 555 | 94 |

A graphical representation of the data provided in Table VIb.1 is shown in Figure VIb.3. It is obvious from this analysis that there is a significant overall reduction (28 %) in average overburden for panels comprising the extended study area.

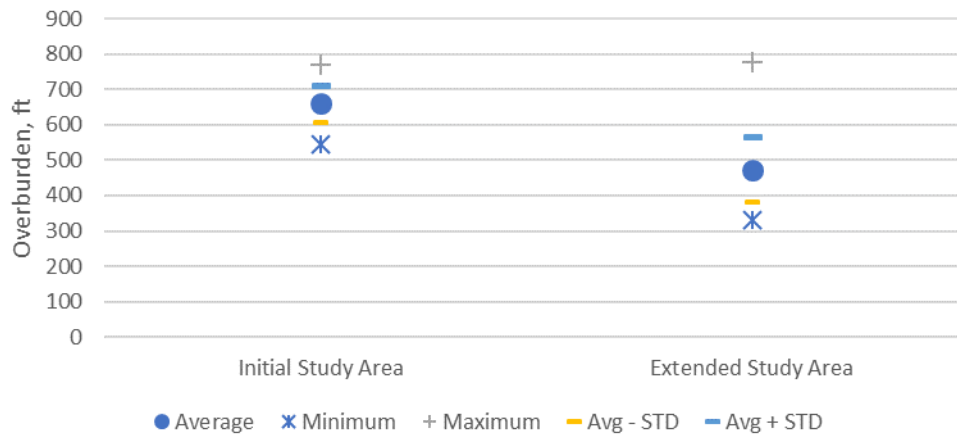


Figure VIb.3 – Graphical representation of the overburden characteristics of the initial study area (Panel 15) and the extended study area comprising potential longwall panels under the I-70 highway alignment between the West Alexander and Claysville Interchanges

According to trends developed in the latest ACT 54 Report (Bain, et al., 2019), the overburden of longwall panels mined between 2013 and 2018 ranged from 416 to 1,293-ft. Three broad categories were identified: shallow (< 705-ft); average (705 to 907-ft); and deep (>907-ft). Overburden within the initial study area is very similar to the average depth of other longwall panels mined recently in Pennsylvania. However, the University estimates that the majority of panels within the extended study area will have overburdens significantly below average and should be classified as ‘shallow’ for Pennsylvania conditions (Table VIb.2). If all other variables are left constant, less overburden will produce higher vertical subsidence and greater surface deformations and strains.

Table VII.2 - Overburden characteristics for the seven longwall mines operating in Pennsylvania from 2013 to 2018 (Bain, et al., 2019)

| Mine | Avg. | SD* | Min | Max | Category |
|-------------------|-------------|------------|------------|------------|-----------------|
| Bailey | 890.7 | 150.7 | 511.5 | 1269.6 | Average |
| Cumberland | 893.6 | 102.5 | 616.5 | 1191.6 | Average |
| Emerald | 734.8 | 79.5 | 449.4 | 894.8 | Average |
| Enlow Fork | 634 | 93.1 | 416 | 850 | Shallow |
| Harvey | 870.9 | 95.4 | 688.7 | 1258.2 | Average |
| Monongalia County | 977.2 | 123.9 | 743.3 | 1293.1 | Deep |
| Tunnel Ridge | 642.8 | 61 | 470.8 | 723.1 | Shallow |

*SD - Standard Deviation

Section VIc – Embankment Stability

A major focus of this research study has been to understand how embankments, constructed to carry the I-70 alignment, would perform when subjected to subsidence from longwall mining. Two of these embankments (Embankments #1 and #2) are located above or adjacent to Panel 15 (Figure VIc.1). The University has provided extensive field and laboratory analysis to help characterizing embankment performance throughout this report. Embankment #1 was subjected to over 4-ft of vertical subsidence at its base. Consolidation and spreading of the embankment added to this total resulting in as much as 5-ft of vertical subsidence. In addition, shear bands near the base of the embankment were partially mobilized, indicating a potential instability in parts of the embankment. The threat of instability was overcome by the strain-hardening material properties of the embankment fill (see Section V). As a result, Embankment #1 did not fail. Embankment #2 was located on the edge of the Panel 15 subsidence basin and was not adversely affected.

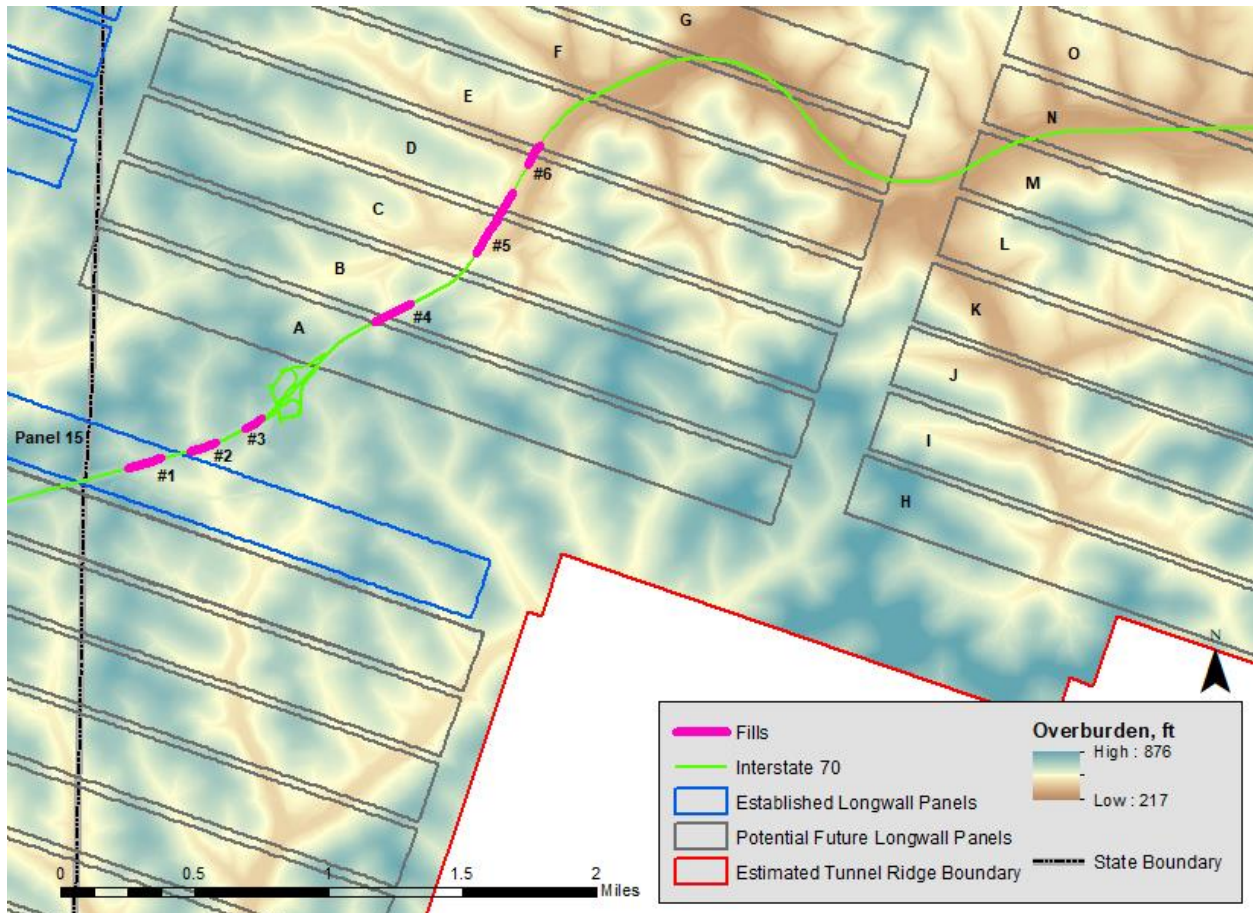


Figure VIc.1 – Five significant embankments were constructed between the West Virginia State Line and the Claysville Interchange. Two of the embankments, #4 and #5, are located within the extended study area.

Three other embankments occur within the extended study area (Figure VIc.1). Embankment #3 is close to the West Alexander Interchange and is not expected to be undermined by longwall mining. Embankment #4 will likely be undermined with an overburden ranging from 500 to 730-ft. The angle of the I-70 highway alignment with the projected orientation of the longwall face will be approximately 10-deg less than the 35-deg angle formed by Panel 15. This embankment is approximately 650-ft long and 52-ft tall. Embankment #5 will likely be undermined with an overburden ranging from 410 to 640-ft. The embankment and I-70 highway alignment are both parallel to the longwall face. It is approximately 650-ft long and 70-ft tall. Embankment #5 represents an increased risk and will be analyzed in greater detail in the coming months.

Section VIId – I-70 Highway Alignment Damage Susceptibility Maps

The University is currently working to produce a series of maps that will forecast potential damage to I-70 within the extended study area. These damage susceptibility maps will rely on overburden calculations and panel characteristics discuss above. Various overburdens and highway orientations will be modeled using the SDPS program to predict minimum, maximum, and average strains conditions within the extended study area.

REFERENCES

- Bain, D., DaCanal, T., Iannacchione, A., Kautz, A., Shirey, P., Tonsor, S. Copeland, M., Deglmann, J., Hill, M., Kandanarachchi, D., Trout, S. and Winn, R. (2019). The Effects of Subsidence Resulting from Underground Bituminous Coal Mining in Pennsylvania, 2013-2018, Bituminous Mine Subsidence and Land Conservation Act, Act 54 Amendments, 5th Five-Year Report, University of Pittsburgh.
- ABAQUS Analysis User's Manual (2016).
- Adelsohn, E., Iannacchione, A., and Winn, R. (2019). *Investigations on Longwall Mining Subsidence Impacts on Pennsylvania Highway Alignments*. 38th International Conference on Ground Control in Mining. Morgantown, WV, pp. 239-250.
- Dawson, E. M., Roth, W. H., & Drescher, A. (1999). Slope stability analysis by strength reduction. *Geotechnique*, 49(6), 835-840.
- Donaghe, R. T., & Torrey, V. H. (1979, September). Scalping and replacement effects on strength parameters of earth-rock mixtures. In *Proc. Conf. on Design Parameters in Geotechnical Engineering* (Vol. 2, pp. 29-34).
- Graybill, F. A., & Iyer, H. K. (1994). MINITAB Laboratory Manual to Accompany Regression Analysis: Concepts and Applications. Duxbury Press.
- Griffiths, D. V., & Lane, P. A. (2001). Slope stability analysis by finite elements. *GEOTECHNIQUE-LONDON*-, 51(7), 653-654.
- Gutierrez, J. J. (2010). *Estimating highway subsidence due to longwall mining* (Doctoral dissertation, University of Pittsburgh).
- Iannacchione, A., Tonsor, S.J., Witkowski, M., Benner, J., Hale, A., and Shendge, M. (2011). "The Effects of Subsidence Resulting from Underground Bituminous Coal Mining on Surface Structures and Features and on Water Resources, 2003 to 2008," PA DEP Website http://www.dep.state.pa.us/dep/deputate/minres/bmr/act54_2008_report/cover.htm, published January 10, 2011, 499 pages and 1 plate.
- Iannacchione, A.T., N.E. Iannacchione, and M. Keener (2013). "Selected Factors Affecting Longwall Mine Layouts in the Pittsburgh Coalbed of Southwestern Pennsylvania," SME Annual Meeting, Preprint 13-151, Denver, CO, Feb. 24-27, 2013, 7 p.
- Iannacchione, A., and Vallejo, L.E. (2000). Shear strength evaluation of clay-rock mixtures. In:

Slope Stability 2000, American Society of Civil Engineers, *Geotechnical Special Publication 101*, pp. 209-223.

Iannacchione, A., Vallejo, L., Li, M., Adelsohn, E., and Winn, R. (2019). Identification of Factors Controlling the Development of Subsidence Impacts Forecasting Methodology to the I-70 Alignment over Longwall Mining of the Tunnel Ridge Mine, Washington, County, PA. PennDOT Contract No. 4400011482, WO #16, Task 1 Report, July 2019, 129 p.

Johnson, A.M. (1970). *Physical Processes in Geology*. Freeman, Cooper and Co., San Francisco.

Mark, C, and T.P. Mucho (1994). "Longwall Mine Design for Control of Horizontal Stress," in New Technology for Longwall Ground Control: Proceedings of the USBM Technology Transfer Seminar, USBM Special Publication 94-01, pp. 53-76.

Matsui, T., & San, K. C. (1992). Finite element slope stability analysis by shear strength reduction technique. *Soils and foundations*, 32(1), 59-70.

Miller, E. A., & Sowers, G. F. (1958). The strength characteristics of soil-aggregate mixtures & discussion. Highway research board bulletin, (183).

Miller, J.S. and W.Y. Bellinger. (2014). "Distress Identification Manual for the Long-Term Pavement Performance Program," 4th edition, U.S. Department of Transportation, Federal Highway Administration, Report No. FHWA-HRT-13-092, 142 p.

Newmark, N.M. (1960). Failure hypothesis for soils. *Proceedings of Conference on the Shear Strength of Soils*. Boulder, Colorado, pp. 17-32.

Peng, S. S., Ma, W. M., & Zhong, W. L. (1992). Surface subsidence engineering. Littleton, CO: Society for Mining, Metallurgy, and Exploration.

Roscoe, K. H. (1970). The influence of strains in soil mechanics. *Geotechnique*, 20(2), 129-170.

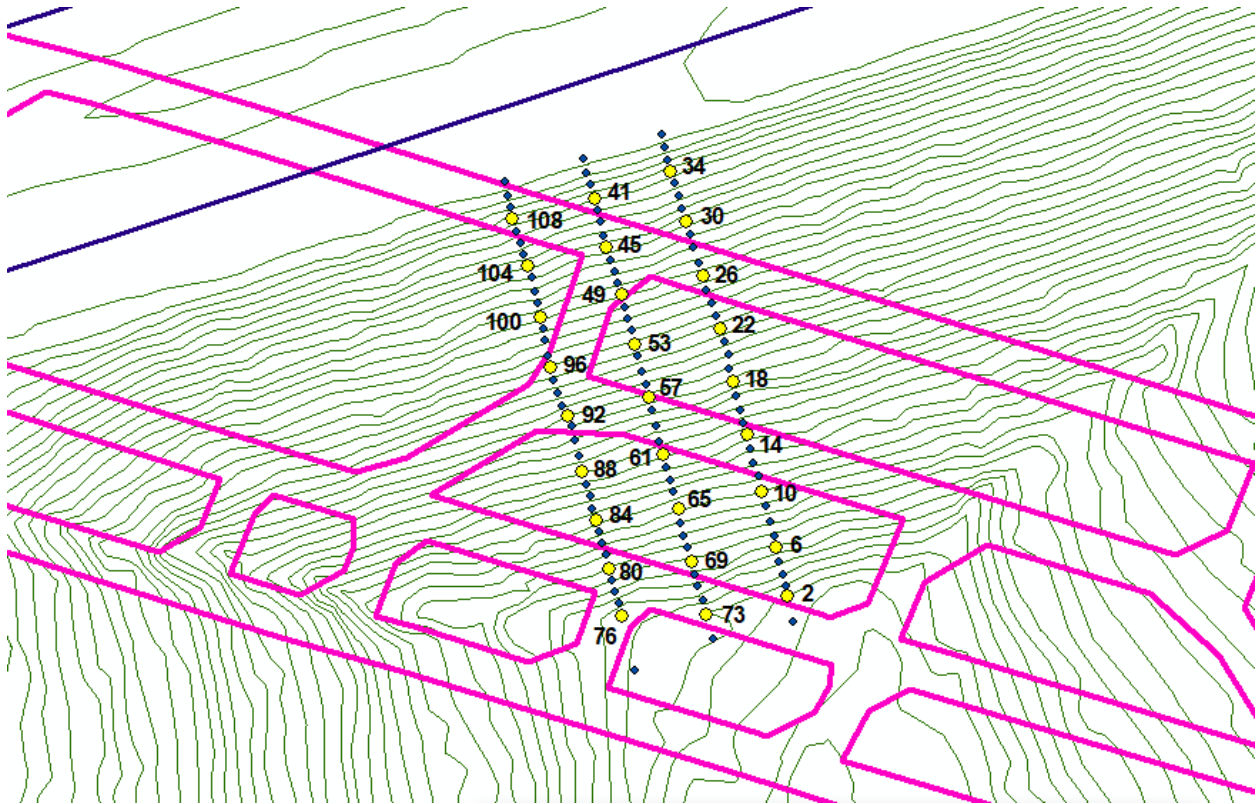
Scovazzo, V.A. (1999). *The Propagation Mechanics of Liquefied Sand Lenses due to Cyclic Loading*. Ph.D. Dissertation, University of Pittsburgh.

Vallejo, L.E. (1982). Development of a shear zone structure in stiff clays. *Proceedings of the 4th Int. Conference on Numerical Methods in Geomechanics, Canada*, 1: 255-262.

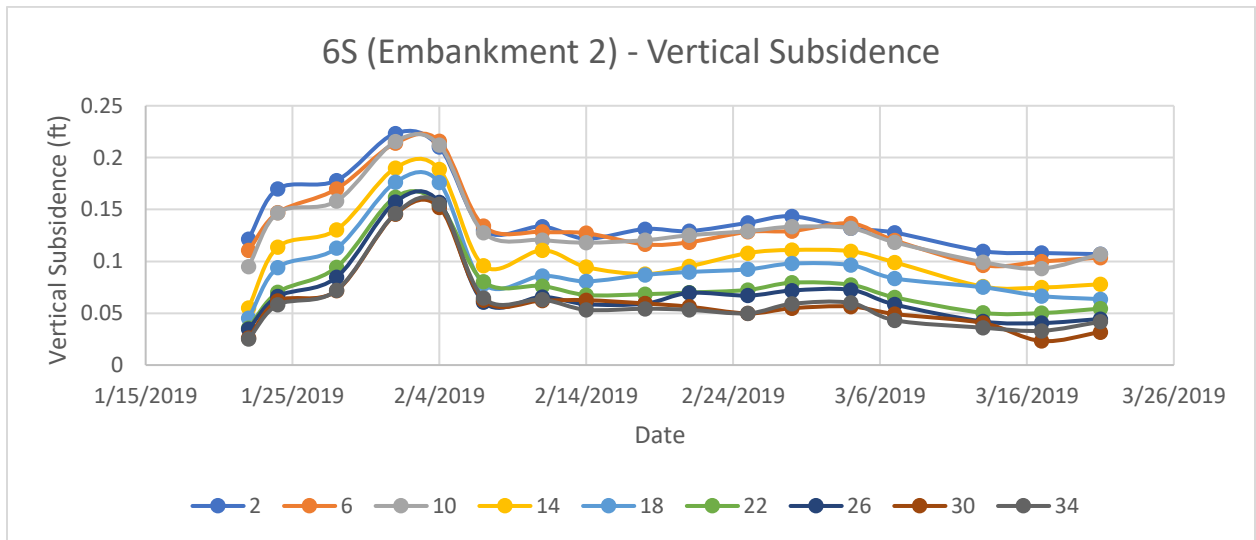
- Vallejo, L.E. and Lin, J.S. (2010). *A Study of Highway Subsidence due to Longwall Mining using data collected from I-79*. Commonwealth of Pennsylvania: Department of Transportation, T. H., & Kraft, L. M. (1970). Safety analysis of slopes. *Journal of Soil Mechanics & Foundations Div.*
- Vallejo, L. E., Lobo-Guerrero, S., & Seminsky, L. F. (2014). Shear strength of sand-gravel mixtures: laboratory and theoretical analysis. In *Geo-Congress 2014: Geo-characterization and Modeling for Sustainability* (pp. 74-83).
- Wu, T.H. and Kraft, L. M. (1970). Safety analysis of slopes. *Journal of Soil Mechanics & Foundations Div.*
- Zhao, Y. and Liu, Z. (2018). Study of Material Composition Effects on the Mechanical Properties of Soil-Rock Mixtures. *Advances in Civil Engineering*, Vol. 2018, Article ID 3854727.
- Zheng, Y. R., Zhao, S. Y., Kong, W. X., & Deng, C. J. (2005). Geotechnical engineering limit analysis using finite element method. *Yantu Lixue(Rock Soil Mech.)*, 26(1), 163-168.
- Zienkiewicz, O. C., Humpheson, C., & Lewis, R. W. (1975). Associated and non-associated visco-plasticity and plasticity in soil mechanics. *Geotechnique*, 25(4), 671-689.

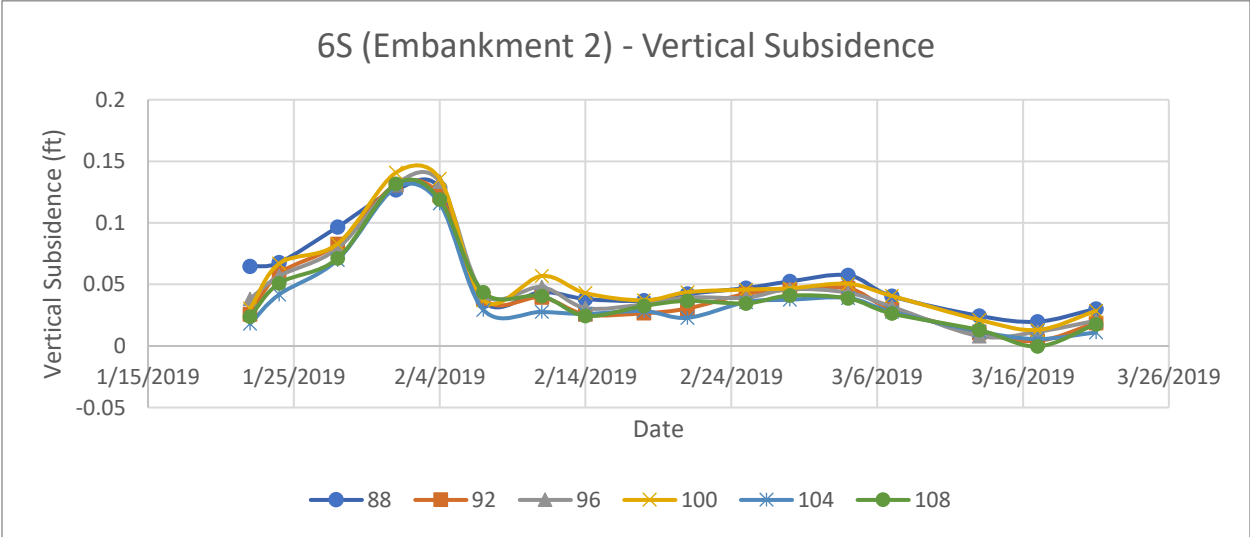
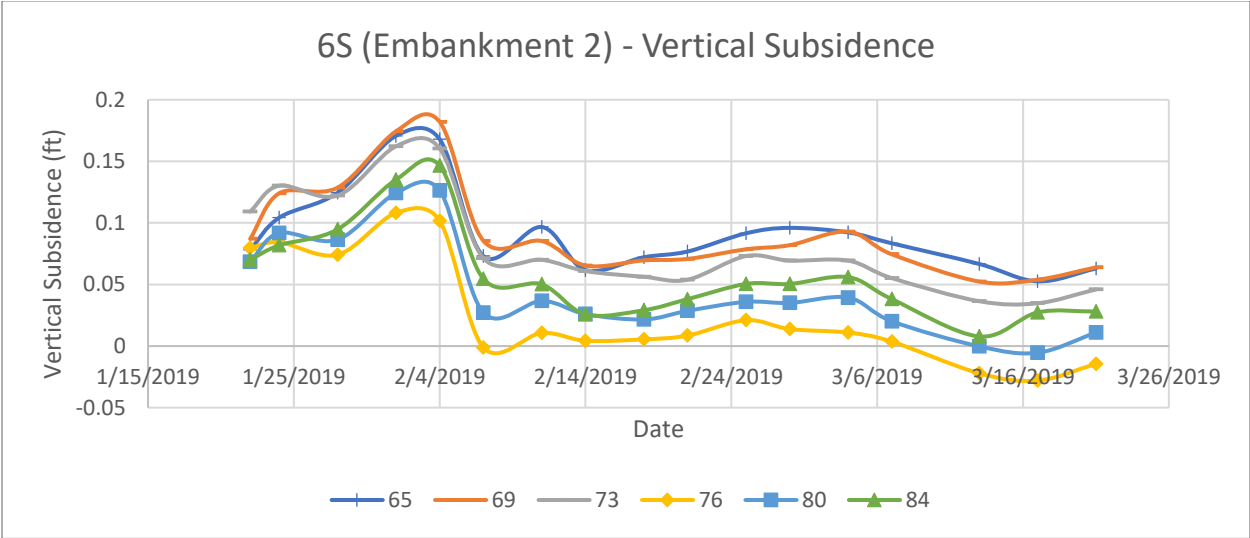
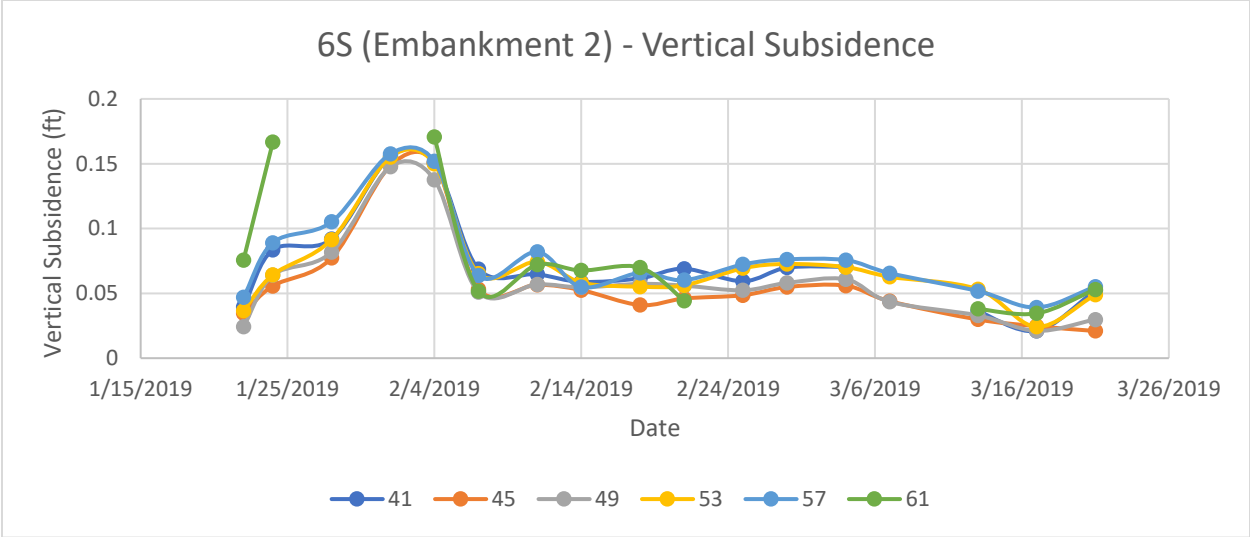
APPENDIX I – Detailed SPK Survey Stake Data

EMBANKMENT #2

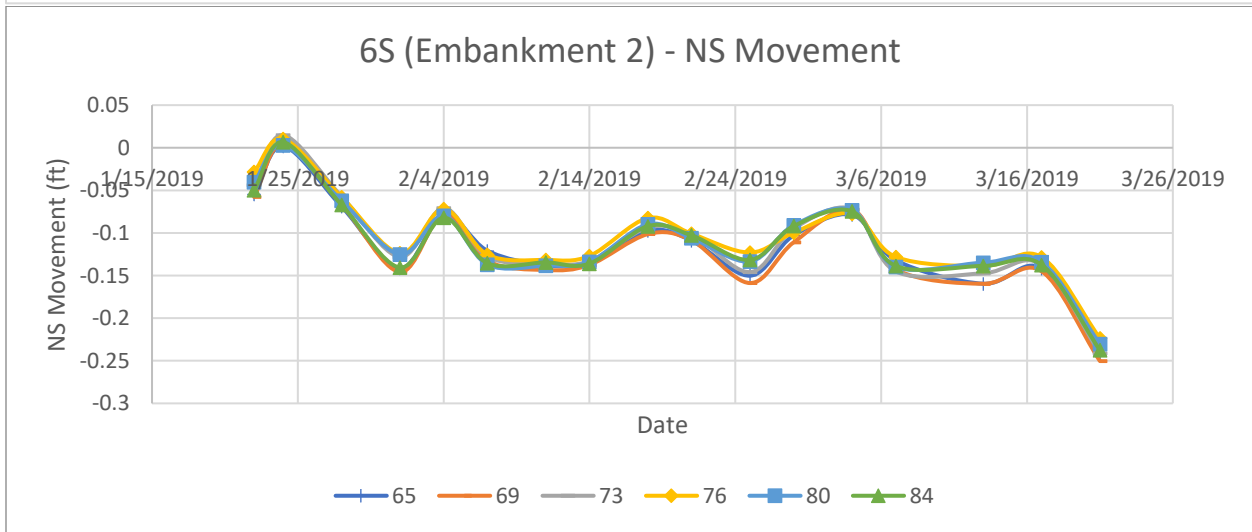
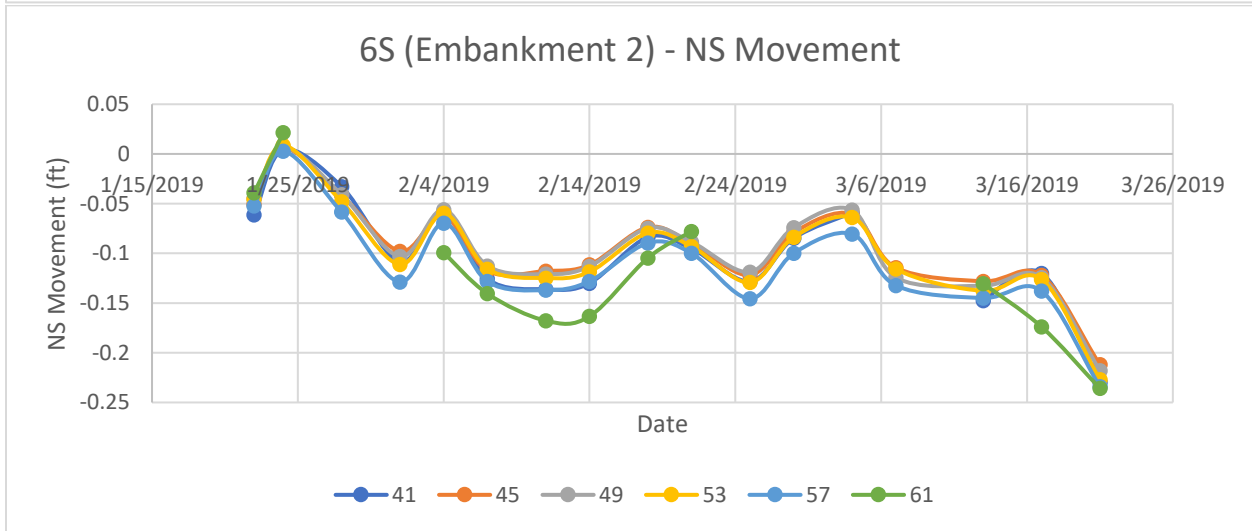
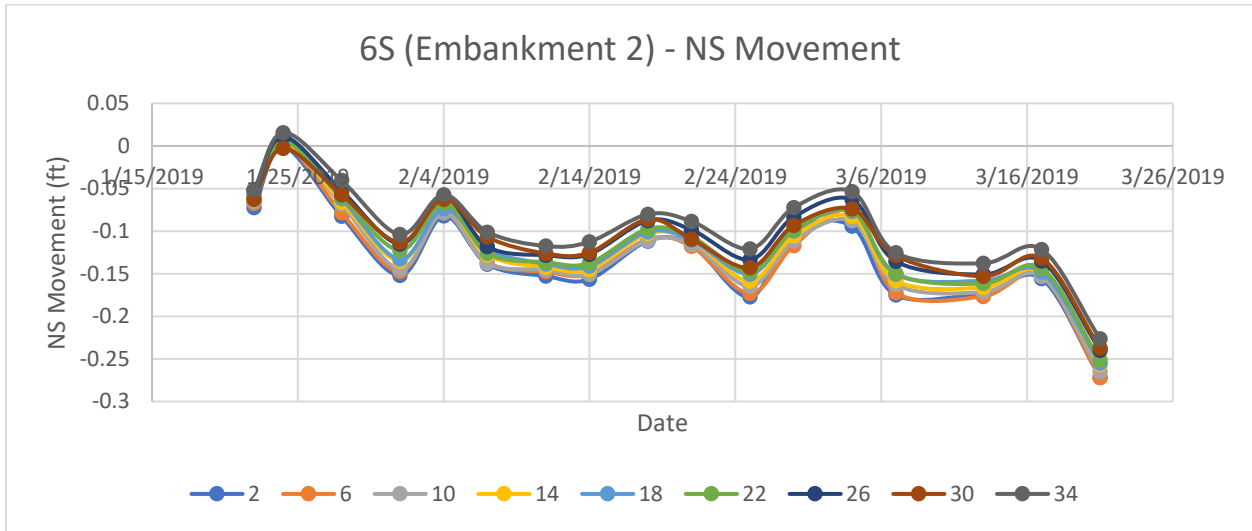


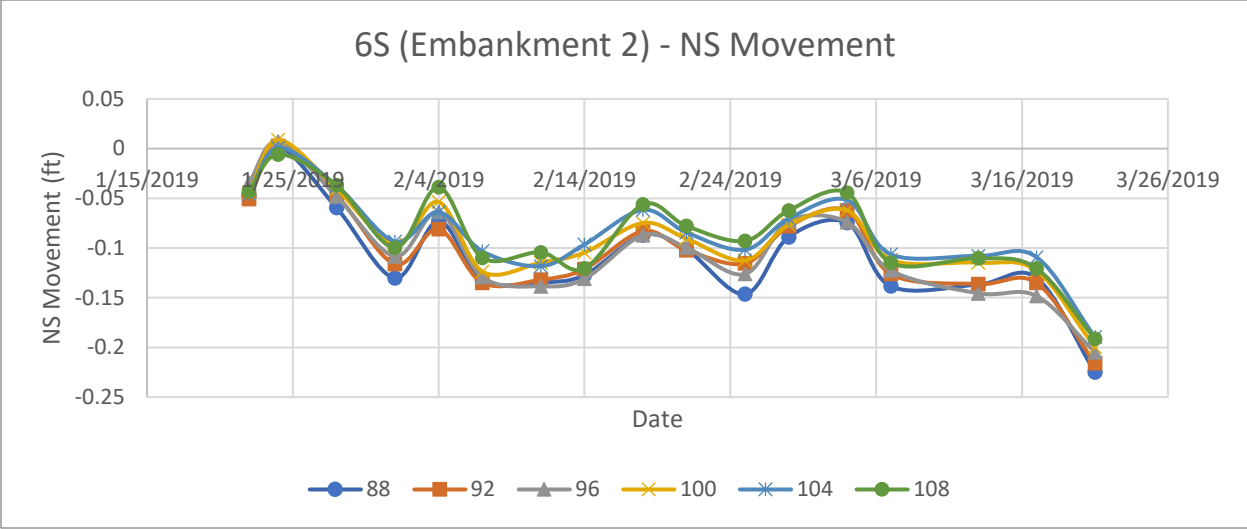
Vertical Movement



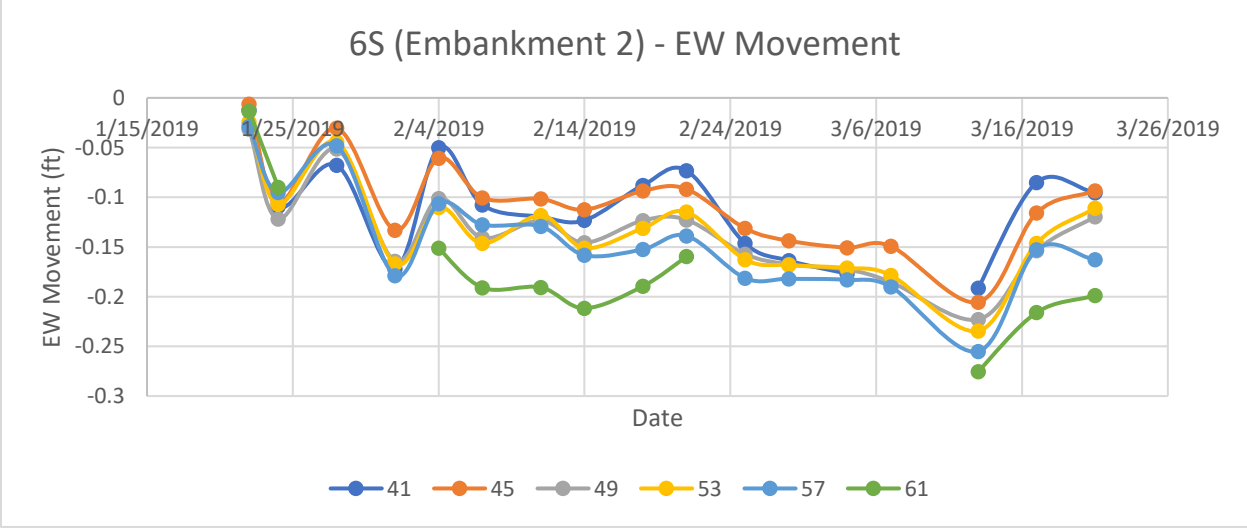
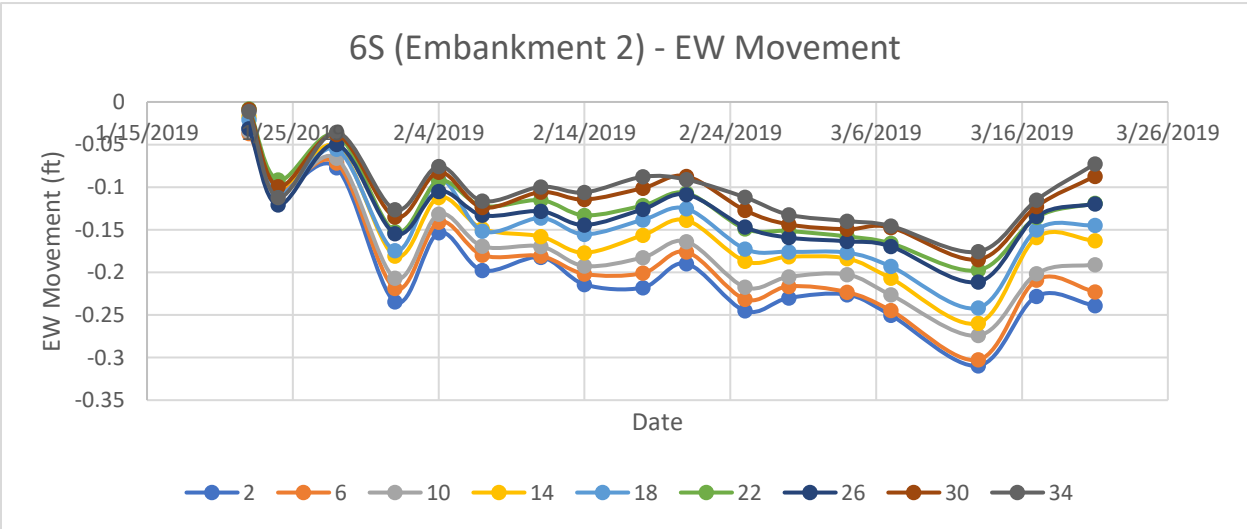


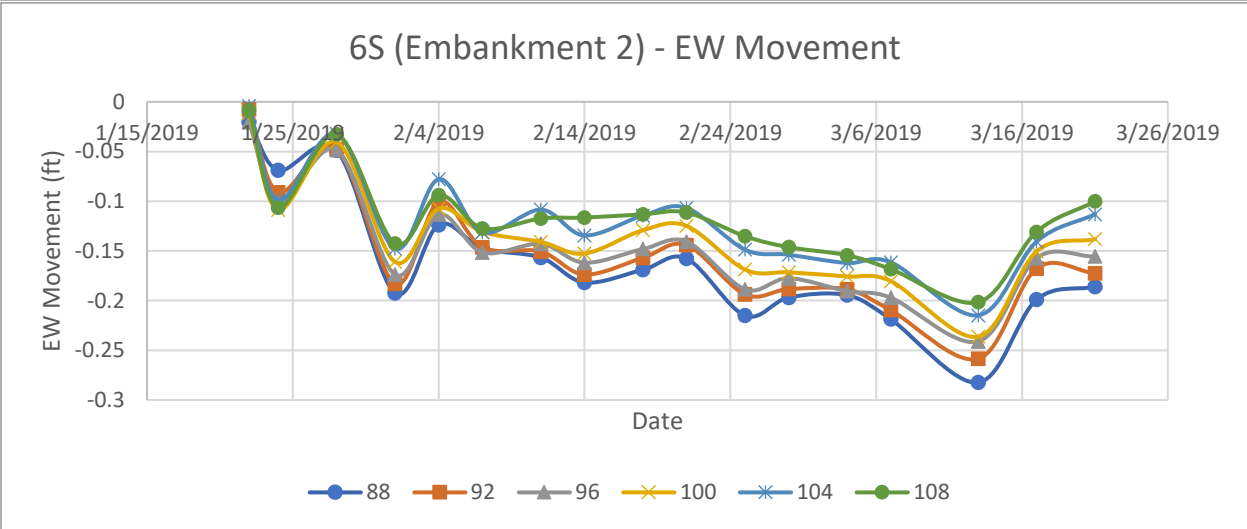
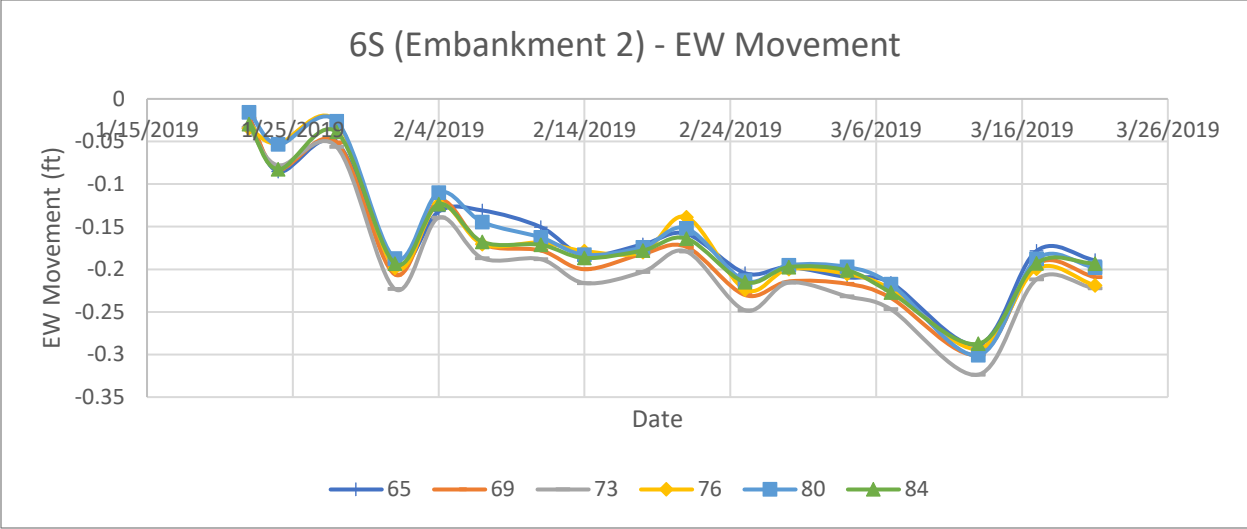
North-South Horizontal Movement



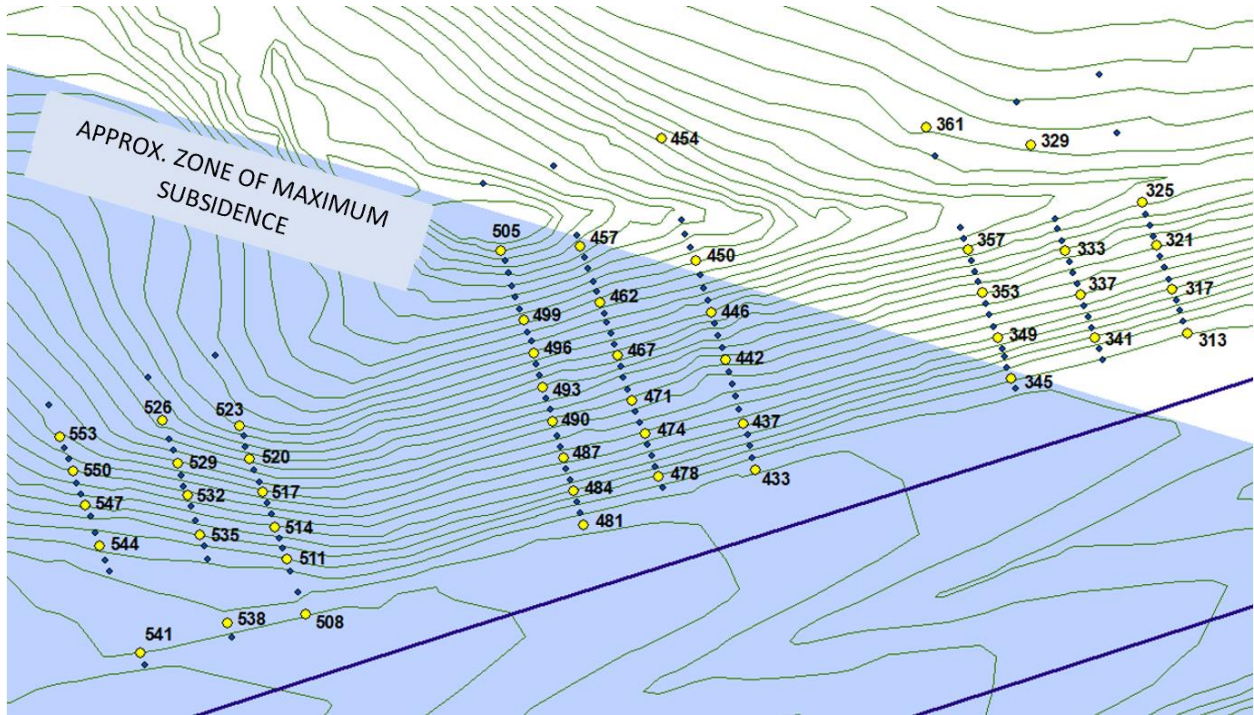


East-West Horizontal Movement

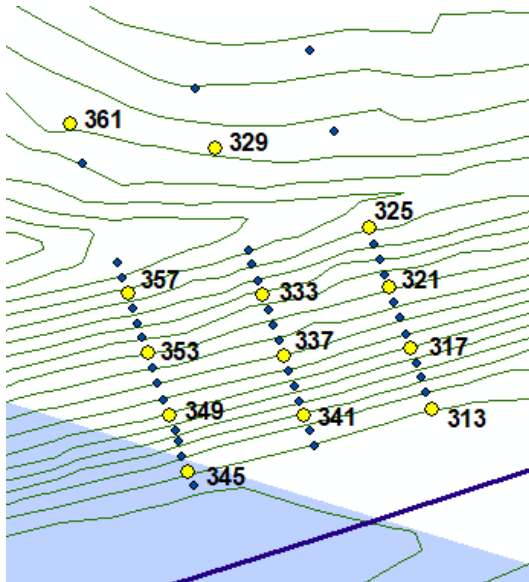




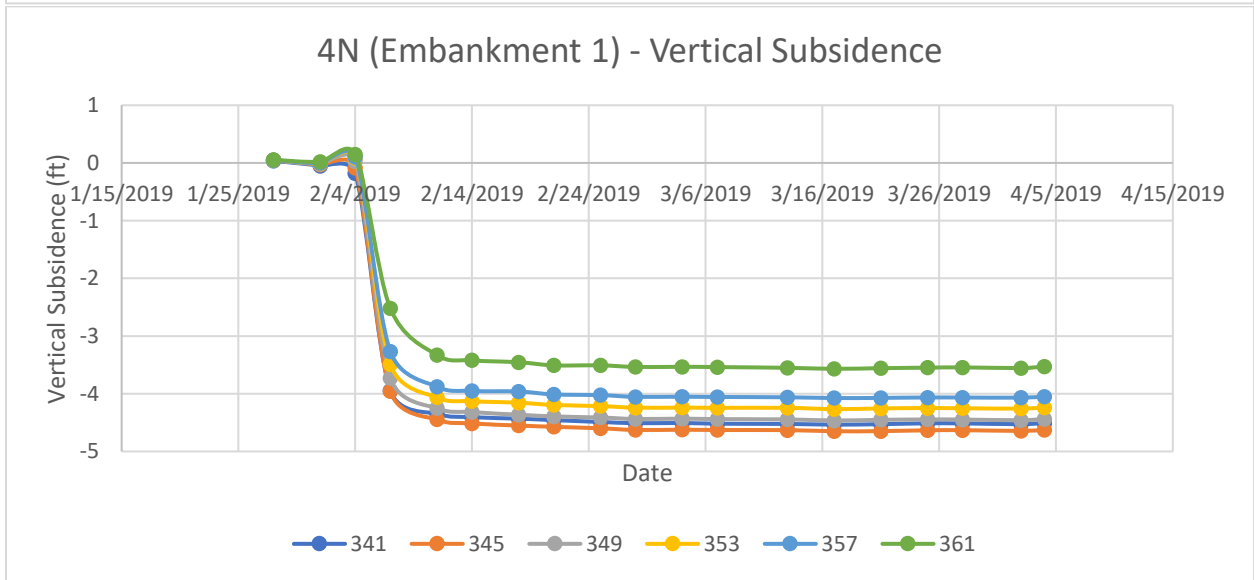
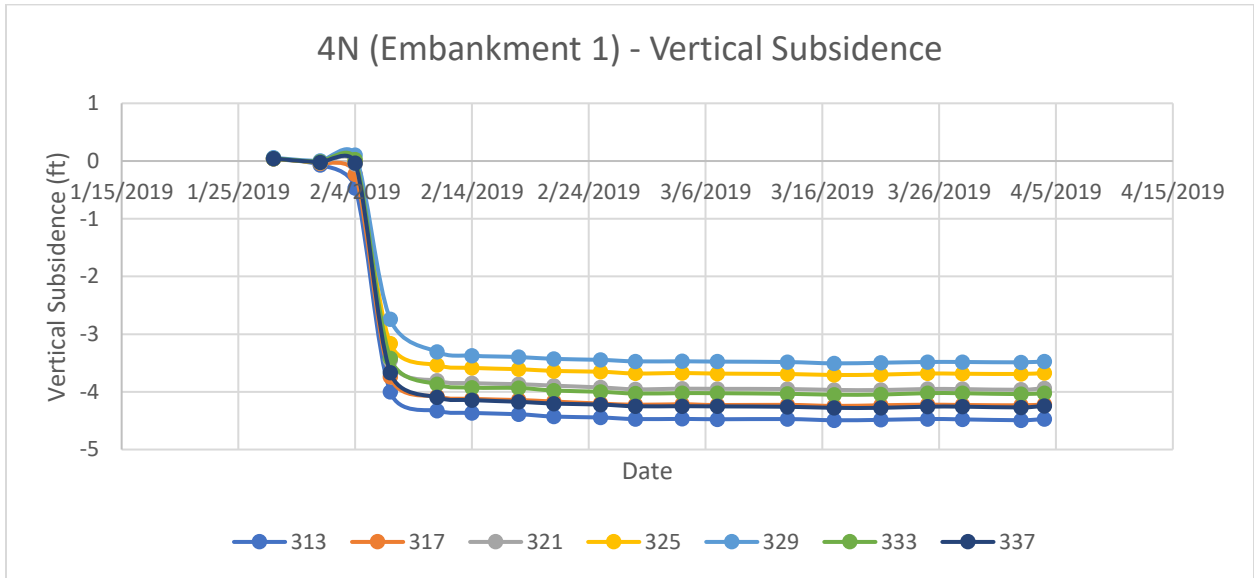
EMBANKMENT #1 – NORTH SLOPE



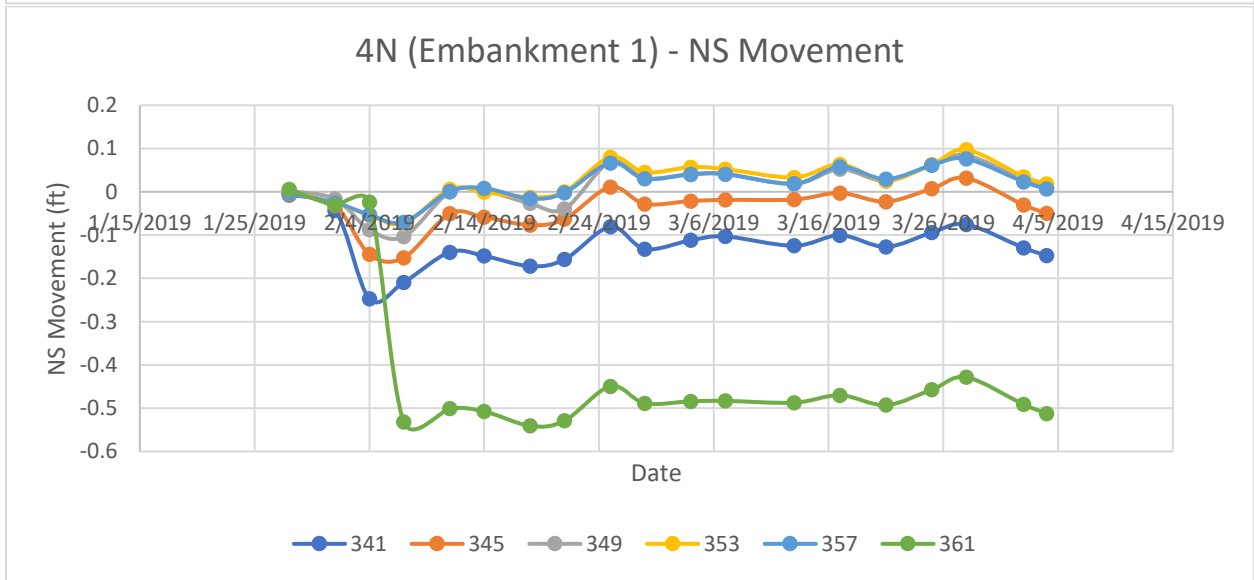
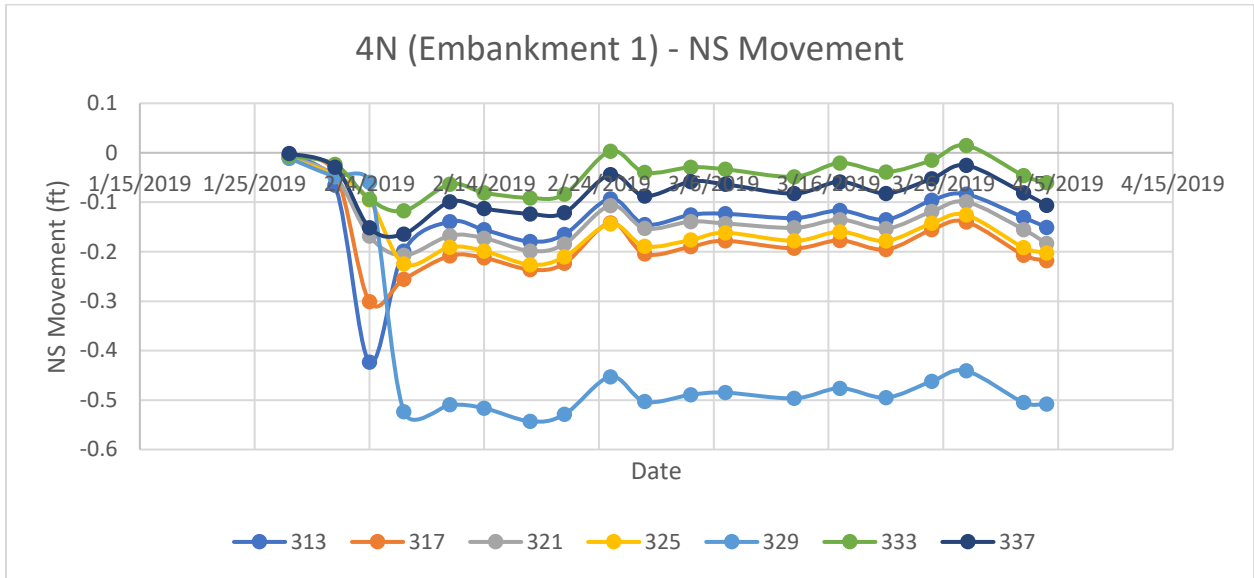
Group 4N



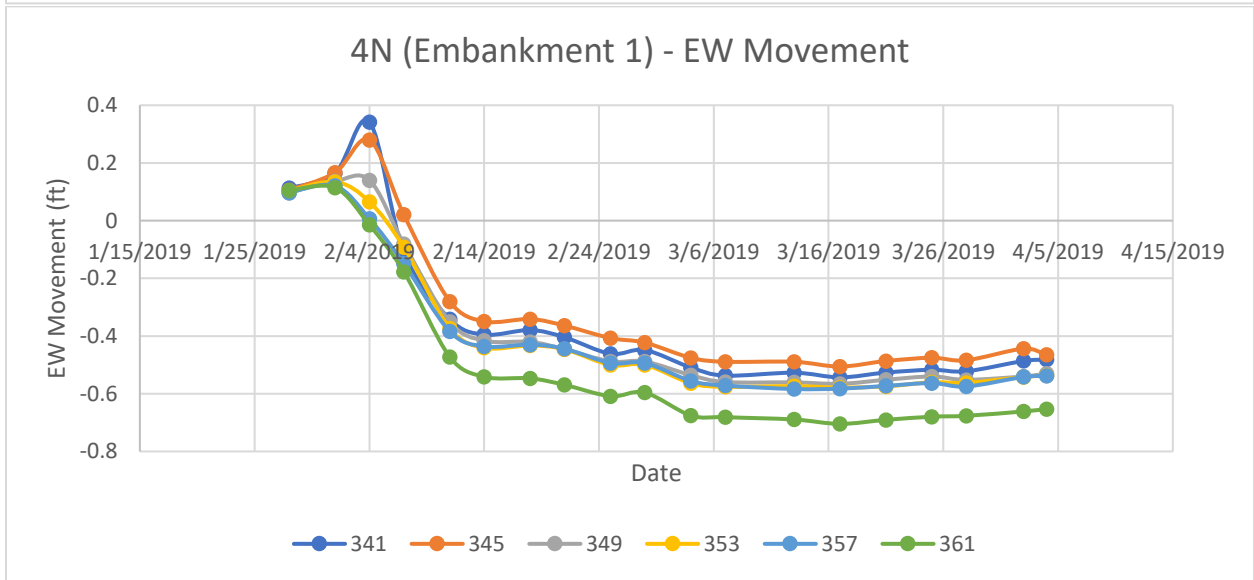
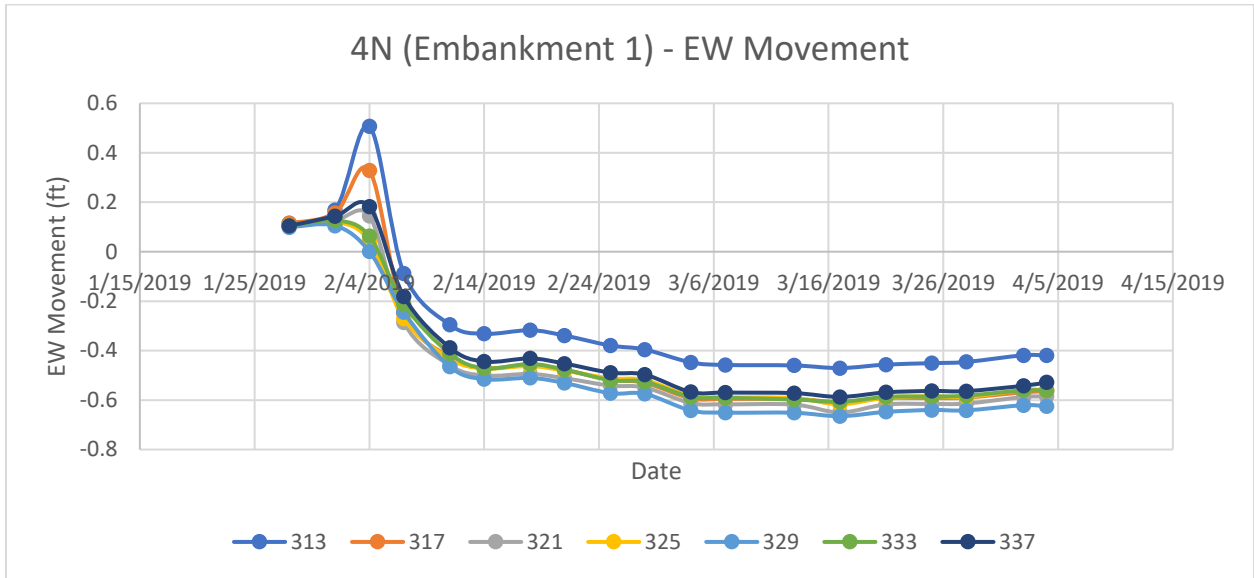
Vertical Movement



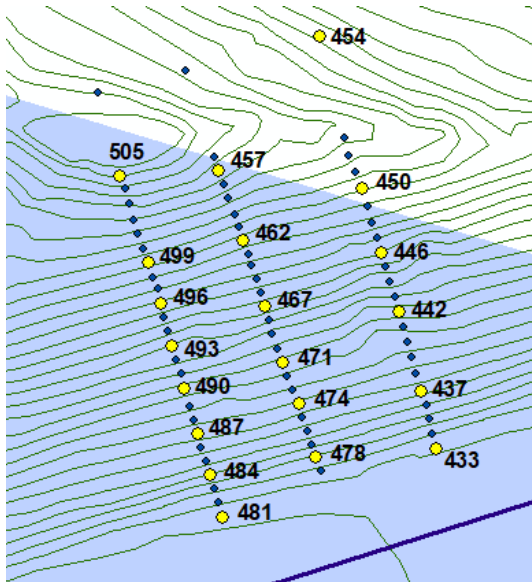
North-South Horizontal Movement



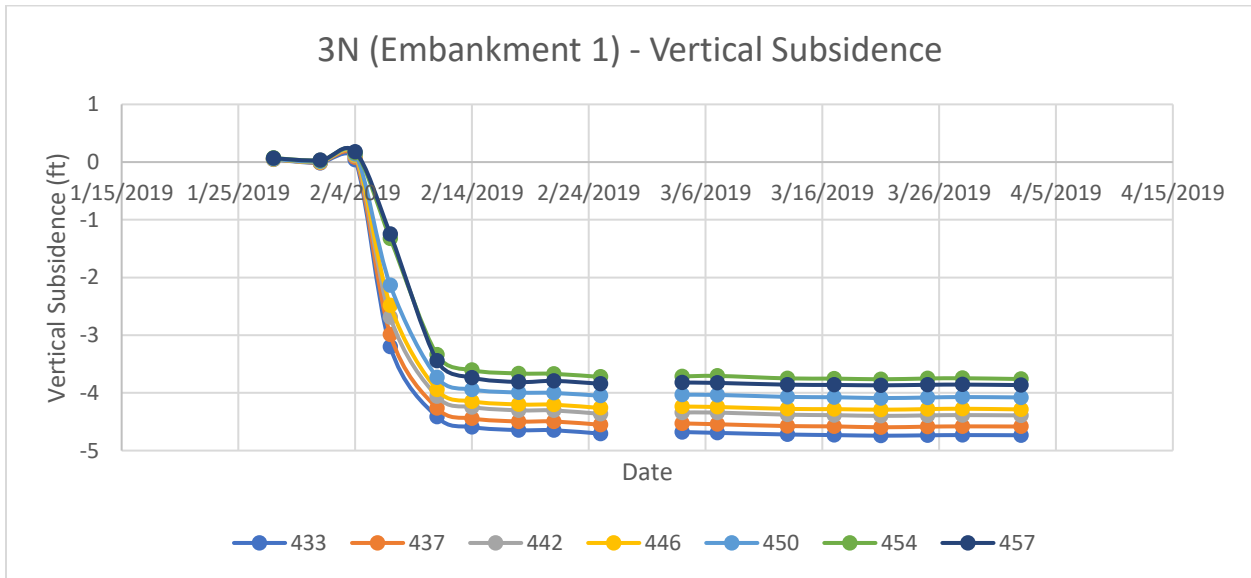
East-West Horizontal Movement



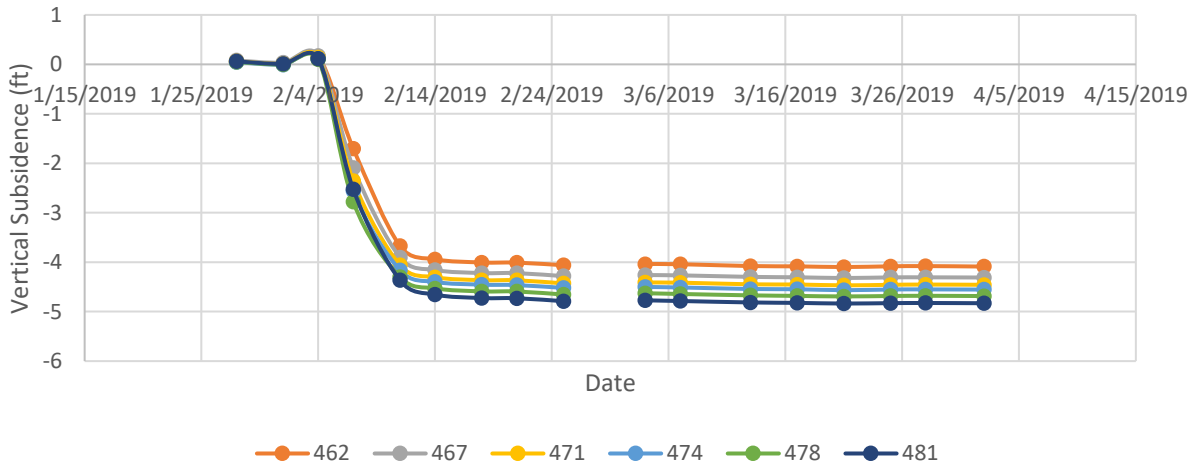
Group 3N



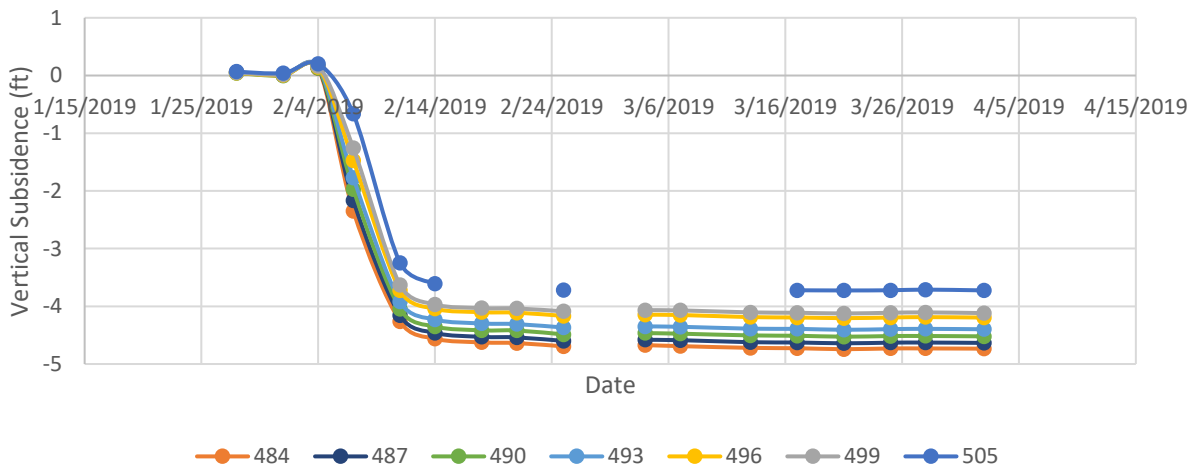
Vertical Movement



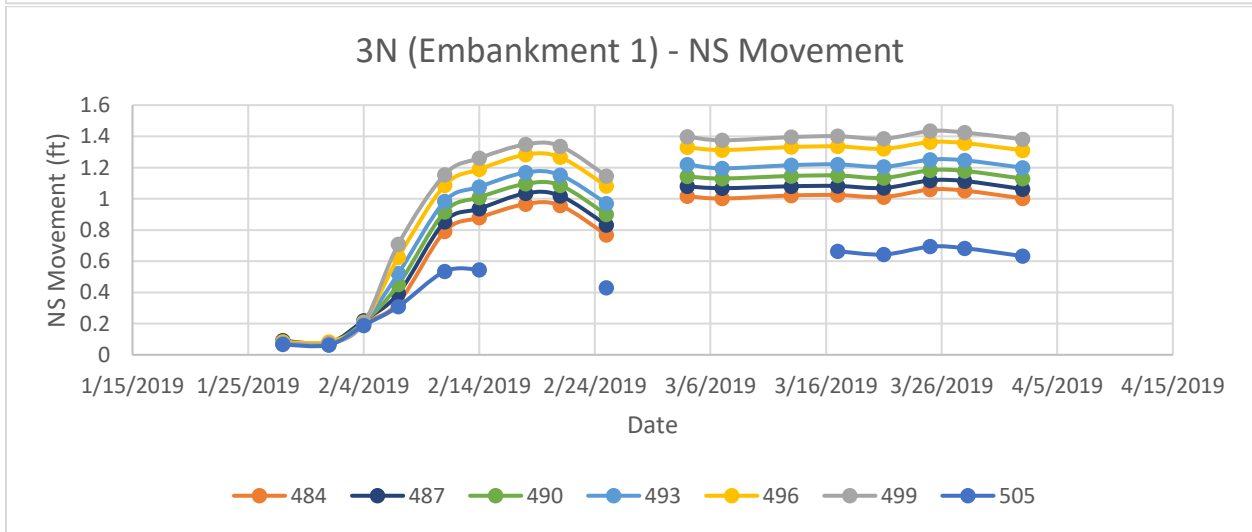
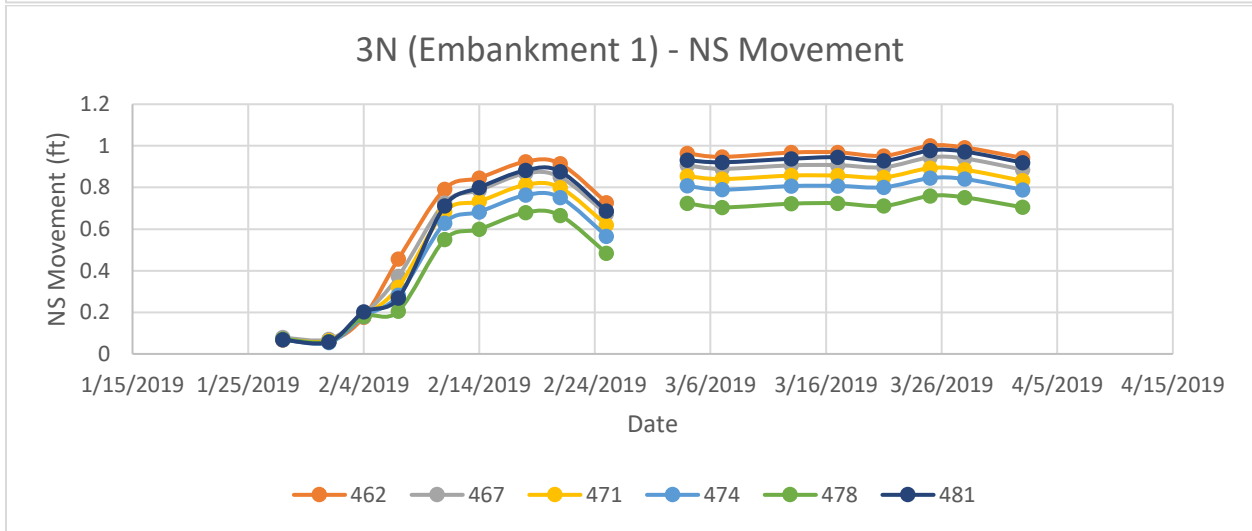
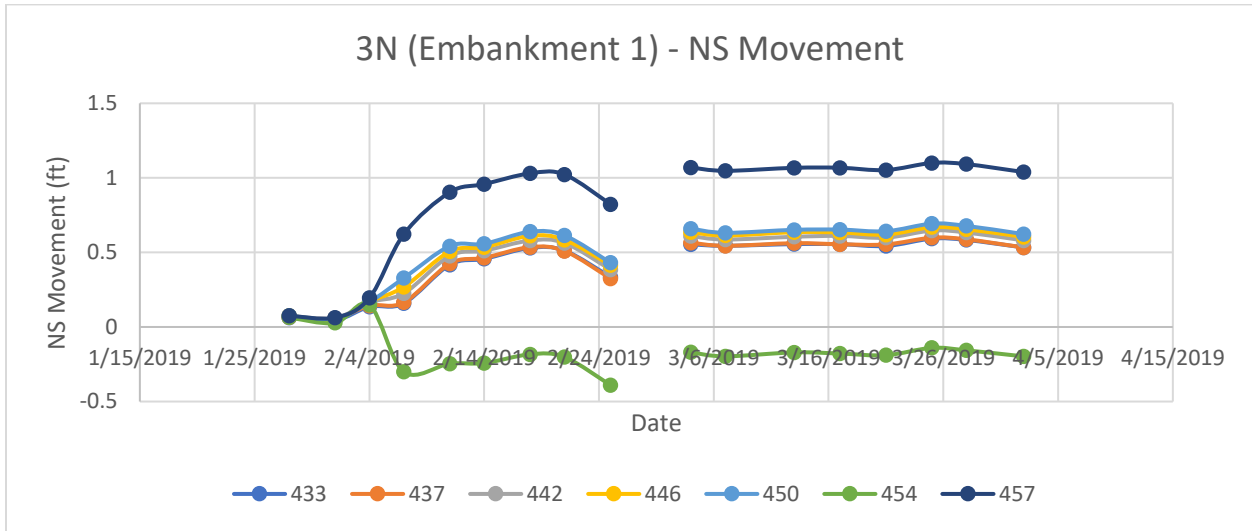
3N (Embankment 1) - Vertical Subsidence



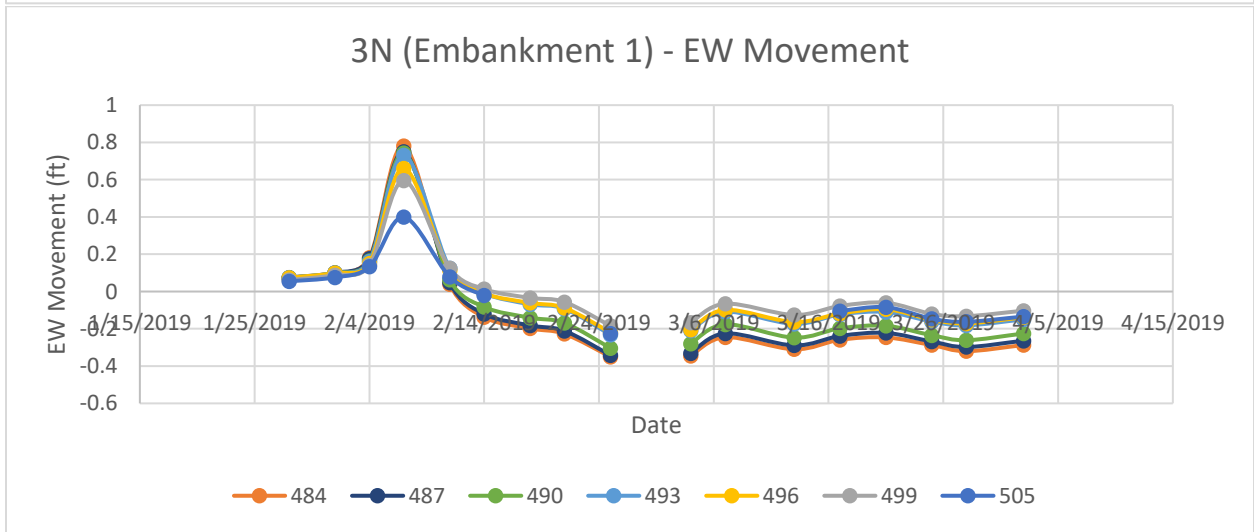
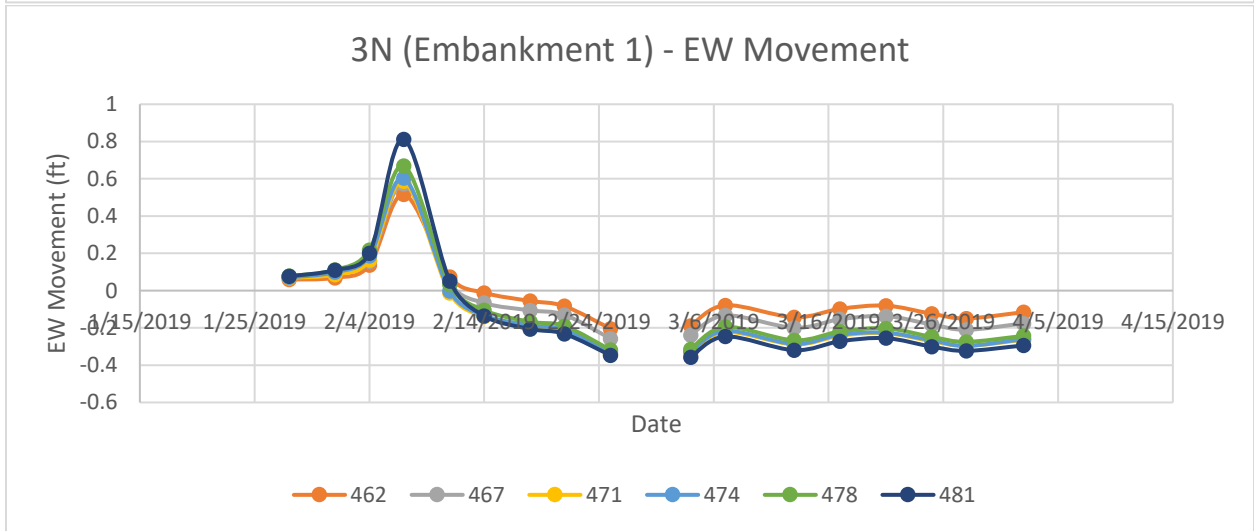
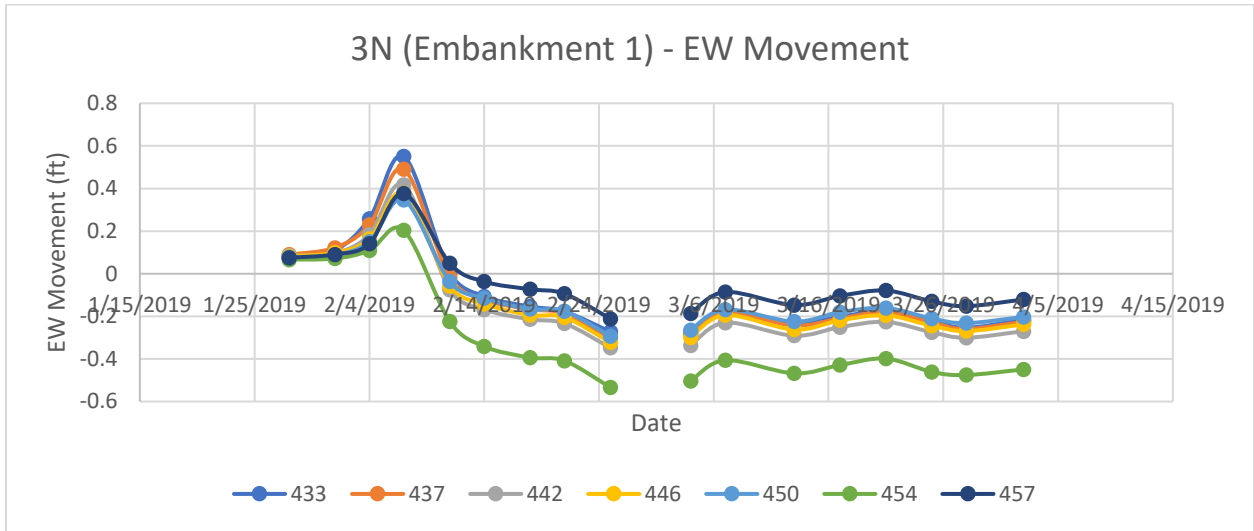
3N (Embankment 1) - Vertical Subsidence



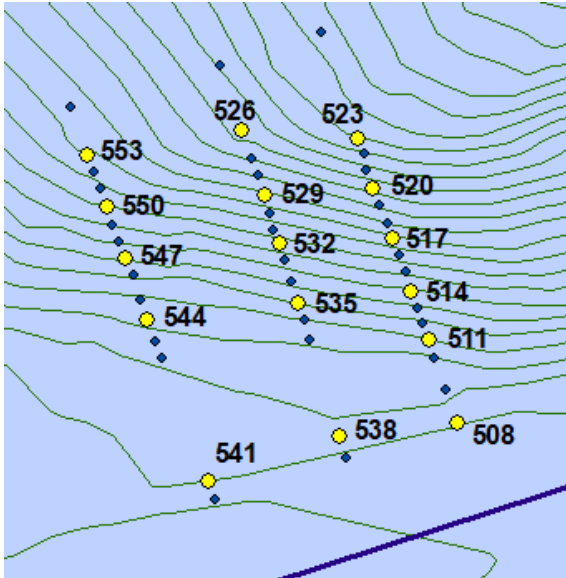
North-South Horizontal Movement



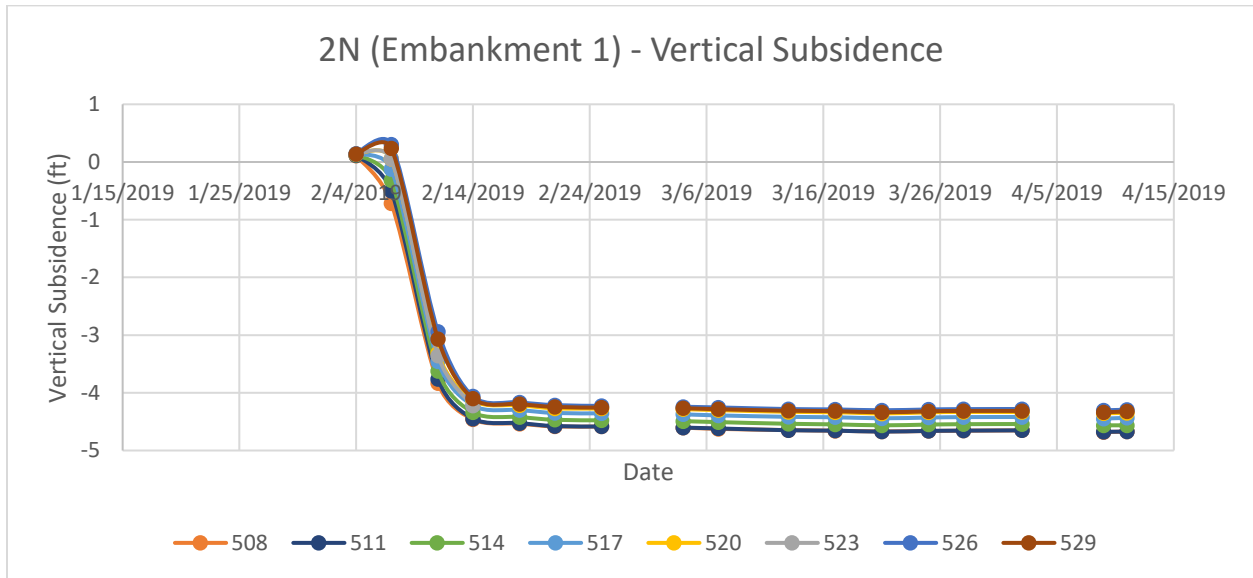
East-West Horizontal Movement

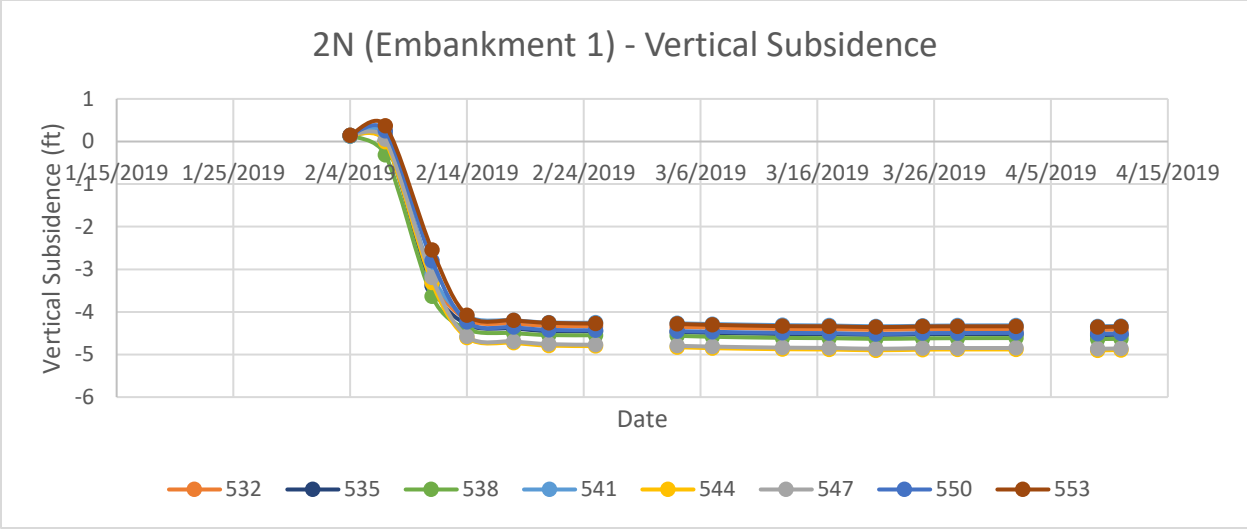


Group 2N

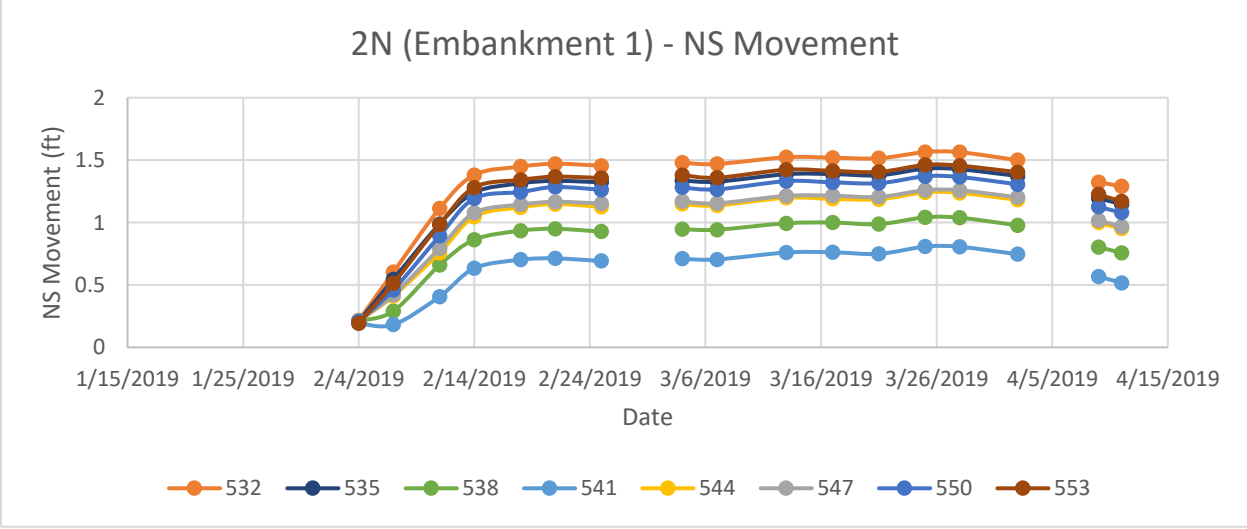
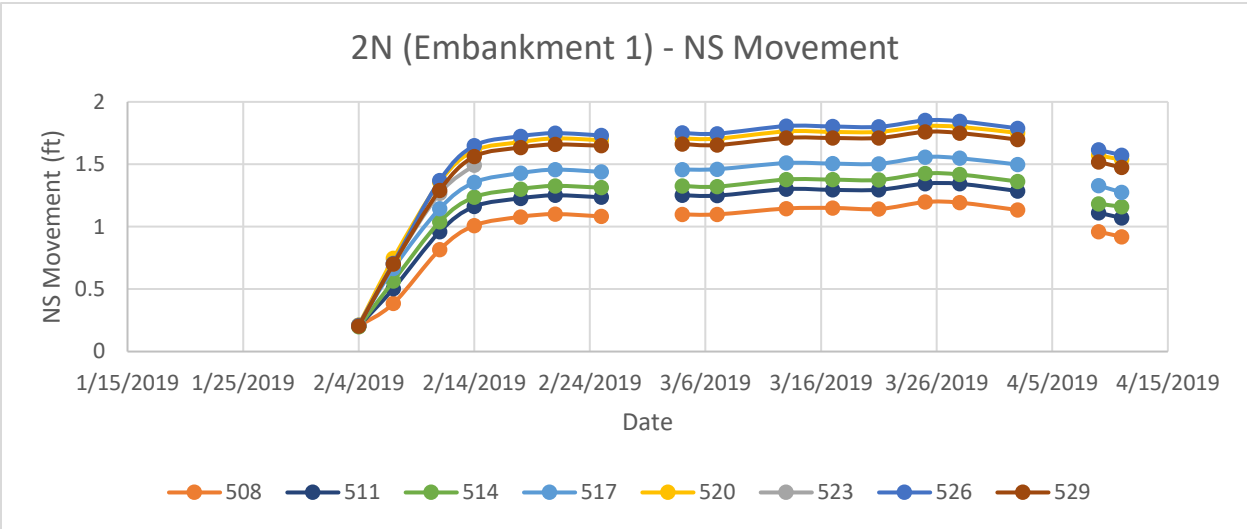


Vertical Movement

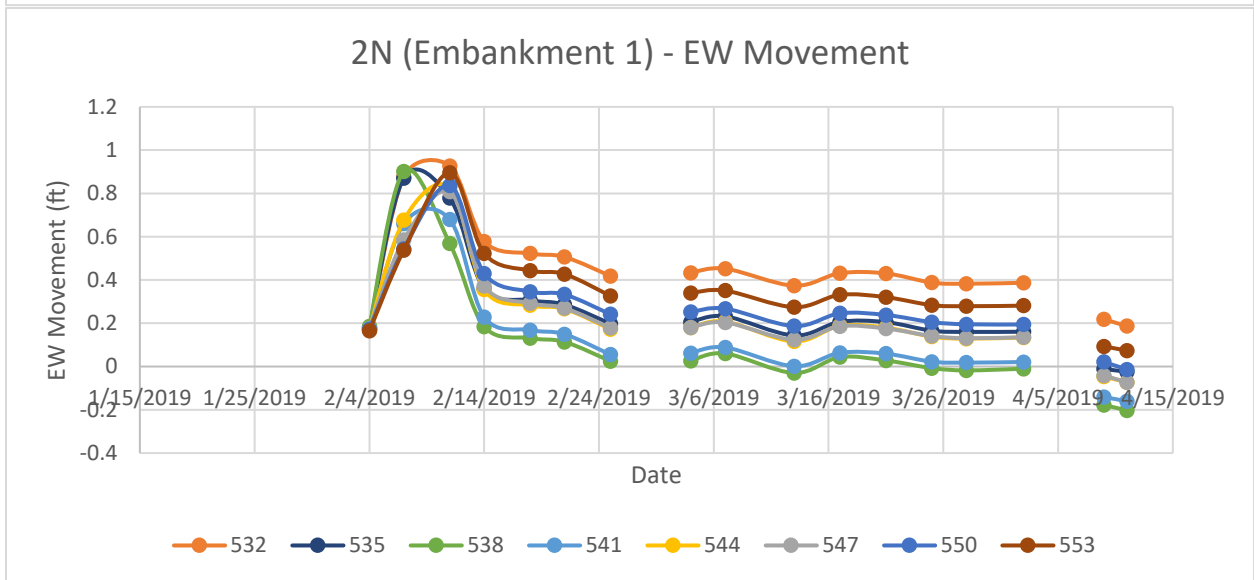
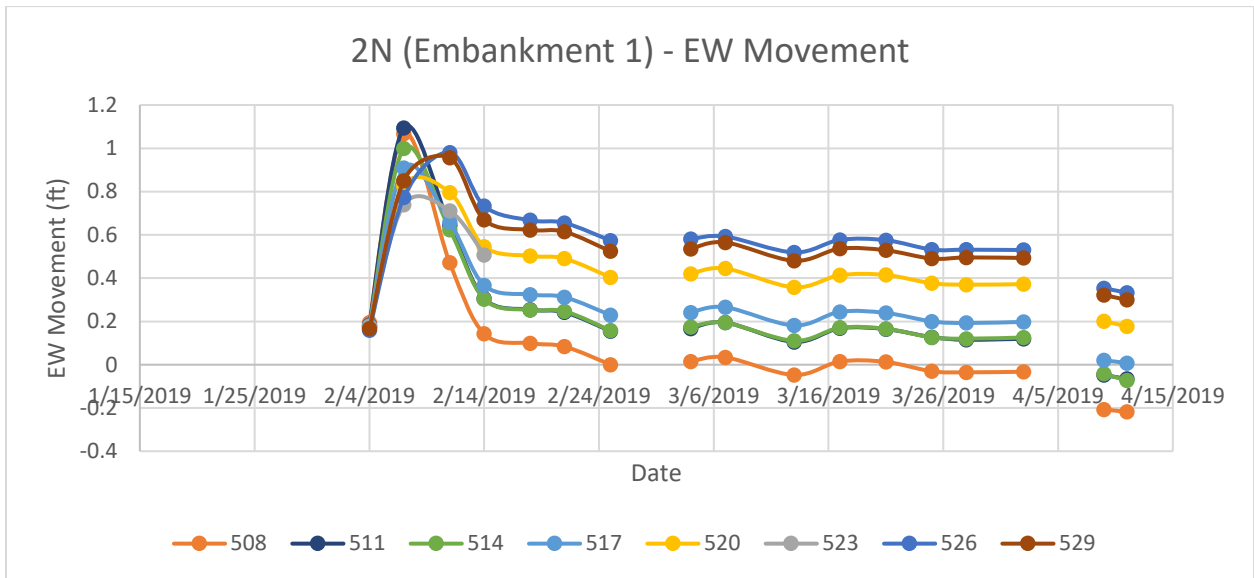




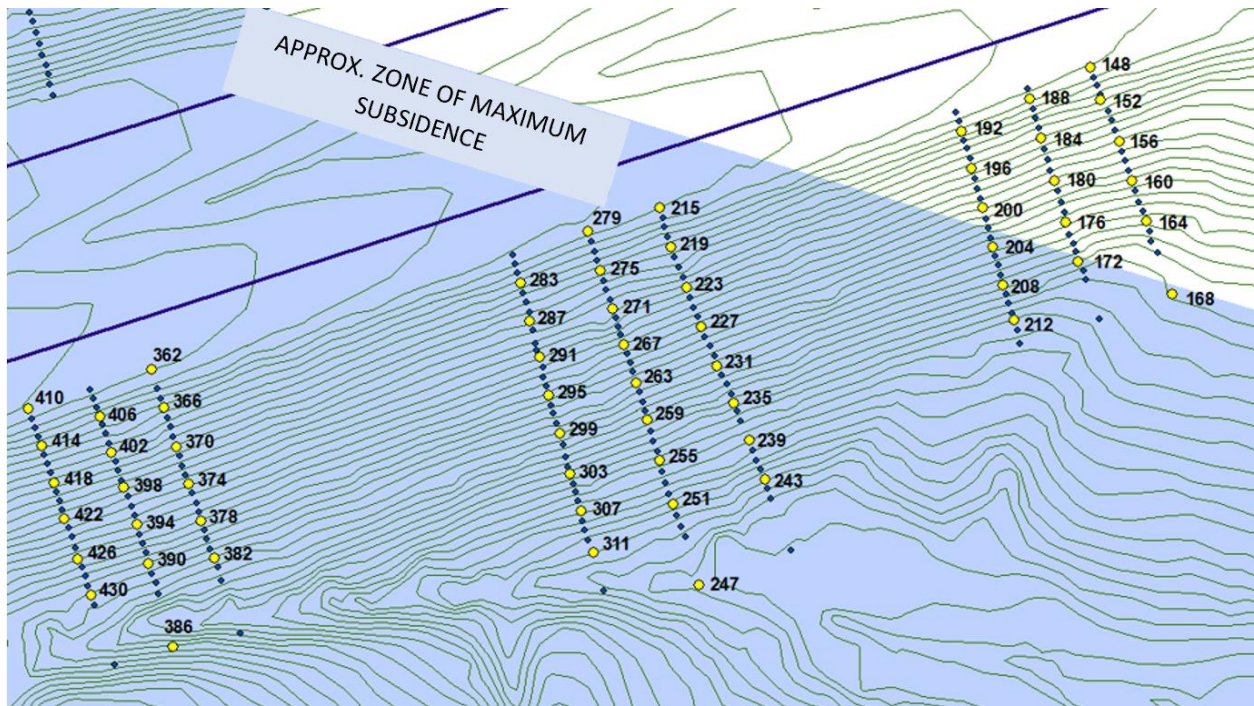
North-South Horizontal Movement



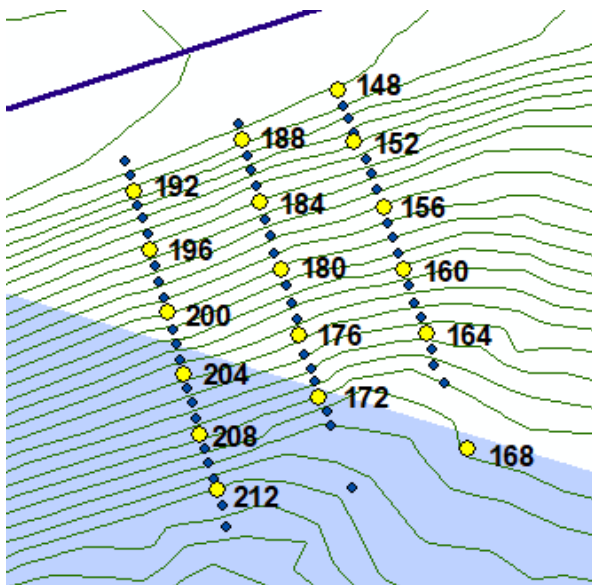
East-West Horizontal Movement



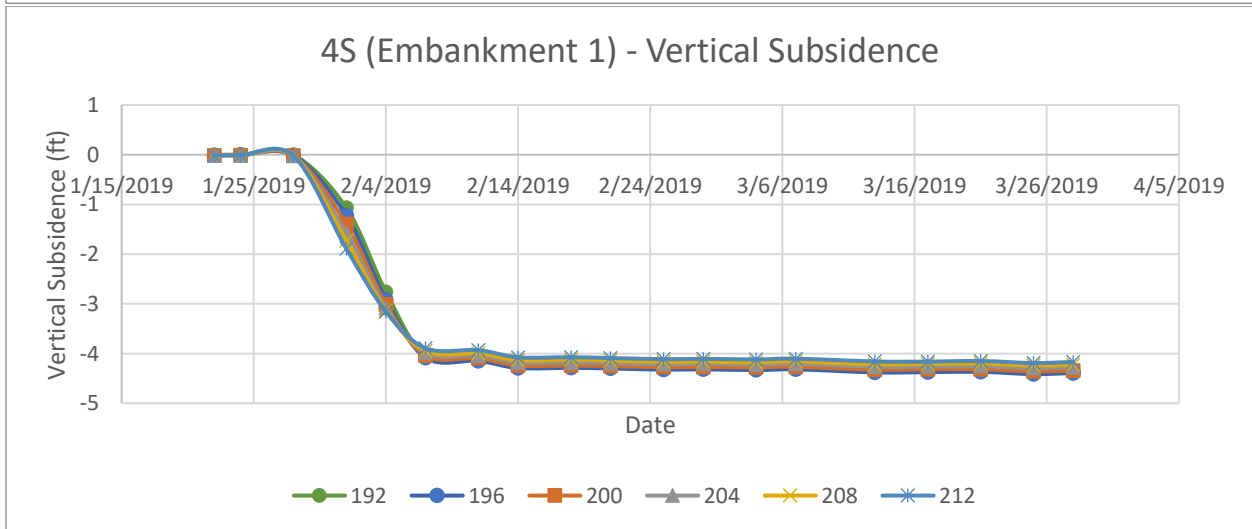
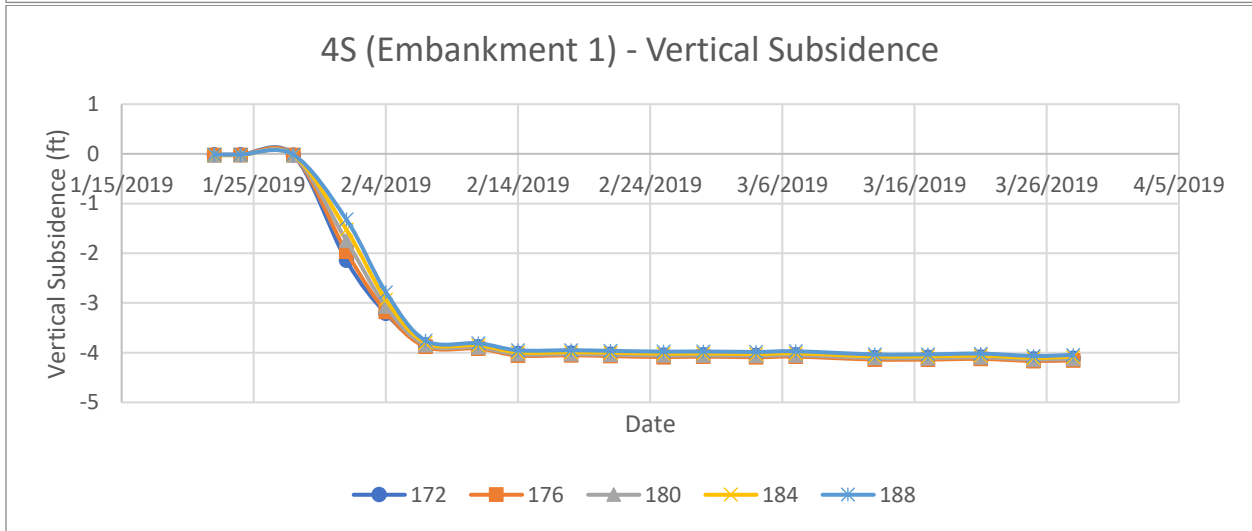
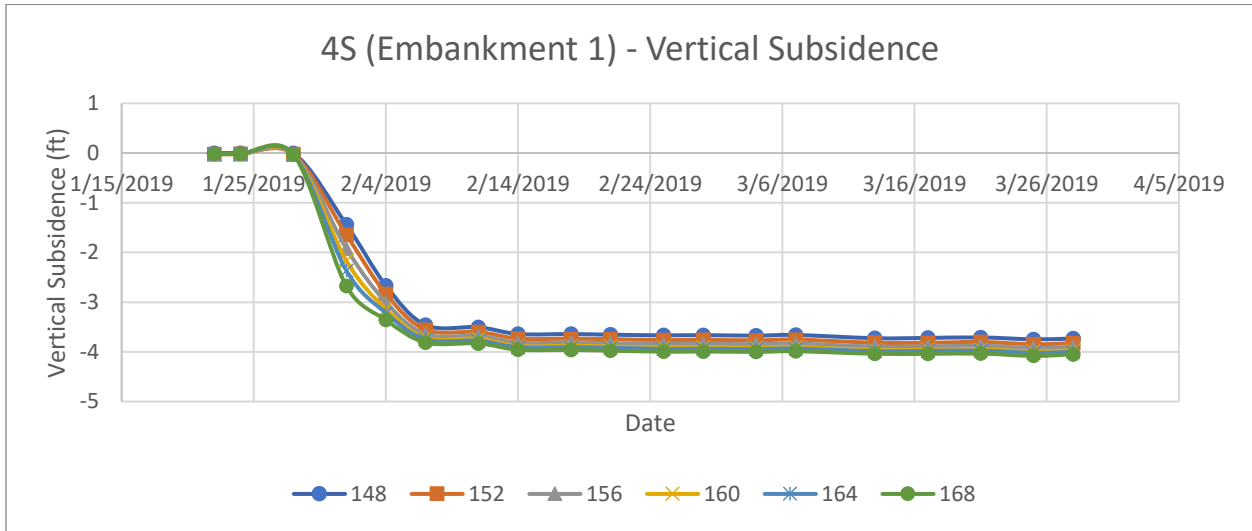
EMBANKMENT #1 – SOUTH SLOPE



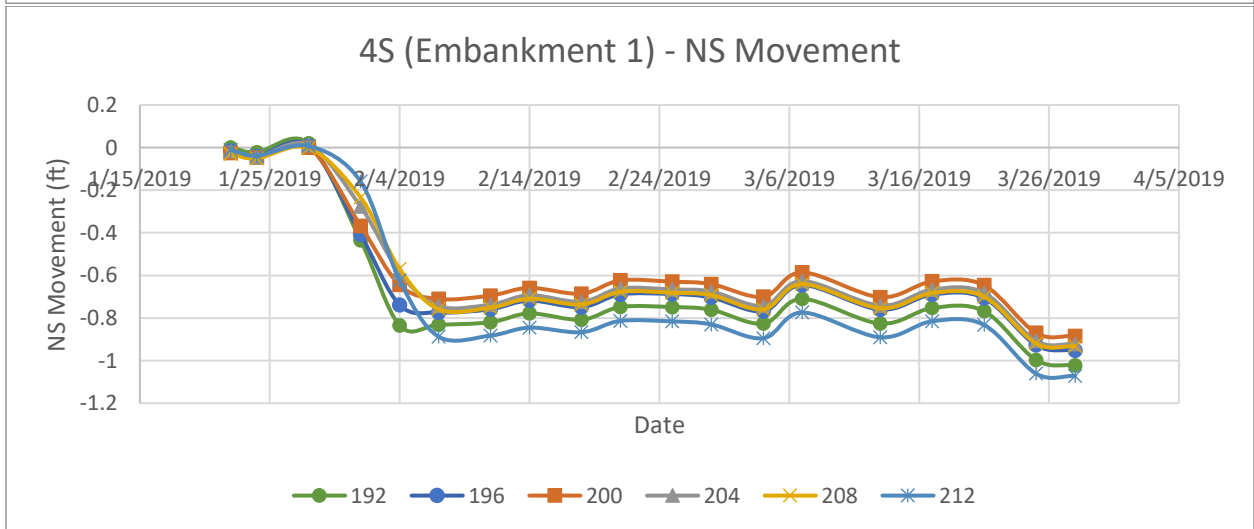
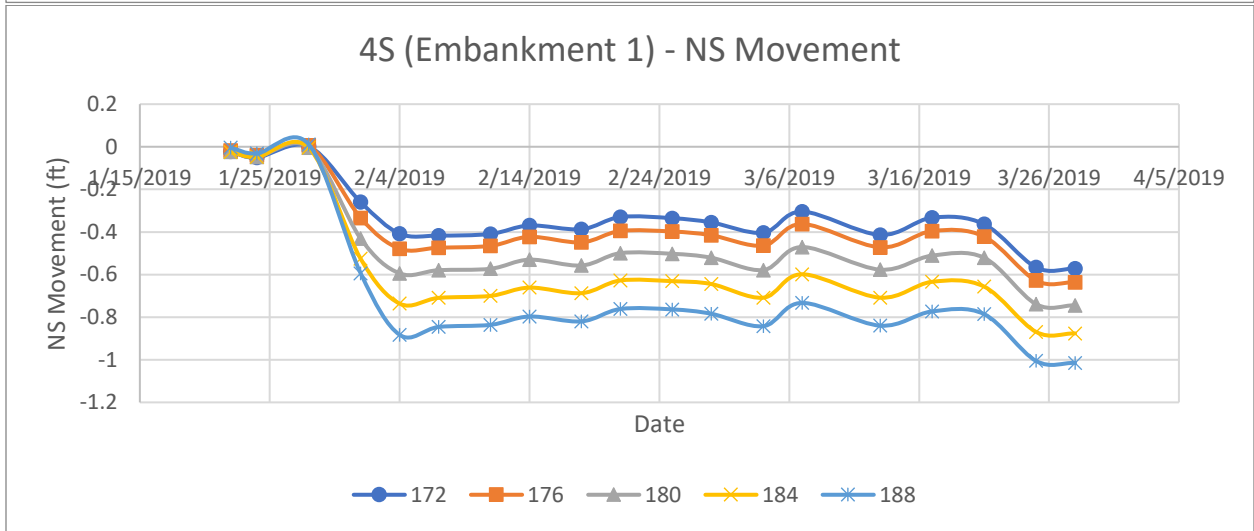
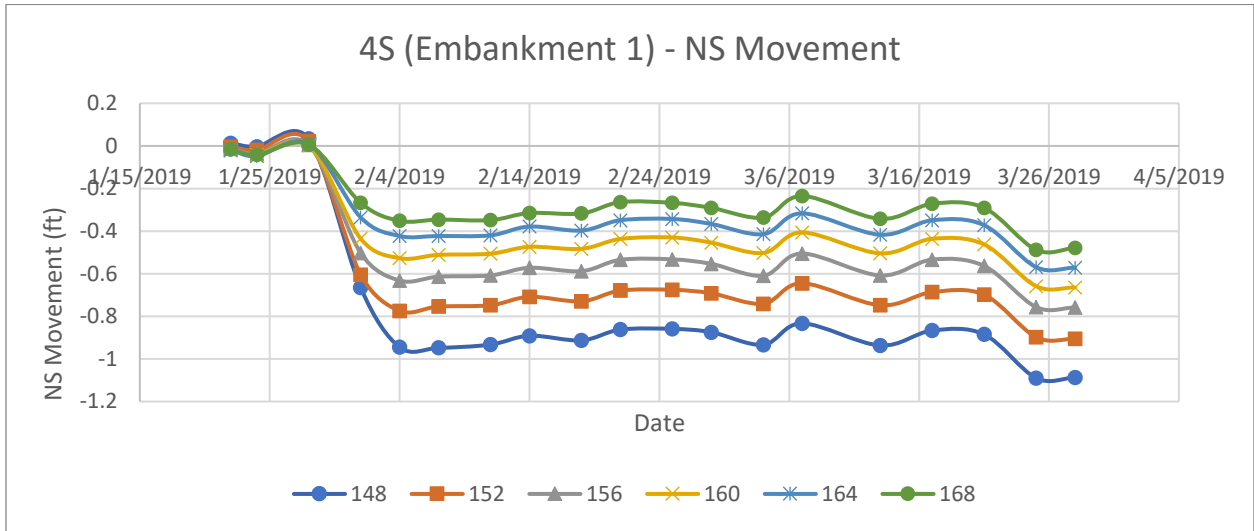
Group 4S



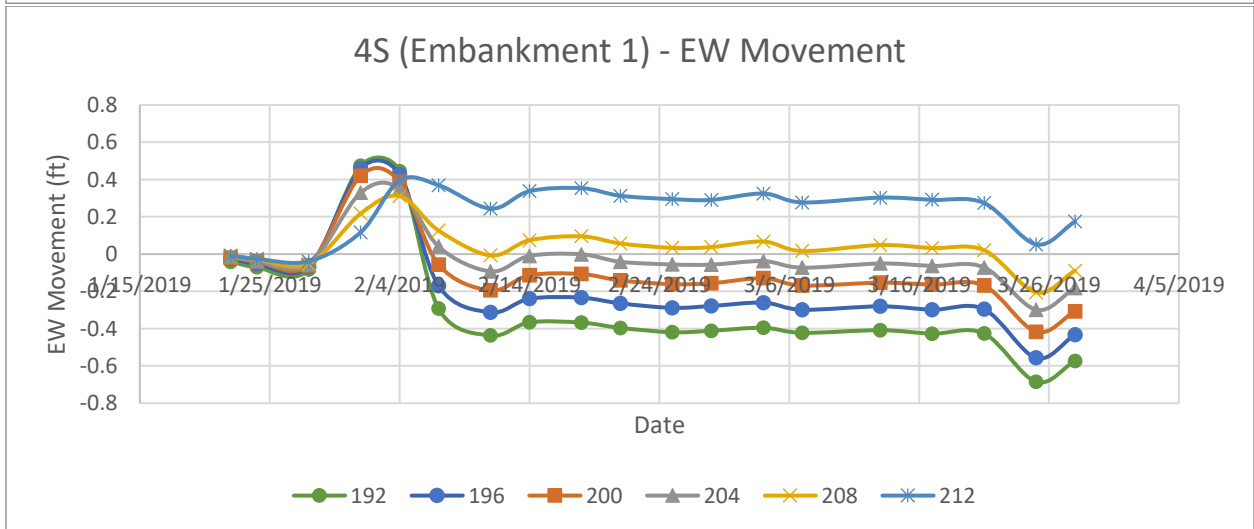
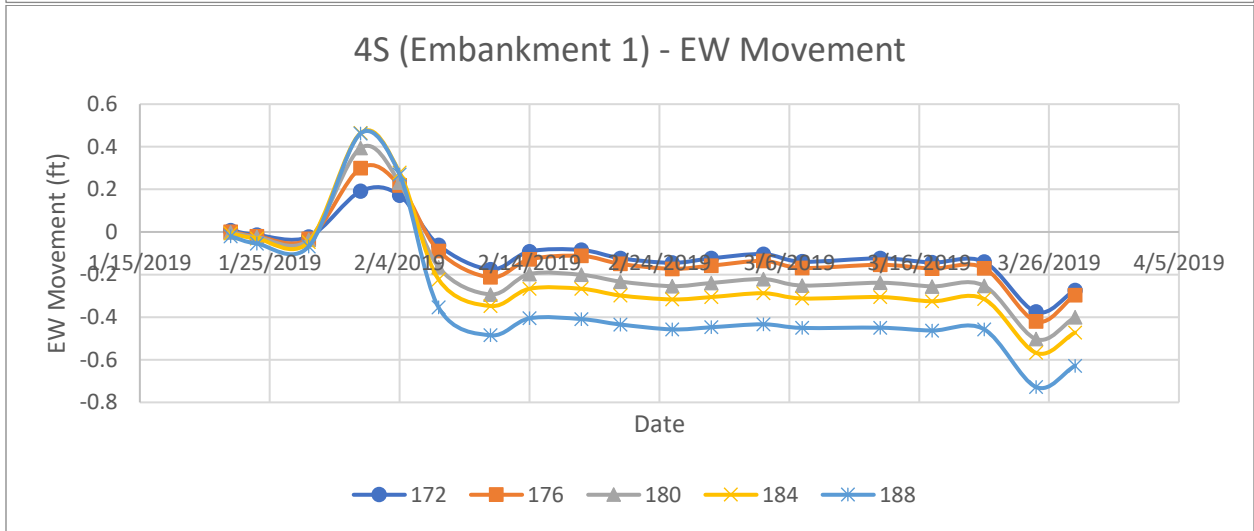
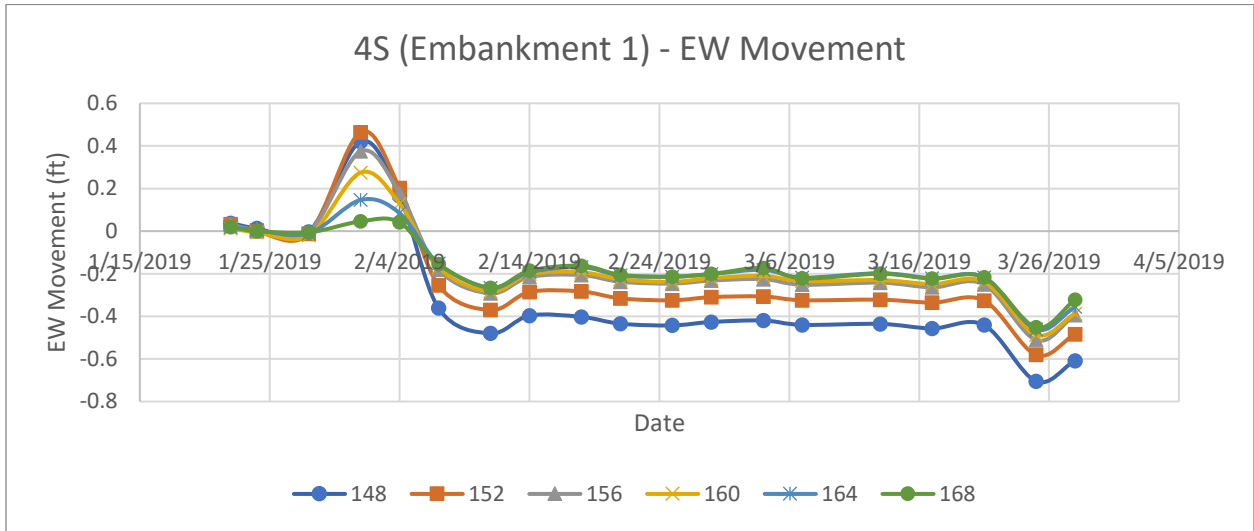
Vertical Movement



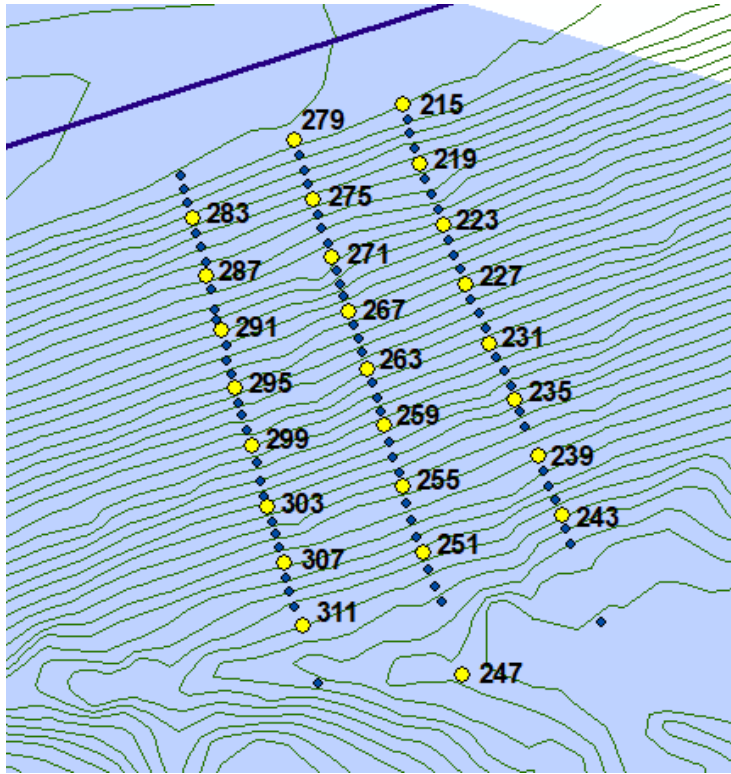
North-South Horizontal Movement



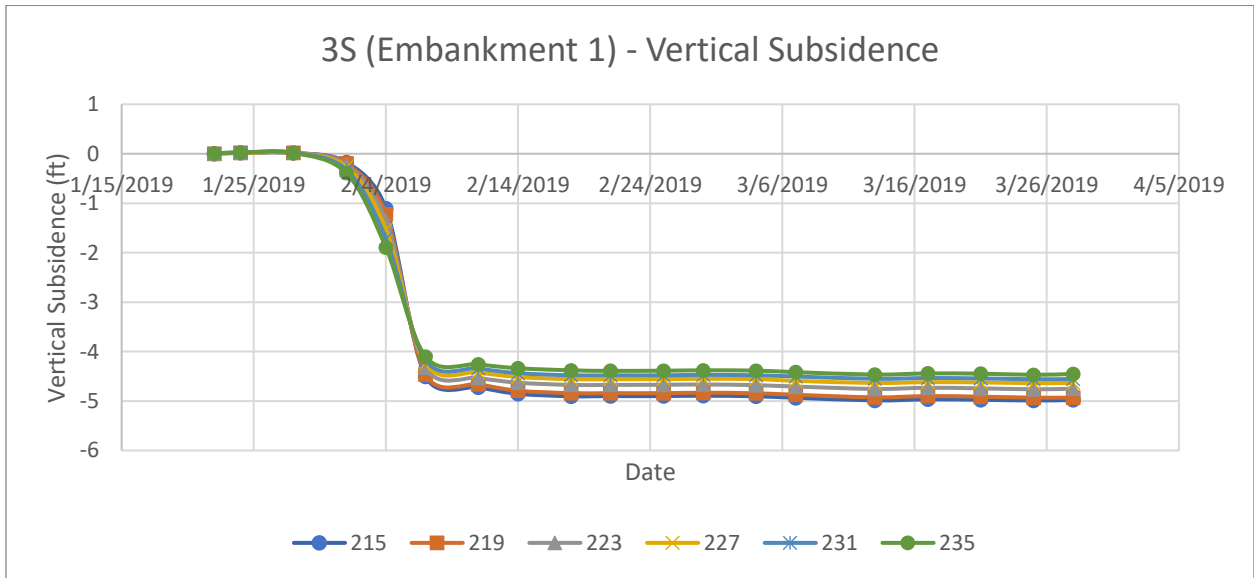
East-West Horizontal Movement

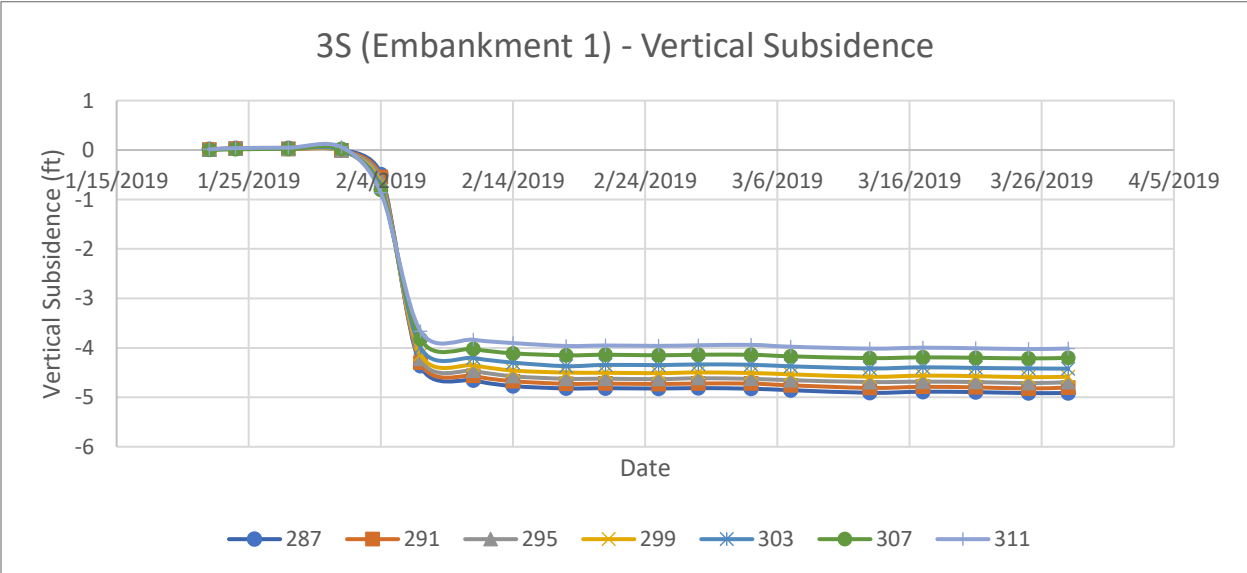
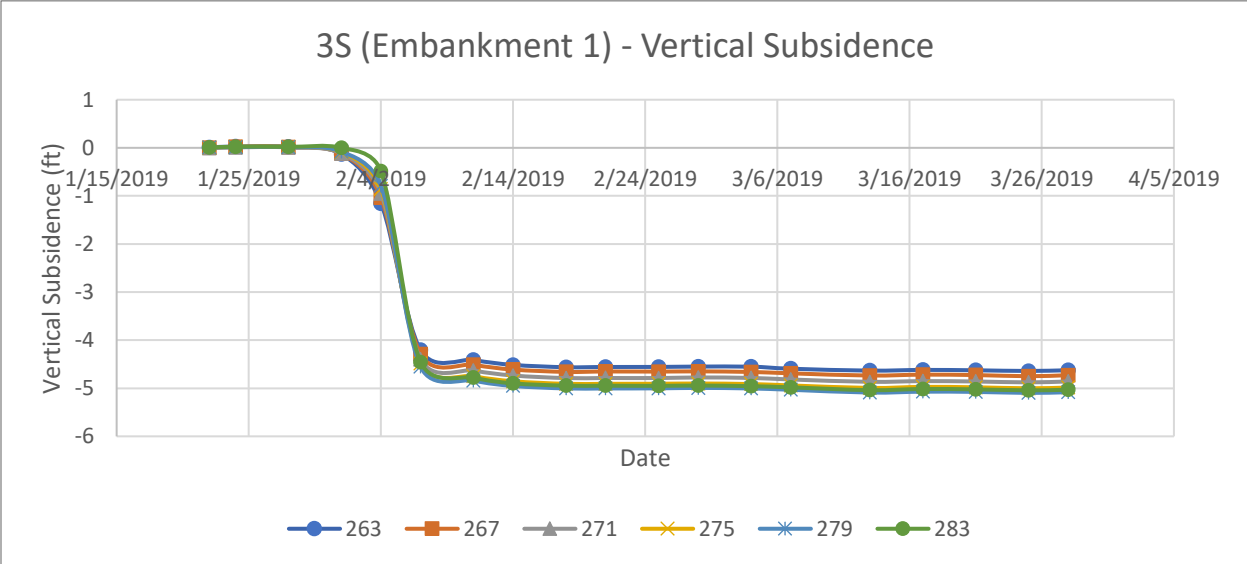
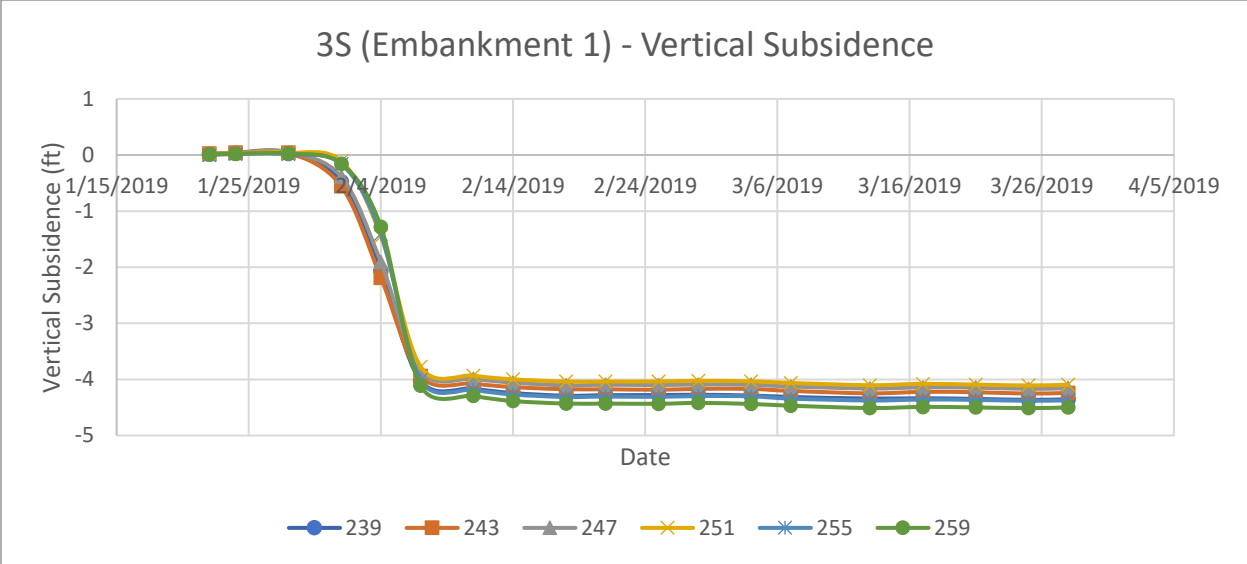


Group 3S

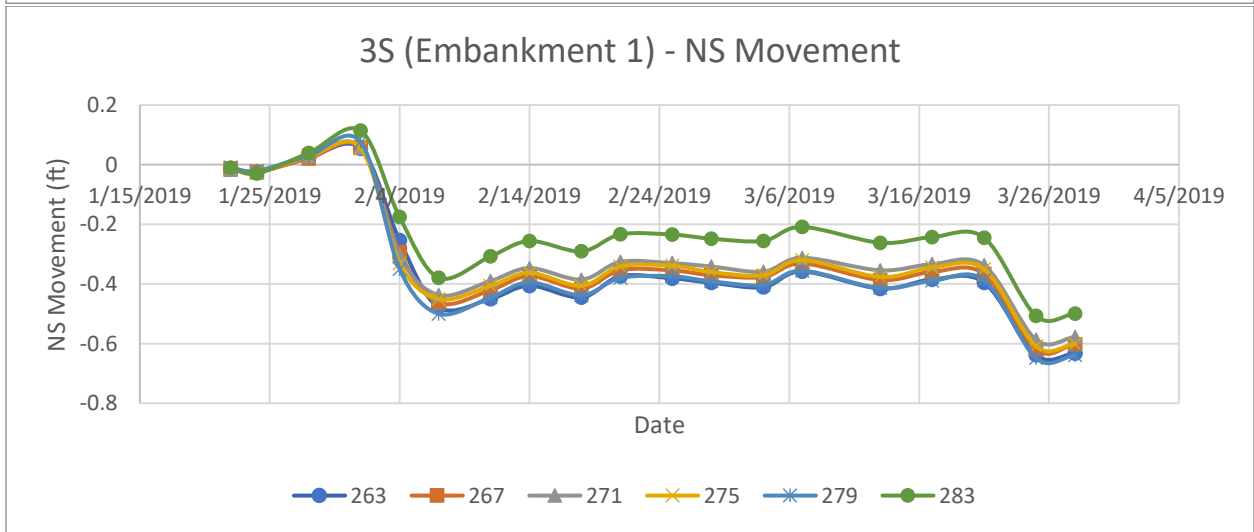
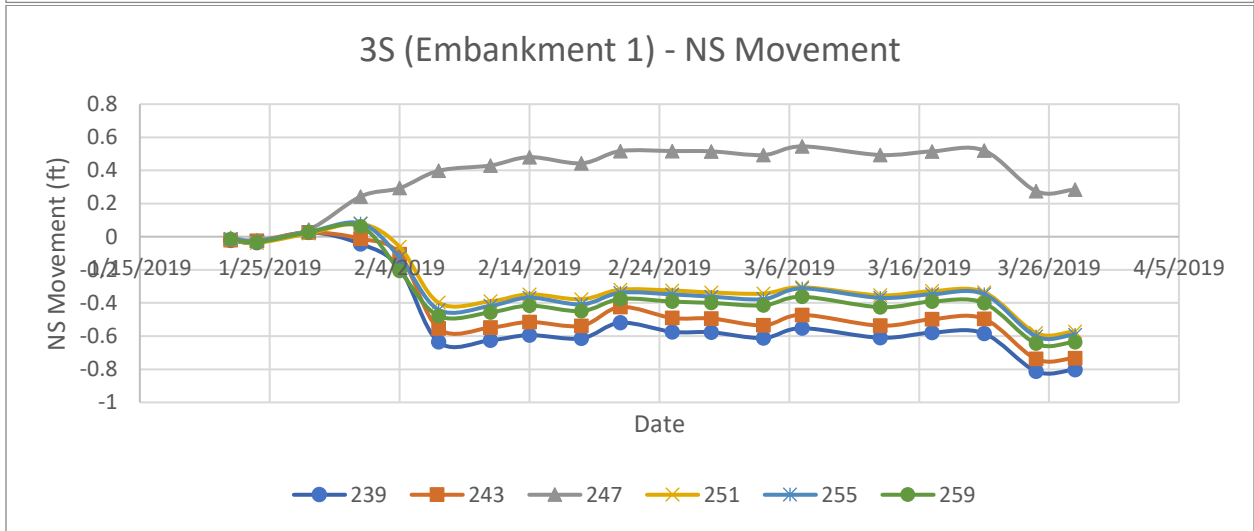
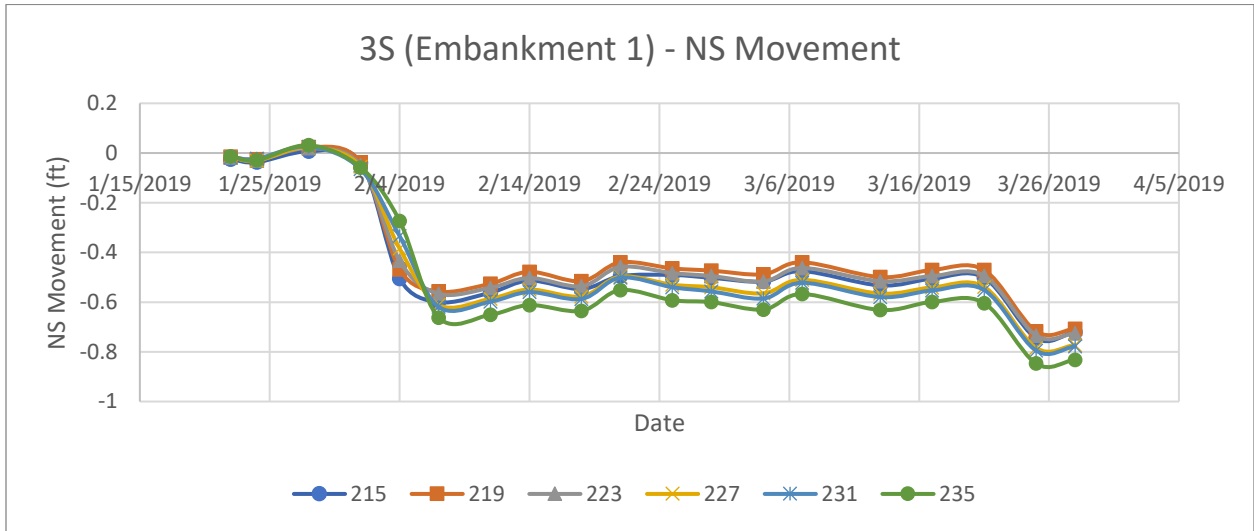


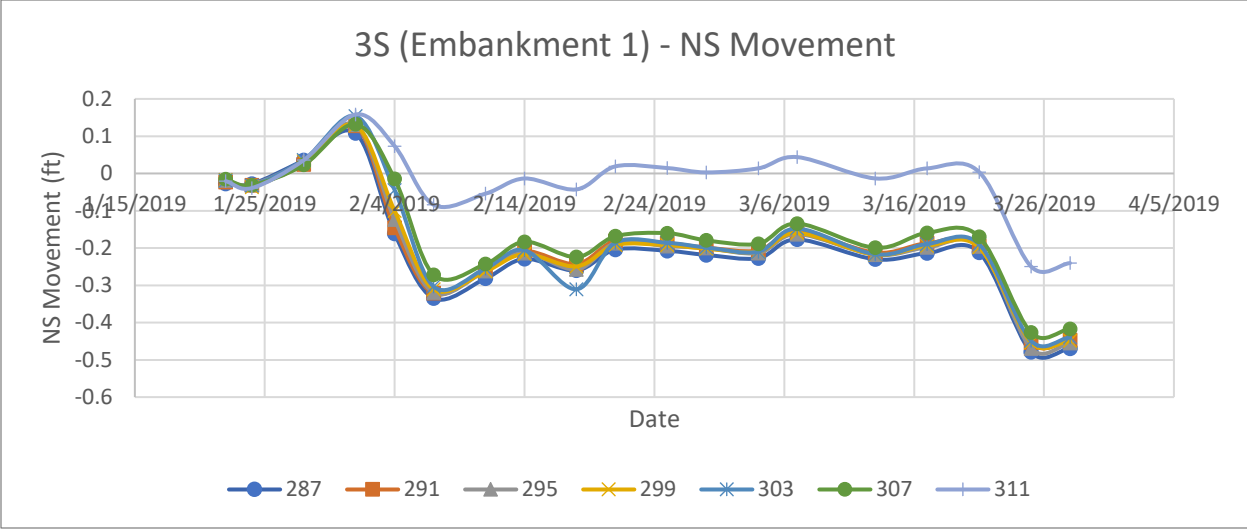
Vertical Movement



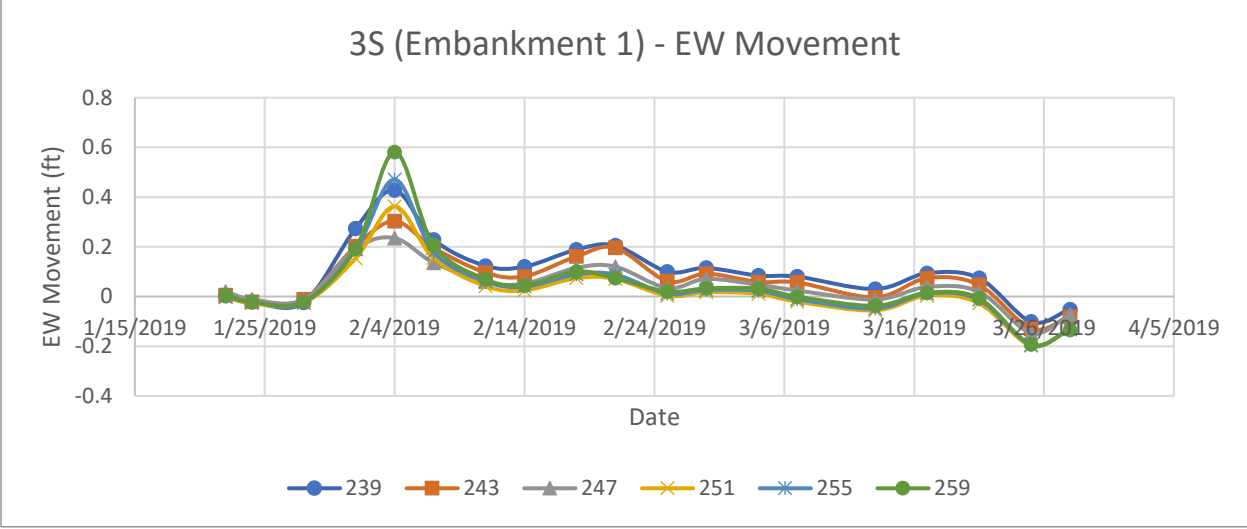
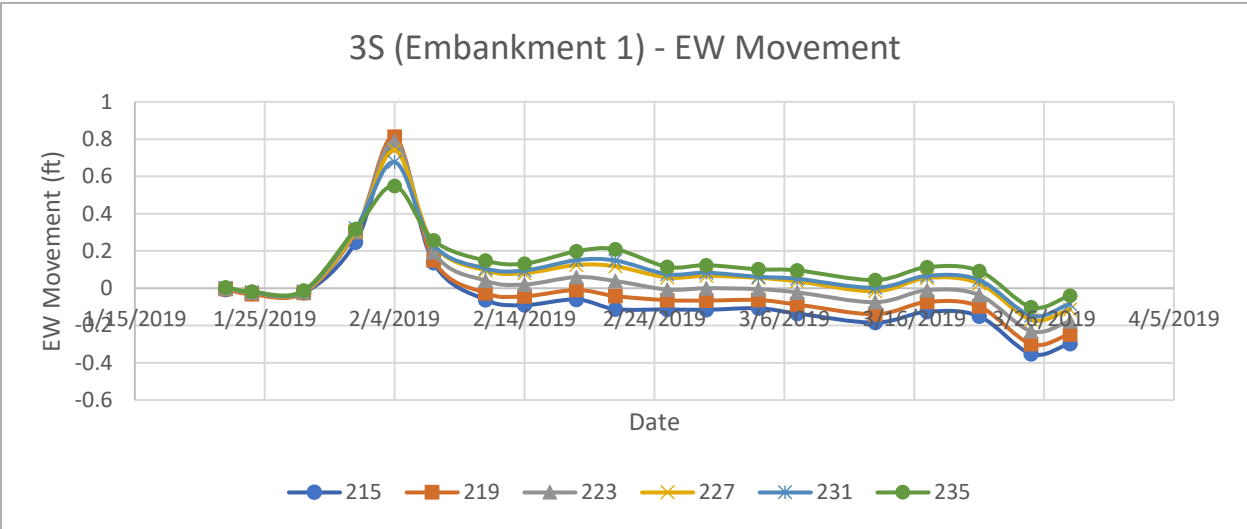


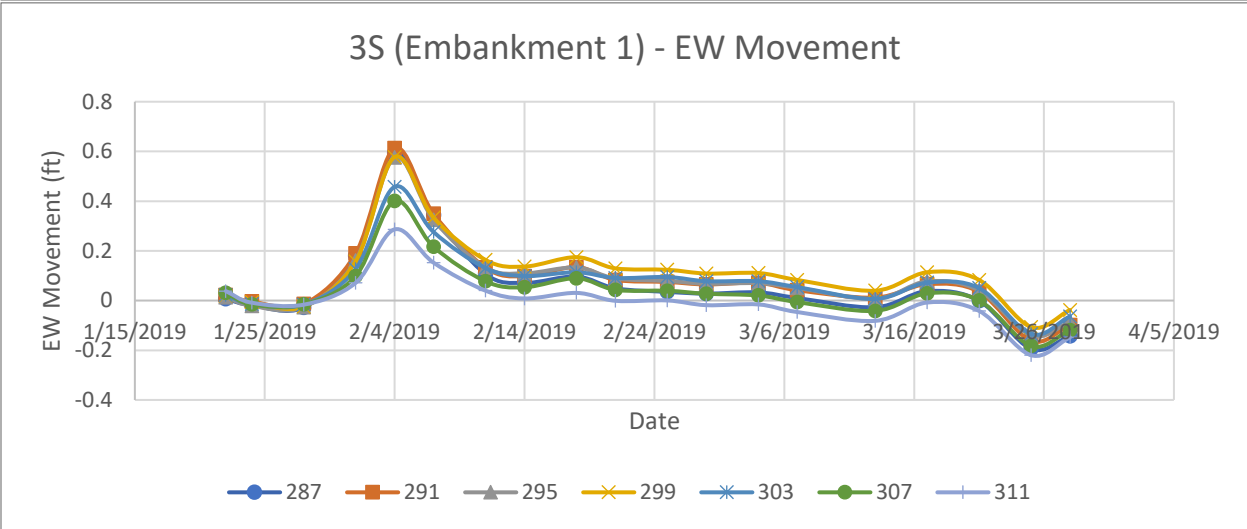
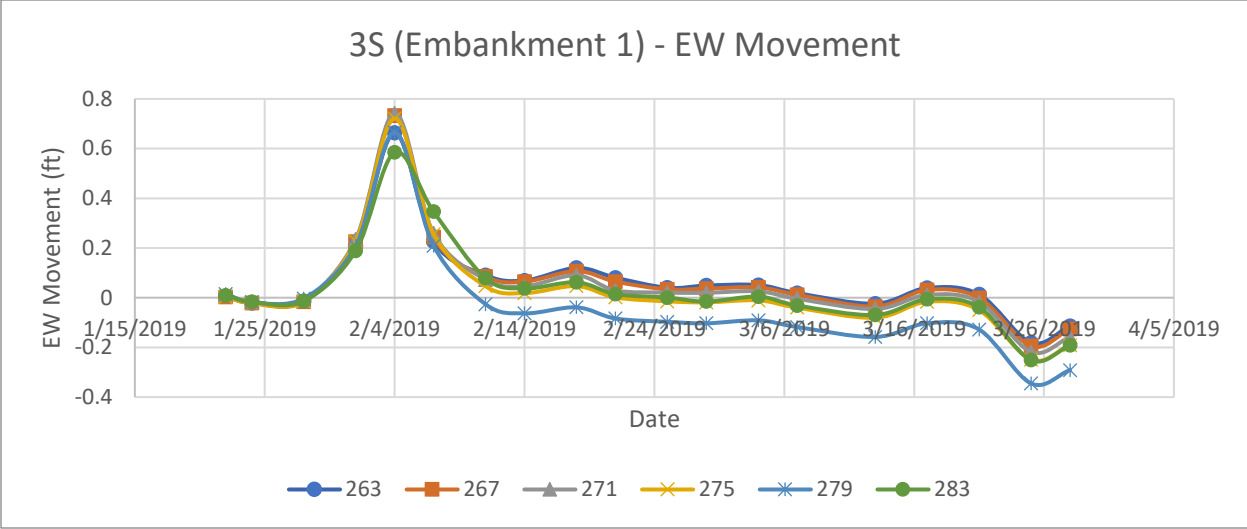
North-South Horizontal Movement



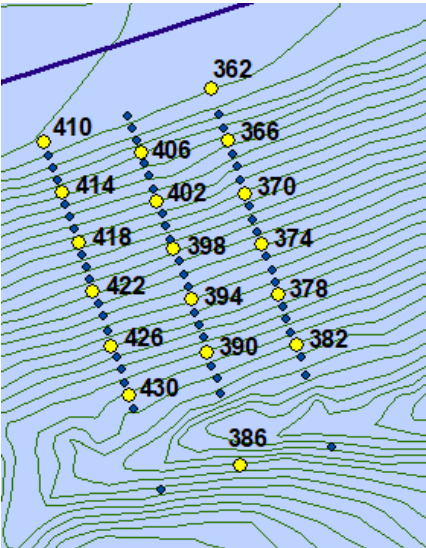


East-West Horizontal Movement

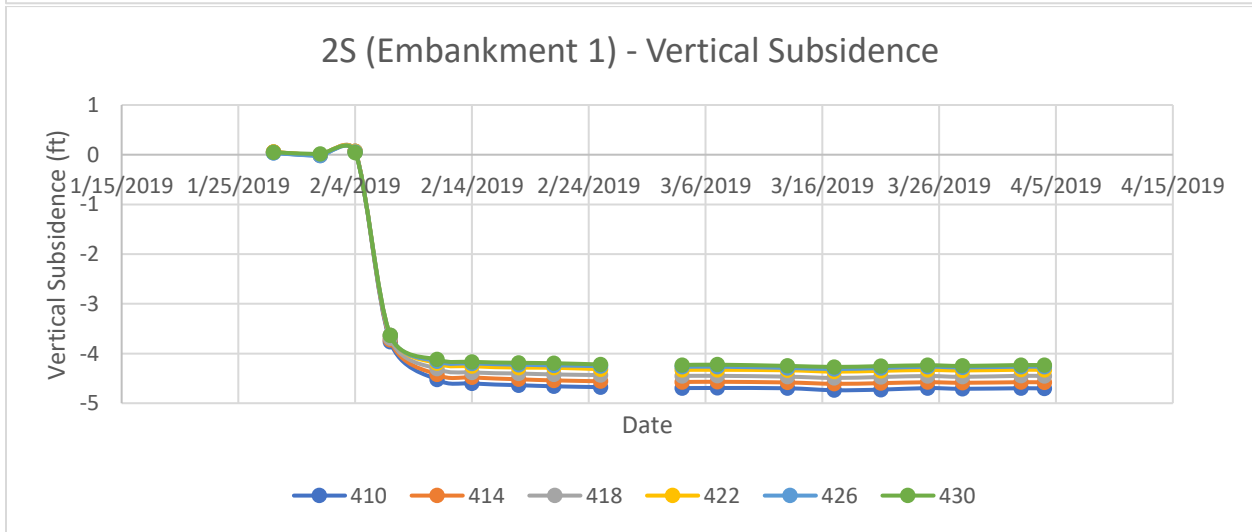
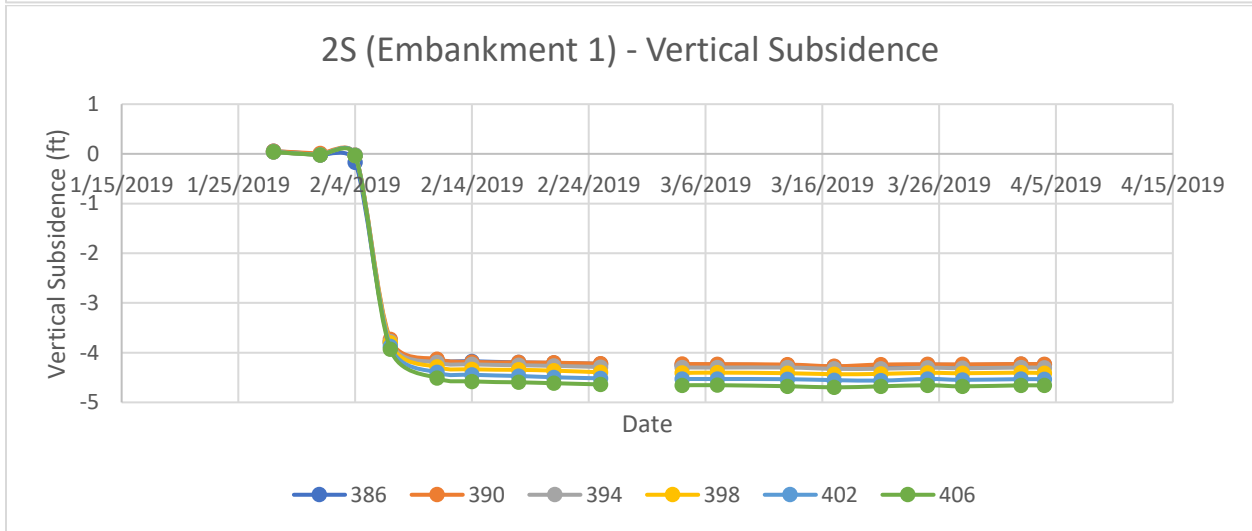
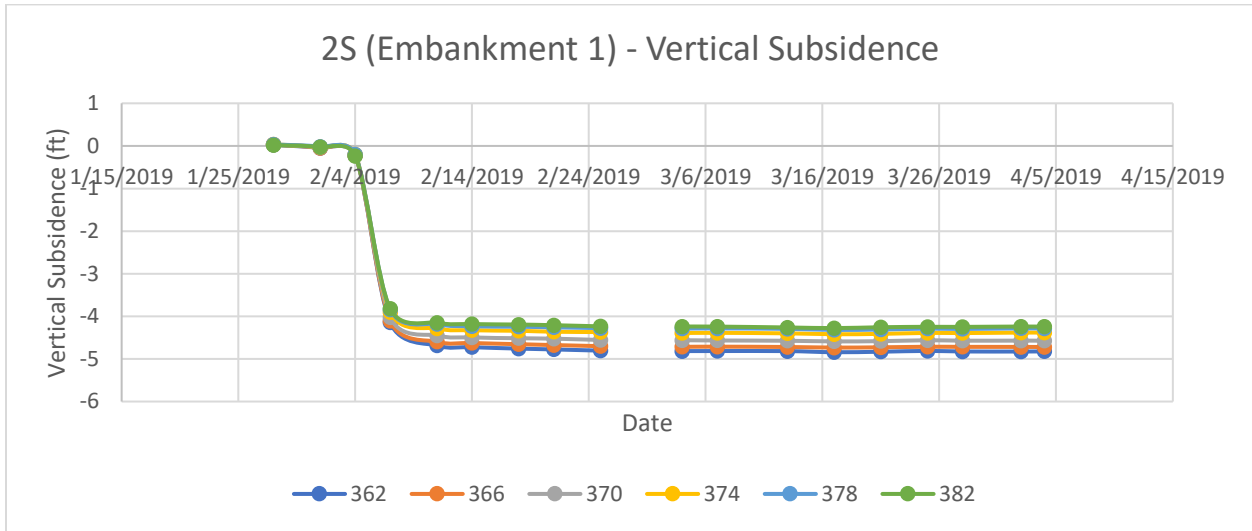




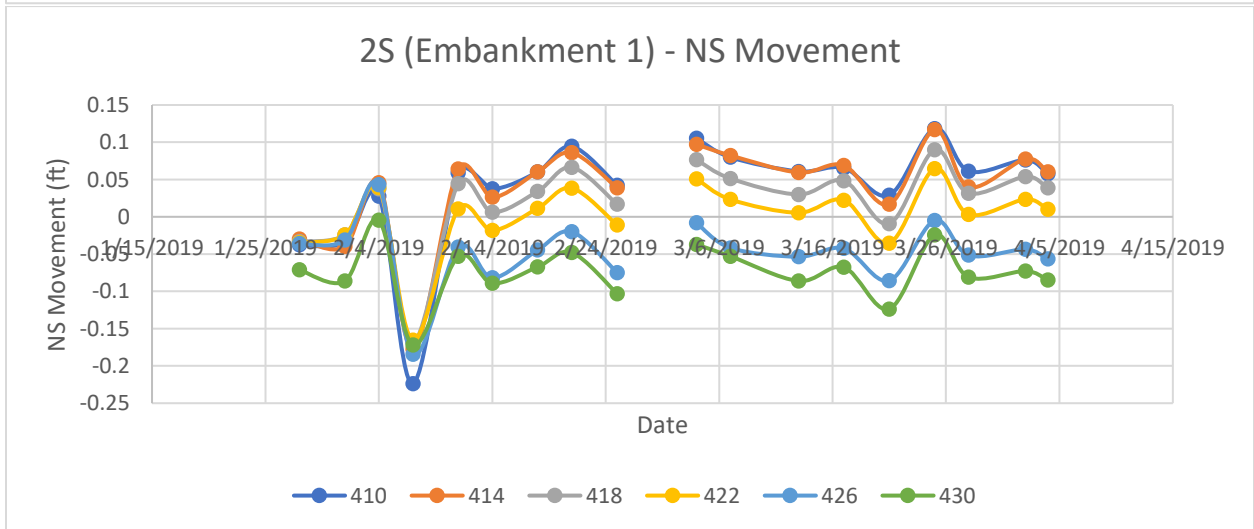
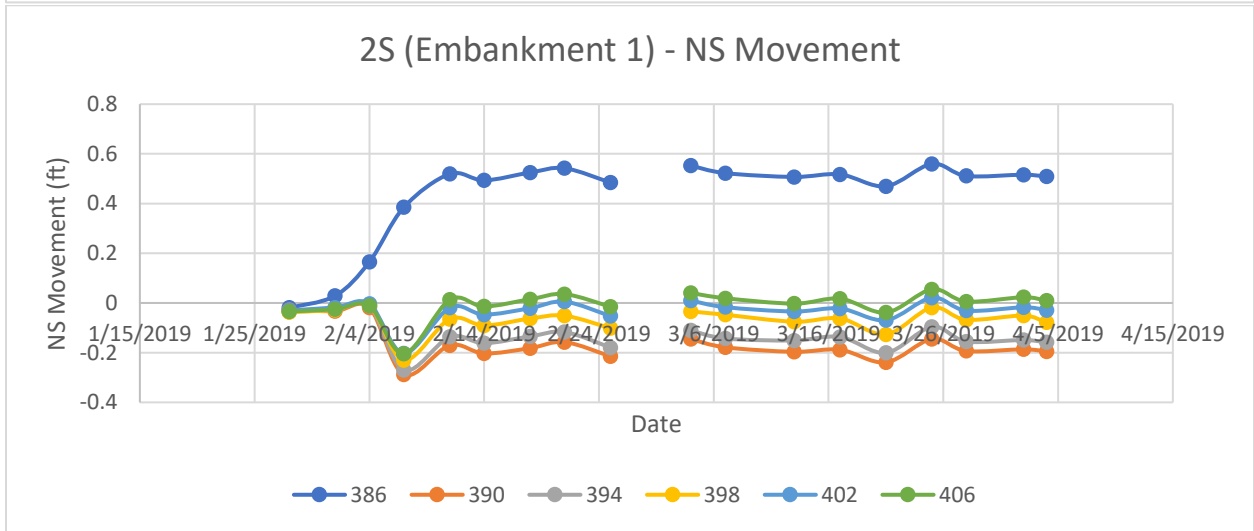
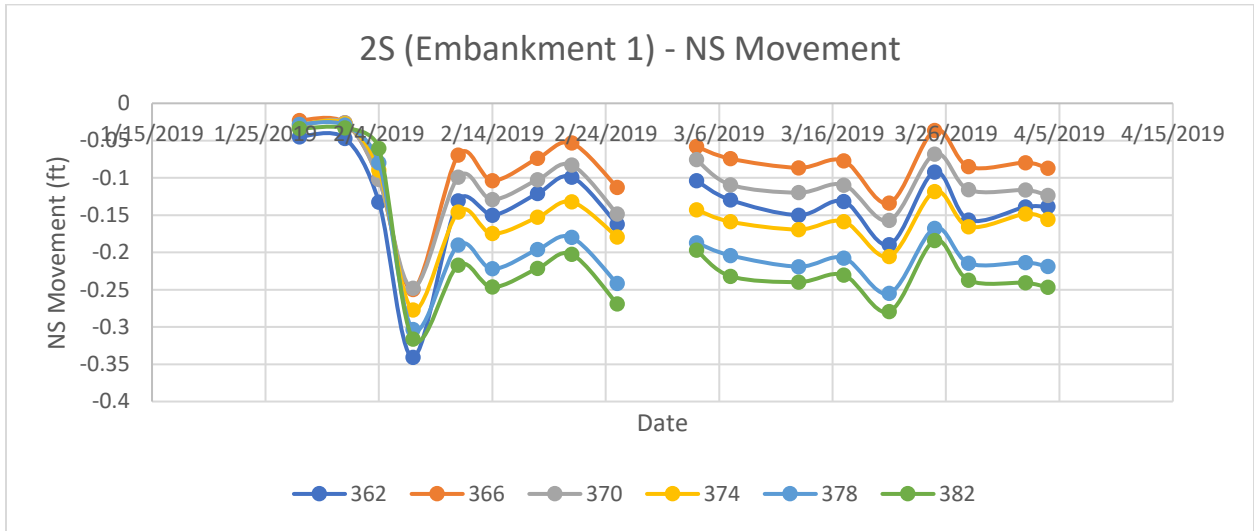
Group 2S



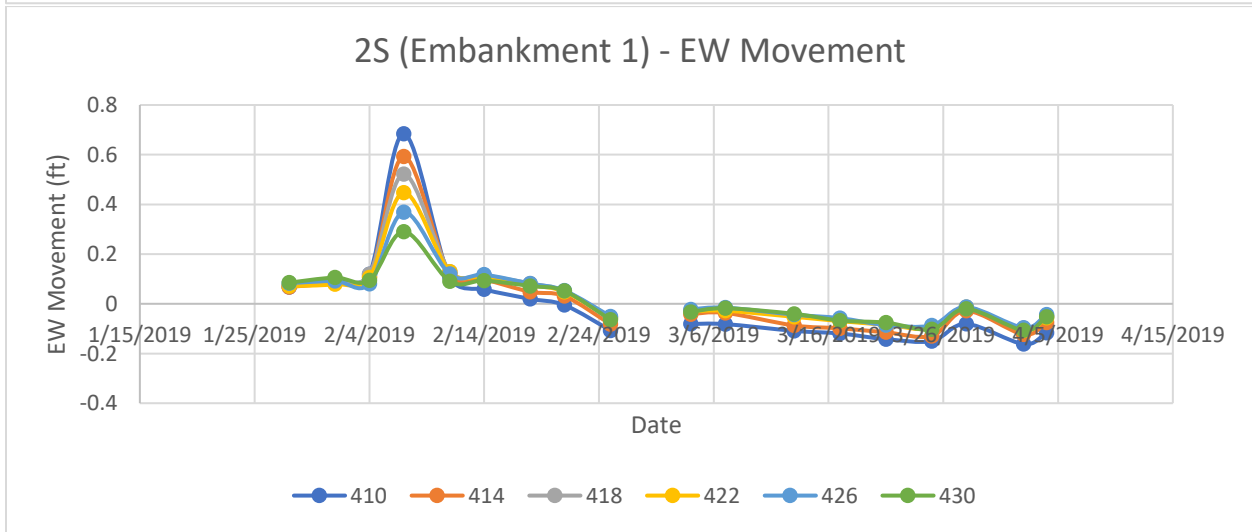
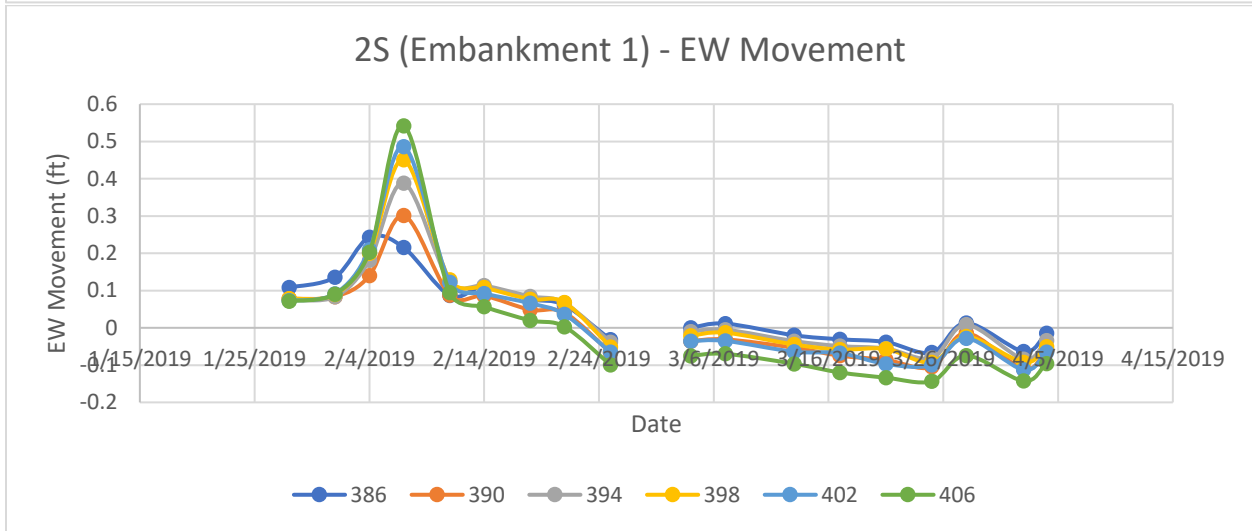
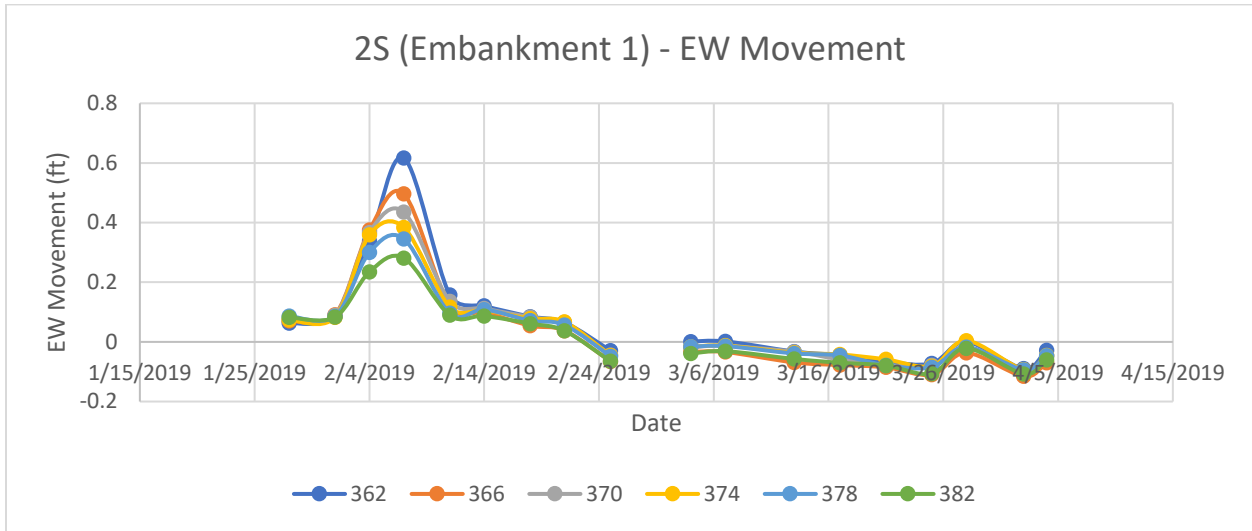
Vertical Movement



North-South Horizontal Movement



East-West Horizontal Movement

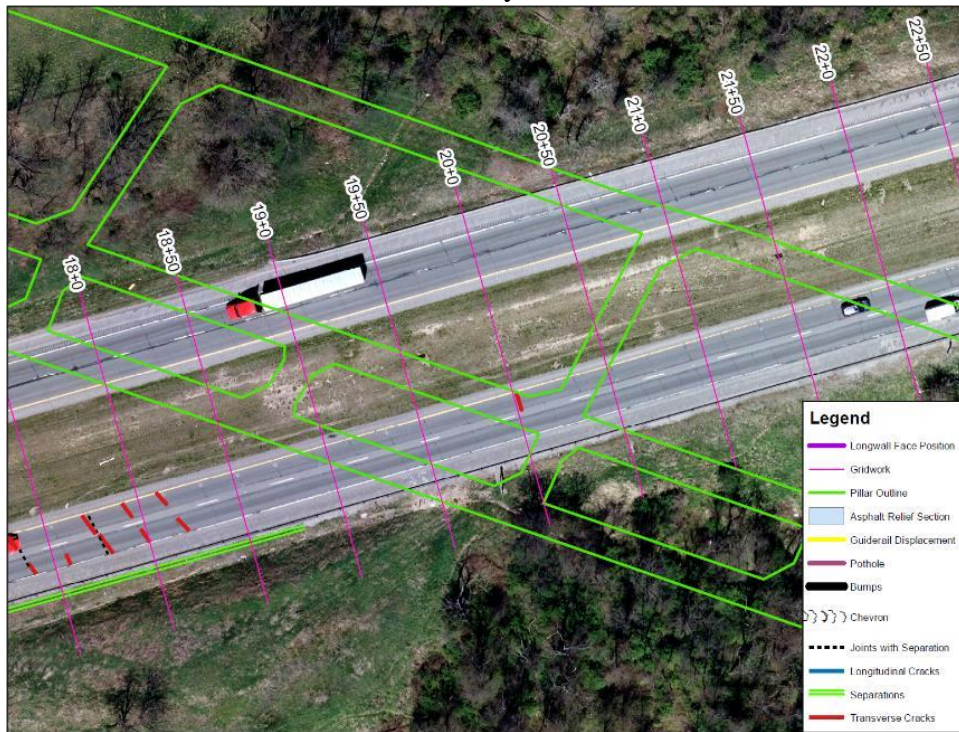


APPENDIX II – Complete Record of Observed Features on Pavement

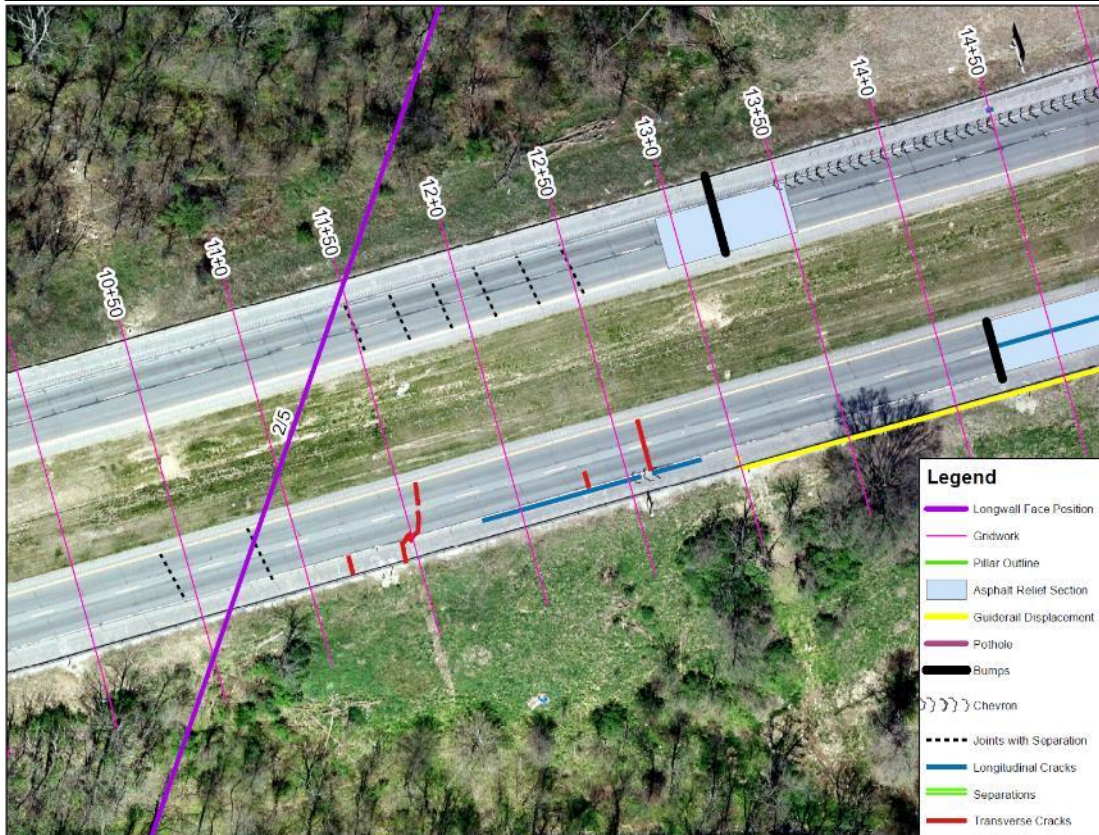
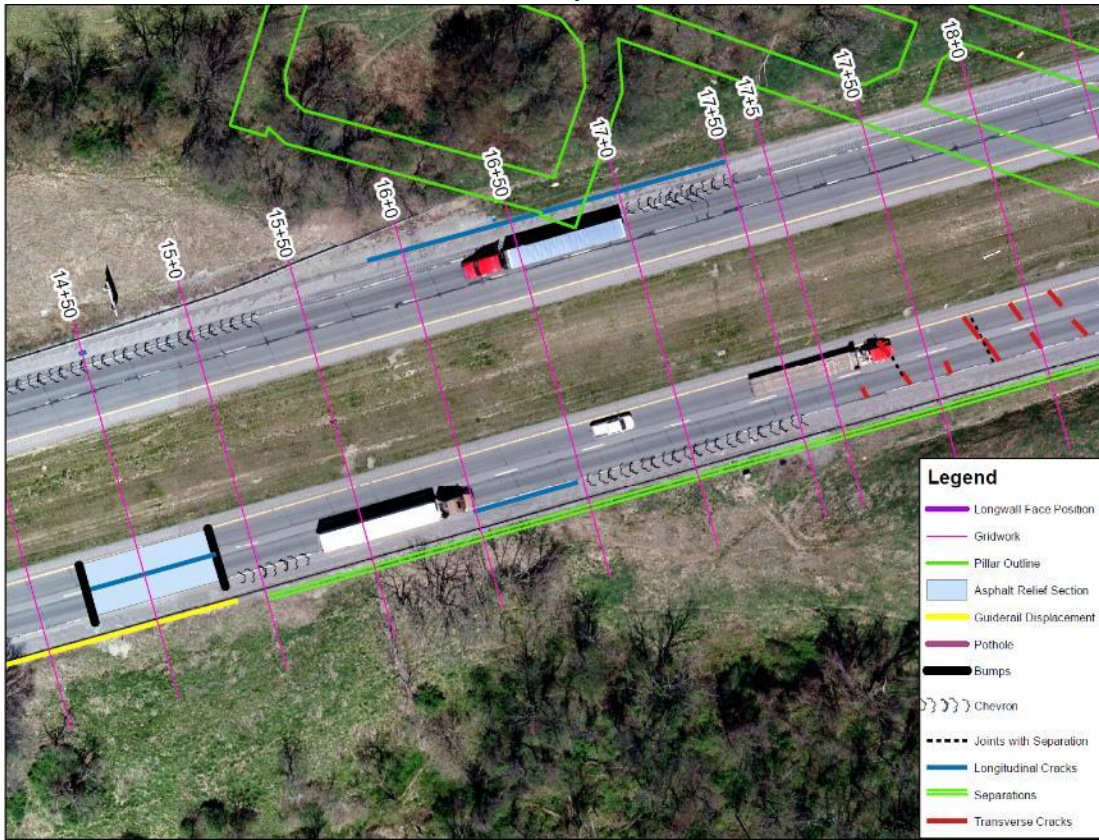
29 January 2019



5 February 2019



5 February 2019



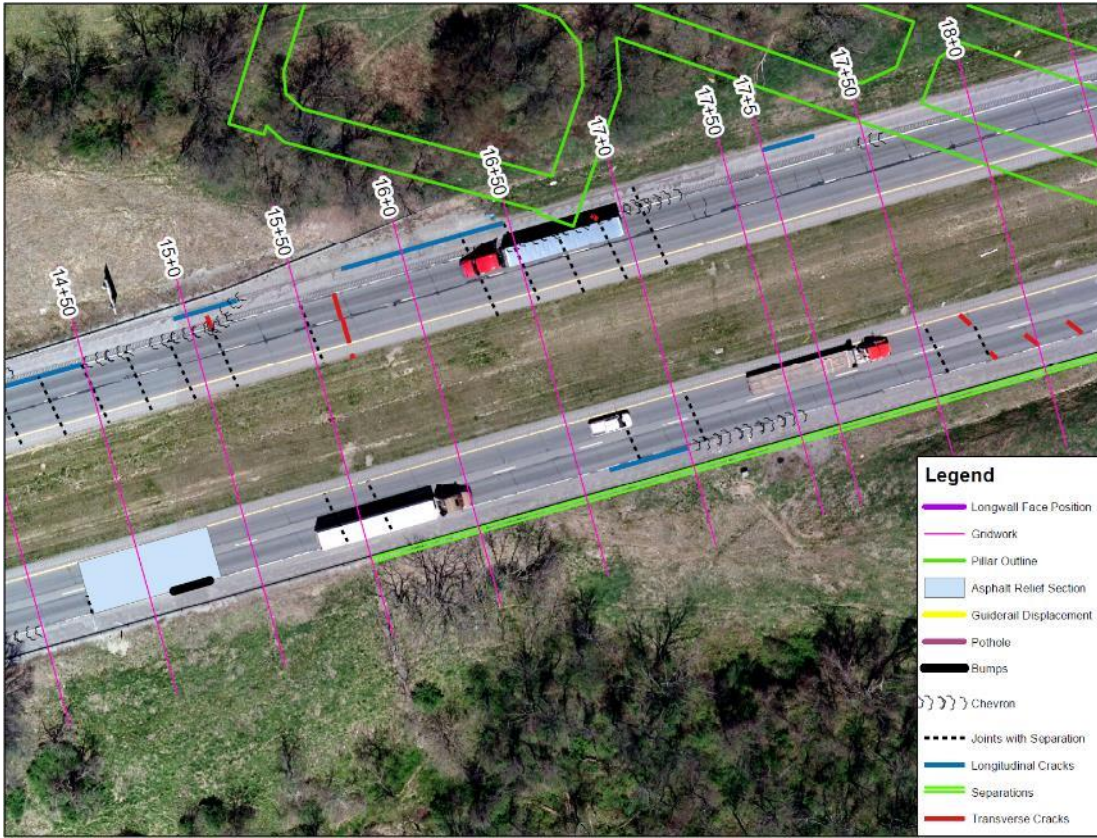
5 February 2019



14 February 2019



14 February 2019



14 February 2019



19 February 2019



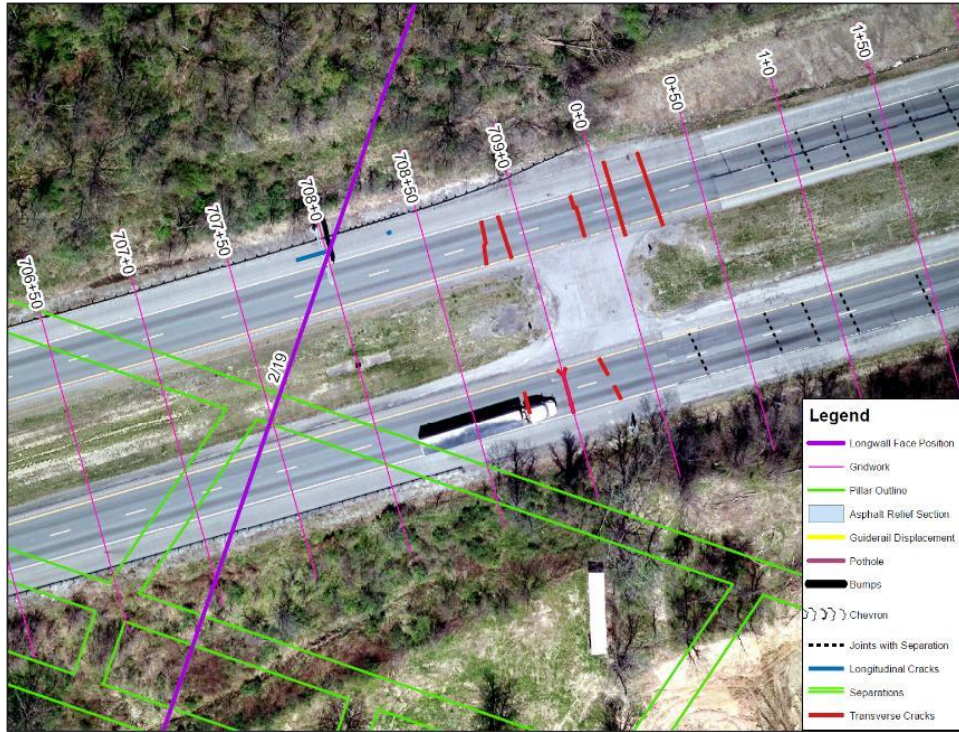
19 February 2019



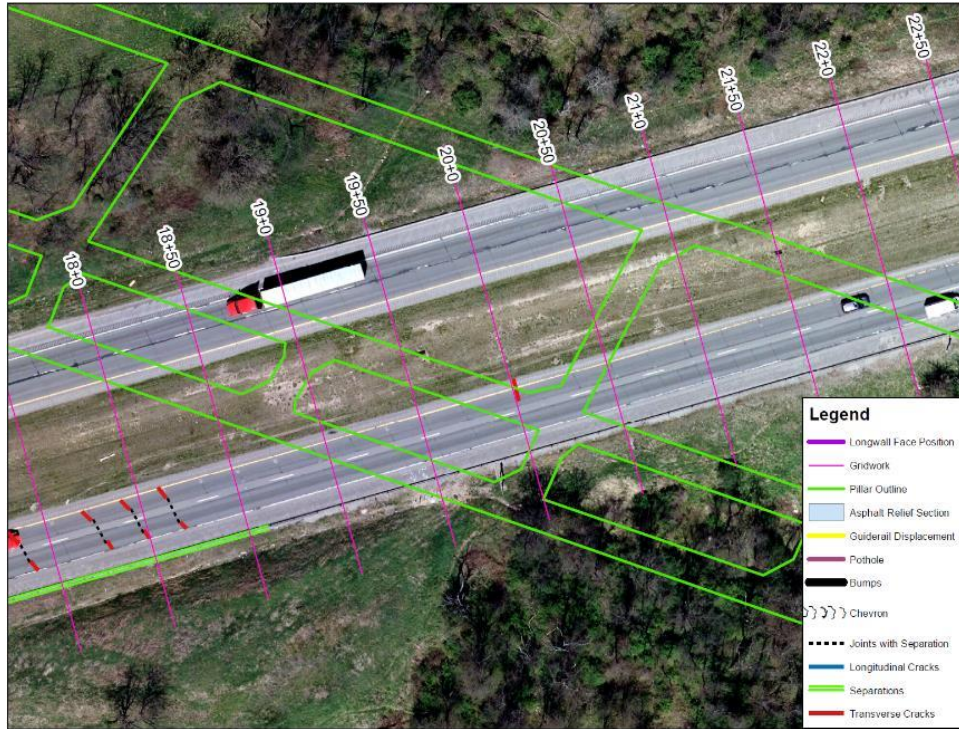
19 February 2019



19 February 2019



26 February 2019



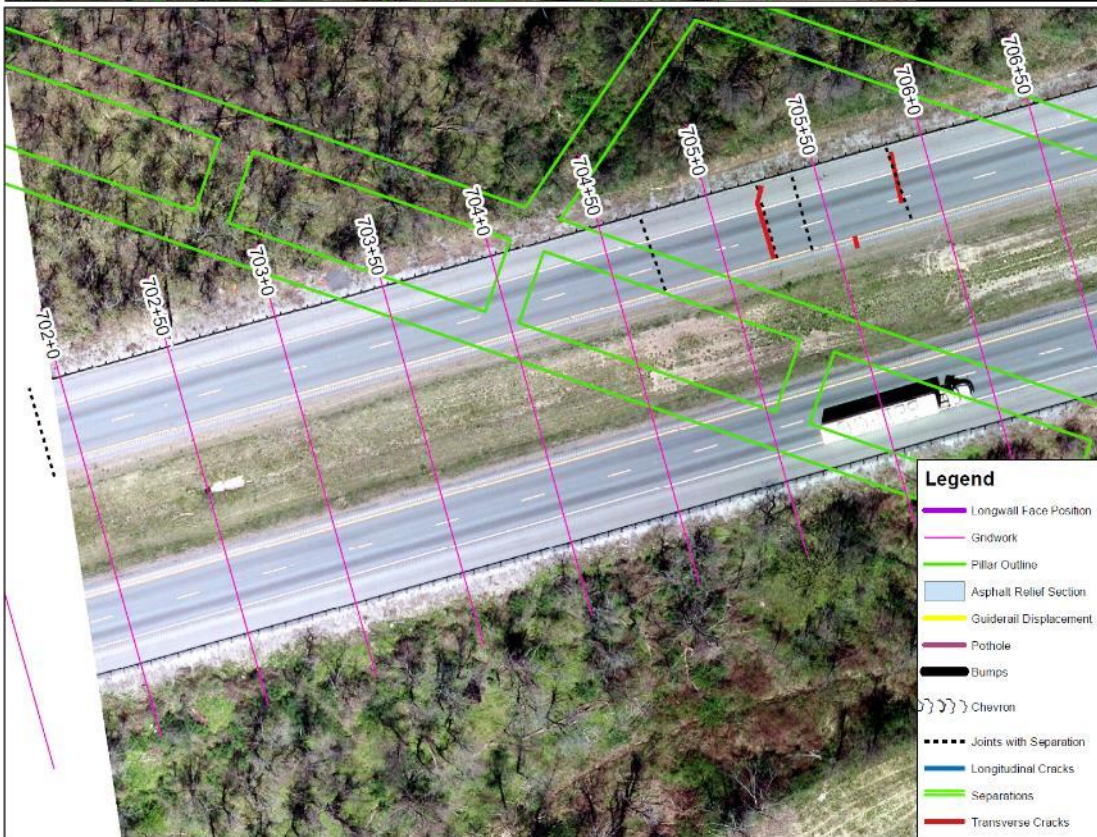
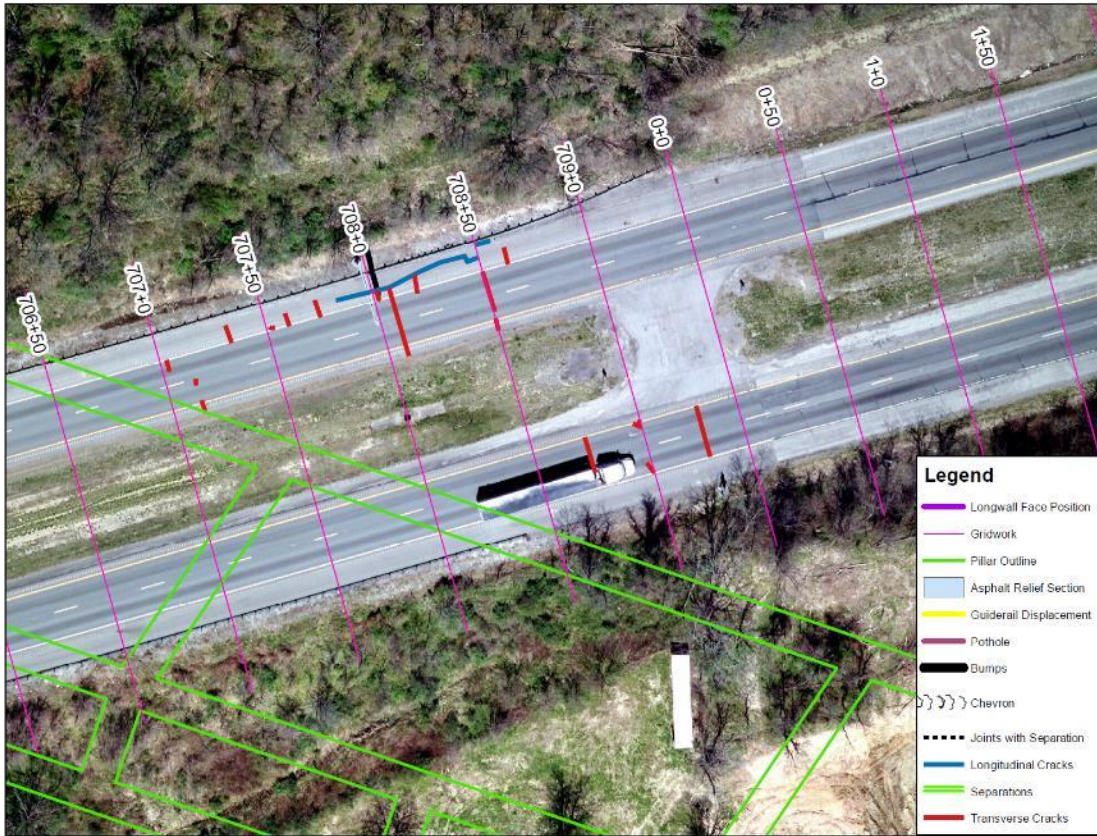
26 February 2019



26 February 2019

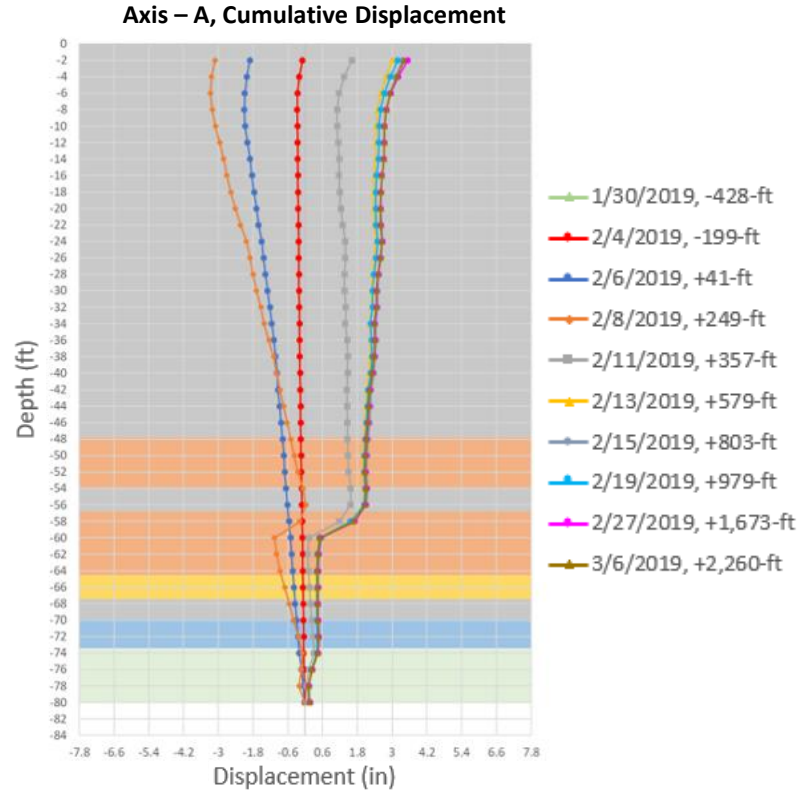


26 February 2019



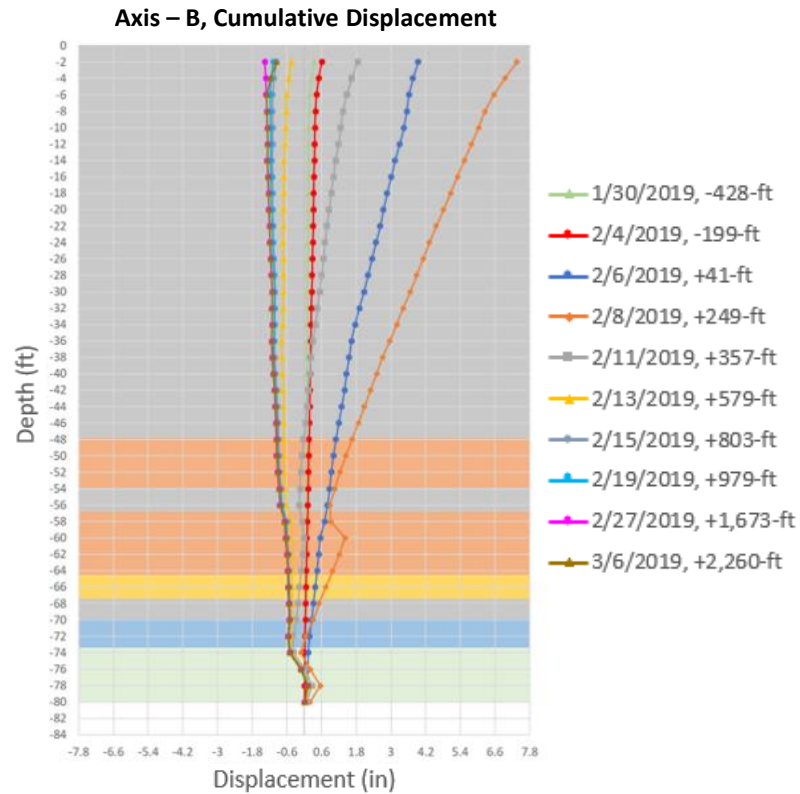
APPENDIX III – Inclinometer Data

TB-2 Cumulative Displacement

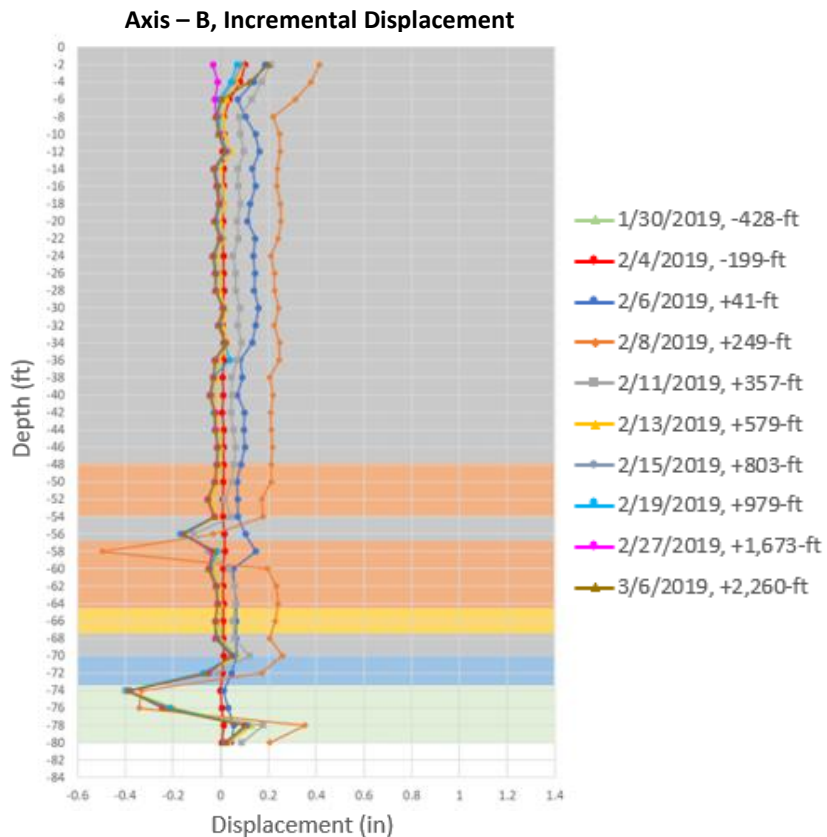
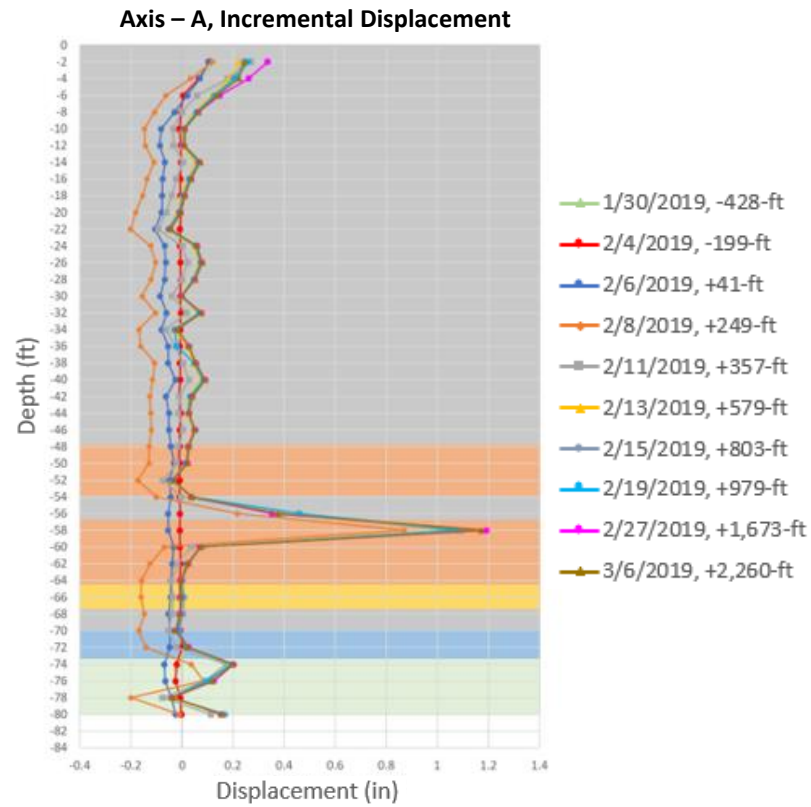


“-“ signs indicate distances as the longwall face approached the inclinometer, while “+” signs indicate distances as the longwall face progressed beyond the inclinometer

- = Clay
- = Gravel
- = Sand and Clay
- = Claystone
- = Limestone



TB-2 Incremental Displacement

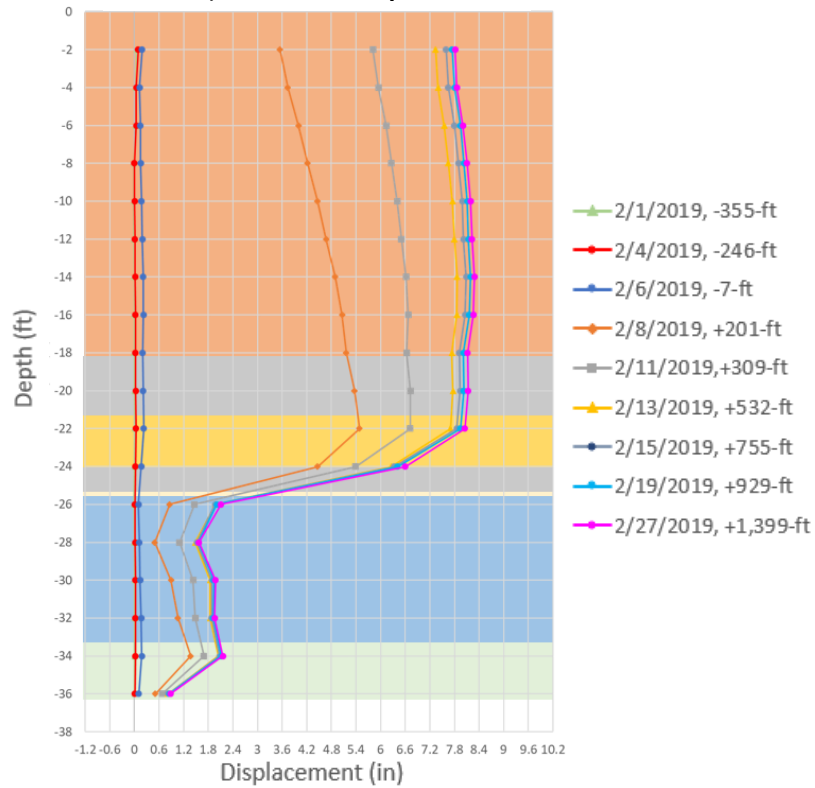


“-“ signs indicate distances as the longwall face approached the inclinometer, while “+” signs indicate distances as the longwall face progressed beyond the inclinometer

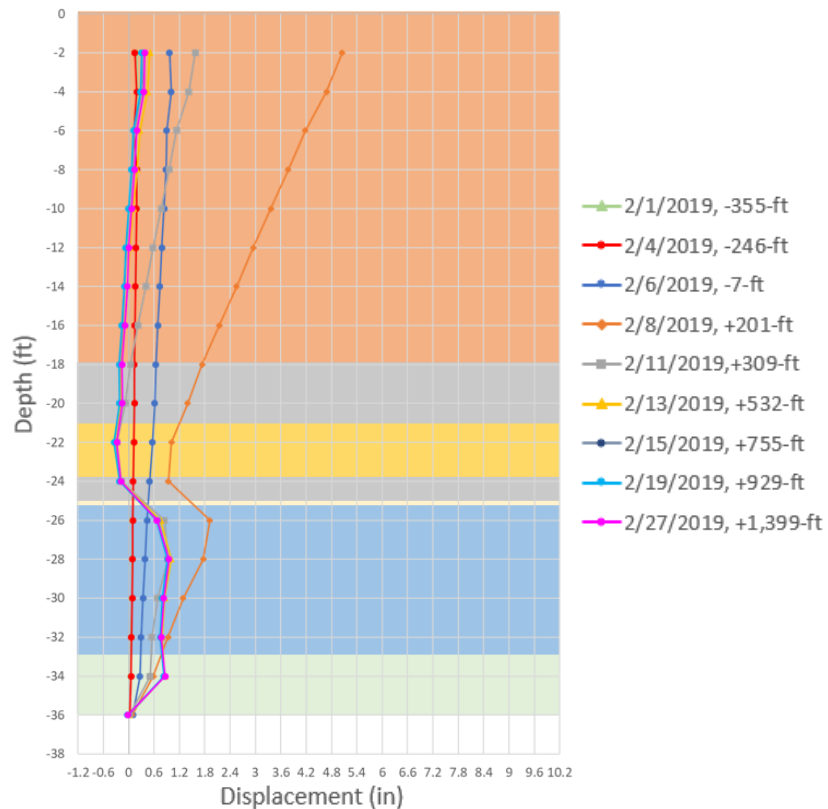
- = Clay
- = Gravel
- = Sand and Clay
- = Claystone
- = Limestone

TB-4 Cumulative Displacement

Axis – A, Cumulative Displacement



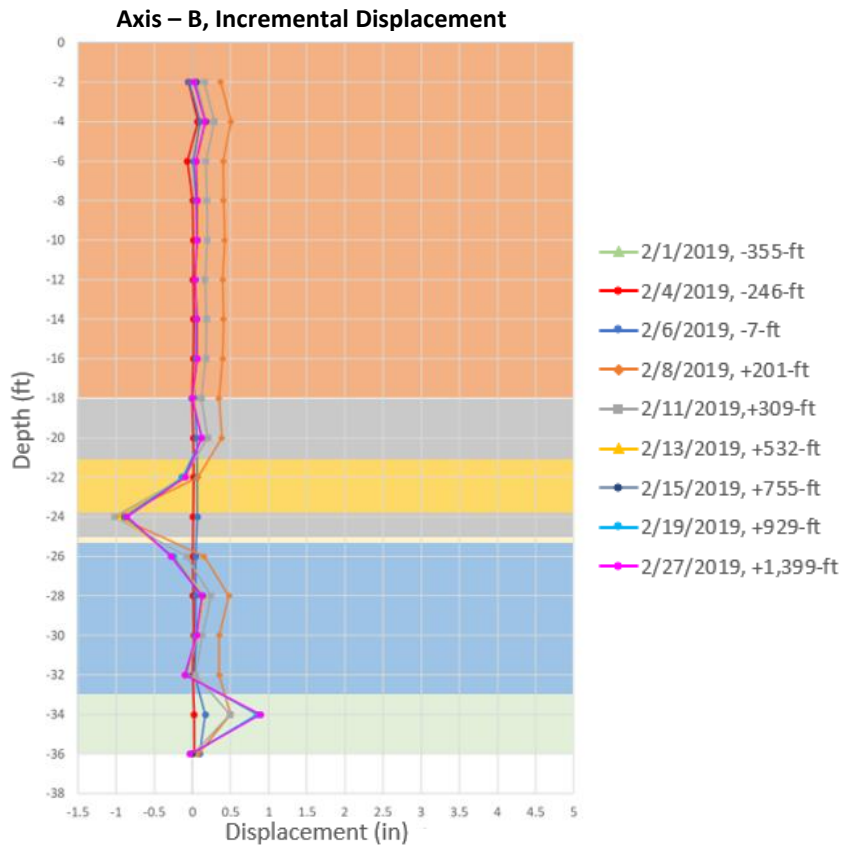
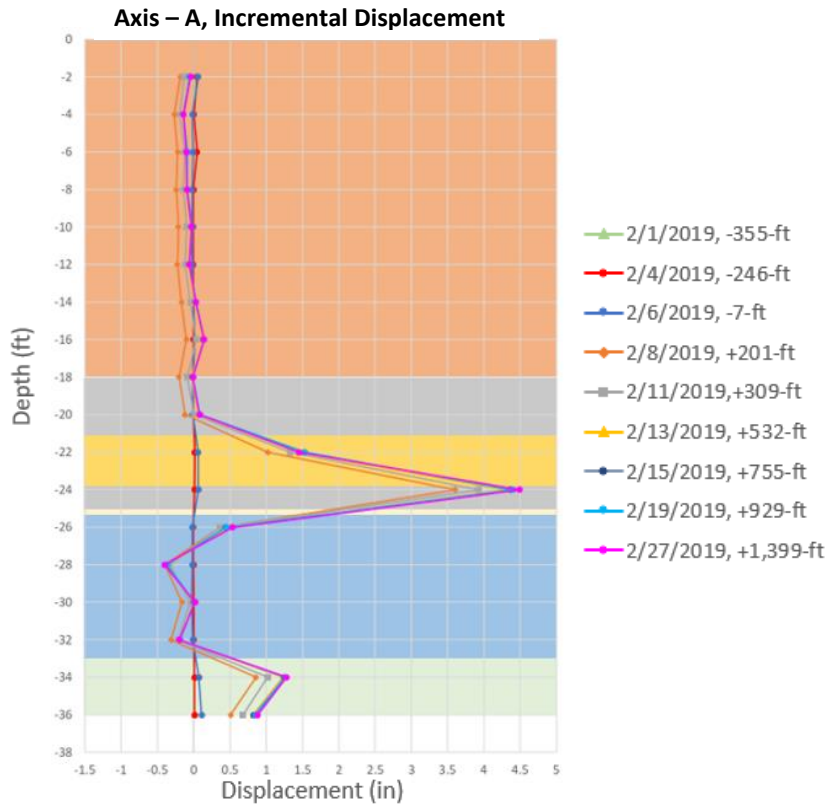
Axis – B, Cumulative Displacement



“-“ signs indicate distances as the longwall face approached the inclinometer, while “+” signs indicate distances as the longwall face progressed beyond the inclinometer

- = Clay
- = Gravel
- = Sand and Clay
- = Sandstone
- = Claystone
- = Limestone

TB-4 Incremental Displacement

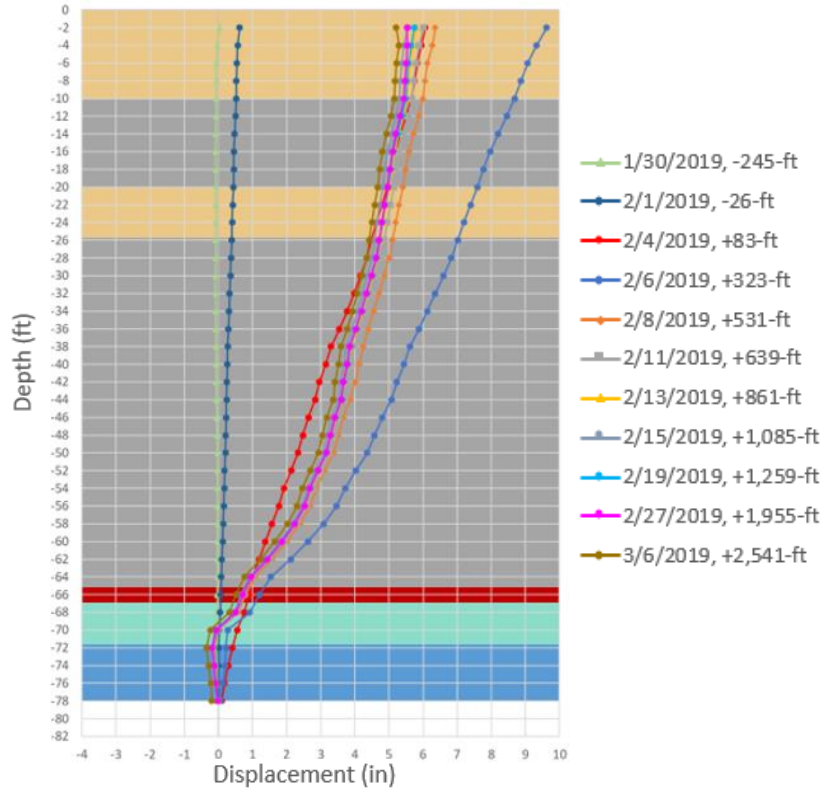


“-“ signs indicate distances as the longwall face approached the inclinometer, while “+” signs indicate distances as the longwall face progressed beyond the inclinometer

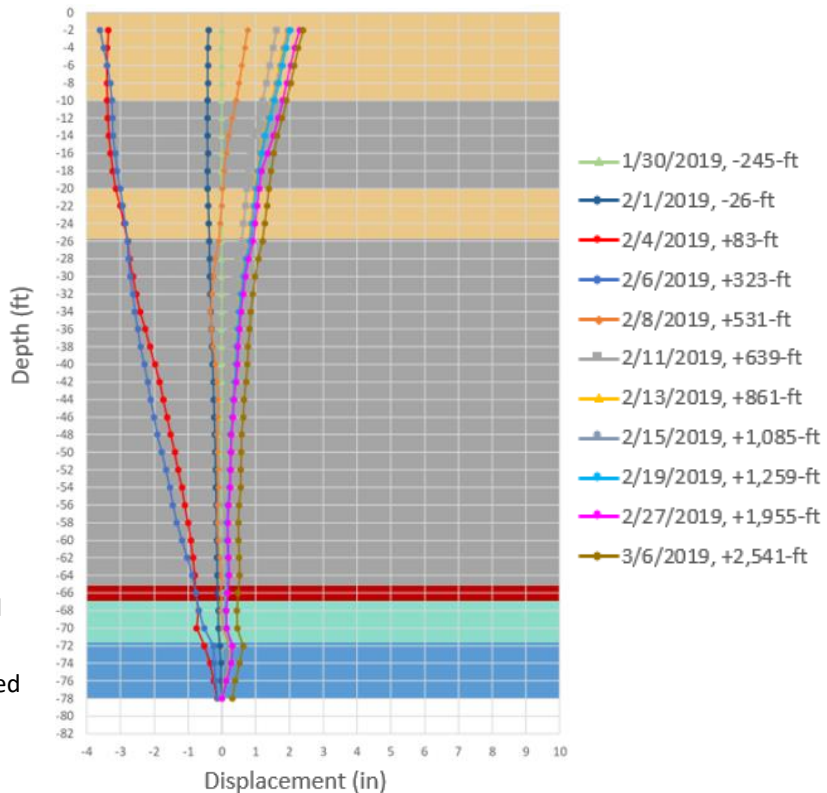
- = Clay
- = Gravel
- = Sand and Clay
- = Sandstone
- = Claystone
- = Limestone

TB-6 Cumulative Displacement

Axis – A, Cumulative Displacement



Axis – B, Cumulative Displacement

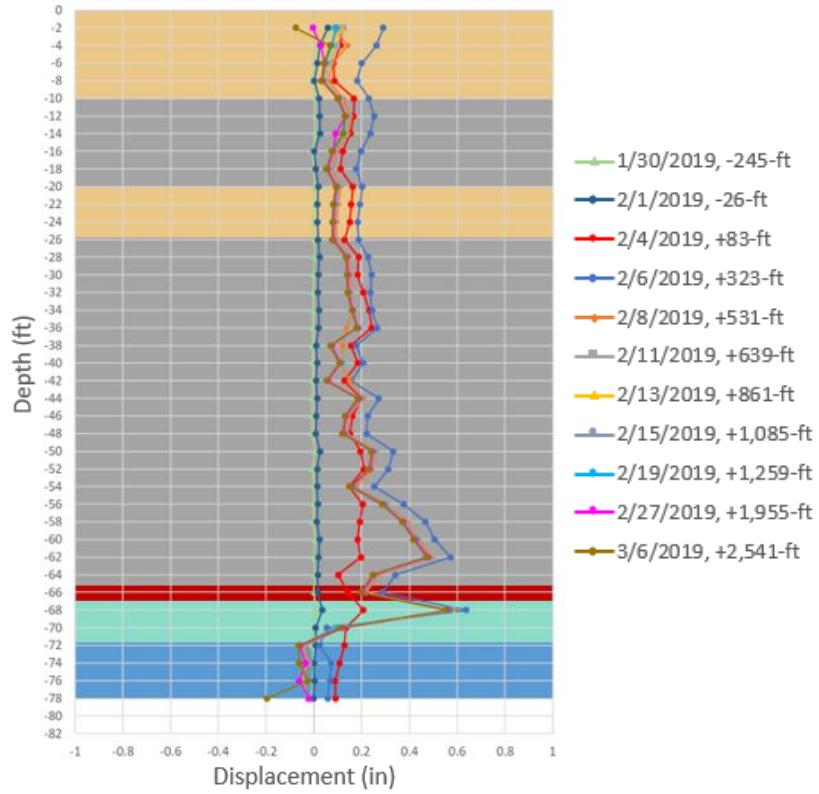


“-“ signs indicate distances as the longwall face approached the inclinometer, while “+” signs indicate distances as the longwall face progressed beyond the inclinometer

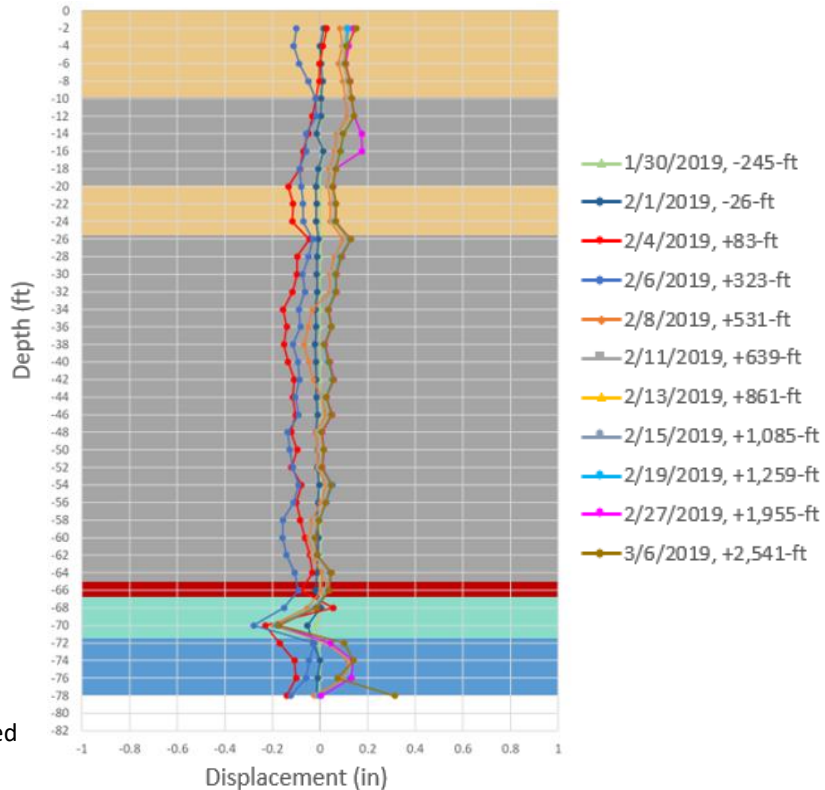
- = Silt and Clay
- = Silt and Sand
- = Silt and Gravel
- = Siltstone interbedded with Limestone
- = Limestone interbedded with Siltstone

TB-6 Incremental Displacement

Axis – A, Incremental Displacement



Axis – B, Incremental Displacement

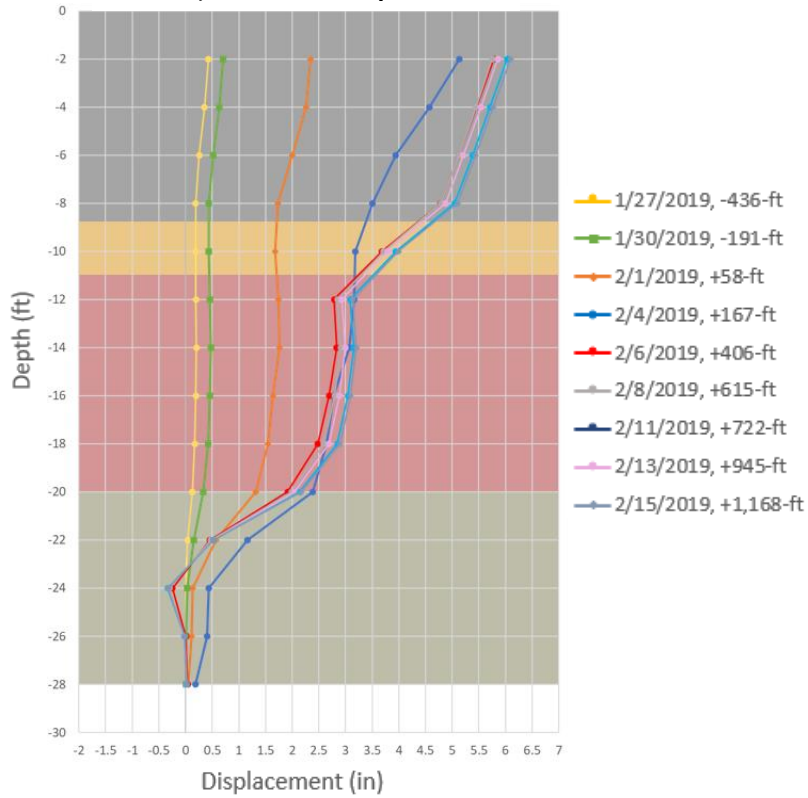


“-“ signs indicate distances as the longwall face approached the inclinometer, while “+” signs indicate distances as the longwall face progressed beyond the inclinometer

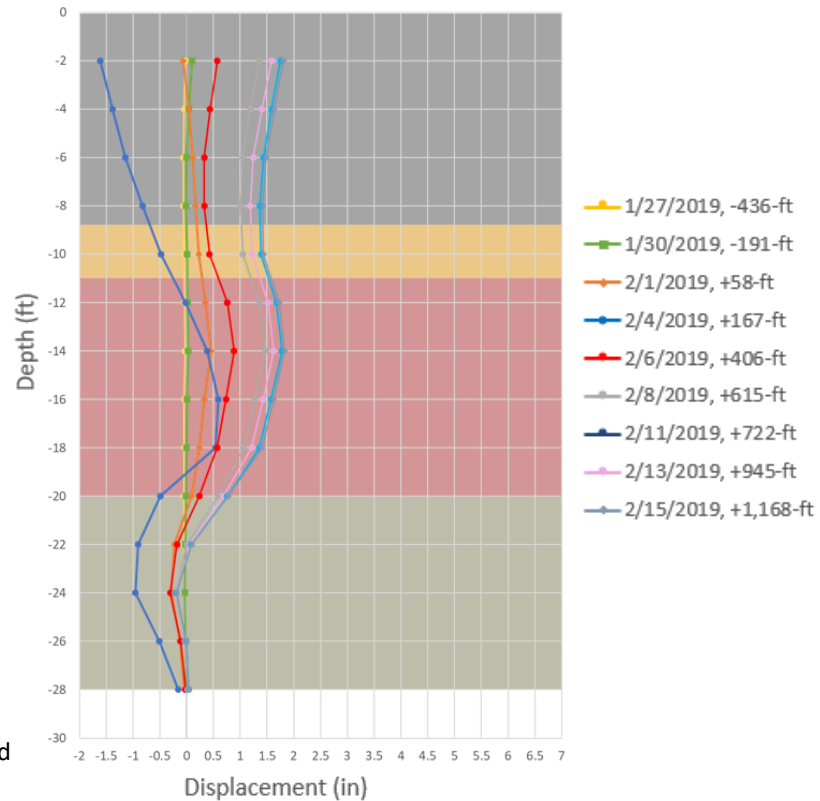
- = Silt and Clay
- = Silt and Sand
- = Silt and Gravel
- = Siltstone interbedded with Limestone
- = Limestone interbedded with Siltstone

TB-8 Cumulative Displacement

Axis – A, Cumulative Displacement



Axis – B, Cumulative Displacement

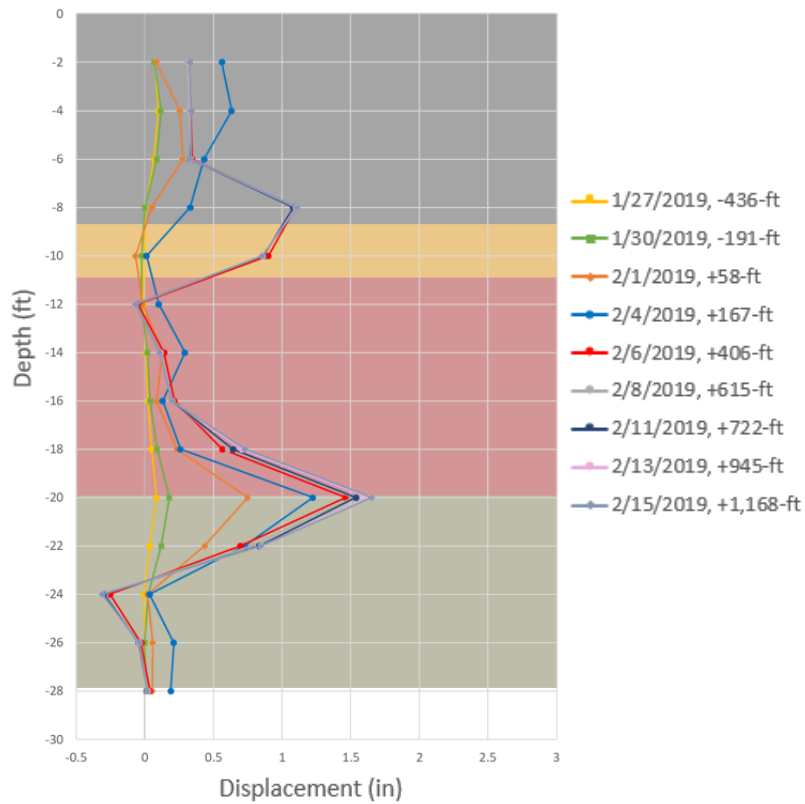


“-“ signs indicate distances as the longwall face approached the inclinometer, while “+” signs indicate distances as the longwall face progressed beyond the inclinometer

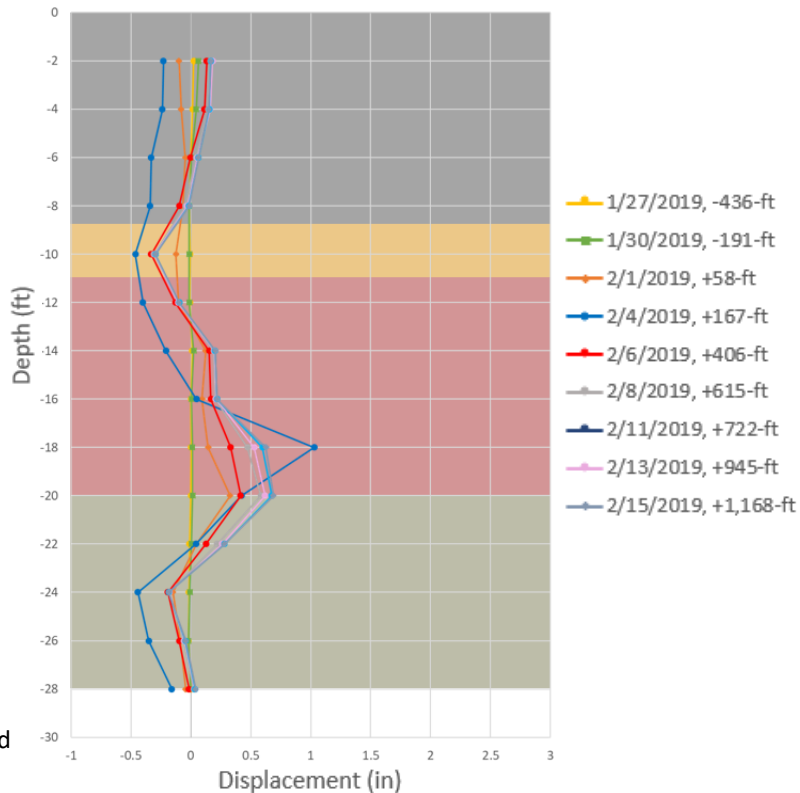
- = Silt and Clay
- = Silt and Sand
- = Siltstone
- = Sandstone interbedded with Siltstone

TB-8 Incremental Displacement

Axis – A, Incremental Displacement



Axis – B, Incremental Displacement

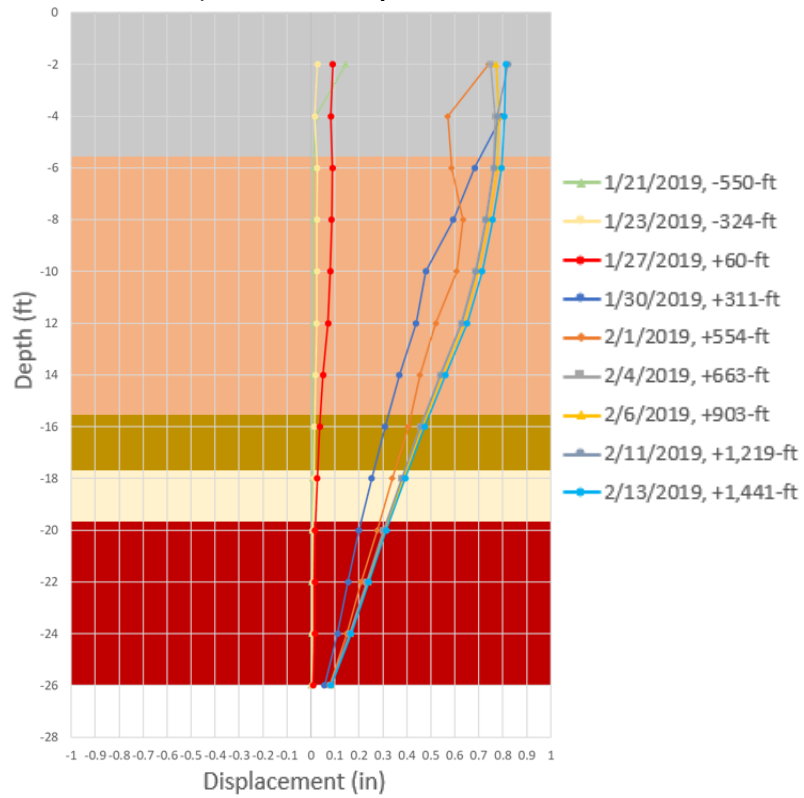


“-“ signs indicate distances as the longwall face approached the inclinometer, while “+” signs indicate distances as the longwall face progressed beyond the inclinometer

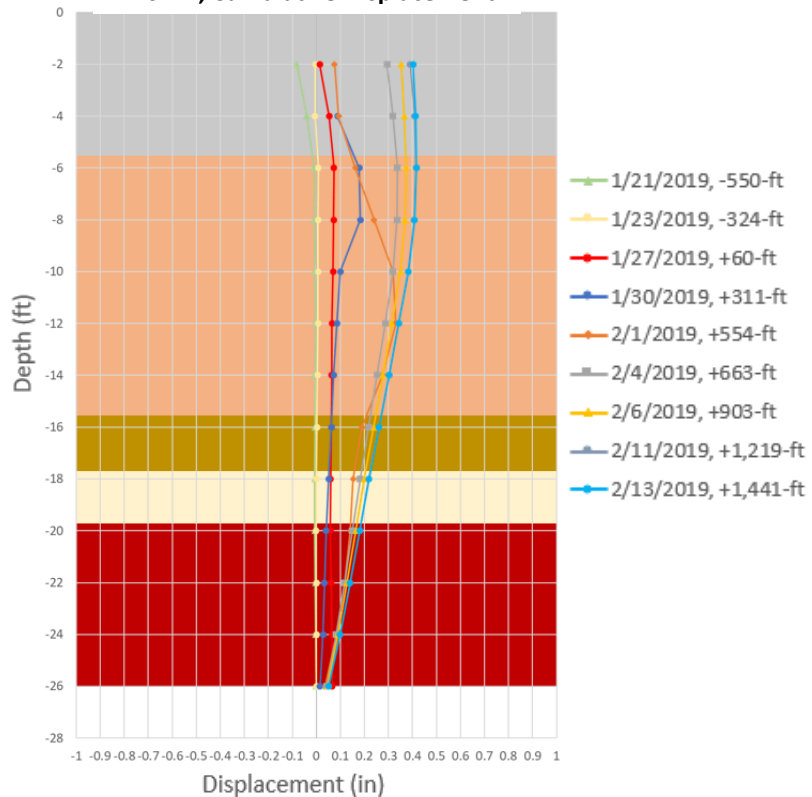
- = Silt and Clay
- = Silt and Sand
- = Siltstone
- = Sandstone interbedded with Siltstone

TB-9 Cumulative Displacement

Axis – A, Cumulative Displacement



Axis – B, Cumulative Displacement

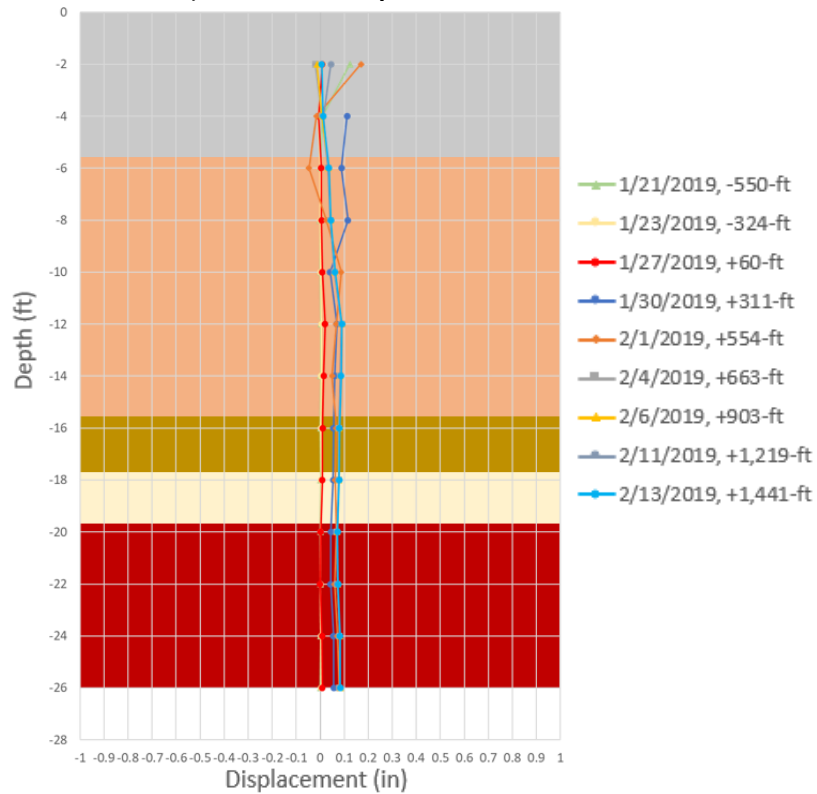


“-“ signs indicate distances as the longwall face approached the inclinometer, while “+” signs indicate distances as the longwall face progressed beyond the inclinometer

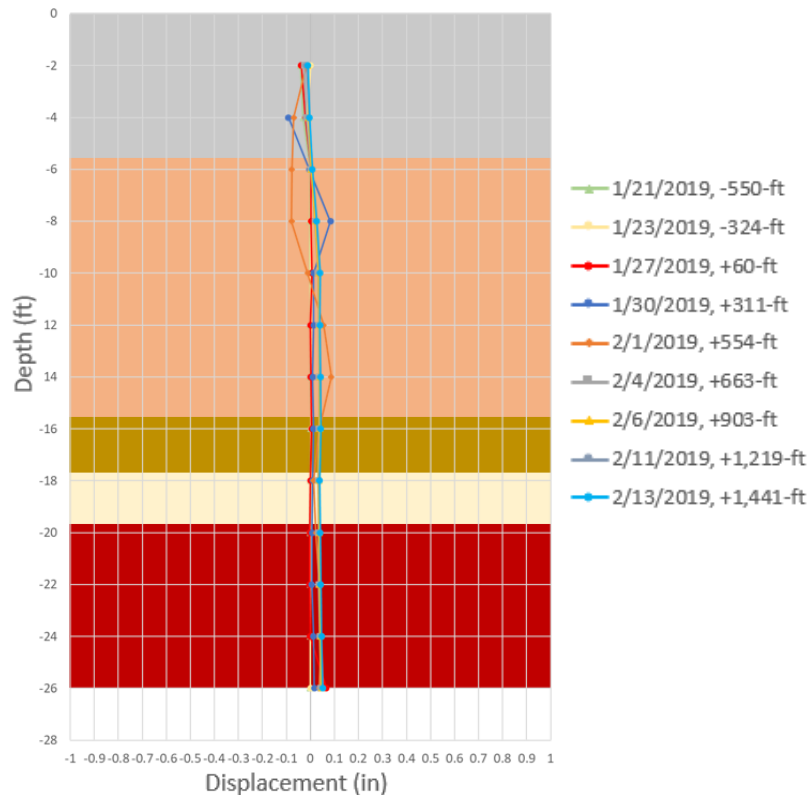
- = Clay
- = Gravel
- = Sand
- = Sandstone
- = Shale

TB-9 Incremental Displacement

Axis – A, Incremental Displacement



Axis – B, Incremental Displacement

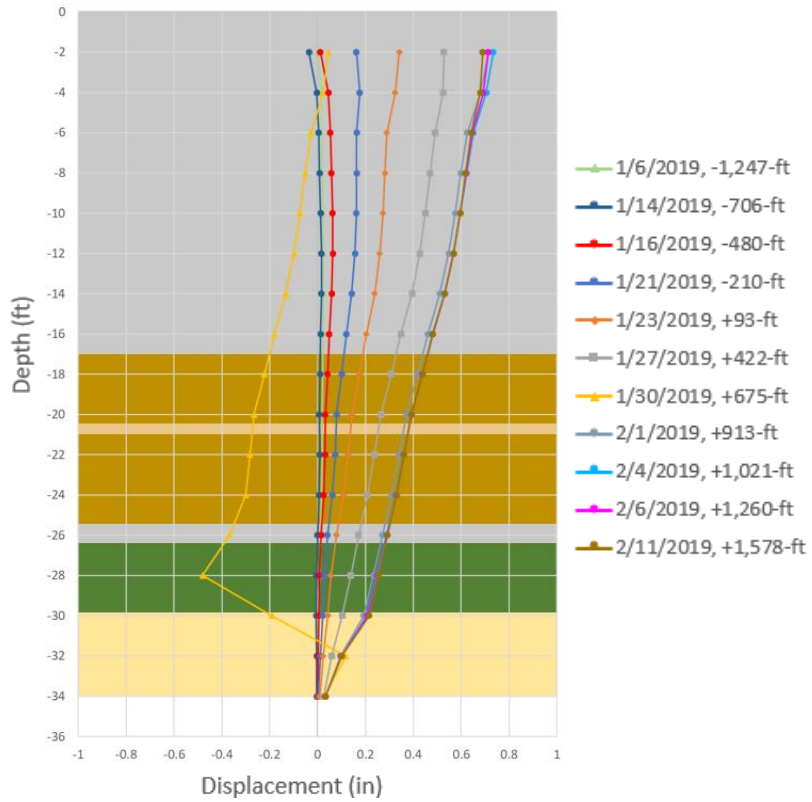


“-“ signs indicate distances as the longwall face approached the inclinometer, while “+” signs indicate distances as the longwall face progressed beyond the inclinometer

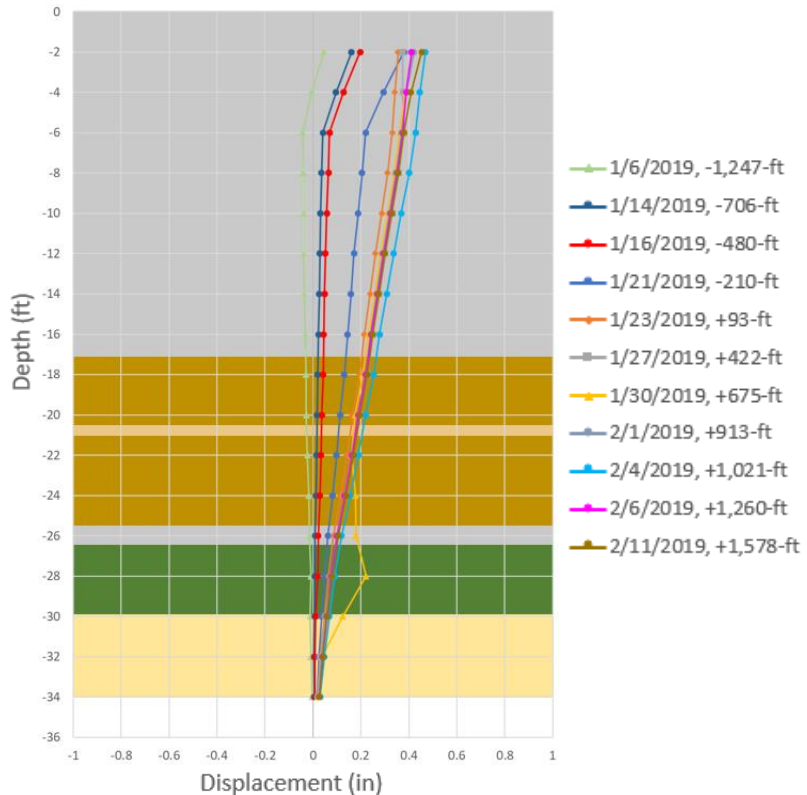
- = Clay
- = Gravel
- = Sand
- = Sandstone
- = Shale

TB-13 Cumulative Displacement

Axis – A, Cumulative Displacement



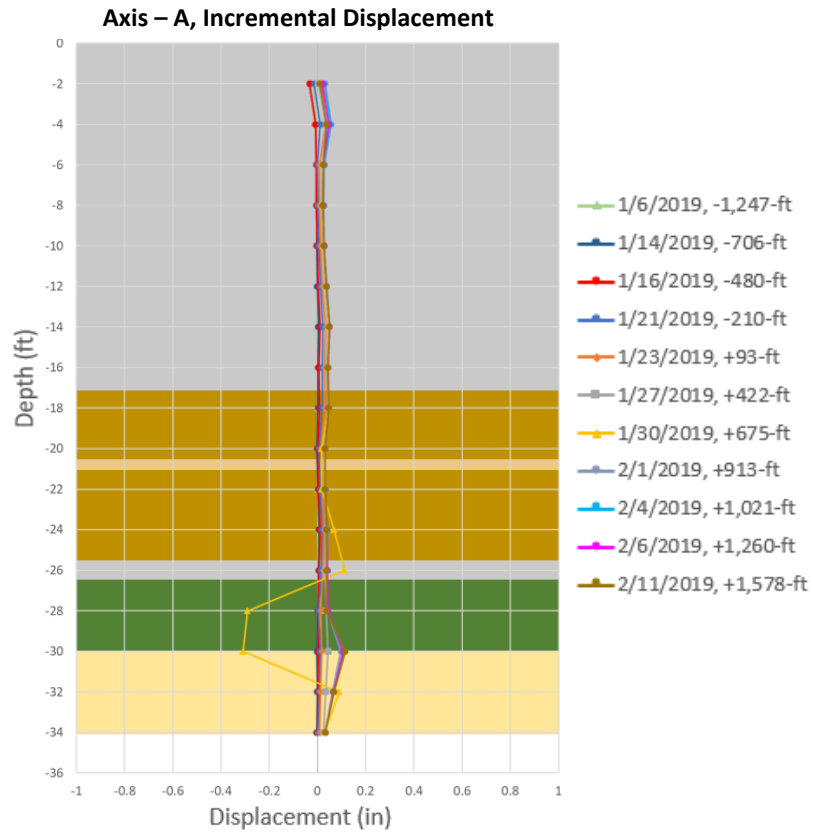
Axis – B, Cumulative Displacement



“-“ signs indicate distances as the longwall face approached the inclinometer, while “+” signs indicate distances as the longwall face progressed beyond the inclinometer

- ☐ = Gravel
- ☐ = Sand
- ☐ = Silt and Sand
- ☐ = Siltstone interbedded with Sandstone
- ☐ = Sandstone

TB-13 Incremental Displacement



“-“ signs indicate distances as the longwall face approached the inclinometer, while “+” signs indicate distances as the longwall face progressed beyond the inclinometer

- = Gravel
- = Sand
- = Silt and Sand
- = Siltstone interbedded with Sandstone
- = Sandstone

